Understanding the Factors which Influence the Interactions of Iron (II) and Iron (III) in Porphyrins and the Chemistry of Silicon Phthalocyanine

By

Shanti Anandan [B.Sc. (H), GRSC]

A thesis submitted in partial fulfilment of the requirements of the University of Greenwich for the Degree of Doctor of Philosophy

May, 2012

School of Science
University of Greenwich,
Medway Campus,
Chatham Maritime,
Kent ME4 4TB, UK

the UNIVERSITY of GREENWICH

DECLARATION

"I certify that this work has not been accepted in substance for any degree, and is not concurrently being submitted for any degree other than that of the PhD being studied at the University of Greenwich. I also declare that this work is the result of my own investigations except where otherwise identified by references and that I have not plagiarised another's work".

S. Anandan (Candidate)

……

PhD Advisor

Prof. B. Z. Chowdhry

20/05/2012

ACKNOWLEDGEMENTS

This PhD has been quite a journey for me. Many years passed before I could reach my dream. Many life's obstacles may have robbed some of my precious time that severely delayed my work but never can I give up my research, passion and interest in my subject.

First and foremost, I would like to take this opportunity to thank Prof. Martin J. Snowden who relentlessly encouraged me to never give up my work. Then, in the last few months, Prof. Babur Z. Chowdhry helped and encouraged me with the submission of the thesis.

However, there are many wonderful people who helped me during my research years. I will always be grateful to Professor Jack Silver and Dr Mike Thomas for their wonderful ideas, encouragement, support and understanding throughout my early PhD years. Thank you also to Paul Marsh and Dominic Davies for their excellent suggestions and advice. I would like to take this opportunity to say thank you to Dr C. McCammon for the usage of the facilities in Geoinstitut, Bayreuth, Germany. The people in the Geoinstitut who made my stay and work there very pleasant especially to Professor D. C. Rubie, Dr. J. Sowerby and Dr. N. Miyajima.

Thanks also to people who worked with me in Lab237 especially George Fern, Huma Ahmad and Lyn Gallagher (helped with all the glasswares!) and Kevyn Knight, my best buddy! Without their help, sense of humour and ideas the work would have been much more difficult. Enrico Furia was wonderfully encouraging in some part of my achievement for this thesis. Russell who stayed up with me when I was burning the midnight oil!

Finally, many thanks to most of the friendly, kind and helpful staffs of the University, my families in Malaysia and USA as well as to all my friends in London and elsewhere.

ABSTRACT

Understanding the Factors which Influence the Interactions of Iron (II) and Iron (III) in Porphyrins and the Chemistry of Silicon Phthalocyanine

The work presented in this thesis involved the study of iron(II) and iron(III) porphyrins using high-pressure Mössbauer spectroscopy. Further work was aimed at the formation of a new complex between iron(III) tetraphenylporphyrin chloride [Fe(III)TPPCl] and silicon phthalocyanine di-4pyridinecarboxylic acid [Si-Pc(4PyCOO)$_2$].

The synthesis of tetraphenylporphyrin (H_2TPP) and Fe(III)TPPCl was achieved and verified using CHN analysis, UV spectrometry and ambient pressure Mössbauer spectroscopy. However the synthesis of pure Si-Pc[PyCOO]$_2$ proved to be difficult. The intention to form a complex between Fe(III)TPPCl and Si-Pc[PyCOO]$_2$ was not successful, despite many attempts. The reason for this was due to the nature of Si-Pc[PyCOO]$_2$. The axial ligand $[PyCOO]^-$ has higher affinity for H^+ than $[Fe(III)TPP]^+$. The difference in solubility of Fe(III)TPPCl and Si-Pc[PyCOO]$_2$ in chloroform caused another problem in the formation of the complex due to the nature of the solvent. Chloroform is too hygroscopic and even a limited exposure to the atmosphere decomposes the Si complex.

An understanding of some of the factors that control the spin state of Fe(III)OEPCl and Fe(III)PPIXCl was made possible using high-pressure Mössbauer spectroscopy studies. Many synthetic porphyrins have been studied to model the structure and the reactions of haemoproteins. One of the reasons for this is that [PPIXFe(II/III)] (haem)

is difficult to crystallise whereas Fe(TPP) and Fe(OEP)-compounds readily crystallise.

Mössbauer spectroscopy was used to study the spin state of iron(III) and its changes in ^{57}Fe(III)OEPCl under high-pressure conditions. This area of study is an extension of previous work on ^{57}Fe(III)PPIXCl using the same technique. Evidence of the nuclear interactions parameter (quadrupole splitting, ΔE_Q) was established for the change in the spin state from high spin to the spin admixed S = +/- $^3/_2$, +/- $^5/_2$ state. Furthermore, high-pressure Mössbauer spectroscopy was shown to be a powerful technique to study this kind of spin state - "spin admixed". Examples were used from previous studies to compare the change in the spin state.

^{57}Fe(III)OEP[4-NH_2Py]$_2$ was also synthesised and compared with [^{57}FePPIX[HIm]$_2$]Cl using high pressure Mössbauer study. The Mössbauer data for these compounds when compared with a whole range of [Fe(III)Por(L)$_2$]$^+$ complexes provided a better understanding of the structural conformation, the orientation of ligands [parallel or perpendicular positions] in relation the Fe-N plane. The comparative study using similar substituted ligands of imidazoles demonstrated that ligands binding to the iron influence the electronic structure in relation to pressure. Probing with the nuclear interactions using Mössbauer technique explained some of the informations and factors that control the spin state in these compounds.

Shanti Anandan [B.Sc. (Hons), GRSC]

DEDICATION

To my beloved late father

Mr V Maniam

"Who Was My Rock, Inspiration And A Wonderful Dad Who Taught Me Many
Beautiful Wisdoms About Life"

To know the Way,

We go the Way;

We do the Way

The way we do

The things we do.

It's all there in front of you,

But if you try too hard to see it,

You'll only become Confused.

I am me

And you are you,

But when you do

The things that you can do

You will find the Way,

And the Way will follow you.

TABLE OF CONTENTS

TITLE PAGE		**I**
DECLARATION		**II**
ACKNOWLEDGEMENTS		**III**
ABSTRACT		**IV**
DEDICATION		**VI**
TABLE OF CONTENTS		**VII**
ABBREVIATIONS		**XIII**
AIMS OF PROJECT		**XV**
Chapter 1 - Introduction to Porphyrins, Metalloporphyrins and Phthalocyanines		
1.1	Introduction	1
1.2	The Porphyrin System	1
	1.2.1 Porphyrin Nomenclature	5
	1.2.2 Metalloporphyrins	7
	1.2.2.1 Structural Features of Porphyrins	9
	1.2.2.1(a) Coordination Type	9
	1.2.2.1(b) Equatorial Stoichiometry	11
	1.2.2.1(c) Axial Stoichiometry	14
1.3	Iron Porphyrins	14
	1.3.1 Iron(III)	15
	1.3.2 Iron(II)	17
1.4	Physical Characteristics of Porphyrins	18

1.4.1 UV/vis Spectroscopy of Metal Free Porphyrins 18
1.4.2 UV/vis Spectroscopy of Metalloporphyrins 20
1.4.3 Infrared Spectroscopy of Porphyrins 22
1.4.4 Mössbauer Spectroscopy of Iron Porphyrins 22

1.5 Phthalocyanines 24
1.5.1 Metallophthalocyanines 25
1.5.2 General Synthesis 26
1.5.3 Polymeric Variations of Phthalocyanines 26
1.5.4 Electronic Absorption Spectra 27
1.5.5 Infrared (IR) Spectra 27

1.6 References 29

Chapter 2 - Experimental Techniques

Section one - Mössbauer spectroscopy

2.1 Mössbauer spectroscopy 34
2.1.1 Discovery and Definition 34
2.1.2 Resonant Fluorescence and Absorption 35
2.1.3 Theory of emission and absorption of γ -rays by nuclei 35
2.1.4 The Mössbauer Effect 39
2.1.5 Mössbauer Spectroscopy 40
2.1.6 The Doppler Effect 42
2.1.7 Instrumentation 43
2.1.8 The Mössbauer Spectrum 44
2.1.9 Mössbauer Effect Hyperfine Parameters 46
2.1.9.1 Isomer Shift (δ) 46
2.1.9.1a.Second Order Doppler Shift 50
2.1.9.2 Quadrupole Splitting (ΔE_Q) 51
2.1.9.3 Magnetic Hyperfine Interaction 57
2.1.9.4 Line Shape, Width, Area 58

Section two - High pressure Mössbauer Spectroscopy

2.2 High Pressure Mössbauer spectroscopy 59

2.2.1 Discovery and Definition 59

2.2.2 Experimental Techniques 60

2.2.2.1 Diamond 60

2.2.2.2 Gasket 61

2.2.2.3 Hydrostatic Medium 62

2.2.2.4 Diamond Anvil Cell (DAC) 63

2.2.2.5 Pressure Calibration by Ruby Fluorescence 65

2.2.3 The Effect of Pressure 67

2.2.3.1 Chemical Consequences 70

2.3 References 70

Chapter 3 - Synthesis of Iron(III) tetraphenylporphyrin chloride [Fe(III)TPP]Cl and Silicon Phthalocyanine di,4-pyridinecarboxylic acid SiPc[PyCOO]$_2$: Studies aimed at forming complexes between [Fe(III)TPP]Cl and SiPc[PyCOO]$_2$

3.1 Introduction 73

3.1.1 Porphyrin, Metalloporphyrin (H_2TPP and Fe(III)TPPCl) 73

3.1.1.1 Properties, Uses and Applications of Fe(III)TPPCl 74

3.1.2 Silicon Phthalocyanine 75

3.1.2.1 Preparation of Axially Substituted SiPc 78

3.1.2.2 Preparation of Axially Substituted SiPc from $SiPcCl_2$ and $SiPc(OH)_2$ 78

3.1.2.3 Properties, Uses and Applications of Silicon Phthalocyanines 81

3.1.2.3.1 Theory of Non-linear Optics 83

3.1.3 Crystallisation 85

3.1.3.1 Solvents for Crystallisation 86

3.1.3.2 In Search of the 'Right' Solvent 86

3.2 Experimental

3.2.1 Synthesis of Porphyrins 88

3.2.2 Synthesis of H_2TPP 88

3.2.3 Synthesis of Fe(III)TPPCl 89

3.2.3.1 Iron(II) Chloride Method 89

3.2.3.2 Iron(II) Acetate Method 90

3.2.3.2a Crystal Structure of Fe(III)TPPCl 90

3.2.4 Synthesis of $SiPcCl_2$ 94

3.2.5 Synthesis of $SiPc[4\text{-}PyCOO]_2$ 95

3.2.6 Attempted Preparation of a New Complex of Fe(III)TPPCl and $SiPc[PyCOO]_2$ 96

3.3 Results 98

3.3.1 Electronic Absorption (UV) Spectrum of H_2TPP 98

3.3.2 IR Assignment of H_2TPP and Fe(III)TPPCl 99

3.3.3 Synthesis Considerations for $SiPc[PyCOO]_2$ 101

3.3.4 UV Spectrum of $SiPcCl_2$ and $SiPc[PyCOO]_2$ 102

3.3.5 IR Spectrum of $SiPcCl_2$ and $SiPc[PyCOO]_2$ 104

3.4 Conclusions 107

3.5 References 108

Chapter 4 - A High Pressure Mössbauer Spectroscopy Study of 2,3,7,8,12,13,17,18-Octaethylporphyrin ^{57}iron(III) chloride [^{57}Fe(III)OEP]Cl

4.1 Introduction 113

4.1.1 The Fe(III)OEP and Fe(III)PPIX System 115

4.2. Experimental 119

4.2.1 Methods 120

4.2.1.1 Synthesis of H_2OEP 120

A. Synthesis of 4-Nitro-3-hexanol 121

B. Synthesis of 4-Aceoxy-3-nitrohexanol 122

C. Ethyl 3, 4-diethylpyrrole 2-carboxylate 123

D. Synthesis of H_2OEP 124

4.2.1.2 Synthesis of Fe(III)OEPCl 125

4.2.2 Preparation of enriched Fe(III)OEPCl 126

4.2.3 Sample Measurements 126

4.3 Results 128

4.4 Discussion 135

4.5 Conclusions 141

4.6 References 141

Chapter 5- Comparative High Pressure Mössbauer Spectroscopic Studies Of Low Spin Iron Porphyrins

5.1 Introduction 145

5.1.1 Cyctochrome b 145

5.1.2 Models for Cyctochrome b 147

5.2 Experimental 149

5.2.1 Materials 149

5.2.2 Preparation of $^{57}FeOEP[4\text{-}NH_2Py]_2Cl$ 150

5.2.3 Preparation of $^{57}FePPIXCl$ 151

5.2.5 Mössbauer Measurements 151

5.3 Results 153

5.4 Discussion 156

5.4.1 Effects of Pressure on the Linewidth of $^{57}FeOEP(NH_2Py)_2Cl$ 159

5.4.2 Studies on $[Fe(III)PPIX(HIm)_2]^+$ 159

5.4.3 Previous Work 166

5.5 Further Discussion 167

5.5.1 Drickamer's Result 169

5.6 Conclusions 171

5.5 References 171

Chapter 6 - Summary and Conclusions

6.1 Summary and General Conclusions 176

6.2 Future Work 177

ABBREVIATIONS

Abbreviation	Description
ClO_4	Perchlorate
EtOH	Ethanol
Fe(OEP)Cl	Iron octaethylporphyrin chloride
$Fe(OEP)ClO_4$	(Octaethylporphyrinato)- iron perchlorate
$Fe(OEP)ClO_4.2EtOH$	*Di*ethanol iron octaethylporphyrinato perchlorate
$FeOEP[4\text{-}NH_2Py]_2$	Iron octaethylporphyrin *bis* 4- aminopyridine
Fe(PPIX)Cl	Iron protoporphyrin IX chloride
$Fe(PPIX)(CN)_2$	*di*cyano protoporphyrin IX iron
$Fe(PPIX)(HIm)_2Cl$	Iron protoporphyrin IX chloride *bis* imidazole chloride
$Fe\ (PPIX)(Im)_2$	Iron protoporphyrin IX *bis* imidazole
Fe(PPIX)(NCS)(Py)	Isothiocyanato(pyridine)(protoporphyrinIX) iron
FeTPPCl	Iron tetraphenylporphyrin chloride
$Fe(TPP)ClO_4$	(Tetraphenylporphyrinato) iron perchlorate
$Fe(TPP)(Im)_2Cl$	*Bis* imidazole tetraphenylporphyrin iron chloride
$FeTPP\ (2\text{-}MeIm)_2ClO_4$	2-Methyl imidazole (tetraphenylporphyrin) iron perchlorate
FeTPP (2-MeIm)(EtOH)	*Di*ethanol 2-methyl imidazole (tetraphenylporphyrin) iron perchlorate
$[Fe(TPP)_2]N$	Nitrido *bis*[(tetraphenylporphyrin) iron]
FeTPP(NCS)Py	Isothiocyanato(pyridine) (tetraphenylporphrinato) iron
$[Fe(TPP)]_2O$	[μ] – Oxo *dimer* of (5,10,15,20 tetraphenylporphyrin) iron
$FeTPP\ (PiP)_2$	*Di*piperidyl (tetraphenylporphyrin) iron
$FeTPP\ (THF)_2$	*Bis* tetrahydrofuran (*meso* tetraphenylporphyrin) iron
Im	I H-Imidazole
2-Me-Im	2-Methylimidazole
NCS	N-Chlorosuccinimide or isothiocyanato
$4\text{-}NH_2Py$	4-Aminopyridine
$OEPH_2$	Octaethylporphyrin
Pip	Piperidine
Ppiv	"picket fence" porphyrin
PPIXCl	Protoporphyrin IX chloride
PMXPP	α, β, γ, δ –(*p*-anisidyl)porphyrin

Py	Pyridine
Py-COOH	Isonicotinic acid or Pyridine-4-carboxylic acid
$[Rh(CO_2)]_2OEP$	*di* (rhodium carbonyl)octaethylporphyrin
Si-Pc	Silicon Phthalocyanine
SiPc(PyCOOH)Cl	Silicon Phthalocyanine pyridine carboxylic acid chloride
$Sn(IV)(Pc)_2$	Tin *bis* phthalocyanine
THF	Tetrahydrofuran
TPP	Tetraphenylporphyrin
$U(Pc)_2$	Uranium *bis* phthalocyanine
$U(TPP)_2$	Uranium *bis* tetraphenylporphyrin

AIMS OF PROJECT

The research reported in this thesis was conducted on iron porphyrins and silicon phthalocyanine compounds to further the understanding of these compounds. The overall aim was to study and enhance our knowledge of the mechanisms controlling the chemistry of the iron site. Iron(II) and iron(III) complexes have high, intermediate and low spin states.

Understanding the chemistry of iron protoporphyrin IX in the absence of protein is of interest to both chemists and biochemists because of its biological role. A synthetic compound that has similar chemical properties is iron octaethyl porphyrin, which is one of the most widely studied and easily synthesised model porphyrin systems. Silicon phthalocyanine compounds were also prepared for some of the aspects of their synthesis, structure and properties in this work.

The work reported in this thesis is as follows.

1. The attempted formation of a crystalline iron tetraphenyl porphyrin and silicon phthalocyanine *di* 4-pyridine carboxylic compound. For the aforementioned:
    - FeTPPCl was synthesised,
    - PyCOOH (*isonicotinic acid*) ligands were bound to the axial positions of $SiPcCl_2$ and
    - the formation of $[FeTPP]^{+}$- $[SiPc(PyCOO)]^{2-}$ containing FeTPPCl and $SiPc[PyCOO]_2$ was attempted and various tests were carried out for ascertaining the solubility of these compounds and other ligands.

2. Interest in the admixed spin species [$^3/_2$, $^5/_2$] in iron(III) compounds led to the synthesis of enriched ^{57}Fe(III)OEPCl and comparative studies with

^{57}Fe(III)PPIXCl, using high pressure Mössbauer spectroscopy so that the results could be compared with previous studies.

3. Finally, ^{57}Fe(III)OEP[4-NH_2Py]$_2$Cl was synthesised and the properties of this complex were studied using the high pressure Mössbauer spectroscopic techniques in order to understand the effect of increased pressure on the axial position of the ligand in the compound.

Chapter 1: Introduction to Porphyrins, Metalloporphyrins and Phthalocyanines

1.1 Introduction

Porphyrins are compounds that are ubiquitous in nature and occur in the well-known *chlorophyll a* and *b* complexes, found in plants and haem which is found in blood. Of particular interest is the group of structural analogues of natural porphyrins, which include synthesised porphyrins, phthalocyanines and their various metal derivatives. Synthesis and development of various types of porphyrins and phthalocyanines are extremely important in the study of the biological, chemical and physical properties of naturally occurring haem proteins.

This research was conducted on iron-containing porphyrins and silicon phthalocyanine compounds to further the understanding of these compounds. The overall aim was to study and enhance the understanding of the mechanisms controlling the chemistry of the iron site. Iron(II) and iron(III) complexes have high, intermediate and low spin states. Silicon phthalocyanine compounds were also prepared to study some of the aspects of their synthesis, structure and properties in this work.

1.2 The Porphyrin System

Küster first suggested the porphyrin structure in 1912[1], but the proposal was not accepted because such a large structure was thought to be intrinsically unstable. In 1929, Fischer succeeded in synthesising iron(III) protoporphyrinIX chloride (haemin), from pyrrolic starting materials and this structure was fully accepted[2].

In 1965, Webb and Fleischer[3] first published the x-ray crystal structure of this molecule, which is a macrocycle, deep red in colour and is very nearly planar in structure.

The name, porphyrin, is given to a family of intensely coloured compounds, which are all substituted analogues of a large macrocycle of twenty carbon and four nitrogen atoms (Figure 1.1) The macrocycle itself is built up from four smaller pyrrole rings, each made up of four carbon and one nitrogen atom. The structure was first suggested by Kuster in 1912[1].

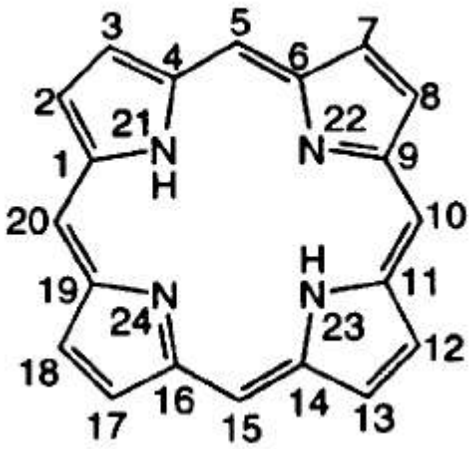

Figure 1.1 All number IUPAC systematic nomenclature of a macrocycle[4].

The bare tetrapyrrole nucleus has unique chelating properties, a central metal atom displaces two hydrogen ions from the porphyrin and thus finds itself in a symmetrical electrostatic field of four nitrogen atoms with which it may form four equivalent coordinate donor-acceptor bonds.

The effects of the substituents on the porphyrin nucleus and the effects of extra ligands (which may be added perpendicularly to the porphyrin plane) mean that the

physiochemical properties of metalloporphyrins can be subjected to great variation. Such modification of metalloporphyrins leads to a wide range of finely tuned properties found in natural compounds. These derivatives play an essential role in the life of bacteria, fungi, plants and animals.

In nature, several dozen compounds contain the porphyrin skeleton, with varying degrees of unsaturation, bonded to a wide range of functional groups; examples of these include:

(i) catalyse, a magnesium(II) [Mg^{2+}] - containing enzyme which catalyses the decomposition of cellular hydrogen peroxide; *chlorophyll a* and *chlorophyll b* (Figure 1.2)[2], two of several photosynthetic pigments which transduce light into chemical energy in plants and other autotrophs;

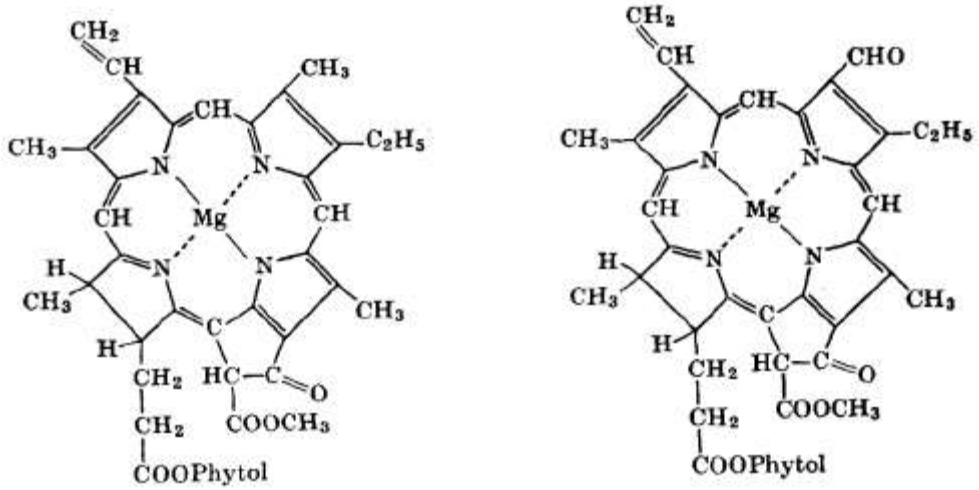

(a) **(b)**

Figure 1.2 Schematic of the structure of (a) chlorophyll-a and (b) chlorophyll-b.

(ii) haemoglobin & myoglobin (Figure 1.3)[3], the iron(II) ion is responsible for transporting dioxygen and carbon monoxide in mammals and birds; The iron atom of cytochromes alternate between the iron(II) state and iron(III) state. Biosynthesis of heme including involves enzyme and mechanisms[4].

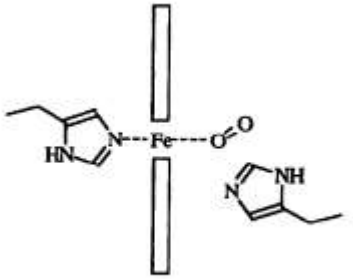

Represents the porphyrin plane

Figure 1.3 Binding of oxygen to the haem group of haemoglobin or myoglobin.

(iii)vitamin-B12 (Figure 1.4)[2], the cobalt(III) cofactor required for the synthesis of mammalian red blood cells.

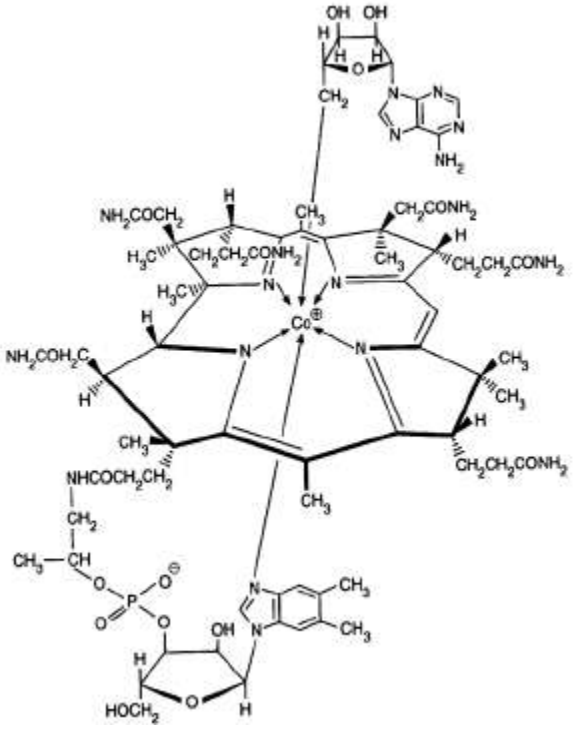

Figure 1.4 Schematic of the structure of vitamin B-12.

The porphyrin ring systems are essential to the function of many biological molecules and are derivatives of the parent porphyrin molecule. These derivatives are named and classified according to the basis of the side chain substituents, for example protoporphyrins, mesoporphyrins, etioporphyrins and coproporphyrins. Of these the most abundant are the protoporphyrins, which may exist in fifteen isomeric forms[2]. These differ in the sequence of substitution of eight different side chains. The function of the side chains is to fine-tune the metalloporphyrin for its specific biological role.

1.2.1 Porphyrins Nomenclature

It was Fischer who derived the first system of nomenclature for porphyrins[2] (Figure 1.1). However, systematic IUPAC nomenclature was introduced in 1979, which numbered all the carbon atoms in the macrocycle (Figure 1.5)[2]. In line with conventional organic chemistry at the time, every new porphyrin was given a trivial name. Many porphyrins are substituted on all eight positions of the pyrrole fragments. When all substituents are the same, naming the porphyrin is relatively simple. For example, eight ethyl (CH_3CH_2) groups attached to the pyrrole positions gives octaethylporphyrin (Table 1.1).

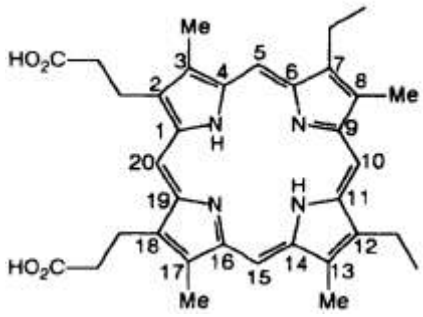

Figure 1.5 Mesoporphyrin IX – systematic nomenclature; 7, 12-diethyl 3, 8, 13, 17-tetramethyl porphyrin 2, 18-dipropionic acid - related numbering system.

Table 1.1 Examples of naturally occurring and synthetic porphyrins[5].

	Position of substituent											
Name	**2**	**3**	**5**	**7**	**8**	**10**	**12**	**13**	**15**	**17**	**18**	**20**
Uroporphyrin I	A	P	H	A	P	H	A	P	H	A	P	H
Coproporhyrin II	M	P	H	P	M	H	M	P	H	P	M	H
Etioporphyrin III	M	E	H	M	E	H	M	E	H	E	M	H
Protoporphyrin IX (PPIX)	M	V	H	M	V	H	M	P	H	P	M	H
Mesoporphyrin IX	M	E	H	M	E	H	M	P	H	P	M	H
Deuteroporphyrin IX	M	H	H	M	H	H	M	P	H	P	M	H
Pyrroporphyrin	M	E	H	M	E	H	M	H	H	P	M	H
Octamethylporphyrin	M	M	H	M	M	H	M	M	H	M	M	H
Octaethylporphyrin (OEP)	E	E	H	E	E	H	E	E	H	E	E	H
Tetramethylporphyrin(TMP)	H	H	M	H	H	M	H	H	M	H	H	M
Tetrapropylporphyrin	H	H	Pr	H	H	Pr	H	H	Pr	H	H	Pr
Tetraphenylporphyrin (TPP)	H	H	Ph	H	H	Ph	H	H	Ph	H	H	Ph

A: CH_2COOH P: CH_2CH_2COOH H: H M: CH3
E: CH_2CH_3 Pr: $CH_2CH_2CH_3$ Ph: C_6H_5 V: $CH=CH_2$

1.2.2 Metalloporphyrin

Porphyrins have the ability to complex with many different metals in the periodic table (Figure 1.6). The metal replaces the two inner pyrrole protons; it coordinates via the lone pairs on the nitrogen atoms.

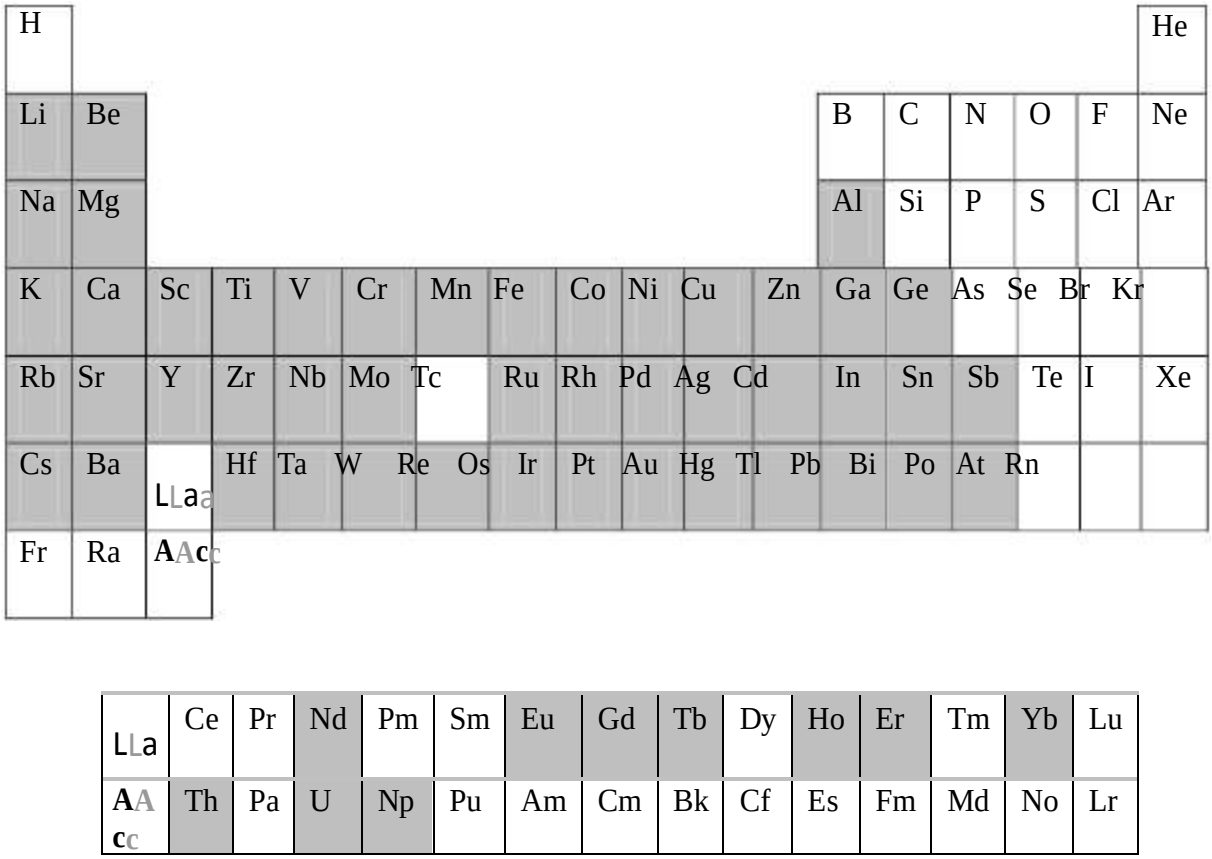

Figure 1.6 Metals (shaded) in the periodic table which can react with porphyrins[7, 8].

In the simplest type of metalloporhyrin the metal ion is often in the (II+) oxidation state. The formation of such a metalloporphyrin involves usually the reaction of the central nitrogen atoms of the metal-free porphyrin, H_2Por, with a metal salt MX_2 (Figure 1.7). Metalloporphyrin and acid HX are formed. This process is known as metallation[6].

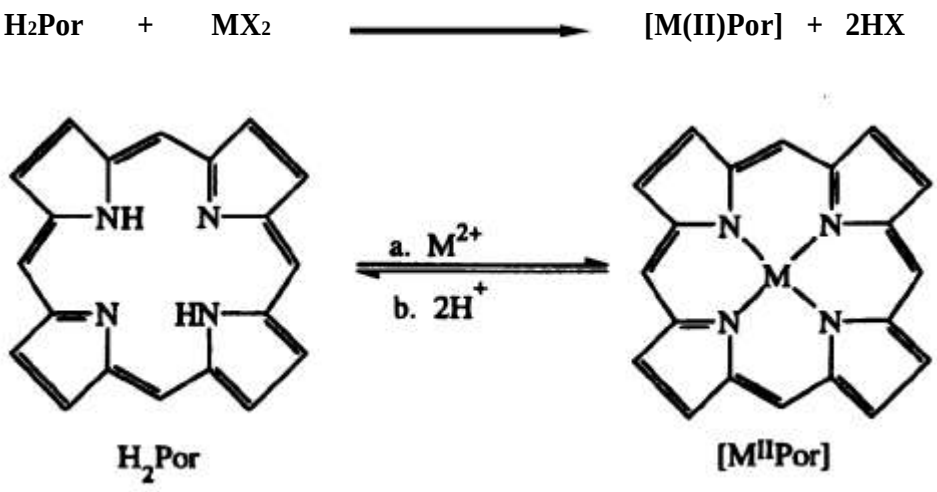

Figure 1.7 Formation of [M(II)Por].

Two possible mechanisms have been proposed for metallation reactions of porphyrins:

1. **dissociation reactions**, in which the –NH hydrogens are removed forming a dinegative Por^{2-} anion, followed by inclusion of the metal ion.
2. **displacement reactions,** in which initially an active metal-porphyrin complex is formed, followed by displacement of the –NH hydrogens by the metal ion to form the metalloporphyrin.

The central metal atom displaces two hydrogen ions from the porphyrin compound and finds itself in a practically symmetrical electrostatic field of four nitrogen atoms with which it may form four almost, coordinate donor-acceptor bonds. If the interaction between the metal and the porphyrin anion is primarily electrostatic, labile ionic complexes are formed. These include complexes of Na^+, K^+, Rb^+, Cs^+, Be^{2+}, Sr^{2+}, Ba^{2+}, Ca^{2+} and some other ions[9].

If the electrostatic interaction involves filling of the vacant orbital of the central atom by the electrons of the donor N atoms of the compound, stable porphyrin complexes that are covalent or predominantly covalent are formed. The transition metal chemistry are revised and studied on widely used isotopes as shown in the shaded area of the periodic table (Figure 1.6) by Gütlich *et al*[10].

1.2.2.1 Structural Features of Metalloporphyrins

The metal ion in the metalloporphyrin may be located either in or out of the plane of the porphyrin ring. The position relative to the plane depends on the:

(a) number of axial ligands,
(b) valence state of the metal,
(c) size of the metal, and
(d) electronegativity of the ligand.

Metalloporphyrins can be classified by different types of structure: coordination type, equatorial stoichiometry and axial stoichiometry.

1.2.2.1(a) Coordination Type

A chemical compound formed by joining independent molecules or ions usually to a central metallic atom by coordinate bonds. A compound may contain one or more coordinate bonds; which forms a link between a pair of electrons in which both electrons are donated by one of the atoms.

(a) Four coordinate (square planar geometry), i.e. the metal ion lies in the porphyrin plane (Fig. 1.8) and is bound to the four nitrogen atoms of the porphyrin ring. [Fe(II)TPP][9] is in this category.

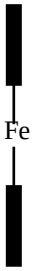

Figure 1.8 [Fe(II)TPP].

(b) Five coordinate (square pyramidal geometry). The metal ion is located out of plane and is coordinated to a single axial unidentate ligand and to the four pyrrole nitrogen atoms. Some high spin iron(III) porphyrins are of this type. An example of this is [Fe(III)PPIXCl] in which the iron(III) is 0.475Å out of the plane[11](Figure 1.9).

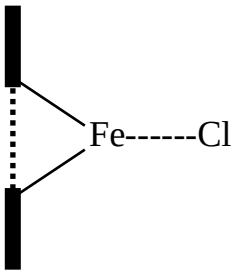

Figure 1.9 [Fe(III)PPIX(Cl)].

(c) Six coordinate (distorted octahedral geometry). Two axial ligands are bound at the fifth and sixth coordination sites. The metal is in the plane of the porphyrin ring. There are many examples of this type of metalloporphyrins in nature. Examples including [Fe(II)TPP(THF)$_2$][12], [Fe(III)TPP(2-MeIm)$_2$]ClO$_4$[13] (Figure 1.10) and [Fe(III)TPP(NCS)(Py)][14].

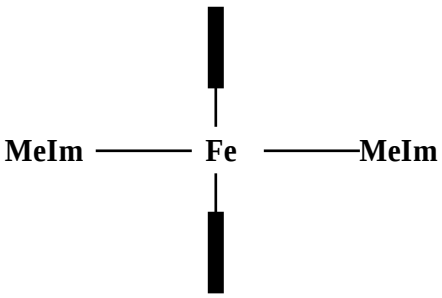

Figure 1.10 Fe(III)TPP(2-MeIm)$_2^+$.

(d) Eight coordination (square antiprism geometry); an unusual sandwich complex formed between two porphyrin molecules. An example of this type is U(TPP)$_2$[14] (Figure 1.11).

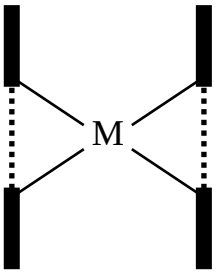

Figure 1.11 Semimetallic porphyrins such as U(TPP)$_2$[15].

1.2.2.1(b) Equatorial Stoichiometry

The equatorial stoichiometry defines the ratio of metal atoms to porphyrin atoms. This can be written as M_hPor_k. The simplest class of metalloporphyrins (Figure1.12) is the monometallic porphyrins (MPor; h = k = 1). All naturally occurring porphyrins belong to this class, e.g. Fe(III)PPIX.

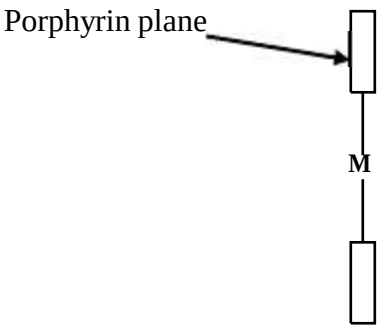

Figure 1.12 A monometallic porphyrin.

Semi-metallic species $M(Por)_2$ (MPor; h = 1, k = 2) occur when two porphyrin molecules are bound to only one metal atom. An example of this class is shown below (Figure 1.13). e.g. $[Sn(IV)(Pc)_2]$[16] and $[U(IV)(Pc)_2]$[17] (see also Figure 1.11).

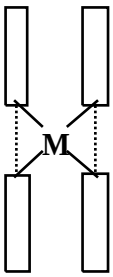

Figure 1.13 Semimetallic porphyrin.

Other classes: bimetallic species M_2Por (MPor; h = 2, k = 1) are shown below (Figure 1.14) e.g. $[\{Rh(CO_2)\}_2OEP]$[18].

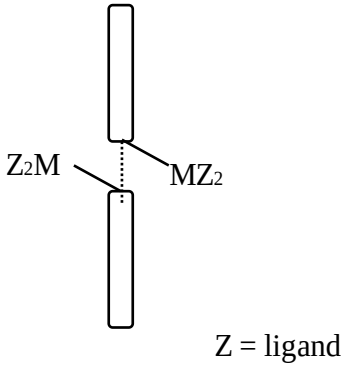

Figure 1.14 Bimetallic porphyrin.

Scheidt *et al*[19] presented the structure of H_4TPPCl_2 as an example of a polymetallic species as shown below (Figure 1.15).

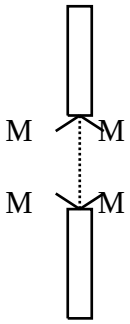

Figure 1.15 Polymetallic porphyrin.

1.2.2.1(c) The Axial Stoichiometry

Taking coordination type (c) [six coordination] as an example, the axial ligands can be specified as follows:

1. neutral unidentate ligands, L
2. uninegative anions, X^-
3. combination of neutral and anion ligands, LX^-

For example, iron(III) porphyrin complexes of coordination type (c) can be further subdivided into subclasses as follows:

1. $[Fe(III)Por(L)_2]^+$ e.g.$[Fe(III)PPIX(Im)_2]^+$ (ref:20)

2. $[Fe(III)Por(X)_2]^-$ e.g. $[Fe(III)PPIX(CN)_2]^-$ (ref:21)

3. [Fe(III)Por(L)(X)] e.g. [Fe(III)TPP(NCS)(Py)] (ref:13)

1.3 Iron Porphyrins

Iron porphyrin complexes have been prepared and characterised with the iron atom in a number of different valence and spin states (Table 1.2).

Table 1.2 Iron porphyrin compounds indicating the spin states.

Iron: oxidation state	**Spin state**	**Example**	**Ref.**
I	$^3/_2$ or $^1/_2$	$[Fe(TPP)]^-$	21
II	2	Fe(TPP)(2-MeIm)(EtOH) $Fe(TPP)(THF)_2$	22 23
	1	Fe(TPP)	23
	0	$Fe(TPP)(PiP)_2$	23
III	$^5/_2$	Fe(TPP)Cl $[Fe(TPP)]_2O$	24 25
	$^3/_2$	$Fe(OEP)ClO_4.2EtOH$	26
	$^3/_2$, $^5/_2$	$Fe(TPP)ClO_4$ $Fe(OEP)ClO_4$	27 28
	$^1/_2$	$Fe(TPP)(Im)_2Cl$	29
IV	1	$[\{Fe(TPP)\}_2O]ClO_4$	30
	1	$[Fe(TPP)_2N]$	30

Only iron(II), iron(III) and iron(IV) have been found in haem proteins. In this work only iron(II) and iron(III) porphyrins were studied.

1.3.1 Iron(III)

Iron(III) high spin porphyrins ($S = ^5/_2$) are the most common type of iron porphyrins. The x-ray structures of a number of five coordinate high spin iron(III) complexes of the type iron(porphyrin)X; (X= Cl, Br, F, I, OH) have been determined (Table 1.3).

Table 1.3 Five coordinate high spin complexes.

Complex	**Fe_N (Å)** **(a)***	**Fe_{ax} (Å)** **(b)***	**Core (Å)** **(c)***	Ref.
Fe(TPP)Cl	2.060(3)	2.193(3)	0.39	31
Fe(PPIX)Cl	2.0629(10)	2.218(6)	0.55	11
Fe(TPP)F	2.072(1)	1.792(3)	0.47	32
Fe(TPP)Br	2.069(9)	2.348(2)	0.56	33
Fe(TPP)I	2.066(11)	2.554(2)	0.53	34
$[Fe(TPP)]_2O$	2.087(8)	1.763(1)	0.54	35

(a)* Fe_N is the mean displacement of the iron(III) atom from the four nitrogen atoms of the plane.

(b)* Fe_{ax} is the iron(III) to axial ligand distance, and

(c)* displacement of the iron(III) atom from the mean plane of the core.

In the iron porphyrin μ-oxo dimer $(FeTPP)_2O$[35] the Fe-O-Fe angle is 174.5(1)° the Fe-O bond length is 1.763(1)Å. High spin iron(III) has also been found to exist in the six-coordination state. In such coordination the large size of the high spin iron(III) atom is accommodated by a radical expansion of the porphinato core with no displacement of the iron atom. An example for this is found in diaquo (*meso* tetraphenyl porphinato) iron(III) perchlorate $[Fe(TPP)(OH_2)_2]ClO_4$ [36].

The average Fe_N distance in the centrosymmetric molecule is 2.045(8)Å, the axial iron-water bond distance is 2.095(2)Å. For an iron(III) complex to have $S = 3/2$ ground state the $d_{x^2-y^2}$ antibonding orbitals lie well above the other *d* orbitals and are

unoccupied, while the remaining four *d* orbitals must fill by Hund's rules. An example of this is $Fe(OEP)ClO_4.2EtOH$[24].

In the low spin iron(III) porphyrin ($S = {}^1/_2$) complexes, the iron is expected to be centred or nearly centred in the porphrinato plane, shorter Fe_N bond distances relative to high spin forms can also be anticipated. The iron(III) ion in $[Fe(III)TPP(Im)_2]Cl$[37] is displaced 0.009Å from the plane of the porphrinato nitrogens. The average Fe_N distance is 1.989Å and 1.991Å.

The spin admixed spin state ($S = {}^3/_2, {}^5/_2$) is found in a series of meso tetraphenyl porphrinato iron(III) complexes of general formula Fe(TPP)X; [X = ClO_4, BF_4, PF_6, SbF_6 and CF_3SO_3]. In $Fe(III)(TPP)ClO_4$[28], the perchlorate ligand is monodentate with an unusually short distance 2.029(4)Å with the iron(III) atom is displaced by an intermediate amount 0.34 Å from the porphyrin plane.

1.3.2 Iron(II)

In high spin iron(II) haems, the iron atoms are located out of plane of the nitrogen atoms. The x-ray structure of 2-methylimidazole Fe(II)(TPP)[38] shows five coordination (square pyramidal), as expected. The iron(II) ion is displaced 0.42Å from the plane of four nitrogen atoms and 0.55Å from the mean porphinato plane. The axial $Fe\text{-}N_{Im}$ bond distance is 2.161(5)Å and the average Fe_N distance is 2.086(4)Å.

Low spin iron(II) ($S = 0$) porphyrin complexes have the iron centred in the porphyrinato plane with much shortened Fe_N bonds. An example of this is $[Fe(II)TPP(PiP)_2]$[39], the iron(II) ion is exactly centred in the porphyrin ring and the axial $Fe\text{-}N_{PiP}$ bonds average to 2.127(3)Å.

In intermediate spin iron(II) haem ($S = 1$) the iron atom is four coordinate and is also centred between the four complexed nitrogen atoms with the Fe-N bond distance

2.01Å. The length of the $Fe(II)_N$ bonds in the intermediate-spin $Fe(TPP)^{11}$ molecule is 1.972Å.

1.4 Physical Characteristics of Porphyrins

1.4.1 Ultra violet/visible Spectroscopy of Metal Free Porphyrins

In metal free porphyrin there are four absorption bands at the region of 400-700 nm and a very intense Soret band at approximately 400 nm ($\varepsilon > 10^5$ $M^{-1}cm^{-1}$). Satellite bands (α and β) are at longer wavelengths. The band α corresponds to the lowest $\pi - \pi^*$ singlet (Q_0) and the band β to the vibronic envelopes (Q_v) [40]. The relative intensities and energies of the four visible bands (I, II, III, and IV) with their own vibronic envelopes are sensitive to the particular type of *meso* substituent. This has led to several ways of classifying porphyrin spectra. The colour of the porphyrin arises from the π- electron system[2].

1. Etio type

   All naturally occurring porphyrins with band intensity diminishing as IV>III>II>I. (Figure 1.16)[2].

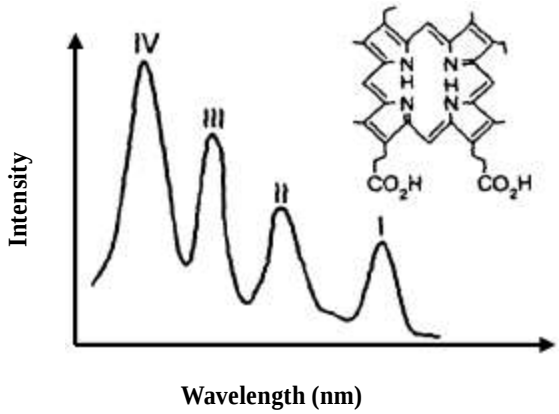

Figure 1.16 Q band porphyrin spectrum of etio type.

2. Rhodo type

These are found among the porphyrins derived from the haem prosthetic groups of the natural haem proteins. Chlorocruorins show this type of spectrum[40]. For this type, band III becomes more intense than IV.

III>IV>II>I (Figure 1.17)[2].

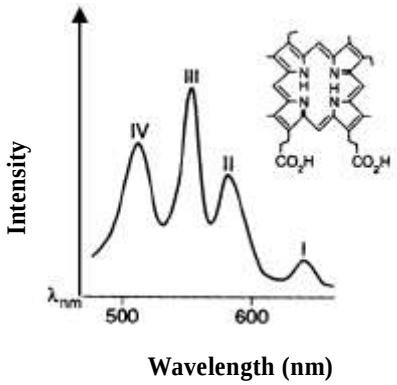

Figure 1.17 Q band porphyrin spectrum of rhodo type.

3. Oxorhodo type

This type of spectrum is found in porphyrins, which possess two rhodofying or 'reddening' groups on diagonally opposite pyrrole rings. Examples include porphyrin a[41]. Band IV becomes less intense than bands III and II. The order is III>II>IV>I (Figure 1.18)[2].

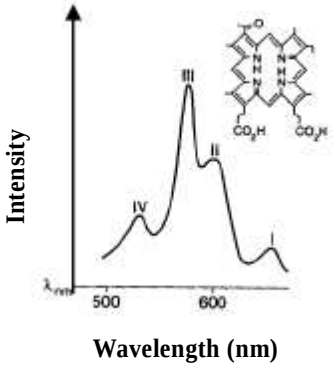

Figure 1.18 Q band porphyrin spectrum of oxorhodo type.

4. Phyllo type

   Many *meso*alklyoxyporphyrins is this type[42]. The band intensity diminishes as IV>II>III>I (Fig. 1.19)[2].

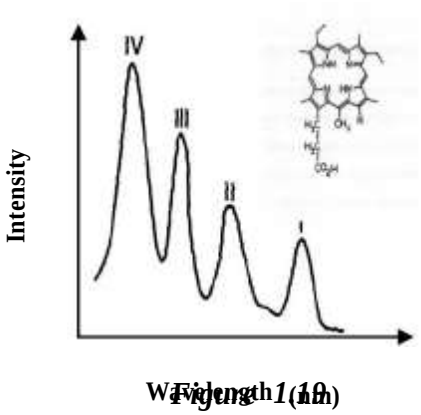

Figure 1.19 Q band porphyrin spectrum of phyllo type.

1.4.2 Ultra violet/visible Spectroscopy of Metalloporphyrins

On comparison of the spectra of the metalloporphyrin with that of the metal free porphyrin, the visible absorption spectrum is observed to change from a two banded (D_{4h} – type) to a four banded (D_{2h} – type). The reason for this is due to the breaking of the D_{4h} symmetry of the porphyrin ring by the central proton axis. These transitions are all doubly degenerate since they are polarised in the plane of the porphyrin[2].

There are three types of absorption spectra for metalloporphyrins.

1. The 'normal' type

   All closed shell metal ions (d^0 or d^{10}) show this type of spectrum. Additional to this, the lanthanoid ions (f^n), VO^{2+} and MoO^{2+} have this type of spectrum. The *d* orbital electrons are deeply buried to disturb the spectrum. Increasing atomic numbers of the metal within a given coordination type and set of axial

ligands results in a small shift to longer wavelength (bathochromic). Examples of the normal type spectrum include [Zn(II)OEP] and [Zn(II)TPP]. The Soret band in this case varies accordingly within a smaller wavelength range[44, 45].

2. The 'hypso' spectrum

   $d^6 - d^9$ metal ions show this type of spectrum. These ions all have been filled d_{xy}, d_{xz} and d_{yz} orbitals. The d_{xz} and d_{yz} orbitals are of correct symmetry to overlap with the empty porphyrin π^* - orbitals. The overlap results in back bonding from the metal to the porphyrin: the π^* energy becomes higher in energy, whereas the d_π energy levels are lowered. As the effect of back bonding on the filled π energy levels are much less, the π-π^* transitions undergo hypsochromic shifts with respect to the normal metalloporphyrins i.e. the bands are shifted to shorter wavelengths. This shift increases with increasing atomic number, for example, in the series:

   Ni(II) < Pd(II) < Pt(II)[45-47].

3. The 'hyper' spectrum

   Hyper type spectrum has the configuration of $d^1 - d^5$. Most of the metal ions in this class (Cr, Mn, Mo, Fe, V) form metalloporphyrin complexes with the metal ion in lower oxidation states which show normal or hypso type spectra. Iron(III) porphyrin gives a 'hyper' type spectrum but iron(II) porphyrin gives 'hypso' type spectrum. A hyper type spectrum consists of the Soret, α and β bands as in the normal type but with additionally one or more bands. This class of spectrum is caused by mixing of charge transfers within the porphyrin

π-π^* transitions. The charge transfer can occur from the axial ligand to the metal, from porphyrin to metal and from metal to porphyrin[48].

1.4.3 Infrared Spectroscopy of Porphyrins

This technique was used for initial characterisation of axial ligands in iron porphyrin complexes and silicon phthalocyanine in this thesis. One important conclusion found in previous studies has been the strong Fe-O-Fe anti symmetric stretch in the 800 – 900 cm^{-1} for a number of μ-oxo-Fe(III) dinuclear compounds[50]. Coordinated iron(II) and iron(III) porphyrins provide a sensitive probe for electronic effects transmitted through the haems; these give different frequencies according to the substituent groups at the periphery of porphyrins.

1.4.4 Mössbauer Spectroscopy of Iron-porphyrins

The Mössbauer spectroscopic technique is used in determining the oxidation and spin state of the iron atom in biological systems. There have been many interesting biological applications of this technique in the last 50 years. Recent advancements in high-pressure work have led to further studies on many samples. A large number of high spin and low spin iron(III) porphyrin complexes have been studied[51]. Intermediate spin state iron(III) porphyrin complexes have also been reported (Table 1.4). Extensive studies of low spin iron(III) porphyrin complexes are presented in Chapter 5 of this thesis.

Table 1.4 Summary of pertinent data on iron(III) porphyrin complexes that have been studied using Mössbauer spectroscopy.

Compounds	Spin state	Temp. (K)	Isomer shift (mms^{-1})	Quadrupole splitting (mms^{-1})	Ref.
Fe(TPP)Cl	$^5/_2$	4.2	0.41	0.46	52
Fe(TPP)Br	$^5/_2$	4.2	0.45	0.72	24
Fe(TPP)I	$^5/_2$	4.2	0.45	0.75	24
Fe(TPP)NCS	$^5/_2$	4.2	0.39	0.49	24
Fe(PMXPP)Cl	$^5/_2$	4.2	0.37	1.03	53
Fe(PMXPP)NCS	$^5/_2$	4.2	0.42	0.63	53
Fe(PMXPP)N_3	$^5/_2$	4.2	0.44	0.67	53
Fe(PMXPP)O_2CMe	$^5/_2$	4.2	0.46	0.92	53
Fe(PMXPP)O_2CCF_3	$^5/_2$	4.2	0.38	1.10	53
Fe(PMXPP)I	$^5/_2$	4.2	0.49	1.33	53
[Fe(TPP)]$_2$O	$^5/_2$	298	0.28	0.62	25
		77	0.40	0.66	25
		4.2	0.41	0.67	25
[Fe(NAPP)]$_2$O	$^5/_2$	298	0.33	0.70	54
		78	0.45	0.73	54
[Fe(OEP)]BF_4	$^3/_2$	4.2	0.38	3.43	54
		115	0.36	3.45	54
		295	0.29	3.17	54
[Fe(OEP)]ClO_4	$^3/_2$	4.2	0.37	3.57	26
		115	0.37	3.52	26
		295	0.29	3.16	26
[Fe(OEP)$(EtOH)_2$]ClO_4	$^3/_2$	4.2	0.38	3.47	26
		115	0.36	3.32	26
		295	0.28	2.97	26
Fe(TPP)$(Py)_2$Cl	$^1/_2$	77	0.16	1.25	29
Fe(TPP)$(Im)_2$Cl	$^1/_2$	77	0.23	2.23	53
		298	0.13	2.11	53
Fe(PMXPP)$(Im)_2$Cl	$^1/_2$	298	0.17	2.06	53
Fe(PMXPP)$(Im)_2$Br	$^1/_2$	298	0.16	2.05	53

1.5 Phthalocyanines

The discovery of phthalocyanine chemistry began serendipitously. Brawn and Tcherniac[55] heated an alcoholic solution of *o*-cyanobenzamide in order to study some of its properties. Phthalocyanine was formed upon cooling the solution. Since their discovery, phthalocyanines have become one of the most important dyestuffs in use. This process is well studied[56], lack of toxicity, ability to resist heat[57], acids and bases[58-61] and light[61] which have all been exploited in the use of these dyes. In the early 1930's, Linstead *et al*[58] synthesised many phthalocyanines and reported that a phthalocyanine contained a ring system of isoindoline units linked by aza nitrogen atoms (Figure 1.20).

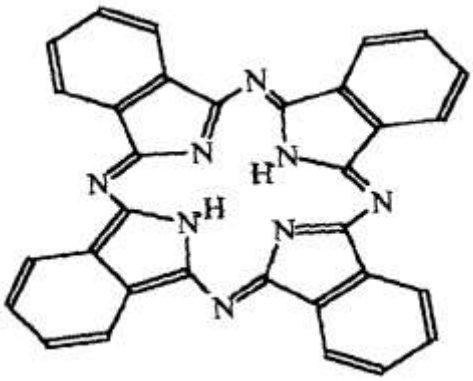

Figure 1.20 Metal free phthalocyanine[58].

Phthalocyanines are therefore related to naturally occuring porphyrins; in latter methine carbons link the 4 pyrrole units. In 1933, Linstead *et al*[58] used for the first time the term "phthalocyanine" which comes from the Greek naphtha (rock oil) and cyanide (dark blue). Robertson *et al*[58] elucidated the structure of phthalocyanine and metallophthalocyanine using single crystal x-ray diffraction analysis. Since then, many studies have been done on photoconductivity, semi conductivity, photochemical reactivity, photosynthetic activity, fluorescence and luminescence. Many bioinorganic

interests have centred on these compounds because metallophthalocyanines have structural similarities to the naturally occurring metalloporphyrins. Studies on electroaluminescence (EL) and photoluminescence in porphyrin derived compounds showed interesting electrical and optical properties[59].

1.5.1 Metallophthalocyanines

The two central hydrogen atoms of metal free phthalocyanine can be replaced by a wide range of metals and metalloids. Such metallophthalocyanines are usually very insoluble in most commonly used organic solvents. Most metallophthalocyanines are thermally very stable and many will sublime unchanged at a high temperature. For example, copper phthalocyanine has been shown to be stable at *circa* 900°C *in vacuo*[63]. The lanthanide and actinide metals form stable sandwich complexes with two phthalocyanine rings (Figure 1.21).

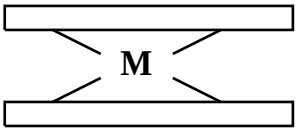

Figure 1.21 Metal sandwiched with two phthalocyanine ring [$M(Pc)_2$].

Phthalocyanines are planar π-conjugated molecules whose electronic characteristics can be modified by peripheral substitution either by electron donating or withdrawing groups.

1.5.2 General Synthesis

Metallopthalocyanines can be prepared by various methods (Figure 1.22).

For example *1,2 di-cyanobenzene* reacts with iron wire at 250°C to yield iron(III) phthalocyanine [Fe(III)Pc], which is readily purified by sublimation[64-66]. The most general methods are given in the following equations where M = metal and Pc = phthalocyanine dianion:

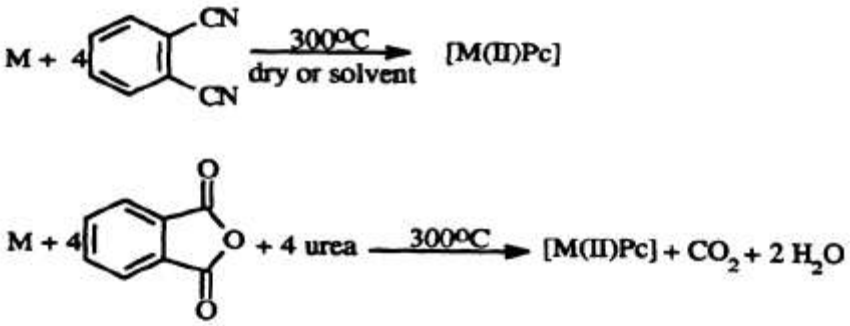

Figure 1.22 Two different synthetic methods for $[M(Pc)_2]$[77].

1.5.3 Polymorphic Variations of Phthalocyanines

The phthalocyanines often exist in two or more polymorphic variations, which may be distinguished by infrared and x-ray diffraction techniques. Metal free phthalocyanine exists in three polymeric forms (α, β and γ)[67,68]. However most of the phthalocyanines exist in two forms (α and β) (Figure 1.23)[67, 69-76].

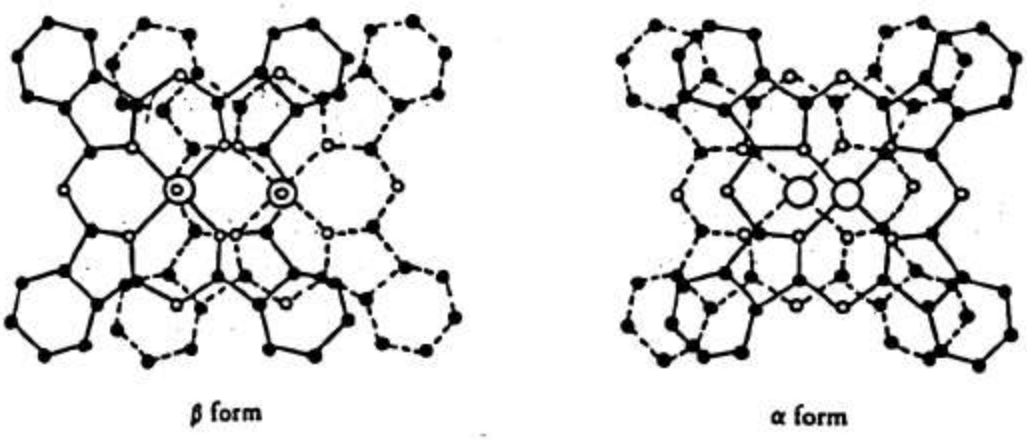

Figure 1.23 Polymorphic forms of metallopthalocyanines (α and β)[77].

1.5.4 Electronic Absorption Spectra

It was reported that as a result of α and β transformation induced by heat sublimation at >300°C, thin films of the α-crystalline forms of H_2Pc and several other metallopthalocyanines, there is a shift to longer wavelengths in the transmission spectra in the 500 – 900 nm region[77].

1.5.5 Infrared (IR) Spectra

Kobayashi *et al*[78]studied the IR and far IR spectra of phthalocyanines and reported all the divalent metallophthalocyanine complexes belongs to the D_{4h} point group and that metal free phthalocyanine belongs to D_{2h} group.

Table 1.5 Absorption frequencies (cm^{-1}) of H_2Pc and metallopthalocyanines in the lower frequency region[78].

D_{2h} symmetry	**D_{4h} symmetry**						
H_2	Fe	Co	Ni	Cu	Zn	Pd	Pt
489	518	519	521	509	512	514	516
498							
552	574	574	578	575	575	578	581
559							
617	642	642	645	640	637	648	645

It is known that the E_u mode of vibration, which if IR active for complexes with D_{4h} symmetry, splits into two other IR active modes, B_{2u} and B_{3u}, with little change in the peak position when, as a result of minor substitution, the symmetry changes to D_{2h}. Such an effect is shown in Table 1.5, for peaks in the lower frequency region.

The characterisation of doublets in the higher frequency region is difficult because of the overlapping of a greater number of peaks. The absorption bands are always shifted in the following order: Ni > Co > Fe > Cu > Zn > H_2.

In the IR far region, there are three metal dependent bands that are observed in each spectrum of metallopthalocyanines[79]. Two of these bands also occur in the metal-free phthalocyanine spectrum. One band is at 324 cm^{-1} and the other appears as a doublet at 259 cm^{-1} and 289 cm^{-1}. The 324 cm^{-1} band is assigned to be out of plane vibrations associated with the isoindoline ring which is closely coordinated to the metal ion. The frequencies of the metal bands shift in the order: H_2 > Cu > Zn > Pd > Fe > Co > Ni >

Pt. The third group of metal bands, which, appears with high intensities in the region 150 – 200 cm^{-1}, are for Fe, Co, Ni and Cu phthalocyanine are assigned to metal ligands vibrations, because these bands are not seen in the spectrum of metal free phthalocyanine[80]. The frequencies of the metal ligand vibrations shift to higher frequency in the order of Zn > Pd > Pt > Cu > Fe > Co > Ni.

1.6 References

1. W. Küster, *Hoppe-Seyler's Z. Physiol. Chem*., **1912**, *82*, 463.
2. L. R. Milgrom, *The Colours of Life*: *An Introduction to the Chemistry of Porphyrins and Related Compounds*, Oxford University Press, Oxford, New York & Tokyo, **1997**.
3. L. Styler, W. Freeman & Co., *Biochemistry*, New York, **1988**, 3rd ed, Chap 17.
4. L. E. Webb and E. B. Fleischer, *J. Am. Chem. Soc*., **1965**, *87*, 667.
5. J. E. Falk, *Porphyrins and Metalloporphyrins*, Elsevier, Amsterdam, **1964**.
6. D. P. E. Dickson and F. J. Berry(eds), *Mössbauer Spectroscopy,* edited by, Cambridge University Press, Cambridge, London, New York, New Rochelle, Melbourne and Sydney, **1986**.
7. G. E. Khalil, E. K. Thompson, M. Gouterman, J. B. Callis, L. R. Dalton, N. J. Turro and S. Jockusch, *Chemical Physics Letters*, **2007**, *435*, 45-49.
8. B. D. Berezin, *Coordination of Compounds of Porphyrins and Phthalocyanines*, John Wiley & Sons, Chichester, New York, Brisbane & Toronto, **1981**.
9. P. Gutlich, E. Bill and A. X. Trautwein, *Mössbauer Spectroscopy and Transition Metal Chemistry,* Springer Heildelberg, London, New York, **2011.**

10. J. P. Collman, J. L. Hoard, N. Kim, G. Lang and C. A. Reed, *J. Am. Chem. Soc*., **1975**, *97*, 2676.

11. D. F. Koeing, *Acta Cryst.*, **1965**, *18*, 663.

12. C. A. Reed, T. Mashiko, W. R. Scheidt, K. Spartalian and G. Lang, *J. Am. Chem. Soc*., **1980**, *102*, 2302.

13. W. R. Scheidt, J. L. Kirner, J. L. Hoard and C. A. Reed, *J. Am. Chem. Soc.*, **1987**, *109*, 1963.

14. W. R. Scheidt, Y. J. Lee, D. K. Geiger, K. Taylor and K. Hatano, *J. Am. Chem. Soc*., **1982**, *104*, 3367.

15. G. S. Girolima, S. N. Milam and K. S. Suslick, *Inorg. Chem*., **1973**, *26*, 930.

16. W. E. Bennett, D. E. Broberg and N. C. Baenziger, *Inorg. Chem*., **1973**, *12*, 930.

17. A. Gierren and W. Hoppe, *Chem. Comm.*, **1971**, 413.

18. A. Takenaka, Y. Sasada, H. Ogoshi, T. Omura and Z-I Yoshida, *Acta Cryst.*, **1975**, *B31*, 1.

19. W. R. Scheidt, *The Porphyrins*, ed. D. Dolphin, Academic Press Inc., New York, **1978**, *3*, 10.

20. T. Higgins, M. K. Safo and W. R. Scheidt, *Inorg. Chim. Acta*, **1990**, *178*, 261.

21. G. S. Srivatsa, D. T. Sawyer, N. J. Boldt and D. F. Bocian, *Inorg. Chem.*, **1985**, *24*, 2123.

22. J. P. Collman, R. R. Gagne, C. A. Reed, C. R. Halbert, G. Lang and W. T. Robinson, *J. Am. Chem. Soc*., **1975**, *97*, 1427.

23. J. P. Collman, J. L. Hoard, N. Kim, G. Lang and C. A. Reed, *J. Am. Chem. Soc*., **1975**, *97*, 2676.

24. H Razavi, E. Mohajerani, N. Safari, H. Shahroosvand and A. Khabbazi, *Journal of Porphyrin and Phthalocyanine*, **2012**, *16*, 396.
25. I. H. Cohen, *J. Am. Chem. Soc.*, **1969**, *91*, 1980.
26. D. H. Dolphin, J. R. Sams and T. B. Tsin, *Inorg. Chem.*, **1971**, *16*, 711.
27. M. E. Kastner, W. R. Scheidt, T. M. Mashiko and C. A. Reed, *J. Am. Chem. Soc.*, **1978**, *100*, 666.
28. C. A. Reed, T. Mashiko, S.P. Bentley, M. E. Kastner, W. E. Scheidt, K. Spartalian and G. Lang, *J. Am. Chem. Soc.*, **1979**, *101*, 2948.
29. L. M. Epstein, D. K. Straub and C. Maricondi, *Inorg. Chem.*, **1967**, *6*, 1720.
30. W. R. Scheidt, D. A. Summerville and I. A. Cohen, *J. Am. Chem. Soc.*, **1976**, *98*, *6*623.
31. J. L. Hoard, G. H. Cohen and M. D. Click, *J. Am. Chem. Soc.*, **1967**, 1992.
32. K. Anzai, K. Hatano, Y. J. Lee and W. R. Scheidt, *Inorg. Chem.*, **1981**, *20*, 2337.
33. B. W. Sketton, and H. A. White, *Aust. J. Chem.*, **1977**, *30*, 2655.
34. K. Hatano and W. R. Scheidt, *Inorg. Chem.*,**1979**, *18*, 877
35. A. B. Hoffman, D. M. Collins, V. W. Day, E. B. Fleisher, T. S. Srivastana and J. L. Hoard, *J. Am. Chem. Soc.*, **1972**, *94*, 3620.
36. W. R. Scheidt, I. A. Cohen and M. E. Kastner, BioChem, **1979**, *18*, 3549.
37. D. M. Collins, R. Countryman and J. L. Hoard, *J. Am. Chem. Soc.*, **1972**, *94*, 2066.
38. N. Kim, J. P. Collman, J. L. Hoard, *J. Am. Chem. Soc.*, **1975**, *94*, 2073.
39. A. D. Adler, L. Sklari, F. R. Longo, J. D. Finarelli and G. Finarelli, *J. Heteronucl. Chem.*, **1968**, *5*, 669.

40. J. R. Platt. *Radiation Biology*, ed. A. Hollaender, McGraw Hill, New York, **1956**, *Vol.3*, Chapter 6.

41. M. Sono and T. Asakura, *BioChemistry*, **1974**, *13*, 4386.

42. P. S. Clezy and C. J. R. Fookes, *Aust. J. Chem.*, **1974**, *27*, 371.

43. H. Fischer and R. Bäuminger *Ann. Chem.*, **1929**, *468*, 58.

44. R. S. Becher and J. B. Allison, *J. Phys Chem.*, **1963**, *67*, 2669.

45. G. Dorough, J. Miller & F. Huennekens, *J. Am. Chem. Soc.*, **1951**, *73*, 4315.

46. J. W. Buchler and L. Puppe, *Justus Liebegs Ann. Chem*., **1974**, 1074.

47. D. W. Thomas and A. E. Martell, *Arch. Biochem. Biophy*, **1958**, *76*, 286.

48. R. S. Becker and J. B. Allison, *J. Phys. Chem*., **1963**, *67*, 2662.

49. J. O.Alben, *The Porphyrins*, ed by D. Dolphin, Acad. Press, New York, San Francisco, London, **1978**, *Vol. III*, Chapter 7, 323.

50. J. W. Butcher, *The Porphyrins*, edited by D. Dolphin, Academic Press, New York, **1978**, *Vol. I*, Chapter 10, 416.

51. P. J. Marsh, J. Silver, M. C. R. Symmons and F. A. Taiwo, *J. Am Soc., Dalton Trans*., **1996**, 2361.

52. T. H. Moss, A. J. Bearden and W. S. Caughey, *J. Chem., Phys*., **1969**, *51*, 2624.

53. M. A. Torréns, D. K. Straub and L. M. Epstein, *J. Am. Chem. Soc.*, **1972**, *94*, 4160.

54. J. R. Sams and T. B. Tsin, *The Porphyrins*, ed. D. Dolphin, Acad. Press, New York, **1978**, *Vol. IV*, Chapter 9.

55. K. Kasuga and M. Tsutsui, *Coord. Chem. Rev*., **1980**, *32*, 67.

56. Y. Kishi, *Pure Appl. Chem*., **1989**, *61*, 313.

57. D. M. P. Mingos and D. R. Baghurst, *Chem. Soc. Rev*., **1991**, *20*, 1.

58. P. Debye, *Polar Molecules*, Chemical Catalog, New York, **1929**.

59. H. Frolich, *Theory of Dielectrics*, 2nd edition, Oxford University Press, London, **1958**.

60. V. Daniel, *Dielectric Relaxation*, Academic Press, New York, **1967**.

61. J. B. Hasted, *Aqueous Dielectrics*, Chapman and Hall, London **1973**.

62. W. R. Tinga, *MRS Symp. Proceed*, **1986**, *60*, 105.

63. R. R. Bowman, *IEEE Trans. Microwave Theory Techn*., **1976**, *MTT-24*, 43.

64. E. A. Lawton, *J. Phys. Chem*., **1958**, *62*, 384.

65. G. T. Byre, R. P. Linstead and A. R. Lowe, *J. Chem. Soc*., **1934**, 1071.

66. P.A. Barrett, D. A. Frye and R. P. Linstead, *J. Chem. Soc*., **1938**, 1157.

67. P.A. Barrett, C. E. Dent and R. P. Linstead, *J. Chem. Soc*., **1936**, 1719.

68. *FIAT Rev. Ger. Sci*., **1972**, *Vol. 3*, 446.

69. M. Shigemitsu, *Bull. Chem. Soc. Japan*, **1959**, *32*, 607.

70. N. A. Ebert and H. O. Gottlieb, *J. Am. Chem. Soc.*, **1952**, *74*, 2806.

71. C. Hammann and I. Storbeck, *Naturswissenschaften*, **1963**, *50*, 327.

72. D. J. E. Ingram and J. E. Bennett, *Discussions Faraday Soc*., **1955**, *19*, 140.

73. F. W. Karasek and J. C. Decius, *J. Am. Chem. Soc.*, **1952**, *74*, 4716.

74. D. N. Kendall, *Anal. Chem*., **1953**, *25*, 382.

75. W. J. Kroenke and M. E. Kenny, *Inorg. Chem*., **1964,** *3*, 696.

76. E. Suito and N. Ueda, *Proc. Japan Acad*., **1956**, *32*, 182.

77. B. Stymne, F. Sauvage & G. Wettermark, *Spectrochim. Acta*, **1979**, *35A*, 1195.

78. A.E Lucia and F. D. Venderame, *J. Chem. Phys*., **1968**, *48*, 2674.

79. T. Kobayashi, F. Kurokawa, N. Uyeda and E. Saito, *Spectrochim. Acta*, **1970**, *26A*, 1305.

80. T. Kobayashi, *Spectrochim. Acta*, **1970**, *26A*, 1313.

Chapter 2: Experimental Spectroscopic Methods and Techniques

This chapter is concerned with the theory and applications of two important experimental spectroscopic techniques used to analyse compounds in this thesis: ambient pressure Mössbauer spectroscopy and high-pressure Mössbauer spectroscopy.

Section one: Ambient Pressure Mössbauer Spectroscopy

2.1 Mössbauer spectroscopy

2.1.1 Discovery and Definition

The Mössbauer effect is described as the recoilless emission from one nucleus and resonant absorption of the γ-ray by a second nucleus without thermal broadening. The temperature dependence of the absorption cross section of ^{191}Ir led Rudolf L. Mössbauer to be the first to discover this phenomenon[1]. The experiment was carried out during his graduate studies at Heidelberg in 1958[2], and he received a Nobel Prize for it in 1961[3]. Kirstner and Sunyar obtained the first indications of hyperfine interactions in a chemical compound in 1960[4]. From these beginnings the Mössbauer effect transitions has been observed in over one hundred isotopes[5] of the elements in the Periodic Table including importantly ^{57}Fe.

As the iron atom absorbs γ-rays of a more accessible energy, than the natural energy of the iron atom itself this rapidly established the importance of the technique for the element as it eliminated the necessity to work only at liquid helium temperatures, which is an absolute requirement for many elements. Using this technique vital information can be obtained about the electronic and magnetic properties of this element.

As iron is so important in living organisms as well as having significant chemical, physical and industrial applications, ^{57}Fe Mössbauer spectroscopy has become a very important tool for a wide range of scientists.

2.1.2 Resonant Fluorescence and Absorption

Nuclear resonant absorption and fluorescence occurs due to the emission of γ-rays when a radioactive nucleus in an excited state decays[6]. Initial attempts to detect this effect were not successful, although it was recognised that the nuclear recoil and Doppler broadening effects were responsible for the failure. Continuing attempts by Kuhn in 1929 to observe nuclear resonant absorption were successful.

All nuclei possess excited states, some of which are accessible from the ground state by photon absorption. Often the excited states of the absorber are long lived and the range of photon energies that will excite the absorption is extremely narrow. If strong absorption is to be observed, a significant fraction of the energy of the source radiation must be within this range. If the nucleus is free, i.e. gas, the recoil momentum and energy are taken by the nucleus itself. In a solid the momentum and energy go into lattice vibrations, i.e. phonons.

2.1.3 Theory of Emission and Absorption of γ-rays by nuclei

In a free atom, resonant absorption occurs when the energy of the γ-ray is equal to the energy difference between the ground and excited state. Emission of γ-rays by decay from an excited nuclear state should be a good source of monochromatic energy. The following illustration (see Figure 2.1) and equations (2.1 - 2.4) refer to one dimension for simplicity, the direction in which the γ-ray is emitted.

If a photon is emitted from a nucleus of mass M moving with an initial velocity V_x in the chosen direction x at the moment of emission, then the total energy above the ground state nucleus at rest is :

$$\textbf{Total Energy} = (E + \tfrac{1}{2}MV_{x2}) \qquad \textit{Equation (2.1)}$$

E is the energy of a nucleus.

Figure 2.1 The energy and momentum are conserved in the γ emission process.

After emission the γ-ray will have an energy E_γ and the nucleus recoils resulting in a nucleus having a new velocity $(V_x + v)$. V_x and v can be in opposite directions. By conservation of energy, the total energy of the new system is:

$$E + \tfrac{1}{2}MV_{x2} = E_\gamma + \tfrac{1}{2}M(V_x + v)^2 \qquad \textit{Equation (2.2)}$$

The difference between the energy of the nuclear transition (E) and the energy of the emitted γ-ray photon (E_γ) is:

$$\delta E = E - E_\gamma = \tfrac{1}{2}M v^2 + MV_x v \qquad \textit{Equation (2.3)}$$

$$\delta E = E_R + E_D \qquad \textit{Equation (2.4)}$$

Thus the γ-ray energy is clearly different from the nuclear energy level separation, δE. This is because it depends on the recoil kinetic energy ($E_R=½Mv^2$) which is independent of the velocity (V_x) and Doppler effect energy ($E_D= MV_xv$) which is proportional to the atom velocity (v).

In the emission process, momentum is conserved so that the momentum of the γ-ray is E_γ/c where c is constant value for the velocity of light, therefore:

$$\mathbf{MV = M(V + v) + E_\gamma/c} \qquad \textit{Equation (2.5)}$$

From equation 2.5, the recoil momentum is $Mv = - E_\gamma/c$. Therefore, the recoil kinetic energy is:

$$\mathbf{E_R= E_\gamma{}^2/2Mc^2} \qquad \textit{Equation (2.6)}$$

Recoil kinetic energy (E_R) is dependent on the mass of the nucleus and the energy of the γ-ray photon. However, the Doppler energy (E_D) is dependent on the thermal velocity of the nucleus and therefore E_D has a distribution of values, and is temperature dependent.

Equation (2.7) shows the mean kinetic energy per translational degree of freedom ($\bar{E}_k$), where k is the Boltzmann constant and T is the absolute temperature.

$$\bar{E}_k \approx ½kT \qquad \textit{Equation (2.7)}$$

$$\bar{E}_D = 2\sqrt{(\bar{E}_k E_R)} = E_\gamma\sqrt{(2\bar{E}_k/Mc^2)} \qquad \textit{Equation (2.8)}$$

Fundamental radiation theory shows that the proportion of absorbed radiation can be determined by the overlap between the exciting and excited energy distributions. Following equation (2.8), the statistical distribution in energy of the emitted γ-rays is displaced from the true excited state energy (E) by $-E_R$ and broadened by E_D into a Gaussian distribution of width $2\bar{E}_D$. The distribution for absorption has the same shape but is displaced by $+E_R$. This is illustrated schematically in Figure 2.2.

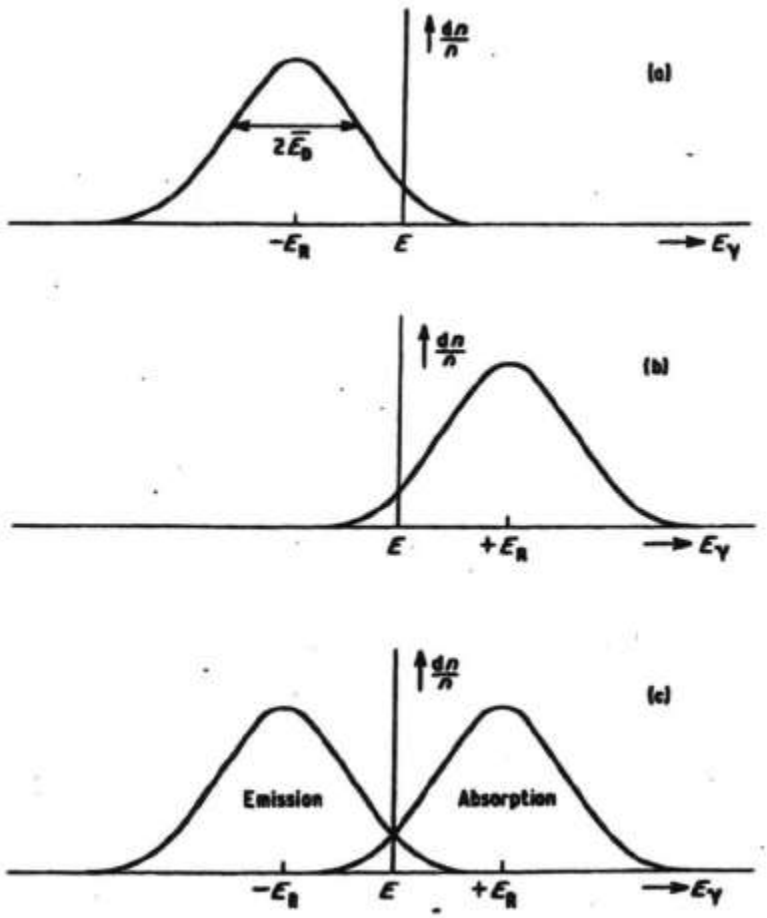

Figure 2.2 The statistical distribution in the γ-ray energy for (a) emission, (b) absorption and (c) the resonant overlap for successive emission and absorption[4].

Nuclear resonant absorption will only be observed if the γ-ray emission overlaps the absorption line. The fraction of energy lost to the recoiling atom is small and therefore insignificant.

2.1.4 The Mössbauer Effect

The Mössbauer effect is the recoilless emission of γ-ray from a solid radioactive material. Since the γ-ray emission is recoilless, it can be resonantly absorbed by atoms, i.e. also in a solid. The nuclear transitions are very sensitive to the local environment of the atom and Mössbauer spectroscopy is a sensitive probe of the different environments an atom occupies in a solid material[7].

Mössbauer eliminated the energy due to the recoil by placing the excited nucleus into a solid state matrix thus fixing it within the lattice. In this situation the recoil energy may be less than the lowest quantised lattice vibrational energy and consequently the γ-ray may be emitted without the loss of energy due to the recoil of the nucleus. The absorber nucleus is held in a solid matrix and the random thermal motion is avoided, hence both energy profiles will overlap (Figure 2.2). In an absorber, atoms are free to vibrate and recoil energy can be transferred to the lattice vibrations, providing the correct quantum of energy. Therefore only a fraction of recoilless, ***f*** events occur. This is given by:

$$f = \exp\left[\frac{-4\pi^2\langle x^2\rangle}{\lambda^2}\right] = \exp\left[\frac{-E_\gamma^2\langle x^2\rangle}{(\hbar c)^2}\right] \qquad \textit{Equation (2.9)}$$

where λ is the wavelength of the γ photon and $\langle x^2 \rangle$ is the mean square vibrational amplitude of the nucleus. Equation 2.9 also shows that ***f*** increases exponentially with decrease in $\langle x^2 \rangle$, which in turn depends on the strength of binding and on the

temperature. The displacement of the nucleus must be small compared to the wavelength λ of the γ-ray. This is why the Mössbauer effect is not detectable in gases and non-viscous liquids. Clearly, ***f*** will be largest for low energy γ absorption at low temperatures in a strong lattice, and thus these are the best conditions under which to measure Mössbauer spectra.

The probability of such recoilless events depends upon the energy of the nuclear γ-ray, hence the Mössbauer effect is restricted to certain isotopes, with low lying excited states (Table 2.1).

Table 2.1 Most common Mössbauer nuclei with nuclear data[8].

Isotope	***E_γ(KeV)**	**I_g**	**I_e**	**N(%)**	**Sign of ΔR/R**
^{57}Fe	14.4	$^1/_2$	$^3/_2$	2.17	negative
^{151}Eu	21.6	$^5/_2$	$^7/_2$	47.80	positive
^{119}Sn	23.9	$^1/_2$	$^3/_2$	8.58	positive
^{121}Sb	37.15	$^5/_2$	$^7/_2$	57.23	negative

*E_γ = energy of γ-ray transition; I_g = nuclear spin quantum number of the ground state

I_e = nuclear spin quantum number of the excited state; N = natural abundance of isotope; ΔR/R = ratio of the radius of nucleus; R = mean value of the nuclear radius.

2.1.5 Mössbauer Spectroscopy

Mössbauer spectroscopy is a technique, which enables the energy levels of nuclei to be investigated by measuring the energy dependence of the resonant absorption of a γ-ray by a nucleus. ^{57}Fe has a series of physical characteristics that qualifies as an approachable isotope[9]. It has great resolution to detect hyperfine interactions between

the probe nucleus and surrounding electrons, which means it, can be used to measure local electronic properties related to magnetism, crystal structure and chemical bonding.

The usual experimental arrangement for Mössbauer spectroscopy involves a radioactive source containing an isotope in an excited state and an absorber consisting of the material to be investigated which contains the same isotope in its ground state. The correct energy is achieved by using a parent isotope, which decays to the excited state of the nuclei being studied. ^{57}Co, which can be alloyed with iron or palladium, is typically the source of ^{57}Fe for laboratory studies. It decays to ^{57}Fe with a half-life of ≈ 200 days. After ≈10^{-7}s, ^{57}Fe decays from the $I = 5/2$ state to the $I = 3/2$ state, emitting a γ-ray with energy of 123keV[10]. The transition of interest is that between the first excited state and the ground state, that is from $I = 3/2$ state to $I = 1/2$, emitting a 14.4 keV γ-ray with a half-life of 1.4 x 10^{-7}seconds. This decay is shown schematically in Figure 2.3.

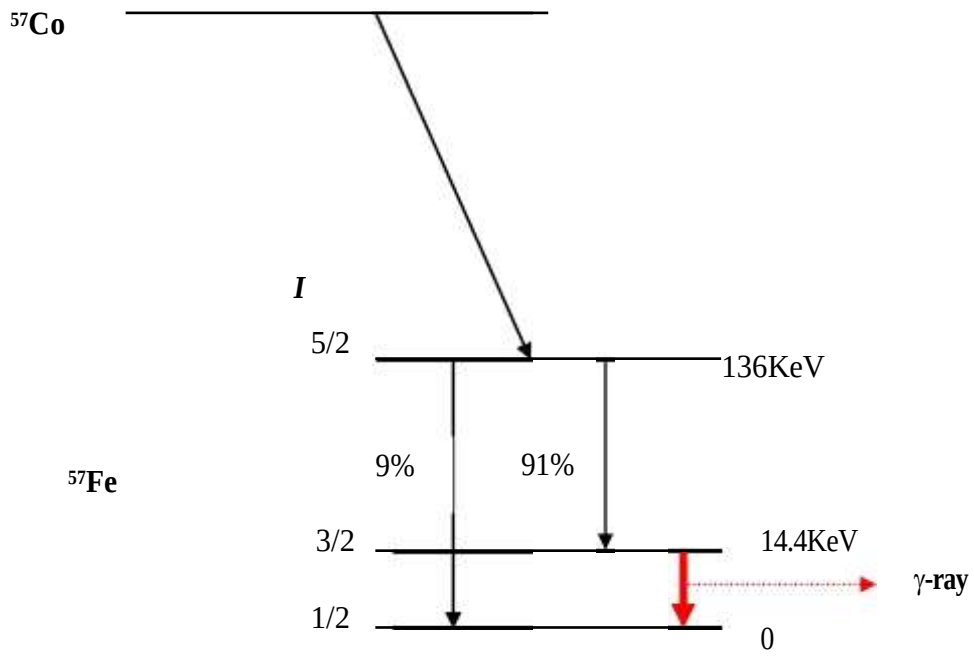

Figure 2.3 The decay of ^{57}Co to ^{57}Fe.

A stable ^{57}Fe nucleus will absorb this γ-ray photon if it is in the same environment as the nucleus in the source. If this is not the case the γ-ray energy must be modulated so that some photons of the correct energy are produced and the resonance condition can be met. This is accomplished by the addition of a Doppler velocity to the source. The required source material is embedded in a matrix such that the energy of emission comes as close as possible to the Heisenberg linewidth for the emitter.

2.1.6 The Doppler Effect

The Doppler effect is the phenomenon in which sound or electromagnetic frequencies are altered by motion of the emitter relative to the observer. Doppler worked out this theory in 1842[11].

If a photon source has an energy (E_γ) and velocity (v_o) moving towards the observer, there will be a change in energy (ΔE_s) and c is the speed of wave. This is given by:

$$\Delta E_s = (v_o/c)\, E_\gamma \qquad \textit{Equation (2.10)}$$

If the source is moving at an angle θ from the line subtended by source and observer then:

$$\Delta E_s = (v_o/c)\, E\gamma . \cos\theta \qquad \textit{Equation (2.11)}$$

In the Mössbauer experiment, the source of γ-ray is mounted on an oscillator and vibrating the source produces the desired range of photon energies. The changes in energy produced by moderate velocities are very small in comparison to E_γ.

2.1.7 Instrumentation

Once the theoretical considerations for the recording of the Mössbauer effect have been considered, then suitable apparatus is required to record a spectrum. The apparatus used is shown diagrammatically in Figure 2.4. A radioactive source is mounted onto a drive system, which contain the transducer and the waveform generator that controls the energy of the emitting γ-rays through the addition of a Doppler effect.

The source may be moved relative to the sample and the counter. The latter will monitor the intensity of the beam after it has passed through the sample. The experimental set-up is very simple, but samples are limited to solids and frozen solutions.

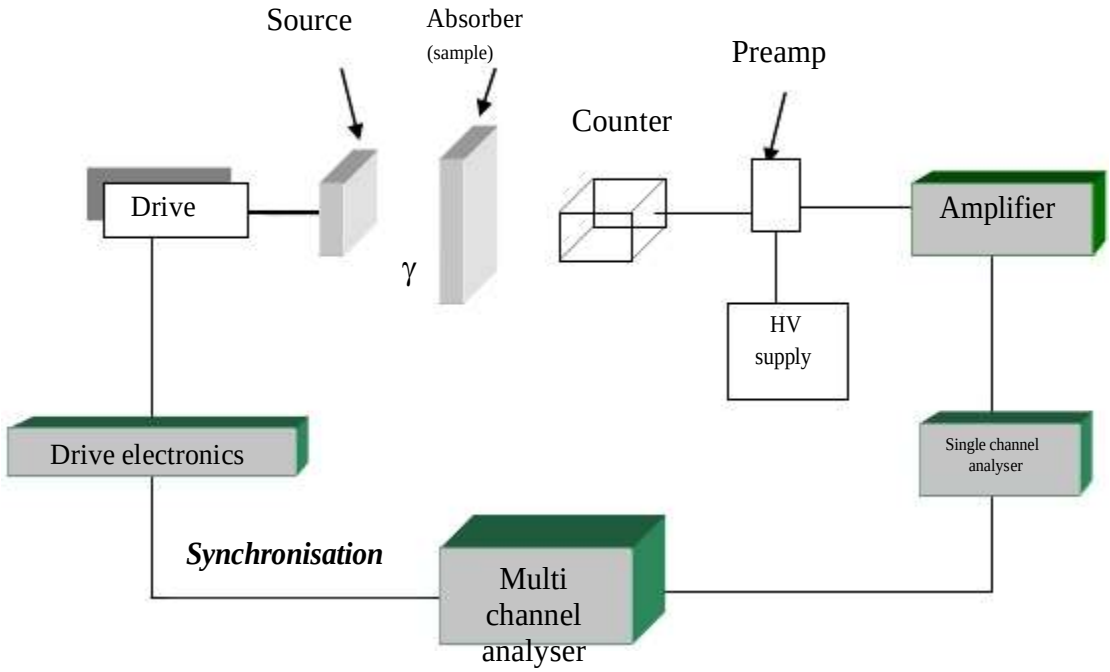

Figure 2.4 Schematic of an experimental set-up for transmission Mössbauer spectroscopy.

The type of detector used is dependent on the energy of the transition being studied. ^{57}Fe Mössbauer spectrometers usually utilise either gas (either argon or krypton) filled proportional counters or scintillation counters. The signal from the detector is then amplified and converted into a Mössbauer spectrum by the single channel analyser (SCA). The signals accepted by the SCA are added to the current of the multichannel analyser (MCA). To increase the recoil-free fraction, ***f*** of the absorber, the sample is often cooled in a cryostat whilst in the γ beam.

2.1.8 The Mössbauer Spectrum

A Mössbauer spectrum is plotted as a function of source velocity (Figure 2.5). The peaks correspond to source velocities at which maximum γ-ray absorption by the sample occurs. Positive relative velocities correspond to moving the source towards the sample and negative velocities correspond to moving the source away from the sample.

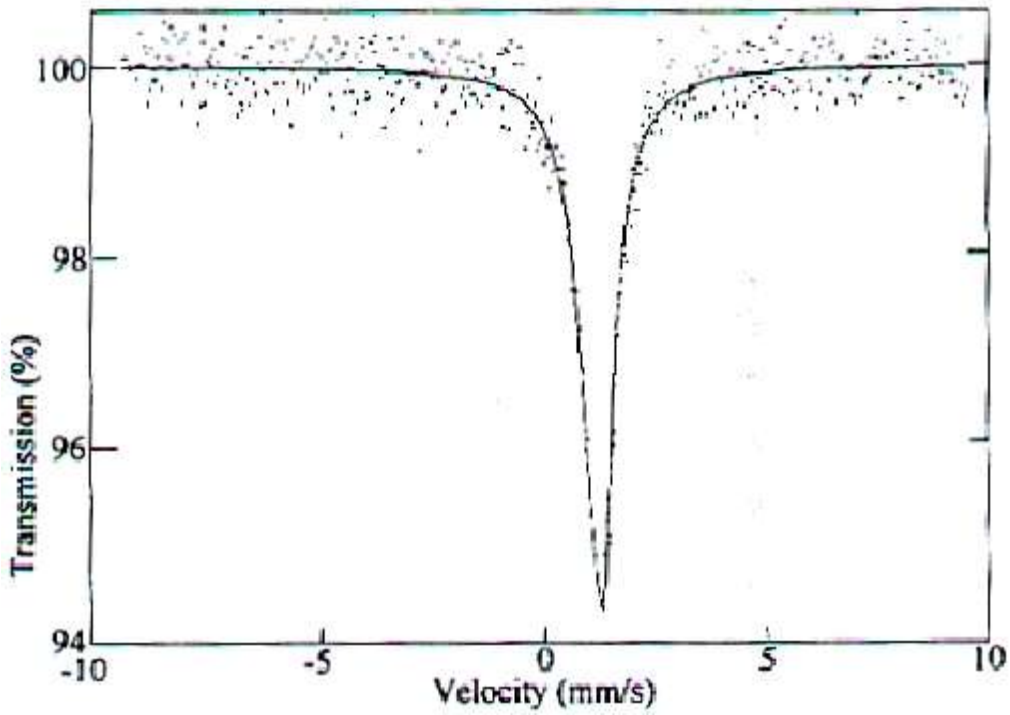

Figure 2.5 A typical Mössbauer transmission spectrum.

A typical sample will have about 1mg/cm^2 of iron in the γ-ray beam. If ^{57}Fe is present in its natural 2% abundance, there will be 2 x 10^{17} ^{57}Fe nuclei/cm^2. The peak resonant cross section is approximately 2 x 10^{-18}cm^2. The spectrometer will typically divide the velocity scale into 256 channels. For a 20 mCi source the total counting rate is usually about 20,000 counts of which about 85% will be 14.4 keV radiations. The spectrometer duty cycle is about 60% and r, the 14.4 keV counting rate per channel, is typically 44 counts/sec/channel. The signal-to-noise ratio, S/N, is given by:

$$S/N = a_p[rT]^{1/2} \qquad \textit{Equation(2.12)}$$

where a_p is the peak absorption intensity and T is the running time. For a given S/N, the run time is inversely proportional to the square of the peak absorption. The

Mössbauer spectrum provides information on the interactions between the nucleus and the magnetic field, which surrounds it.

2.1.9 Mössbauer Effect Hyperfine Parameters

A Mössbauer spectrum reflects the hyperfine interactions of the sample. Several parameters can be extracted from the spectrum. These parameters can be used to identify the chemical and magnetic phases present in the sample like a fingerprint. The chemical environment influences the energies of the nuclear states. It is possible to detect these extremely small changes because the energy of the nuclear state is so well defined, the difference between the hyperfine interaction of the isotopes in the source and the sample can be studied in detail. In ^{57}Fe, the energy uncertainty (natural line width), is $5x10^{-9}$ eV compared to the energy of $14.4x10^{3}$ eV of the radiated photon[12]. This is smaller than the characteristic values for the magnetic dipole, electric monopole (isomer shift) and electric quadrupole interactions (quadrupole splitting) of nuclei with their surrounding electrons. These interactions are collectively known as hyperfine interactions.

2.1.9.1 Isomer Shift (δ)

The sample (absorber) will usually have slightly different resonant absorption energy if the atoms of the absorber are in a different coordination to those of the source. This can be understood quantitatively by noting that the wave functions of *s* electrons are non-zero at the position of the nucleus, so they may interact with the nucleus and alter the nuclear energy levels. In addition the more *d* electrons that are present, the more the nucleus is shielded from *s* electrons. This forces the *s* cloud to expand, reducing

the density at the nucleus. So, increasing *d* electron density can alter the δ absorption energy. This effect is known as isomer shift (or chemical shift).

To measure δ, the nucleus is assumed to be an uniformly charged sphere where the electronic charge density at the nucleus ($\Psi^2(0)$) is assumed to be uniform over the nuclear dimensions, and caused only by *s* electrons.

The basic γ-ray transition between the nuclear excited state and the ground state is considered. Its total energy (ΔE) can be divided into a purely nuclear part that is dependent on the size of the nucleus and the *s* electron density. Only electrons in orbital *s* have electron density at the nucleus. The isomer shift can be written as:

$$\delta = K \{\Sigma_s |\Psi(0)|^2 - \Sigma_a |\Psi(0)|^2\} \qquad \textit{Equation (2.13)}$$

where δ is the isomer shift, K is a positive constant depending on the charge in the nuclear radius, $\Sigma_s |\Psi(0)|^2$ is the electron density of the source nucleus, and $\Sigma_a |\Psi(0)|^2$ is the electron density of the absorber nucleus.

A full mathematical derivation of equation (2.13) is shown is equation (2.14):

$$\delta = 4/5\ \pi Ze^2r^2 (\Delta r/r) [\ |\Psi_s(0)_A|^2 - |\Psi_s(0)_B|^2\ ]$$

Equation (2.14)

where A and B are two different chemical environments of which B is either the source matrix or a reference absorber. Z is the atomic number, e is the charge on an electron, r is the mean nuclear radius and Δr/r is the ratio of the radius of nucleus

where its the relative change between the excited state and ground state. In Table 2.1 there is a list of isotopes with a positive or a negative ratio of the nucleus.

For iron, in order to allow isomer shifts to be measured independently of the nature of the source the centre of the room temperature spectrum of metallic iron has been adopted as the zero of energy and all shifts are measured relative to it. This convention yields:

$$\delta = K_0 - K\Sigma_a \left| \Psi(0) \right|^2 \qquad \textit{Equation (2.15)}$$

where K_0 is a constant.

Before information about changes in electron density can be gained from the δ, the sign and magnitude of Δr/r must be known. For ^{57}Fe (Δr/r) is negative, so that an increase in *s* electron density at the nucleus results in a decrease in isomer shift (Table 2.2). If Δr/r is negative, the nucleus expands on going from the excited state to ground state therefore, δ increases with decreasing electron density at the nucleus.

The 1*s* and 2*s* electron densities at the nucleus are independent of the chemical environment of the iron ion. However, the 3*d* electrons shield the 4*s* electrons and cause a decrease in the electron density at the nucleus. The more delocalised the 3*d* electrons, the smaller the isomer shift.

Hence, the principal contribution to the isomer shift comes from changes in the number of electrons in the highest occupied *s* orbital (4*s* in the case of iron) and from shielding effects owing to electrons in the outer *p* and *d* orbital.

Table 2.2 Isomer shifts for iron in various oxidation states[10].

***d*- Configuration**	**Isomer shift (mm/sec)**	**Oxidation state**
d^2	-0.9 to -0.8	Fe(VI)
d^4	-0.2 to 0.00	Fe(IV)
Low spin d^5	-0.2 to +0.4	Fe(III)
Low spin d^6	0.0 to +0.3	Fe(II)
High spin d^5	+0.3 to +0.7	Fe(III)
High spin d^6	+0.8 to +1.5	Fe(II)

For iron(III), the isomer shift for low spin (S = ½) complexes falls in the range –0.2 to +0.4 mm/sec, for high spin (S = 5/2) and intermediate (S = 3/2) complexes it falls in the range of +0.3 to +0.7 mm/sec. For iron(II), isomer shift values are usually in the range of 0.0 to +0.3 mm/sec in low spin (S = 0), 0.0 to +0.4mm/sec in intermediate spin (S = 1) and +0.8 to +1.5mm/sec in high spin (S = 2).

In all cases, an increase in covalency tends to increase *s* electron density, so that the most ionic complexes have the highest δ values. Compounds, in the presence of a lone pair with high *s* electron character give a positive δ value.

An increase in oxidation state in transition metals will decrease the *p* and *d* electrons through shielding of the *s* electron density and as a result will increase the δ value. Decreases in coordination number contribute to the same result. However, for isotopes where Δr/r is negative, such as ^{57}Fe, all the effects of electron density on δ are reversed. The electronic contribution to the isomer shift is essentially temperature independent and the observed decrease at high temperatures is due to the relativistic

second order Doppler shift (discussed below). Hence, the most valuable information obtained is for classifying various compounds according to oxidation state, degree of covalency, shielding of *s* electron and coordination number.

2.1.9.1a Second Order Doppler Shift

The second order Doppler shift arises from the vibration of absorbing nuclei in the lattice site in the crystal. The vibration of a nucleus in the lattice affects both the energy of the emitted and absorbed γ-ray. It is the second order term for the frequency of the lattice vibration which affects the δ values and gives the variable the name second order Doppler shift. The change in the energy of the γ is described by equation (2.16) in terms of the zero point motion. The extreme right hand side of equation (2.16) is a classically derived high temperature approximation of the effect. The approximation of the effect using the Debye model as expressed in equation (2.17) is more accurate at low temperatures.

However for spectra recorded at similar low temperatures and the same pressures the contribution to γ from second order Doppler shift may be considered equal and small.

$$\frac{\delta E_\gamma}{E_\gamma} = \frac{\delta \nu}{\nu} = \frac{\langle \nu^2 \rangle}{2c^2} = \frac{-3RT}{2Mc^2} \qquad \textit{Equation (2.16)}$$

where E_γ is the energy of the γ-ray and ν is the frequency of the oscillation.

$$\frac{\Delta \nu_0}{\nu} = \frac{-9}{16} \frac{k\theta^2}{Mc^2} \qquad \textit{Equation (2.17)}$$

where M is the mass and $k\theta^2$ is the Debye temperature.

2.1.9.2 Quadrupole Splitting (ΔE_Q) [12]

When charge is distributed asymmetrically around the atomic nucleus (electrons, ions and dipoles) it gives rise to an electric field gradient (EFG), which results in a splitting of the nuclear energy. Nuclei with a spin quantum number, $I > ½$ have a non-spherical charge distribution; this magnitude of the charge distortion is measured by the nuclear quadrupole moment, Q. The sign of Q can be either positive or negative depending on whether the nucleus is respectively prolate (elongated) or oblate (flattened) along the spin axis. Q is zero for nuclei where $I = 0$ or $I = 1/2$.

For ^{57}Fe Mössbauer spectroscopy the transitions are between the $I = 1/2$ ground state and $I = 3/2$ excited state. Therefore, the ground state of ^{57}Fe, with $I = 1/2$ cannot exhibit quadrupole splitting and, also is not affected by non-zero EFG. However the excited state of ^{57}Fe splits into two sub-states, which give rise to a two line spectrum. This is illustrated in the shaded area of the diagram (Figure 2.6).

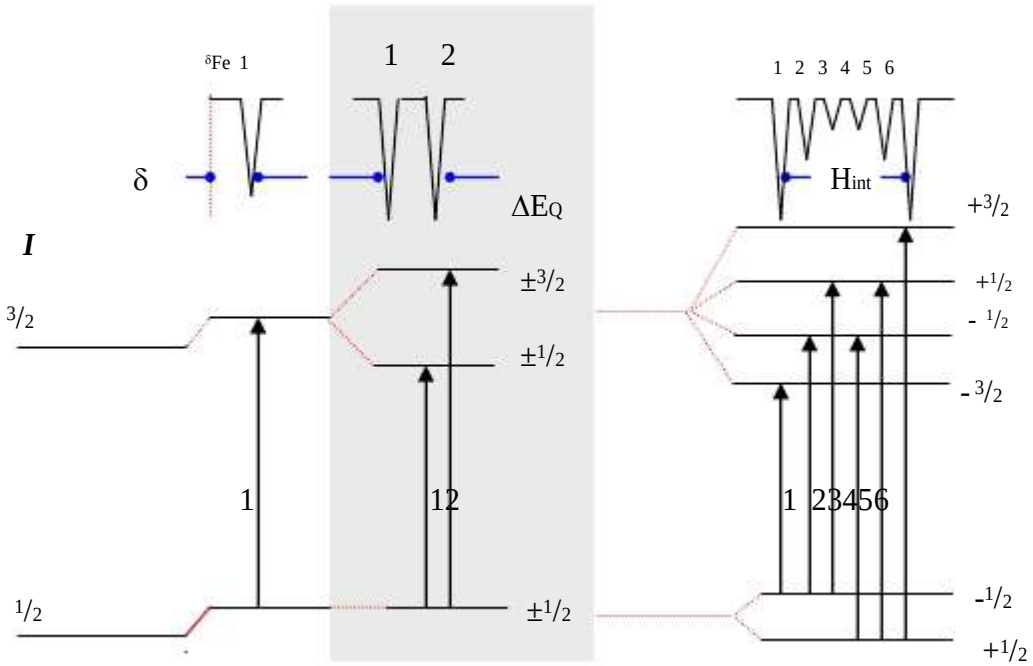

Figure 2.6 Schematic diagram[4] of the nuclear energy level shift and splitting as a
(a) function of chemical environment,
(b) electric field gradient and
(c) internal magnetic hyperfine field.

The nuclear quadrupole moment, Q is expressed by:

$$eQ = \int \rho r^2 (3\cos^2\theta - 1) d\tau \qquad \textit{Equation (2.18)}$$

where +e is the charge on the proton and ρ is the charge density in the volume element dτ at a distance r from the centre of the nucleus and at an angle θ to the axis of the nuclear spin quantisation axis.

The interaction of a nuclear quadrupole moment with the electronic environment is expressed by the Hamiltonian is given on the next page. The electrostatic potential, V

at the nucleus due to a point charge *q* at a distance r is given by $\mathbf{V=q/(4\pi\varepsilon_0 r)}$ where ε_0 is the permittivity of a vacuum.

$$\mathcal{H} = -\,{}^{1}/_{6}eQ.\nabla E \qquad \textit{Equation (2.19)}$$

where ∇E represents the electric field gradient at the nucleus (which is the derivative of the field E and hence the negative of the second derivative of the electrostatic potential, V).

∇E is the tensor quality, which can be expressed as:

$$\nabla E_{ij} = -\frac{\partial^2 V}{\partial x_i\, \partial\, x_j} = -V_{ij}$$

$$(x_i, x_j = x, y, z) \qquad \textit{Equation (2.20)}$$

$$\nabla E = -V_{ij} = \begin{bmatrix} V_{XX} & V_{XY} & V_{XZ} \\ V_{YX} & V_{YY} & V_{YZ} \\ V_{ZX} & V_{ZY} & V_{ZZ} \end{bmatrix} = EFG$$

Equation (2.21)

where $V_{XX} = \frac{\partial^2 V}{\partial X^2}$, $V_{YY} = \frac{\partial^2 V}{\partial Y^2}$, $V_{ZZ} = \frac{\partial^2 V}{\partial Z^2}$ and etc

There are nine values of V_{ij} to express in a Cartesian axis system: x, y, z. A 'principal' axis system may always be defined such that all the V_{ij} terms with $i \neq j$ are zero (the

matrix of the tensor is diagonal), leaving the three finite 'principal' values V_{XX}, V_{YY} and V_{ZZ}. The polar coordinates are defined below (Figure 2.7).

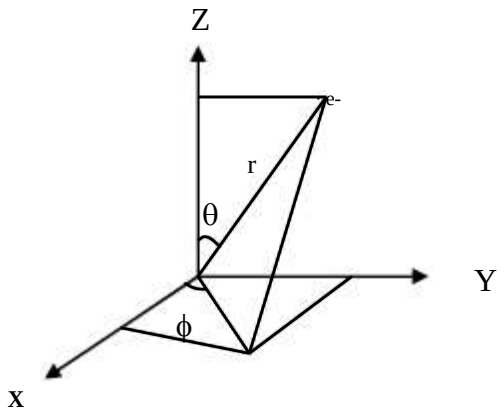

Figure 2.7 Polar coordinates of an electron in free space.

V_{XX}, V_{YY} and V_{ZZ} are not independent. The Laplace equation (2.22) must be satisfied in the regions where *s* electrons are found, due to the fact that they do not contribute to the ∇E by virtue of their spherical symmetry. The Laplace equation dictates that ∇E is real, symmetric and a traceless sensor.

$$\mathbf{V_{XX} + V_{YY} + V_{ZZ} = 0} \qquad \textbf{\textit{Equation (2.22)}}$$

Noting that $\cos^2 x + \sin^2 x = 1$, ($x = \theta, \phi$), it is evident from the expressions in Table 2.3 that equation (2.22) is obeyed. As a result it is only necessary to specify two independent parameters to completely describe an electric field gradient tensor in its principal axis system. These are chosen to be V_{ZZ} and η, where η is the asymmetry parameter:

$$\eta = \mathbf{(V_{xx} - V_{yy})/V_{zz}} \qquad \textbf{\textit{Equation (2.23)}}$$

so that, by convention $|V_{zz}| > |V_{yy}| \geq |V_{xx}|$ which forces $0 \leq \eta \leq 1$ and ensures that the η can only increase ΔE_Q.

Table 2.3 Components of the EFG tensor gradient for a charge of Z electronic units.

$V_{XX} = Ze r^{-3}(3\sin^2\theta\cos^2\phi - 1)$	$V_{XY} = V_{YX} = Ze r^{-3}(3\sin^2\theta \sin\phi \cos\phi)$
$V_{YY} = Ze r^{-3}(3\sin^2\theta\cos^2\phi - 1)$	$V_{XZ} = V_{ZX} = Ze r^{-3}(3\sin\theta \cos\theta \cos\phi)$
$V_{ZZ} = Ze r^{-3}(3\cos^2\theta - 1)$	$V_{YZ} = V_{ZY} = Ze r^{-3}(3\sin\theta \cos\theta \sin\phi)$

The Hamiltonian describing the interaction in equation (2.19) is more often expressed as:

$$\mathcal{H} = \frac{eQ}{2I(2I-1)} \left[V_{ZZ}\hat{I}_{z2} + V_{YY}\hat{I}_{y2} + V_{XX}\hat{I}_{x2} \right],$$

using equation (2.20), the Hamiltonian therefore becomes:

$$\mathcal{H} = \frac{e^2qQ}{4I(2I-1)} \left[3\hat{I}_{z2} - I(I-1) + \eta(\hat{I}_{x2} - \hat{I}_{y2}) \right] \qquad \textit{Equation(2.24)}$$

where $\hat{I}_z$, $\hat{I}_y$ and $\hat{I}_x$ are quantum-mechanical spin operators, I is the nuclear spin and e is the protonic charge(1.602×10^{-19} Coulomb), V_{ZZ} and q is referred to as field gradient. ($V_{ZZ} = q$). If the ∇E tensor has axial symmetry ($\eta = 0$), the energy levels are given by:

$$E_Q = \frac{e^2qQ}{4(2I-1)} \left[3I_{z2} - I(I+1) \right] \qquad \textit{Equation(2.25)}$$

where the quantum number I_z can take the $2I + 1$ values of $I, I-1, \ldots, -I$. If $I = 3/2$, $5/2$, $7/2$ etc., the energy level is split into a series of Kramers' doublets with $\pm I_z$ states

degenerate. An important example is $I = 3/2$, which has two energy levels at $+(e^2qQ/4)$ for $I_z = \pm 3/2$ and $-(e^2qQ/4)$ for $I_z = \pm 1/2$. If the symmetry is lower than axial (i.e. when $\eta > 0$), an exact expression can only be given for $I = 3/2$, and is:

$$E_Q = \frac{e^2qQ}{4I(2I-1)} [3I_z^2 - I(I+1)] \left[1 + \frac{\eta^2}{3}\right]^{1/2}$$

Equation (2.26)

EFG arises from the valence electrons of the Mössbauer atom itself and is associated with asymmetry in the electronic structure. This asymmetry results from partly filled electronic shells occupied by the valence electrons. Other contributions are from the lattice arrangement (V_{ZZ}) of the ligand atoms in non-cubic lattices. Molecular orbitals can contribute to the EFG. The quadrupole splitting observed in a particular system therefore reflects the symmetry of the bonding environment and the local structure in the vicinity of the Mössbauer atom.

Valuable information can be obtained when the data are considered in conjunction with the data on isomer shift. ΔE_Q data can provide information relating to the electronic population of:

1. various orbitals
2. isomerisation phenomena
3. ligand structure
4. short-lived reaction intermediates
5. semiconductor properties, and
6. defect structure of solids.

2.1.9.3 Magnetic Hyperfine Interactions

^{57}Fe nucleus possesses a magnetic moment in both ground and excited states. This moment will interact with a magnetic field, H at the nucleus to lift the degeneracy of a nuclear state with an angular momentum number, $I > 0$. This sub state magnetic splitting results in $2I + 1$ level for each state. Therefore, the ground state ($I = ^1/_2$) is split into two levels ($m_1 = +^1/_2, -^1/_2$) and the excited state ($I = ^3/_2$) into four levels [$m_1 = +^1/_2$, $m_2 = -^1/_2$, $m_3 = +^3/_2$, $m_4 = -^3/_2$] (see Figure 2.6). The energy of these states is given by:

$$E_m = -g_N\mu_N m_1 H \qquad \textit{Equation (2.27)}$$

where g_N is the nuclear gyromagnetic ratio, μ_N is the nuclear magnetic dipole moment, H is the applied magnetic field and m_1 is the magnetic quantum number. The selection rules for these magnetic dipole transitions require that $\Delta m_1 = 0$ or ± 1 and so only six transitions are observed.

Different effects arise depending upon the oxidation state and spin state of the iron atom. For iron(III) all 3 possible spin states ($S = ^1/_2, ^3/_2, ^5/_2$) are half integral.

According to Kramer's theorem, an electronic state must have at least double fold degeneracy and will therefore exhibit magnetic properties. The electrons will have a net hyperfine interaction even in the absence of an applied magnetic field, provided that the spin relaxation time is sufficiently long. For high spin, iron(III) ($S = ^5/_2$), spin lattice relaxation is expected to be important because this state has no orbital angular momentum and the spin system is well insulated from the lattice. However, spin lattice relaxation could be important for intermediate spin ($S = ^3/_2$). In iron(II) complexes there are systems with integral spin ($S = 0, 1, 2$) and the latter two spin

states, are expected to see magnetic interactions. Low spin, iron(II) ($S = 0$) is diamagnetic, no magnetic interactions can be observed in zero field.

2.1.9.4 Line Shape, Width and Area

In most cases, lines depict energy levels. Resonant absorption shows a characteristic energy dependence of the form:

$$I(E) = \frac{\Gamma_{ex}}{2\pi}\left[\frac{1}{(E-E_t)^2 + (1/2\,\Gamma_{ex})^2}\right] \qquad \textit{Equation (2.28)}$$

where Γ_{ex} is the experimentally determined full width at half maximum intensity and E_t is the nuclear transition energy. This distribution shows a Lorenztian shape (Figure 2.8)

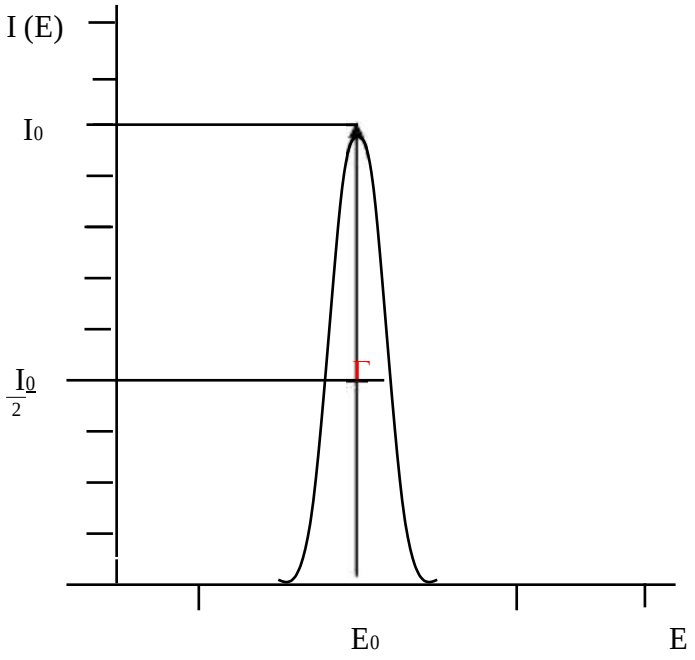

Figure 2.8 Illustration of the width of an energy level.

The line width is controlled by the Heisenberg uncertainty principle:

$$\Delta E \Delta t \geq \hbar \qquad \textit{Equation (2.29)}$$

$$\Gamma.\tau \geq \hbar$$

where ΔE is the distribution in energy, Γ is the linewidth Δt is the mean lifetime and $\tau = t_{½}/\ln 2$ of the nuclear excited state which generates the γ-ray.

Section two: High Pressure Mössbauer Spectroscopy

2.2 High Pressure Mössbauer Spectroscopy

2.2.1 Discovery and Definitions

The resurgence of static high pressure studies in materials science is due to the Diamond Anvil Cell (DAC)[13]. From the pioneering work of Bridgman, during the later part of the 19th century, until the late 1960s, massive hydraulically driven Bridgman-anvil and piston cylinder devices dominated high-pressure science[14]. The Bridgman cell was used to study a range of properties to a pressure of 12Kbar* utilising liquid or gaseous pressure transmitting media[15]. The gasketed DAC has become a standard tool for the generation of high pressures over the last four decades and has been applied to a wide range of experimental studies. Development of the DAC is as significant as a revolution for measurement under non-ambient conditions in physical sciences as that of the invention of the transistor to the whole sphere of electronics and computation. Further development resulted in the multiple anvil cells.

*****The standard measurement unit is the Pascal (Pa). Pressure can be converted in the following manner between the different units: Kbar (kilo bar) = 10^3 bar and Mbar (mega bar) = 10^6 bar. GPa (giga Pascal) = 10^4 bar. One bar = 10^5 Nm^{-2}(Pascal) = 0.9869 atm = 1.0197 $kgcm^{-2}$

2.2.2 Experimental Techniques

High pressure research encompasses a wide range of techniques and specialised apparatus, the literature contains many reviews on the subject [16-20] and some of the details relevant to this work are discussed below.

2.2.2.1 Diamond

Diamonds are suitable as part of an apparatus to generate high pressure for use in Mössbauer spectroscopy. They are capable of withstanding the forces involved in the experiment and are transparent to the Mössbauer gamma and electromagnetic radiation used in the measurement of the pressure in the cell. The diamonds used are high quality, flawless, brilliant-cut gemstones. The culet is removed by grinding a flat, octagonal surface with area of approximately 0.45 mm^2.

The size of the diamond may vary from $^1/_8$ to $^1/_2$ carat and the anvil flat from 0.3 to 0.7 mm similar in area and shape to be used. The recent discovery[21] of perforated diamond anvils has provided a tool for significantly high pressure studies. Pressures of 200-300 GPa can be achieved with bevelled-culet diamond anvils. Figure 2.9 shows the setup of a perforated anvil.

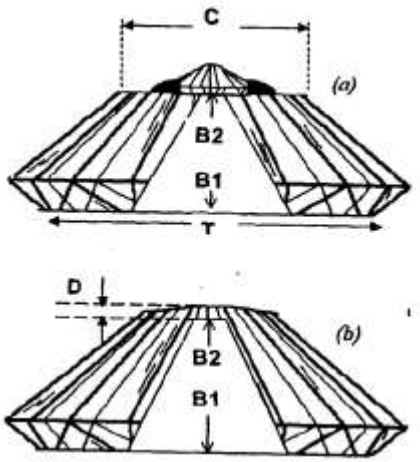

Figure 2.9 *(a)* Sketches of combined diamond backing plate (DBP) and a miniature anvil (MA). The DBP is first centred and glued to the metal BP of the DAC, followed by the same operation with the MA. T and C corresponds to table and culet dimensions. B1 and B2 refer to the larger and smaller conical openings. *(b)* A sketch of a partially perforated anvil with culet flat wall thickness D[21].

2.2.2.2 Gasket[22]

A gasket is used to hold the sample, a hydrostatic medium and ruby chips (for pressure measurement) lay between the facets. Use of a hydrostatic medium is necessary to avoid uneven pressure within the sample chamber. The choice of gasketing material is important. This is because of the nature of the experiment using high pressure. Tantalum tungsten alloy is a preferred material because it is malleable but not soft enough to cause the gasket to fail. The gasket hole is made by a spark-erosion system as shown in Figure 2.10. The size of hole is very precise when compared with micromechanical drilling of the gasket, which often requires time and a lot of adjustment under the microscope.

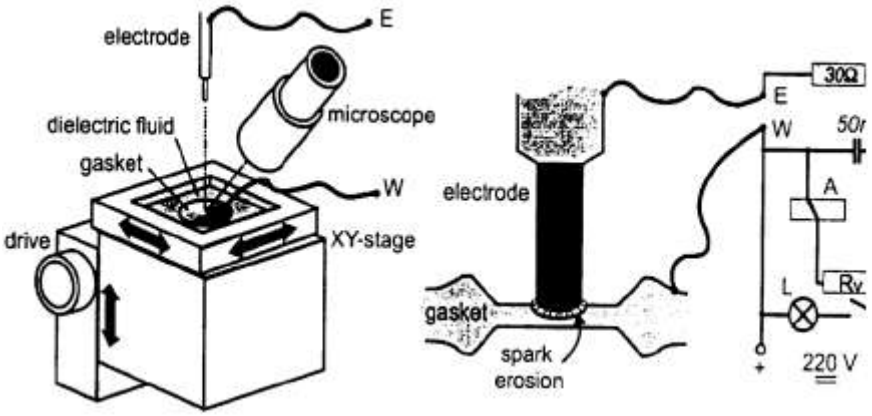

Figure 2.10 Principle of spark-erosion system and the electric circuit[14].

2.2.2.3 Hydrostatic Medium

Hydrostatic media in the sample chamber is the key component of the DAC. As the pressure increases, the fluid within the sample can solidify.

One of the most common pressure media is the 4:1 methanol : ethanol (water saturated) alcohol mixture, which is believed to remain at least quasi-hydrostatic to its glass transition as approximate of 10 GPa[23].

This mixture generates a good approximation of hydrostatic pressure. In Mössbauer experiments, it is important to determine the chemistry aspect of the solid sample. The hydrostatic media must not affect or dissolve the sample. Two commonly used hydrostatic media are [4:1 mixture of methanol:ethanol] and [1:1 mixture of pentane : isopentane]. Condensed gases such as helium, argon and other gases (listed in Table 2.4) retain low shear strength at much higher pressure or low temperatures. The ability to load gaseous material is therefore important for using them as a pressure-transmitting medium. Table 2.4 gives an overview of other alternatives, frequently used pressure transmitting fluids.

Table 2.4 Pressure transmitting media[14].

Medium	freezing pressure point (GPa)	max GPa of (quasi) hydrostaticity	Ref.
Silicon oil		<2.0	24
Water		2.5	24
Isoproyl alcohol		4.3	23
Glycerine: water (3:2)		5.3	25
Petroleum ether		6	26
Pentane: isopentane (1:1)		7.4	23
Methanol		8.6	23
Methanol: ethanol (4:1)		10.4	23
Methanol:ethanol:water(16:3:1)		14.5	27
Hydrogen	5.7	177	28
Helium	11.8	60 -70	29, 30
Neon	4.7	16	29
Argon	1.2	9	29
Xenon		55	31, 32
Nitrogen	2.4	13	33

2.2.2.4 Diamond Anvil Cell (DAC)

The principles of the gasketed DAC are elegantly simple. Figure 2.11 is a diagram of a DAC similar to that used in the experiments reported in this thesis.

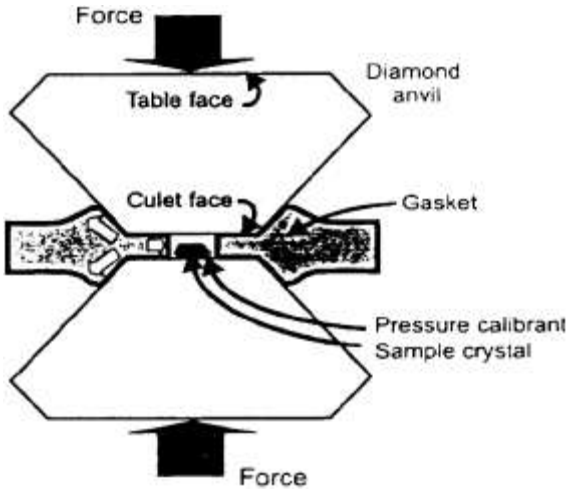

Figure 2.11 Assembly of the gasketed diamond anvil cell: principle of pressure generation[40].

The sample is placed in a pressure chamber created between the flat parallel faces (culets, < 1 mm) of two opposed brilliant-cut diamond anvils. A thin gasket is placed between the culet tips to help to support the load. A hole drilled or spark-eroded in the prepressed gasket defines the sample space.

The space is approximately 150 to 300 μm in diameter and 10-15 μm in thickness for the samples, ruby chips and pressure medium for reducing pressure gradients. The DAC used in the experiments performed in this work is a modified Merrill-Bassett cell.

Figure 2.12 shows a modified Merrill-Bassett cell, in which three screws pull the two triangular plates together when tightened, carrying the diamond anvils with them.

20 GPa is the maximum upper limit pressure for a cell of this design[32].

In the construction of the plates, beryllium (Be) discs are used to support the diamonds and the discs themselves are press-fitted into the stainless steel housings. Although there is no method for adjusting the diamond culets so that they can be made absolutely parallel to one another, three guide screws are kept parallel during

pressurisation. This technique is crucial in order to obtain the right pressure calibration.

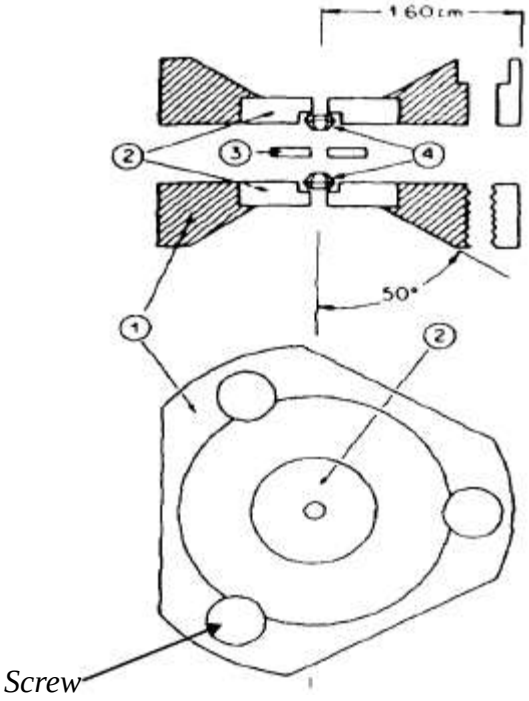

1. Stainless steel plates 2. Beryllium disc 3. Gasket 4. Diamond anvils

Figure 2.12 Merrill-Bassett miniature cells. The diamonds are set in Beryllium backing plates and the thrust applied by tightening the three symmetrically located screws[16].

2.2.2.5 Pressure Calibration by Ruby Fluorescence

The introduction of the ruby fluorescence method (RFM) in 1972[34] marked the beginning of measuring pressure in the DAC during the experiment. It is simple, rapid and requires no alteration, as the measurements are *in situ*. RFM is a versatile and accurate method of determining the sample pressure[35]. However this method is not suitable at higher temperature as the intensity of the fluorescence diminishes significantly[36].

The essential elements of the pressure calibration system, as shown in Figure 2.13 are the laser light source to excite the fluorescent radiation, an optics system for both the

incident laser light and the fluorescent light and a spectrometer for the spectral analysis of the fluorescence signal.

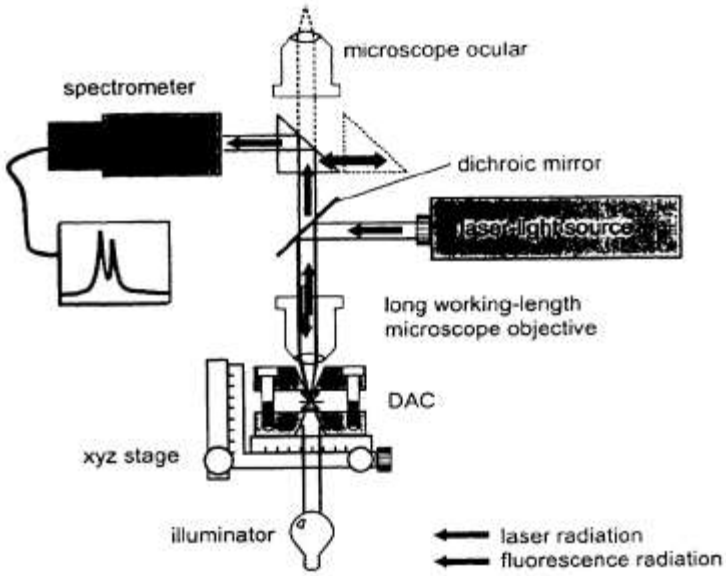

Figure 2.13 Schematic diagram of a fluorescence pressure calibration system[40].

Tiny crystal chips of ruby (Cr^{3+} doped with 0.5% α-Al_2O_3) approximately 5-10 μm in size are placed in the DAC. Ruby fluorescence under blue-green excitation is characterised by an intense doublet ($^2E \rightarrow {}^4A_2$ electronic transition of Cr^{3+} in a distorted octahedral crystal field) with sharp band components centred at R_1= 6928 Å and R_2 = 6942 Å at ambient pressure. The fluorescence spectrum is composed by R_1 and R_2 lines and shifts towards longer wavelengths when pressure increases.

The process of pressure determination requires at least two measurements, one of the fluorescence from a reference sample at ambient pressure (this is achieved by scattering ruby fragments on microscope slides) and one of the equivalent materials within the sample chamber of DAC at higher pressure. The correlation of the measured wavelength shift ($\Delta\lambda$) with applied pressure is the basis for the pressure determination.

This is dictated by the following equation:

$$P\ (GPa) = 380.8\ [(\Delta\lambda/\lambda_{\circ} + 1)^5 - 1] \qquad \textit{Equation (2.30)}$$

The equation shown above has a correct linearity within the experimental range up to 29 GPa[37]. When using this calculation for pressure calibration it is important to be able to make reproducible measurements with an accurate estimation of error. The major contribution of error is usually due to the bench set-up of the system. However this problem is eliminated by setting the calibration system up in a dark room on a shock absorption optical bench dedicated to the calibration of ruby pressure.

2.2.3 The Effect of Pressure

The primary effect of pressure on the electronic structure is to increase the overlap between orbitals of neighbouring atoms especially cation-anion interactions[38]. This directly applies the effect on the recoil free fraction, ***f*** [39] as described in equation 2.31. Since ***f*** is dependent on the Debye-Waller factor (Lamb-Mössbauer factor) applying pressure to the lattice will affect ***f***.

$$f \propto -\langle x^2 \rangle \qquad \textit{Equation (2.31)}$$

where $< x^2 >$ is the mean vibrational amplitude of the emitting atom.

Increasing pressure to the lattice restricts the vibrational modes of the lattice and therefore increases ***f***.

$$\frac{1}{E_\gamma}\left(\frac{\partial \text{i.s.}}{\partial P}\right)_T = \frac{1}{v}\left(\frac{\partial V}{\partial P}\right)_T$$

Equation (2.32)

$$\left(\frac{\partial \nu}{\partial P}\right)_T = K\left(\frac{\partial|\psi(0)|^2}{\partial \ln V}\right)_T\left(\frac{\partial \ln V}{\partial P}\right)_T + \left(\frac{\partial \nu_{rel}}{\partial \ln V}\right)_T\left(\frac{\partial \ln V}{\partial P}\right)_T$$

$$\frac{1}{v}\left(\frac{\partial \nu_{rel}}{\partial \ln V}\right)_T\left(\frac{\partial \ln V}{\partial P}\right)_T \approx \frac{3}{20}\frac{k\theta_D}{Mc^2}\left(\frac{\theta_D}{T}\right)\left(\frac{\partial \ln \theta_D}{\partial \ln V}\right)_T\left(\frac{\partial \ln V}{\partial P}\right)_T$$

Equation (2.33)

Equation 2.32 describes how the isomer shift (i.s.) varies with pressure at constant temperature (T). V is the volume, v is velocity, θ_D is the Debye Waller temperature and k is the Boltzmann constant.

This equation has two terms, describing the effect of pressure on the electronic term and second order Doppler shift. The right hand side of equation 2.33 shows how second order Doppler shift varies with pressure depending on the Grüneisen constant (which can be used to calculate $(\partial \ln\theta_D / \partial \ln V)$), and the compressibility of the sample $(\partial \ln V / \partial P)$. This term is small and for a lattice with a low Debye temperature it can be considered negligible compared to pressure induced changes in the electronic term.

The effect of pressure on the electronic term will depend on how pressure affects both the *s* electron density at the iron nucleus and the shielding of the nuclear *s* electron by *p* and/or *d* electrons. Thus isomer shift is described as shown in equation 2.33, then a decrease in isomer shift with pressure can be caused by an increase in $|\psi(0)|^2_{absorber}$ or by a decrease in the shielding of the *s* electron density at the nucleus by the *p* and *d* electrons. The opposite effects can be used to explain an increase in isomer shift with

pressure. The effect of pressure on quadrupole splitting is very dependant on the compound under investigation.

If pressure causes distortion of the lattice and the valence electron density towards cubic symmetry then the quadrupole splitting will decrease. However, the effect of pressure could also cause a phase change to a lattice structure with a different contribution to quadrupole splitting or to cause a rearrangement of the valence and lattice contributions of a quadrupole splitting. These two effects could be cooperating in a constructive or a destructive fashion towards the variation of quadrupole splitting with pressure.

Equation 2.34 shows quadrupole splitting[18],

$$\Delta E = {}^{1}/_{2}\, e^2 qQ \left[1 + \eta^2/3\right]^{0.5}$$

$$q = (1 - \gamma_\infty)\, q_{lat} + (1 - R) q_{val}$$

Equation (2.34)

where η is asymmetry parameter, eq is the EFG, eQ is the nuclear quadrupole moment which causes a splitting of degenerate nuclear levels. γ_∞ is the Sternheimer shielding factor and R the Sternheimer anti-shielding factor. Of these variables only q_{val} and q_{lat} are usually considered pressure dependent.

Pressure also causes changes in a magnetic sextet. However it is beyond the discussion for this work.

2.2.3.1 Chemical Consequences

The effect of pressure causes a number of phenomena in the electronic orbital of the compounds. Delocalisation of electrons and broadening of the bands of allowed energy transitions are two examples. Another effect is to displace one orbital with respect to another. Orbitals with different quantum numbers have different orbital angular momentum, therefore some orbitals will be more compressible than others, which will increase or decrease the broadening effect[37].

2.3 References

1. R. L. Mössbauer, *Z. Physik*, **1958**, *151*, 124.
2. G. K. Wertheim, *Mössbauer Effect*: *Principles and Applications*, Academic Press, New York and London, **1964**.
3. A. Vertes, L. Korecz and K. Burger, *Mössbauer Spectroscopy* : *Studies In Physical And Theoretical Chemistry*, Elsevier Scientific Publishing Company, Amsterdam, Oxford and New York, **1979**.
4. N. N. Greenwood and T. C. Gibb, *Mössbauer Spectroscopy*, Chapman and Hall Ltd., London, **1971**.
5. D. P. E. Dickson and F. J. Berry, *Mössbauer Spectroscopy*, Cambridge University Press, Cambridge, **1986**.
6. T. C. Gibb, *Principles of Mössbauer Spectroscopy*, Chapman and Hall Ltd., London, **1975**.
7. B. W. Fitsimmons, *Chemistry of Iron*, edited by J. Silver, Blackie Academic, Glasgow, **1993**.
8. Muir, Anda & Coogan, *Mössbauer Effect Data Index*, 1985-1965.

9. F. J. Erazo, *Mössbauer Spectroscopy of Iron Porphyrin*, Knox College Hughes Fellowship Summer Research, **1999**.
10. *An Introduction to Mössbauer Spectroscopy*, ed. L. May, Plenum, New York, **1971**.
11. Gary J. Long, *Mössbauer Spectroscopy Applied to Inorganic Chemistry, Vol.1,* Plenum Press, New York & London, **1984**.
12. G. M. Bancroft, *Mössbauer Spectroscopy*: *An Introduction for Inorganic Chemists and Geochemists*, McGraw Hill Book Company (UK) Ltd., **1973**.
13. M. P. Pasternak and R. D. Taylor, *Hyperfine Int.*, **1990**, *62*, 89.
14. R. M Hazen and R. T. Downs, *Reviews in Mineralogy and Geochemistry*, **2000,** *41*, 451.
15. R. D Taylor and M. P. Pasternak, *Hyperfine. Int.*, **1990**, *53*, 159.
16. A. Jayaraman, *Rev. Mod. Phys.*, **1983**, *55*, 65
17. W. B. Hopfazel, *High Temperatures-High Pressures*, **1970**, *2*, 241
18. G. Amthauer in *High Pressure Research in GeoSciences*, edited by W. Schreyer, E. Schweizerbart'sche Verlagsbuchhandlung, Stuttgart, **1982**.
19. M. P. Pasternak and R. D. Taylor, *Hyperfine Int.*, **1989**, *47*, 415.
20. R. D Taylor and M. P. Pasternak, *Hyperfine. Int.*, **1992**, *72*, 241.
21. A. Dadashev, M. P. Pasternak and G. Kh. Rozenberg, *Rev. Sci. Instum.*, **2001**, *72(6)*, 2633.
22. E. Stearer, M. P. Pasternak and R. D. Taylor, *Rev. Sci. Instum.*, **1990**, *61*, 1117.
23. G. J. Piermanni, S. Block and J. D. Barnett, *J. Appl. Phys.*, **1973**, *44*, 5377.
24. R. J. Angel, *Reviews in Mineralogy and Geochemistry*, edited by R. M. Hazen and R. T. Downs, **2000,** *41*, 100.
25. V. A. Sidorov and O. B.Tsiok, *Fizika I Technika Vysokikh Davlenii*, **1991**, *34*, 74.

26. J. D. Barnett and C. D. Bosco, *J. Applied Phys.*, **1969**, *40*, 3144.

27. I. Fujishiro, G. J. Piermanni, S. Block and R. G. Munro, *High-Pressure in Research and Industry, Proc 8th AIRPART Conf, Uppsala*, edited by C. M. Backman, T. Johannison and L. Tegner, **1981**, 608.

28. H. K.Mao and P. M. Bell, Science, **1979**, *103*, 1004.

29. P. M. Bell and H. K. Mao, *Carnergie Inst. Wash Yrbk.*, **1981**, *80*, 404.

30. M. I. Eremets, *High Pressure Experimental Methods*, Oxford University Press, Oxford, *New* York & Tokyo, **1996**.

31. D H. Liebenberg, *Phys. Lett.*, A(73), **1979**, 74.

32. D. H. Liebenberg, R. L. Mills, J. C. Bronson, *High Pressure Science and Technology*, edited by K. D. Timmerhaus and M. S. Barber, Plenum, New York, **1979**, 1, 395.

33. K. Asaumi and A. L. Ruoff, *Phys Rev. B*, **1986**, *33*, 5633.

34. R. LeSar, S. A. Ekberg, L. H. Jones, R. L. Mills, L. A. Schwalbe and D. Schiferl, *Solid state Comm.*, **1979**, *32*, 131.

35. R. A. Forman, G. J. Piermanni, J. D. Barnett and S. Block, *Science*, **1972**, *176*, 284.

36. J. D. Barnett, S. Block and G. J. Piermarini, *Rev. Sci. Instrum.*, **1973**, 44, 1.

37. G. J. Piermarini and S. Block, *Rev. Sci. Instrum.*, **1975**, 46, 973.

38. M. J. Carney, G. C. Papaefthymiou, K. Spartalian, R. B. Frankel and R. H. Holm, *J. Am. Chem. Soc.* **1988**, 110, 6084.

39. G. R. Fern, *PhD Thesis*, Essex University, **1998**.

40. R. Miletich, D. R Allan and W. F Kuhs, *High Pressure Single – Crystal Technique*, *Reviews in Minereology and Geochemistry*, **2000**, *Vol.41*, 445.

Chapter 3: Synthesis of Chlorotetraphenylporphyrinato iron(III) [Fe(III)TPP]Cl and Silicon phthalocyanine *bis* 4-pyridinecarboxylic acid SiPc[PyCOO]$_2$: Studies aimed at forming complexes between [Fe(III)TPP]Cl and SiPc[PyCOO]$_2$

3.1 Introduction

This chapter is concerned with the synthesis of tetraphenylporphyrin - H_2TPP, chlorotetraphenylporphyrinato iron(III) – Fe(III)TPPCl, silicon pthalocyanine dichloride - $SiPcCl_2$ and silicon phthalocyanine *bis* 4-pyridinecarboxylic acid - $SiPc[PyCOO]_2$. The synthesis of the silicon phthalocyanine compound from the reaction of 4-pyridinecarboxylic acid (4-PyCOOH) and silicon phthalocyanine dichloride acid ($SiPcCl_2$) is presented in detail. The aim of this work was to produce a new complex between $SiPc[PyCOO]_2$ and Fe(III)TPPCl.

A number of other substituted imidazoles were also used to attempt to form new compounds. In addition, the charge transfer properties of $SiPc[PyCOO]_2$ were also examined.

3.1.1 Porphyrin and Metalloporphyrin (H_2TPP and Fe(III)TPPCl)

All forms of life depend on the ability of metalloporphyrins to undergo oxidation-reduction and electron transfer reactions[1]. The structures of naturally occurring iron porphyrins in proteins are very complex. So, in order to study their properties, a 'simpler' version of these molecules was synthesised in this work, namely *meso* tetraphenylporphyrin (H_2TPP) (Figure 3.1). In addition to their biological implications, the cyclic tetradentate framework of the four central nitrogen atoms makes H_2TPP a unique chelating agent[1-5]

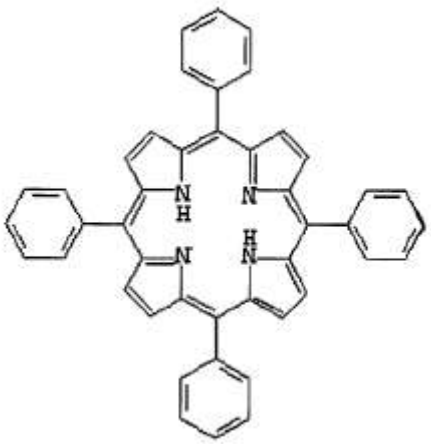

Figure 3.1 Structure of H_2TPP[6].

Synthetic H_2TPP has been widely used in studies on molecular symmetry, solubility and crystal structure. The recent trend has been to abandon research using "biologically active" porphyrins in favour of synthetic compounds having a better defined behaviour, especially H_2TPP and most of all its *para* substituted derivatives[7]. As a result, there is a considerable interest in the synthesis of porphyrin compounds that exhibit predictable and ideal behaviour in solution without having to deal with naturally occurring active matters in porphyrins.

3.1.1.1 Properties, Uses and Applications of Fe(III)TPPCl

Each of the 4 possible combinations of iron(II) and iron(III) in a high or a low spin ground state are realised in one or more of the naturally occurring iron porphyrins. Elucidation of the structural principles governing iron porphyrin stereochemistry carries many biologically significant implications. A five coordinate square pyramidal geometry, with the iron(III) ion displaced (0.475Å out of plane from the porphinato core – was established earlier (Chapter One) as typical for the coordination group in a high spin iron(III) porphyrin[10].

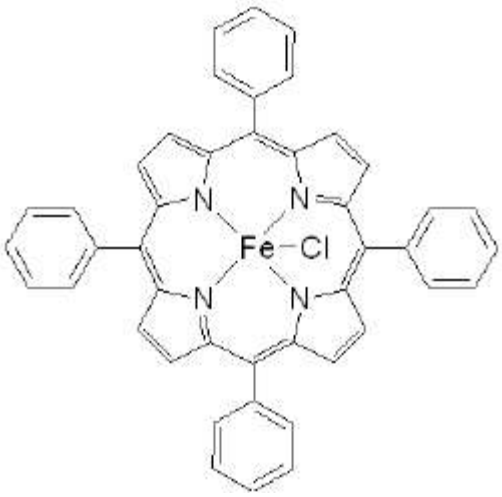

Figure 3.2 Structure of Fe(III)TPPCl[9].

Fe(III)TPPCl (Figure 3.2) is only soluble in non-aqueous solvents. In the absence of an aqueous base, it does not readily lose the coordinated chloride. Fe(III)TPPCl is soluble in chloroform and therefore allows the extension of the study of bridged electron transfer reactions[11].

Before an atom transfer mechanism can be considered for the electron transfer reaction, the highly conjugated system and highly stable compound must be met regarding as the characters of the Fe(III)TPPCl.

3.1.2 Silicon Phthalocyanine

Silicon phthalocyanine (Figure 3.3) was first reported in 1960 and in the following years a number of other silicon phthalocyanine complexes were prepared[10 - 12].

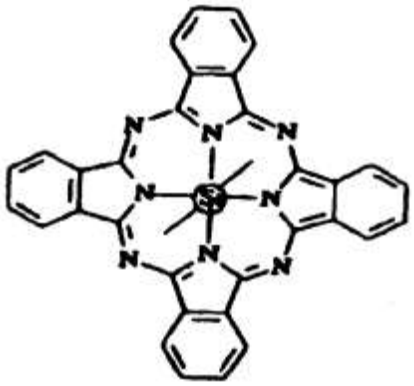

Figure 3.3 Structure of silicon phthalocyanine[28].

The early work on the synthesis of the silicon phthalocyanine compounds concentrated on the apparent hexacoordination of the silicon and the stability of the Si-N bonds[12]. The *bis* siloxy ligated silicon phthalocyanine complexes were understood to have a structure which contained both a tetra coordinate silicon in the siloxy group and a hexa coordinate silicon atom in the centre of the phthalocyanine[13]. Preparation of silicon phthalocyanines was carried out in a quinoline solvent (method 1) and resulted in low yields of $SiPcCl_2$, so an alternative method was developed to improve the yields of $SiPcCl_2$ hexachlorodisiloxane instead of silicon tetrachloride (method 2)[14]. These methods (1 - 5) are illustrated in Figure 3.4.

Two methods on the synthesis of $SiPcCl_2$ in quinoline (method 3 and 4)[16] which were reported in 1965 showed higher yield of $SiPcCl_2$ than methods 1 and 2.

The insertion of silicon into peripherally substituted phthalocyanines in toluene and tri-n-butyl amine reported in 1977 showed that the yields by this method (method 5) are dependent on the nature of the peripheral substitution of the macrocycle[17]. However, this is an important discovery as many peripherally substituted phthalocyanines can be prepared and thus a large range of peripherally substituted silicon phthalocyanines can be synthesised.

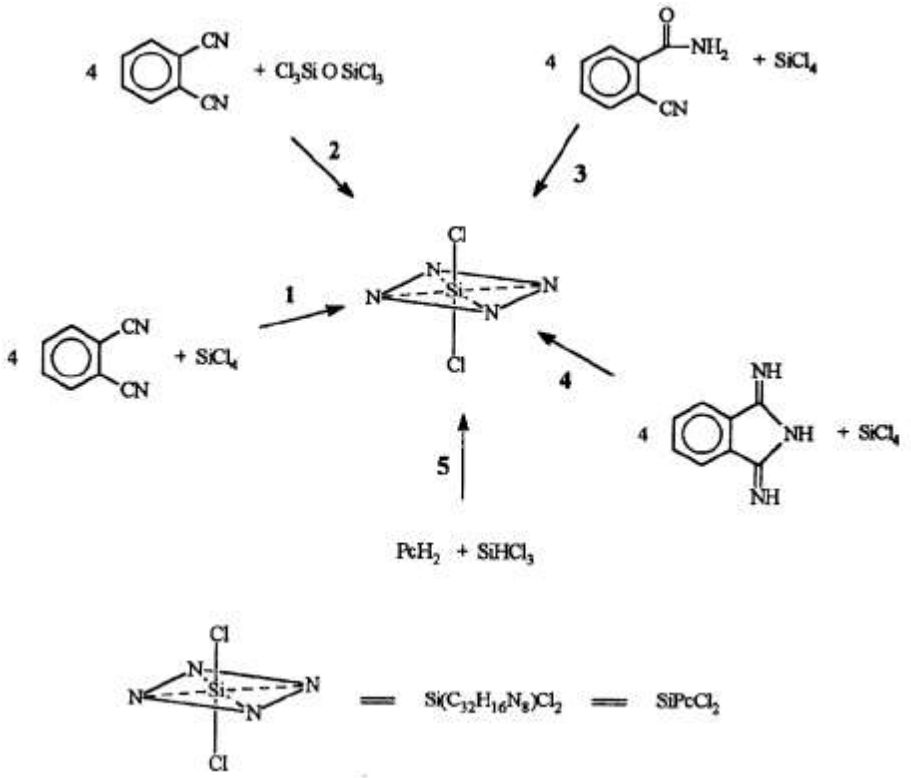

Figure 3.4 Synthetic routes to silicon phthalocyanine[18].

Low yields of $SiPcCl_2$ in the first four methods are caused by various factors. Quinoline is very difficult to dry and the presence of water causes the decomposition of silicon halides to silanols[16]. Also longer reflux times lead to the thermal decomposition of the quinoline solvent[18], Diiminoisoindolene (DII) can also be used for the preparation of $SiPcCl_2$ but DII decomposes at circa 200ºC[15] (about the temperature of refluxing quinoline), so DII should not be introduced until the $SiCl_4$/quinoline mixture has almost attained refluxing conditions. Experimentation has proved that the literature conditions are essentially optimum for minimum hydrolysis of $SiPcCl_2$ – longer reflux times resulting in decomposition[18].

3.1.2.1 Preparation of Axially Substituted Silicon Phthalocyanines

Axially substituted silicon phthalocyanines can be prepared by a range of methods, two of which are as follows.

The first method is by reacting chloro or hydoxy silicon phthalocyanine [$SiPc(OH)_2$] with different reagents[20], such as organic acids and alcohols. [$SiPc(OH)_2$] can be prepared from $SiPcCl_2$ by using a metal hydroxide in pyridine[21] or by dissolving $SiPcCl_2$ in an excess of concentrated sulphuric acid followed by the addition of water[22].

Secondly, silicon phthalocyanines can be prepared by the reaction of DII organo trichlorosilanes. Using this method a range of asymmetrically substituted silicon compounds were prepared (SiPcXCl, X = $CH_3C_6H_5$; C_2H_5; C_3H_7)[22-24], where the highest yield was achieved when X = CH_3 (52%)[21] and the lowest yield when X = C_2H_5 (5.11%)[23].

3.1.2.2 Preparation of Axially Substituted Silicon Phthalocyanines from $SiPcCl_2$ and $SiPc(OH)_2$

A variety of silicon phthalocyanines can be prepared from $SiPcCl_2$ and $SiPc(OH)_2$ as illustrated in Figure 3.5

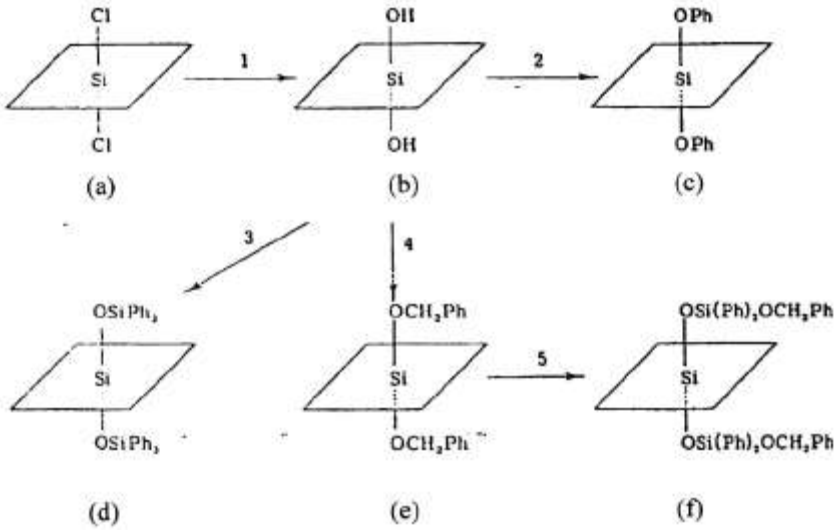

Figure 3.5 Some reactions of silicon phthalocyanines.
(Reactions pathway: (1) Py/NH_4OH; (2) Py/C_6H_5OH; (3) Ph_3SiOH; (4) $C_6H_5CH_2OH$; (5) $Ph_2Si(OH)_2$[21]

$SiPc(OH)_2$ reacts with phenol in pyridine to form diphenoxysilicon phthalocyanine (c); with benzyl alcohol the dibenzyloxy derivate $SiPc[(OCH)_2Ph]_2$ (e) is formed and with triphenylsilanol $SiPc(OH)_2$ forms the siloxy complex (d). The dibenzyloxy complex (e) reacts with diphenylsilanediol and forms bis (benzyloxydiphenylsiloxy) silicon phthalocyanines (f). These complexes sublime readily without decomposition[21].

Preparation of the alkoxy derivates may be carried out by the reaction:

$$SiPc(OH)_2 + 2ROH \rightarrow SiPc(OR)_2 + 2H_2O$$

According to Krueger and Kenney, siliconium ions are the most likely intermediate; i.e. in the case of ROH. [14, 20]

$$HOPcSiOH + ROH \rightarrow HOPcSiOH_{2+} + RO^-$$

$$HOPcSiOH_{2+} \rightarrow HOPcSi^+ + H_2O$$

$$HOPcSi^+ + RO^- \rightarrow HOPcSiOR$$

The acidity of ROH is important (the more acidic ROH, the easier the alkoxy derivates are formed) [14, 20], and silicon probably delocalises its positive charge into the ring by the use of its d_{xz} and d_{yz} orbitals.

$SiPc(OR)_2$ reacts readily with trichloroethanol forming the alkoxide $SiPc(OR)_2$ where $R = CH_2CCl_3$, while neopentyl alcohol requires a high reflux temperature to form $SiPcCl_2$ with alcohol:-

$$SiPcCl_2 + 2ROH \rightarrow SiPc(OR)_2 + 2HCl.$$

Some of the alkoxy compounds, such as diethoxy silicon phthalocyanine, have been prepared from the reaction of an alcohol and $SiPcCl_2$ in the presence of sodium borohydride[25].

Due to the flexibility of the side chain attached to the silicon atom, the higher alkoxides are soluble in benzene, but these complexes are thermally unstable so cannot be sublimed. These compounds can undergo hydrolysis and are readily converted to $SiPc(OH)_2$ in the presence of an acid (i.e HCl)[21].

Triorganosilanols are the most common axial substituting group used. The triorganosilanoxy silicon phthalocyanine derivates are prepared by condensation of $SiPc(OH)_2$ with silanol forming $SiPc(OSiR_3)_2$ or $SiPc(OSiR_3)(R')$ compounds which are stable and soluble in organic solvents[22,23,25]. These compounds have been observed to be more stable than the alkoxy derivates of silicon phthalocyanine.

Dehydration of $SiPc(OH)_2$ at high temperatures and reduced pressures leads to formation of oligomers of SiPcO units, where the degree of oligomerisation is dependent on the temperature and pressure conditions[27,28]. The reaction between $SiPcCl_2$ and $SiPc(OH)_2$ under controlled conditions results in the formation of dimers[29]. Using the same method as for monomers it is possible to modify the terminal axial ligands of these oligomers by reactions with a triorganosilanol[27, 29]. The

reaction between $SiPcCl_2$ and a diamine results in formation of oligomers containing SiPc units linked by $NHCH_2CH_2NH$ bridges. A schematic representation of the axial substitution of silicon phthalocyanines is shown in Figure 3.6.

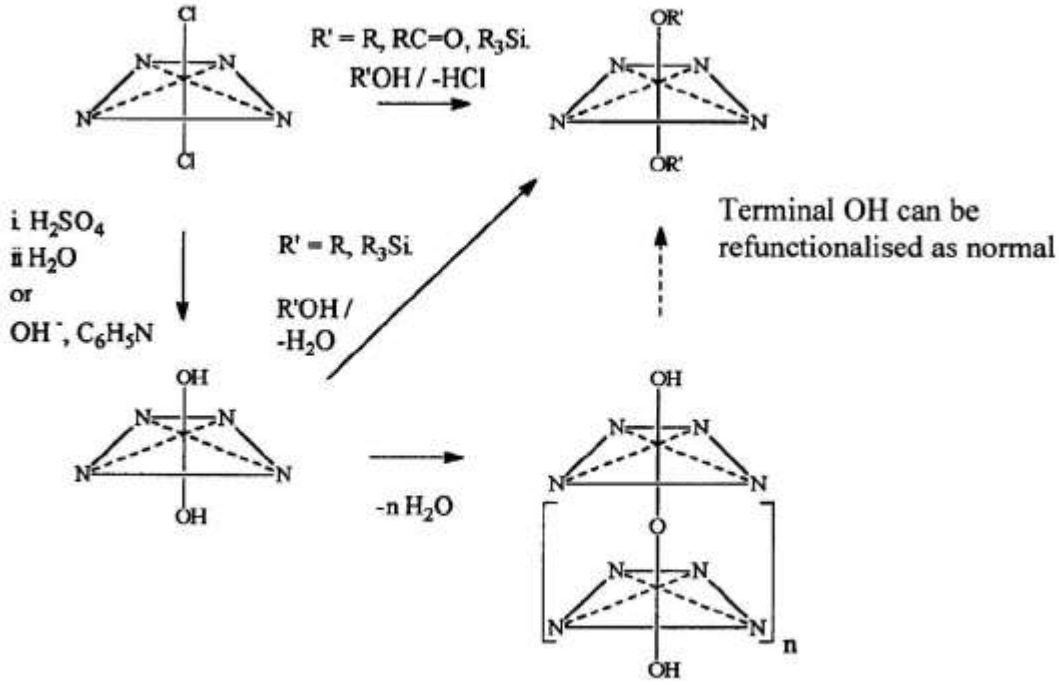

Figure 3.6 Axial substitution of silicon phthalocyanines[30].

3.1.2.3 Properties, Uses and Applications of Silicon Phthalocyanines

The properties, uses and applications of phthalocyanines are well documented in the literature[31] and some of the properties and uses are also presented in Chapter 1. The properties of silicon phthalocyanines will be discussed here to highlight the range of uses of silicon phthalocyanine generally.

The strong blue colour of silicon phthalocyanines, due to strong absorption of silicon phthalocyanines in the visible absorption region at around 700 nm (Q band) and two absorptions at lower intensity, is a reason for their use in the dye industry[32].

The use of silicon phthalocyanines in medicine is based on their photobiological activity against viruses[33] and tumors[34]. Therefore, silicon phthalocyanines are of use in indirect photodynamic therapy, where molecular oxygen, activated by visible light or near visible ultraviolet light, acts as the therapeutic agent.

Photo conducting studies of silicon phthalocyanines polymers have shown that bridged polymeric silicon phthalocyanines $(SiPcL)_n$ exhibit properties with high photosensitivity. The high photosensitivity is a result of the conducting band formed by π-orbitals in the phthalocyanine ring overlapping each other[35].

Non-linear optical (NLO) studies on phthalocyanines have shown that the strength of the optical absorption band (related to its transition dipole moment) allows large optical nonlinearities[36]. Silicon phthalocyanines exhibit an efficient third harmonic generation (THG) activity due to their extensively delocalised two-dimensional 18 π-electron system[36 - 38].

The third-order NLO properties of phthalocyanines are important because they have centro-symmetric components i.e. non-substituted and identically substituted on the four isoindoline moieties. The necessary requirement of non centro-symmetry is the reason for limited investigation in the second round harmonic generation (SHG) response of phthalocyanines[37]. However, it has been pointed out that unsymmetrical phthalocyanines with donor and acceptor groups should possess second-order NLO properties[38].

Silicon phthalocyanines fluorescence spectra mirror the Q band absorption spectra when excited at the wavelength of the Q band (600-700 nm) or the Soret band (300-400 nm) [39].

The stability of $SiPcCl_2$ both thermal and chemical, as well as the low toxicity and natural abundance of silicon would make them suitable for industrial applications.

3.1.2.3.1 Theory of Non-linear Optics[36]

The interaction of a non-linear optical (NLO) material with the electromagnetic field of high intensity laser light can result in the generation of new electromagnetic fields. When light passes through a material, its electric field interacts with inherent charges in the material causing the original light to be altered in phase, amplitude, frequency or polarisation. Therefore, the field of non-linear optics is a field that describes deviations from linear behaviour as defined by the classical laws or optics.

NLO experiments are mostly carried out on macroscopic materials and the linear polarisation is:

$$P = \chi E \qquad \textit{Equation (3.1)}$$

where χ, the linear susceptibility of the materials and E is is the electric field of the light.

When a high intensity electric field (laser light) is applied, the polarisability of the molecule can change from a linear to a non-linear regime. The non-linear molecular polarisation (P_m) leads to non-linear effects and is a function of the applied field, shown in equation (3.2).

$$P_m = \alpha E + \beta E^2 + \gamma E^3 + \ldots\ldots\text{etc} \qquad \textit{Equation (3.2)}$$

Where α is the linear polarisability, β is first molecular hyperpolarisibility (SECOND ORDER EFFECT) and γ is second molecular polarisability (THIRD ORDER EFFECT).

An analogous expression of the polarisation of the material is shown in Equation (3.3) where P_o is static dipole of the sample and $\chi^{(n)}$ is n^{th} order NLO susceptibility.

$$P = P_o + \chi^{(1)}E + \chi^{(2)}E^2 + \chi^{(3)}E^3 + \ldots\ldots\ldots\chi^{(n)}E^n \qquad \textit{Equation (3.3)}$$

If an intense light passes through a second order NLO material, then light at twice the input frequency will be produced - the principle of second order harmonic generation (SHG).

The interaction of an intense light with a third order NLO produces a polarisation component at the third harmonic (third harmonic generation is represented by $\chi^{(3)}$).

Designs of second order NLO materials follow well defined guidelines, and are as follows:

1. polarisable material;
2. asymmetric charge distribution (incorporation of donor – acceptor molecules);
3. a pathway of π-conjugated electrons;
4. non-central symmetric crystal packing.

Materials for third order NLO should be materials with extended π-electron conjugation (ideal for $\chi^{(3)}$) and the large π-electron delocalisation length creates a large anharmonic component in the non-resonant electron oscillations. There are no inherent symmetry restrictions for the third order effects, and it is hoped that the use of metal atoms will improve the design order NLO species that do not involve large delocalised electronic systems.

3.1.3 Crystallisation[40 - 49]

The second part of this chapter is aimed at trying to form a complex between $SiPc[PyCOO]_2$ and Fe(III)TPPCl. A central part was spent in the choice of appropriate solvents for crystallisation.

In order to carry out crystallisation, it is important to measure the degree of solubility of the compound[40]. The compounds were dissolved in minimum amounts of various hot solvents to determine the solubility. If insoluble impurities were present, the hot solution was then filtered. If the solution was contaminated with coloured impurities, it was treated with decolourising charcoal and filtered. The hot, saturated solution was then allowed to cool at a moderate rate. When the crystals were fully formed, they were isolated from the mother liquor (the solution) by filtration.

Crystallisation occurs in stages. As the hot saturated solution cools, it becomes supersaturated; and then crystal nuclei forms. These nuclei often form on the walls of the container, at the liquid surface, or on a foreign body because there is a proper molecular association at these locations. Once the crystal has been formed, additional molecules migrate to their surface by diffusion and join the crystal lattice. Because the molecule must migrate from the bulk of the solution to the growing crystal surface, the solution surrounding the crystal becomes less concentrated than the bulk of the solution.

Crystal growth is usually exothermic. So the heat released from the growing crystal increases the solubility of the compound near the surface. For crystallisation to continue the concentration of solute at the crystal site must be increased and the heat must be dissipated. These processes occur by diffusion and take time. Premature chilling or agitation can increase the rate of crystal growth to the point at which the

solid precipitates. The purest crystals are obtained when crystallisation occurs slowly from an undisturbed solution.

3.1.3.1 Solvents for Crystallisation

The ideal solvent for the crystallisation of a particular compound is the one that:

- does not react with the compound,
- boils at temperature below the compound's melting point,
- dissolves a moderately large amount of the compound when hot.
- dissolves only a small amount of compound when cool,
- is moderately volatile so that the final crystals can be dried readily, and
- non-toxic, non-flammable and inexpensive.

The primary consideration in choosing a solvent is that the compound be moderately soluble in hot solution and less so in the cold solvent. Most commonly, in the selection of a specific solvent for a specific compound, the solubility of the compound in various solvents is determined by *trial and error*.

General guidelines for predicting solubilities based upon the structures of organic compounds do exist. If the best solvent for crystallising a compound is not known; small portions of the compound can be tested with a variety of likely solvents.

3.1.3.2 In Search of the 'Right' Solvent

When a chemical similarity is present, the solution of the two components will usually have a structure similar to the one of the pure materials (alcohol-water mixture). For example:

Methanol – benzene

Water – N, N – dimethylformamide (DMF)

Aniline – diethyl ether

Polystyrene – chloroform

On the other hand, insolubility can occur in spite of similarity of the two partners. Thus, *polyvinyl* alcohol does not dissolve in alcohol. Between the extremes there is a whole range of possibilities where the two materials dissolve each other to a limited extend. Rather than like dissolve like, there is an intermolecular interaction, between solvent and solute molecules, which determines the mutual solubillity.

Experiments were conducted, based on these theories, given in Table 3.1, when attempting to make various crystalline complex. A compound 'A' dissolves in a solvent 'B' only when the intermolecular forces of attraction K_{AA} and K_{BB} for the pure compounds can be overcome by the forces K_{AB} in solution. The sum of the interaction forces between the molecules of solvent and solute can be related to the so-called polarity of 'A' and 'B'. Denoting compounds with large interactions A……A or B…….B respectively as polar and those with small interactions as nonpolar, four cases of qualitative prediction of solubility can be distinguished, as shown in Table 3.1.

Table 3.1 Solubility and polarity of two different solvents[42].

Solute A	**Solvent B**	**Interaction**			**Solubility of A and B**
		A……A	**B…..B**	**A…..B**	
nonpolar	nonpolar	weak	weak	weak	can be high[a]
nonpolar	polar	weak	strong	weak	probably low[b]
polar	nonpolar	strong	weak	weak	probably low[c]
polar	polar	strong	strong	strong	can be high[a]

[a] not much change for solute or solvent; [b] difficult to break up B……B; [c] difficult to break up A…..A

3.2 Experimental

3.2.1 Synthesis of Porphyrins

The porphyrin system was discussed in detail in Chapter One.

3.2.2 Synthesis of H_2TPP[51, 52]

H_2TPP was formed by a condensation reaction between benzaldehyde and pyrrole (Figure 3.7).

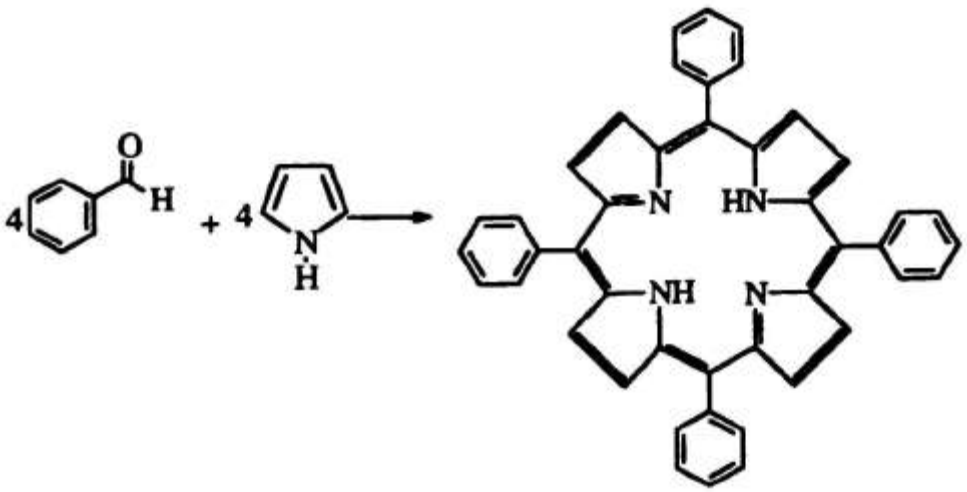

Figure 3.7 Synthesis of H_2TPP[53].

Benzaldehyde, pyrrole and propionic acid were purchased from Aldrich Chemical Co. Pyrrole was distilled and a clear liquid was collected for use in the second part of the synthesis in refluxing conditions. Benzaldehyde (used without further purification) (75 mL, 0.7 mol) was heated under refluxing conditions in propionic acid (700 mL). Freshly distilled pyrrole (75 mL, 1.2mol) was added to the reaction mixture (using a dropping funnel) slowly over 40 to 50 minutes.

The reaction mixture was heated for a further 40 minutes. During the reaction, a dark purple precipitate formed. The precipitate was filtered, washed thoroughly using methanol and hot water until the filtrate was clear. The purple, crystalline solid was

collected and analysed using electronic absorption spectroscopy, infrared spectroscopy and elemental analysis technique to be H_2TPP. The H_2TTP produced was used for the next experiment.

[*Anal.* Calc. For $C_{44}H_{30}N_4$: C, 85.90; H, 4.92; N, 9.12%; Found C, 84.34; H, 4.83; N, 8.96%]

3.2.3 Synthesis of Fe(III)TPPCl

Fe(III)TPPCl can be synthesised using two different methods; iron(II) acetate in trichloromethane or iron(II) chloride in *N,N*-dimethylformamide (DMF). Both methods were attempted.

3.2.3.1 Iron(II) chloride [$Fe(II)Cl_2$] Method[49]

Iron(II) chloride, $Fe(II)Cl_2$ [light green powdered material] was prepared by adding hydrochloric acid to iron wire until there was no further reaction. Excess hydrochloric acid and water were removed at low pressure.

In order to synthesise Fe(III)TPPCl**,** H_2TPP (2g, 3.3×10^{-3} mol) was dissolved in DMF (500 mL). Anhydrous iron(II) chloride (7 g, 7.7×10^{-2} mol) was added. The reaction mixture was heated under refluxing conditions. After 35 minutes, the reaction mixture was allowed to cool to room temperature. Concentrated hydrochloric acid (2 mL) was added to the reaction followed by 250 mL of distilled water. Instead of a purple precipitate, a dark brown precipitate formed. No further steps were carried out, due to the presence of iron(III) impurities which explained the brown coloured material. Moisture must have been introduced during the experiments therefore the insertion of iron(III) did not happen but formation of iron oxide occurred.

3.2.3.2 Iron(II) acetate [2($C_2H_3O_2$) Fe] Method[54]

1g of H_2TPP was dissolved in 100 mL of chloroform and 400 mg of sodium chloride was added. Into this solution was added 150 mL of filtered, hot iron(II) acetate. Iron(II) acetate was prepared freshly using iron filings in boiling acetic acid. After refluxing for 2 hours, the volume of the reaction mixture was concentrated to approximately 50 mL. The mixture was cooled and filtered. Approximately 500 mg of impure crystals were obtained.

The crude product was dissolved in methanol and soxhlet extracted for 5 hours to remove unreacted material. Dark purple needle-like crystals were obtained after drying the solvent containing purified FeTPPCl_2. Verification was made by electronic absorption, infrared spectroscopy, mass spectrometry, single crystal x-ray crystallography and elemental analysis.

[*Anal.* Calc. For $C_{44}H_{28}N_4$FeCl: C, 75.06; H, 4.00; N, 7.96 %; Found C, 74.67; H, 4.18; N, 8.04 %].

[*Mass Spec*. Calc.: $C_{44}H_{28}N_4$FeCl, molar mass: 703.99; Found: 703.14]

3.2.3.2a Crystal Structure of Fe(III)TPPCl

Crystals of FeTPPCl were grown in chloroform over a period of 8 weeks. The crystal structure was determined using x-ray crystallography[55] by Prof. C. Frampton formerly of Roche Ltd. A deep purple crystal of FeTPPCl, chosen for analysis was mounted on a glass fibre and was cooled with an Oxford Cryosystem. Data collection: MSC/AFC Diffractor Control Software (Molecular Structure Corporation, 1993). Cell refinement: MSC/AFC Diffractor Control Software. Data Production: TEXSAN (Molecular Structure Corporation, 1993). Program used to solve structure:

SHELXS86 (Sheldrick, 1990). Program used to refine structure: TEXSAN. Details of data are as follows:

Summary of crystal data:

[FeCl($C_{44}H_{28}N_4$)	Mo Kα radiation
M_r = 704.03	λ = 0.71073 Å
Monoclinic	Cell parameters from 20 reflections
$P2_1/a$	θ = 21.1-36.4º
a = 10.254(2) Å	μ = 5.6 cm^{-1}
b = 15.969(3) Å	T = 293 K
c = 20.180(4) Å	Prism
β = 90.48(2)º	Purple crystal
V = 3407.7 $Å^3$	0.4 x 0.25 x 0.10mm
Z=4	
D_x = 1.37 gcm^{-1}	
D_m not measured	

Data Collection

Rigaku AFC-7R diffractometer	R_{int} = 0.047
ω scans	θ_{max} = 55º
Absorption correction: none	hkl = 11-12, 0-19, 0-24.
8420 measured reflections	4 standard reflections
7581 independent reflections	
3357 observed reflections	
[I = 3σ(I)]	intensity decay : none

Refinement:

Refinement on F	$(\Delta/\sigma)_{max}$ =0.02
R = 0.047	$\Delta\rho_{max}$ = 0.37e $Å^{-3}$
wR = 0.045	Extinction correction: none
S = 1.45	Atomic scattering factors from International Tables for X-ray Crystallography (**1974**, Vol. IV)
All non H-atom refined anisotropically	

$w = 1/\sigma^2(F)$

Details of bond distances and angles of the crystal structure of five-coordinate high spin Fe(III)TPPCl are given in Tables 3.3 and 3.4.

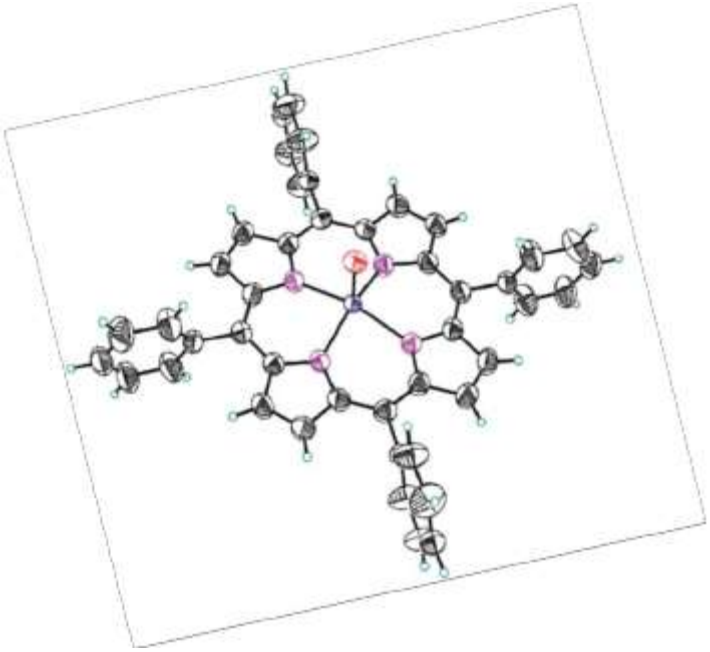

Figure 3.7 Crystal structure of Fe(III)TPPCl

Table 3.2 Fractional atomic coordinates and equivalent isotropic displacement parameters (Å^2).

$$U_{eq} = (1/3) \sum_i \sum_j U_{ij} a_i^* a_j^* a_i . a_j .$$

	x	***y***	***z***	U_{eq}
Fe	0.36716	0.32539	-0.351436	2.95
Cl	0.17639(11)	0.26438(4)	-0.33596(5)	4.55
N(1)	0.3616(3)	0.36420(20)	-0.44581(15)	3.0
N(2)	0.4852(3)	0.22799(20)	-0.38271(15)	3.1
N(3)	0.4598(3)	0.31402(20)	-0.26331(4)	3.0
N(4)	0.3314(3)	0.44932(20)	-0.32694(15)	3.0
C(*a*1)	0.3027(4)	0. 43607(27)	-0.46895(19)	3.3
C(*a*2)	0.3857(4)	0. 31516(26)	-0.49877(18)	3.1
C(*a*3)	0.4962(4)	0.19801(26)	-0.44463(19)	3.4
C(*a*4)	0.5492(4)	0.17026(28)	-0.34401(19)	3.5
C(*a*5)	0.5235(4)	0. 24271(28)	-0.24060(19)	3.4
C(*a*6)	0.4427(4)	0. 36507(27)	-0.21061(18)	3.1
C(*a*7)	0.3356(4)	0. 48369(26)	-0.26589(19)	3.3
C(*a*8)	0.2815(4)	0. 51138(26)	-0.36617(20)	3.5
C(*b*1)	0. 2903(4)	0. 43042(28)	-0.53741(19)	3.7
C(*b*2)	0. 3418(5)	0. 35744(29)	-0.55602(19)	3.8
C(*b*3)	0. 5668(5)	0. 12059(29)	-0.44450(21)	4.0
C(*b*4)	0. 5976(5)	0. 10341(29)	-0.38306(22)	4.2
C(*b*5)	0. 5426(4)	0. 25036(29)	-0.17288(19)	3.8
C(*b*6)	0.4925(4)	0. 3237(3)	-0.15406(19)	3.7
C(*b*7)	0.2874(5)	0. 56762(27)	-0.26757(20)	3.7
C(*b*8)	0.2555(5)	0. 58481(26)	-0.32938(21)	4.0
C(*m*1)	0. 4487(4)	0. 23761(26)	-0.49964(19)	3.2
C(*m*2)	0. 5654(4)	0. 17622(28)	-0.27768(18)	3.3
C(*m*3)	0. 3862(4)	0. 44450(26)	-0.21087(18)	3.2

C(*m*4)	0. 2649(4)	0. 50513(26)	-0.43288(19)	3.3
C(1)	0.4725(5)	0. 20021(26)	-0.56443(19)	3.5
C(2)	0. 5886(5)	0.2129(3)	-0.59448(23)	4.7
C(3)	0. 6057(5)	0.1882(4)	-0.65769(25)	5.7
C(4)	0.5064(6)	0.1494(3)	-0.69009(22)	4.8
C(5)	0.3910(6)	0.1345(3)	-0.66049(24)	5.1
C(6)	0. 3734(5)	0. 1601(3)	-0.59788(21)	4.6
C(7)	0.6425(5)	0.1087(3)	-0.24471(20)	3.8
C(8)	0.5828(5)	0.0387(4)	-0.21992(24)	5.1
C(9)	0. 6561(8)	-0.0248(4)	-0.19080(27)	6.1
C(10)	0. 7863(10)	-0.0172(5)	-0.1875(3)	6.0
C(11)	0.8471(7)	0.0520(6)	-0.2107(3)	6.6
C(12)	0.7754(6)	0.1151(4)	-0.23964(24)	5.6
C(13)	0.3884(5)	0.49359(26)	-0.14956(20)	3.4
C(14)	0.2775(5)	0.5116(3)	-0.11663(22)	4.5
C(15)	0.2810(6)	0.5578(3)	-0.06013(23)	5.0
C(16)	0. 3990(7)	0.5880(3)	-0.03807(23)	4.8
C(17)	0.5101(6)	0.5710(3)	-0.07071(24)	4.9
C(18)	0.5060(5)	0.5238(3)	-0.12612(21)	4.3
C(19)	0.2044(5)	0.57705(27)	-0.46893(20)	3.4
C(20)	0.2761(4)	0.62110(28)	-0.51346(22)	4.0
C(21)	0.2187(5)	0.6837(3)	-0.55042(21)	3.4
C(22)	0.0897(6)	0.7023(3)	-0.54301(24)	4.6
C(23)	0.0187(5)	0.6608(3)	-0.49844(27)	5.1
C(24)	0.0747(5)	0.59741(29)	-0.46127(22)	4.5

Table 3.3 Bond lengths(Å) in the [FeCl(TPP)] molecule.

Fe-N(1)	2.060(3)	C(*b*5)-C(*b*6)	1.338(6)
Fe-N(2)	2.078(3)	C(*b*7)-C(*b*8)	1.351(5)
Fe-N(3)	2.066(3)	C(*m*1)-C(1)	1.496(5)
Fe-N(4)	2.077(3)	C(*m*2)-C(7)	1.499(5)
Fe-Cl	2.211(1)	C(*m*3)-C(13)	1.498(5)
N(1)-C(*a*1)	1.382(5)	C(*m*4)-C(19)	1.503(6)
N(1)-C(*2a*2)	1.376(5)	C(1)-C(2)	1.365(6)
N(2)-C(*a*3)	1.380(5)	C(2)-C(3)	1.386(6)
N(2)-C(*a*4)	1.386(5)	C(3)-C(4)	1.364(7)
N(3)-C(*a*5)	1.394(5)	C(4)-C(5)	1.360(7)
N(3)-C(*a*6)	1.379(5)	C(5)-C(6)	1.379(6)
N(4)-C(*a*7)	1.384(5)	C(1)-C(6)	1.384(6)
N(4)-C(*a*8)	1.379(5)	C(7)-C(8)	1.377(7)
C(*a*1)-C(*b*1)	1.432(5)	C(8)-C(9)	1.398(7)
C(*a*2)-C(*b*2)	1.438(5)	C(9)-C(10)	1.342(10)
C(*a*3)-C(*b*3)	1.433(6)	C(10)-C(11)	1.359(11)
C(*a*4)-C(*b*4)	1.433(6)	C(11)-C(12)	1.383(8)
C(*a*5)-C(*b*5)	1.426(5)	C(7)-C(12)	1.370(7)
C(*a*6)-C(*b*6)	1.440(5)	C(13)-C(14)	1.363(6)
C(*a*7)-C(*b*7)	1.429(6)	C(14)-C(15)	1.388(6)
C(*a*8)-C(*b*8)	1.428(6)	C(15)-C(16)	1.377(7)
C(*a*1)-C(*m*4)	1.391(5)	C(16)-C(17)	1.358(7)
C(*a*2)-C(*m*1)	1.397(5)	C(17)-C(18)	1.378(6)
C(*a*3)-C(*m*1)	1.392(5)	C(13)-C(18)	1.383(6)
C(*a*4)-C(*m*2)	1.392(5)	C(19)-C(20)	1.380(6)
C(*a*5)-C(*m*2)	1.383(5)	C(20)-C(21)	1.389(6)
C(*a*6)-C(*m*3)	1.394(6)	C(21)-C(22)	1.368(6)
C(*a*7)-C(*m*3)	1.401(5)	C(22)-C(23)	1.356(7)
C(*a*8)-C(*m*4)	1.401(5)	C(23)-C(24)	1.394(6)
C(*b*1)-C(*b*2)	1.338(6)	C(19)-C(24)	1.380(6)
C(*b*3)-C(*b*4)	1.343(6)		

Table 3.4 Bond angles (º) in the [FeCl(TPP)] molecule.

N(1)FeN(2)	86.4(1)	C(*b*4)C(*a*4)C(*m*2)	125.0(4)
N(1)FeN(3)	151.8(1)	N(3)C(*a*5)C(*b*5)	109.0(4)
N(1)FeN(4)	86.8(1)	N(3)C(*a*5)C(*m*2)	125.8(4)
N(2)FeN(3)	87.0(1)	C(*b*5)C(*a*5)C(*m*2)	125.4(4)
N(2)FeN(4)	153.4(1)	N(3)C(*a*6)C(*b*6)	109.4(4)
N(3)FeN(4)	87.0(1)	N(3)C(*a*6)C(*m*3)	126.4(4)
N(1)FeCl	104.7(1)	C(*b*6)C(*a*6)C(*m*3)	124.4(4)
N(2)FeCl	103.5(1)	N(4)C(*a*7)C(*b*7)	110.0(4)
N(3)FeCl	103.4(1)	N(4)C(*a*7)C(*m*3)	125.6(4)
N(4)FeCl	103.0(1)	C(*b*7)C(*a*7)C(*m*3)	124.4(4)
FeN(1)C(*a*1)	126.2(3)	N(4)C(*a*8)C(*b*8)	110.3(3)
FeN(1)C(*a*2)	126.1(3)	N(4)C(*a*8)C(*m*4)	125.2(4)
FeN(2)C(*a*3)	127.2(3)	C(*b*8)C(*a*8)C(*m*4)	124.7(4)
FeN(2)C(*a*4)	126.2(3)	C(*a*2)C(*m*1)C(1)	116.4(4)
FeN(3)C(*a*5)	125.7(3)	C(*a*3)C(*m*1)C(1)	120.1(4)
FeN(3)C(*a*6)	126.4(3)	C(*a*2)C(*m*1)C(*a*3)	123.4(4)
FeN(4)C(*a*7)	126.8(3)	C(*a*4)C(*m*2)C(7)	117.6(4)
FeN(4)C(*a*8)	127.2(3)	C(*a*5)C(*m*2)C(7)	117.5(4)
C(*a*1)N(1)C(*a*2)	105.9(3)	C(*a*4)C(*m*2)C(*a*5)	124.8(4)
C(*a*3N(2)C(*a*4)	105.6(3)	C(*a*6)C(*m*3)C(13)	118.0(4)
C(*a*5)N(3)C(*a*6)	106.0(3)	C(*a*7)C(*m*3)C(13)	117.7(4)
C(*a*7)N(4)C(*a*8)	105.5(3)	C(*a*6)C(*m*3)C(a7)	124.1(4)
N(1)C(*a*1)C(*b*1)	109.2(4)	C(*a*1)C(*b*4)C(19)	116.9(4)
N(1)C(*a*2)C(*m*4)	126.4(4)	C(*a*8)C(*m*4)C(19)	119.1(4)
C(*b*1)C(*a*1)C(*m*4)	124.3(4)	C(*a*1)C(*m*4)C(*a*8)	124.0(4)
N(1)C(*a*2)C(*b*2)	109.8(4)	C(*a*1)C(*b*1)C(*b*2)	108.1(4)
N(1)C(*a*2)C(*m*1)	126.9(4)	C(*a*2)C(*b*2)C(*b*1)	106.9(4)
C(*b*2)C(*a*2)C(*m*1)	123.2(4)	C(*a*3)C(*b*3)C(*b*4)	107.0(4)
N(2)C(*a*3)C(*b*3)	110.1(4)	C(*a*4)C(*b*4)C(*b*3)	107.9(4)
N(2)C(*a*3)C(*m*1)	125.4(4)	C(*a*5)C(*b*5)C(*b*6)	108.3(4)
C(*b*3)C(*a*3)C(*m*1)	124.5(4)	C(*a*6)C(*b*6)C(*b*5)	107.3(4)
N(2)C(*a*4)C(*b*4)	109.3(3)	C(*a*7)C(*b*7)C(*b*8)	107.1(4)
N(2)C(*a*4)C(*m*2)	125.6(4)	C(*a*8)C(*b*8)C(*b*7)	107.4(4)

According to x-ray analysis iron atom of Fe(III)TPPCl is in a square pyramidal environment and is displaced by 0.57Å from the basal plane of the four nitrogen atoms towards the chlorine atom. From the table it shows the iron(III) ion is coordinated to chloride ion [Fe-Cl = 2.211(1)Å] and four porphrinato nitrogen atoms, averaged [Fe-N = 2.070(9)Å]. This analysis was conclusive for producing crystal structure of Fe(III)TPPCl.

3.2.4 Synthesis of $SiPcCl_2$

In a 1L round bottomed flask equipped with a Liebeg condenser, a thermometer and a nitrogen inlet, a mixture of 1, 3 – diiminoisoindoline (DII) (36.5 g, 0.25 mol), tetrachlorosilane [$SiCl_4$] and *dry quinoline** (415mL) was brought to reflux with stirring (equation 3.1). Reflux was maintained at circa 210 ºC for 30 minutes and then

the reaction mixture was allowed to cool down to room temperature and then filtered. The cooled purple crystalline product was washed with chloroform (300 mL) and identified by infrared spectroscopy. Yield of $SiPcCl_2$ was 56%.

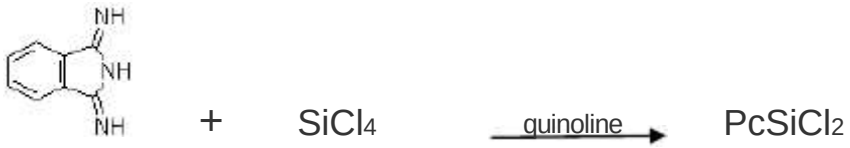

Equation (3.1)

3.2.5 Synthesis of SiPc[4-PyCOO]$_2$

500 mg (0.82 mmol) of $SiPcCl_2$ was dissolved in 10 mL of *dry quinoline** in a round-bottomed flask and fitted with a condenser. The reaction was carried out under nitrogen atmosphere. 5 g (0. 041 mol) of 4-pyridine carboxylic acid was added. The mixture was refluxed for approximately 90 minutes. After cooling for an hour, *dry diethyl ether** was added. The reaction mixture was filtered through a sintered glass funnel and rinsed with dry ethanol several times. The precipitate that formed consisted of dark green crystals. The crude product was dried in an oven overnight at 100^{o}C. Pure $SiPc(PyCOO)_2$ was extracted using soxhlet extraction in chloroform for 5 hours.

Figure 3.7 Axial substitution reaction of $SiPcCl_2$ and 4-pyridinecarboxylic acid[30].

The solvent containing the product was evaporated dry using a rotary evaporator to obtain green powders which was verified as $SiPc(4\text{-}PyCOO)_2$ using electronic absorption and IR spectroscopy. The yield was 20%.

[*Mass Spec*. Calc.: $C_{44}H_{24}N_{10}SiO_4$, molar mass: 784.33; Found: 785.0]

** Drying solvents*

Quinoline *was dried with sodium sulphate overnight and vacuum distilled over zinc chippings very slowly.*

Diethyl ether *was dried by shaking repeatedly with equal amount of aqueos sodium chloride (saturated) in a separating funnel. The layers were allowed to separate (at least for several hours) and the ether layer was extracted and added calcium chloride in a round bottom flask and distilled after 48 hours.*

3.2.6 Attempted Preparation of a Complex between SiPc[PyCOO]$_2$ and Fe(III)TPPCl

This second part of this chapter describes an attempt to produce a complex of the form [Fe(III)TPP-OOCPy]$_2$ SiPc.

Crystallisation of [Fe(III)TPP-OOCPy]$_2$ SiPc was attempted, but crystals were not obtained. Attempts were made to grow the crystals by layering 2:10 (mL) of a methanol/chloroform solution of Fe(III)TPPCl and SiPc[PyCOO]$_2$. After 2 months at room temperature, large, well formed Fe(III)TPPCl crystals were removed. The sample was analysed using x-ray crystallography by Prof C. Frampton[52] at Roche Ltd. The sample that was shown to be Fe(III)TPPCl. SiPc[PyCOO]$_2$ remained in the filtrate and the crystallisation process was not successful.

At the same time, attempts were made to produce new compounds from Fe(III)TPPCl and substituted imidazoles as ligands. Table 3.2 shows the relevant data for the ligands used with Fe(III)TPPCl and the search for the 'right' solvent. X-ray crystallography showed that only Fe(III)TPPCl had been produced.

Table 3.5 Solubility test for substituted imidazoles.

Ligand- substituted Im	H_2O	Methanol	Ethanol	Acetone	$CHCl_3$	Hexane
Guanine	x	§	§	x	x	x
Theophylline	§	§	§	✓	x	x
Urocanic acid	§hot	x	x	§hot	x	x
Cytosine	§hot	x	x		x	x
4,5-Imidazoledicarboxylic acid	x	x	x		x	x
3,4 Pyridinedicarboxylic acid	x	x	§hot		x	x
Imidazole	✓	✓	§hot	✓	✓	x
1-chlorobenzyl –L- histidine	✓	✓	§hot		x	x
4-Imidazoleacetic hydrochloric acid	✓	✓	✓	✓	x	x
5-chloro –1- methyl imidazole	✓	§	✓	✓	✓	x
5,6- dimethylimidazole	✓	✓	✓	✓	x	x
4(5)-Imidazolecarboxyaldehyde	§hot	✓	✓	✓	x	x
4,5-dicyanoimidazole	✓	§	§	§	x	x
4-methylimidazole	✓	✓	✓	✓	✓	x

✓ - soluble x - not soluble § - slightly soluble (cold) §hot - soluble when hot

Solubility data for guanine, theophylline, urocanic acid, cytosine, 4,5-imidazoledicarboxylic acid and imidazole were obtained from the literature[57]. All attempts were unsuccessful. In most of the solutions, Fe(III)TPPCl crystallised out and separately the ligand precipitated slightly in the liquor solution.

Table 3.6 Solubility test for Fe(III)TPPCl.

ORGANIC SOLVENTS	SOLUBILITY
Hexane	x
Chloroform	✓
Acetone	✓
Diethyl ether	✓
Methanol	✓
Ethanol	✓

✓ - *soluble* x - *not soluble*

3.3 Results

3.3.1 Electronic Absorption Spectrum of H_2TPP

The colours of porphyrins are derived from the π - electron system. Often, the electron absorption spectrum of a porphyrin consists of a very intense band at *circa* 410 - 420 nm, known as the Soret band and the satellite bands (α and β) at longer wavelengths. The Soret band is found in all tetrapyrroles in which the nucleus is fully conjugated. It is well known that α corresponds to the lowest π -π^* singlet and β to the Q_v vibronic envelope. These transitions are all doubly degenerate since they are polarised in the plane of porphyrin (Figure 3.9). All the absorption spectra shown in Fig. 3.9, 3.11 and 3.12 were measured on a KONTRON –UNIKON Model 860 series spectrophotometer. All spectra were taken on solutions by using different solvents in quarts cell of 1cm path length. Pure solvents were used as a reference.

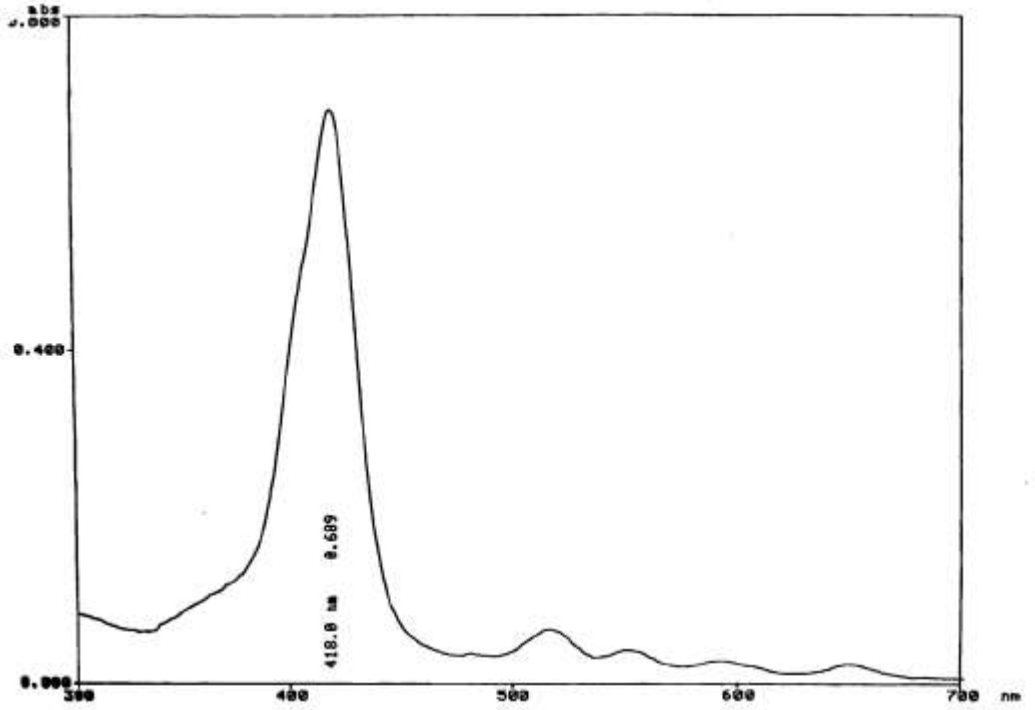

Figure 3.9 The Uv/vis spectrum of H_2TPP.

3.3.2 Infrared Assignments for H_2TPP and Fe(III)TPPCl

All spectra (Figure 3.10, 3.13 and 3.14) reported were obtained with a Perkin- Elmer Model Paragon 1000 FT-IR spectrometer. Potassium bromide discs were prepared for the infrared spectra of H_2TPP and Fe(III)TPPCl. The data are shown below in Tables 3.7 and 3.8, respectively.

Table 3.7 IR assignments for Fe(III)TPPCl

Wavenumber (cm $^{-1}$)	**Assignment[58]**
1473s	C-H bend
1441s	C-H bend
1350s	C=N stretch
1155m	[arene] C=C
1000w	C=C stretch
980s	C-H rock
729s	[arene] C-H bend

Table 3.8 IR assignments for H_2TPP.

Wavenumber (cm $^{-1}$)	**Assignment**
1595m	N-H bend
1440s	C-H bend
1333m	C=N stretch
1175s	
1001	C-H rock
835m	C-H rock
750s	[arene] C-H bend

Band intensity: s=strong, m=medium, w=weak

This important observation for Fe(III)TPPCl (Figure 3.10) is that there is no vibration due to N-H indicating a successful insertion of the iron atom into the centre of the porphyrin system.

The infrared spectrum of $[Fe(III)TPP]_2O$ (dimer) and the Fe(III)TPPCl (monomer) were similar. The only notable difference in the spectrum was the band which appeared at ~835 cm^{-1} in the spectrum for iron-oxide stretches. The dimer compound shows a strong absorption at approximately 878 cm^{-1} in a crystalline state[59]. This clearly proves that prepared sample is monomeric and not the dimeric [Fe(III)TPP]-O-[Fe(III)TPP] compound.

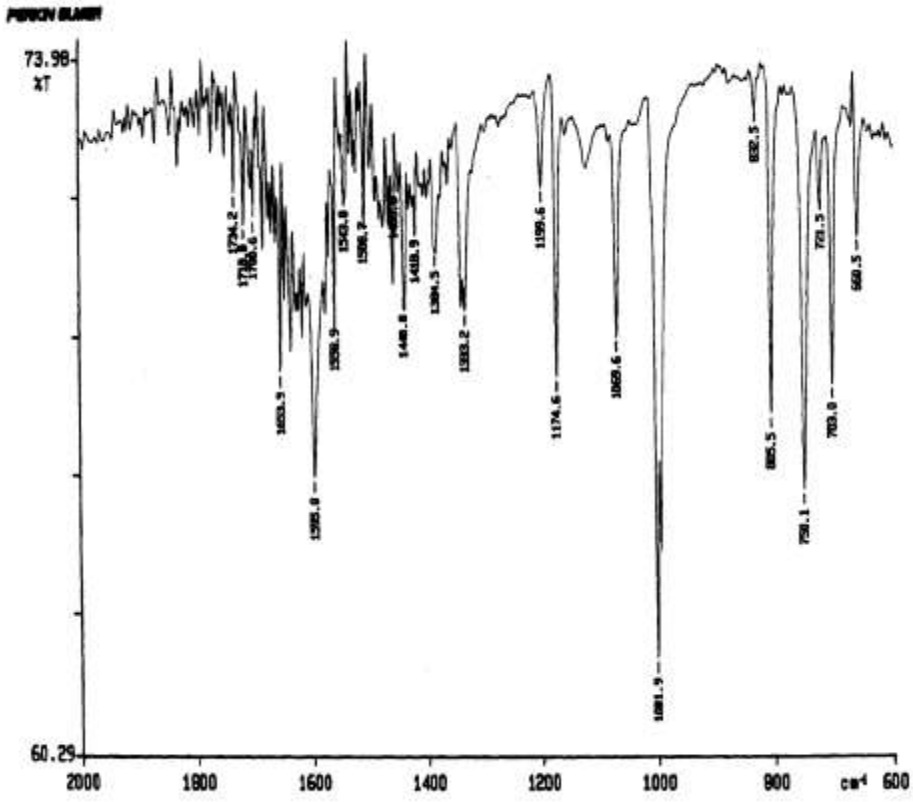

Figure 3.10 The IR spectrum of Fe(III)TPPCl.

3.3.3 Synthesis considerations for SiPc[PyCOO]$_2$

The reaction was carried out under nitrogen atmosphere to prevent hydrolysis and formation of oligomeric compounds caused by the presence of water and oxygen from the atmosphere. The reaction heating times were kept at minimum (1 hour at reflux), as it has been shown that the longer heating times lead to decomposition of product and solvent[50] and also lead to oligomeric species. Heating of the crude product under high vacuum was avoided where possible because of possibility of oligomerisation as well.

A range of methods were applied, none of which resulted in the formation of the desired substituted SiPc without significant contamination from unreacted starting

materials and by-products formed by the side chains. The purity of the crude product was not improved despite variation of the concentrations of the starting reagents.

3.3.4 UV Spectrum of $SiPcCl_2$ and $SiPc[PyCOO]_2$

The electronic absorption spectrum for $SiPcCl_2$ (shown in Figure 3.11), obtained using chloroform as solvent, shows four main bands at 694, 624, 364 and 285 nm. The absorption bands at 694 nm and 624 nm are assigned as the Q-band and its vibronic overtone. The Soret band is split into two separate vibrations, the B_1 - band at 364 nm (higher intensity) and B_2 - band at 306 nm (lower intensity).

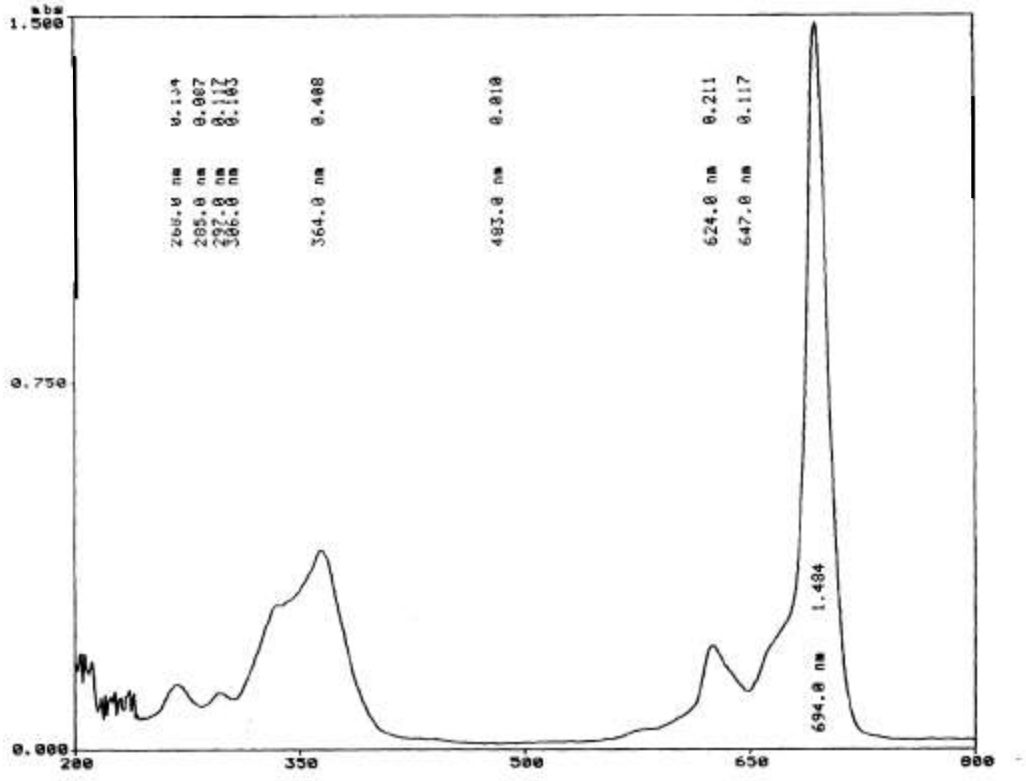

Figure 3.11 Electronic absorption spectrum of $SiPcCl_2$ in chloroform.

The electronic absorption of $SiPc[PyCOO]_2$ in methanol (Figure 3.12) showed a strong absorption at 688 nm (Q band) and the Soret band at around 358 nm. The spectra although similar were different enough to indicate that the Si-O-C interaction was significant between the axially bound substituents. The spectrum clearly showed an overtone at approximately 650 nm (Figure 3.12). Conjugation of the 4-pyridinecarboxylic acid had little effect on the spectrum. Both spectra showed intense optical transitions in the 600 - 700 nm and 300 - 400 nm regions which are analogous to porphyrin "Q-band" and "Soret-band" π-π^* transitions.

The $SiPc[4\text{-}PyCOO]_2$ compound showed solvatochromic (change in the position of the UV-Vis absorption band with a change in solvent polarity) behaviour, which is a useful indicator for NLO activity. The position of the absorption of the $SiPc[4\text{-}PyCOO]_2$ compound was different when recorded in two different solvents - chloroform (Figure 3.12) and chlorobenzene (694 nm, 648 nm, 361 nm and 332 nm). The absorption bands appeared at shorter wavelength in chloroform than chlorobenzene.

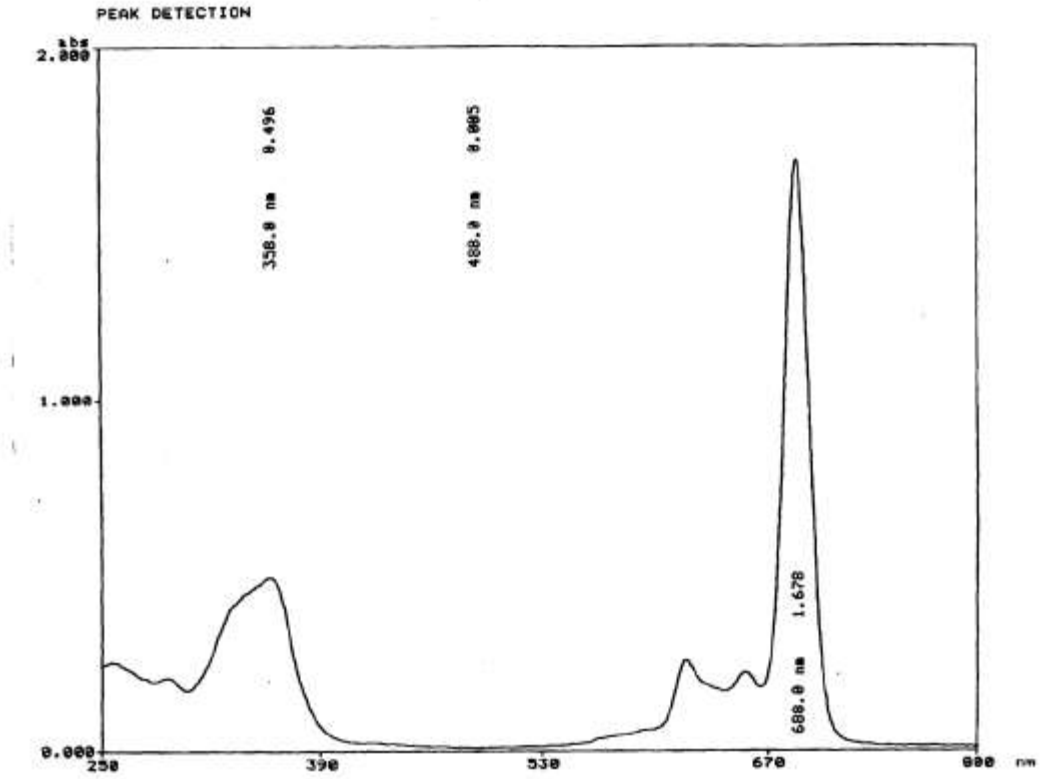

Figure 3.12 The electronic absorption of $SiPc[PyCOO]_2$ in chloroform.

3.3.5 Infrared Spectra of $SiPcCl_2$ and $SiPc[PyCOO]_2$

The infrared spectrum of $SiPcCl_2$ (Figure 3.13) and the axially derivatised silicon phthalocyanine were obtained using KBr discs. The corresponding data are summarised in Table 3.9.

Table 3.9 Infrared frequencies (cm^{-1}) for the silicon phthalocyanine complexes using KBr discs.

$SiPcCl_2$	**$SiPc[PyCOO]_2$**
466s	458m
531m 573m	502m 537m 576m
648vw 693w	668m 684m
733vs 760s 784m	733vs 762s
866vw 883vw	
913s 960m	915s
1060m 1080vs	1070w 1082m
1120vs 1163m	1123vs 1160vw
1290s	1290s
1336vs	1304vs 1323vs 1339vs
1430s 1472m 1490m	1430s 1472m
1532s 1539m 1576m	1533vs 1576m
1635m	1653vs 1684vs
	1733s 1771m

Band intensities: vs=very strong, s=strong, m=medium, w=weak, vw=very weak.

All the assigned range for both compounds are similar except for the Si-O and N-H bonds which exists only in the $Si[4\text{-}PyCOO]_2$.

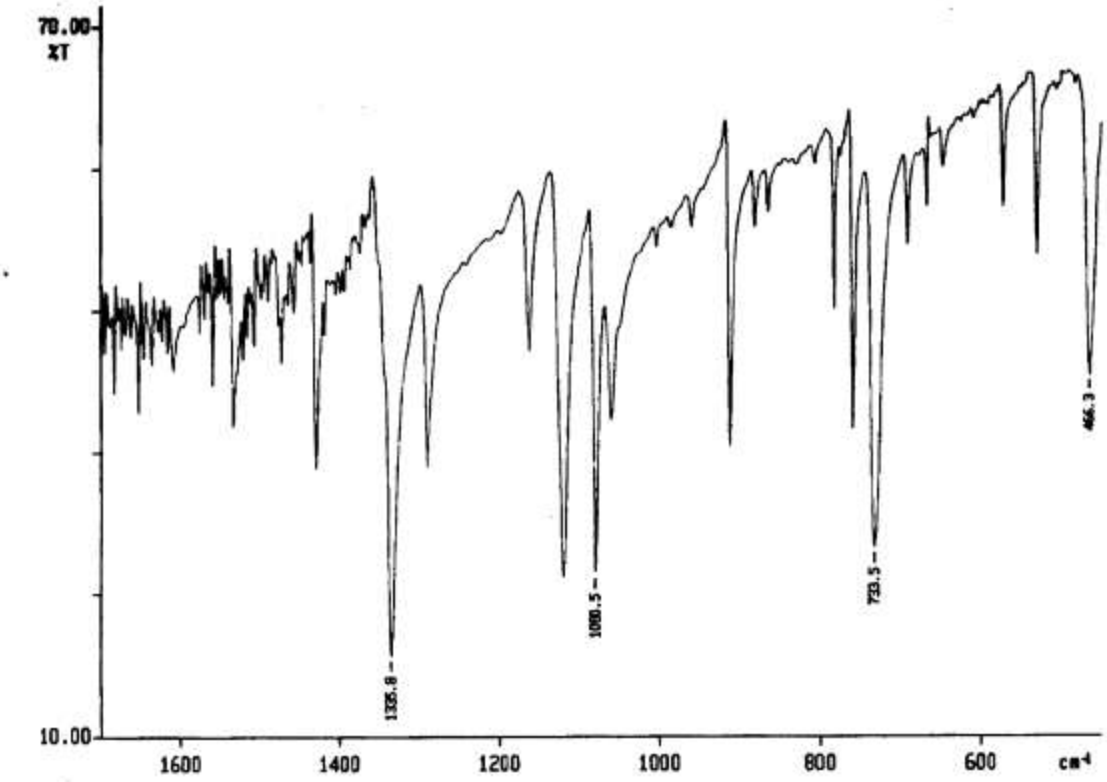

Figure 3.13 The IR spectrum of $SiPcCl_2$.

The IR spectrum exhibits, as expected, the characteristic absorption bands of the phthalocyanine macrocycle. In general, the positions of the absorptions assigned to the macrocycle [Si-Pc] remain relatively constant.

Only a few differences that depend on the nature of the axial ligand bound to the silicon atom were observed. In the $SiPcCl_2$, a strong band at 466 cm^{-1} corresponds to the stretching frequency of the Si-Cl bond and disappears after the reaction. For $SiPc[PyCOO]_2$ the new absorption bands of medium intensity appear between 822-938 cm^{-1} depending on the carboxylic acid (Figure 3.14). The spectrum showed band occurred at 915 cm^{-1}.

- Aliphatic carboxylic acid absorbs at 910-938 cm^{-1}.
- Aromatic carboxylic acid absorbs at 822-852 cm^{-1}.

From the spectrum, C=O stretching mode of carboxylate group was observed at 1684 cm^{-1}. This confirms that a substitution reaction has occurred, but offers little information as to the nature of any contamination.

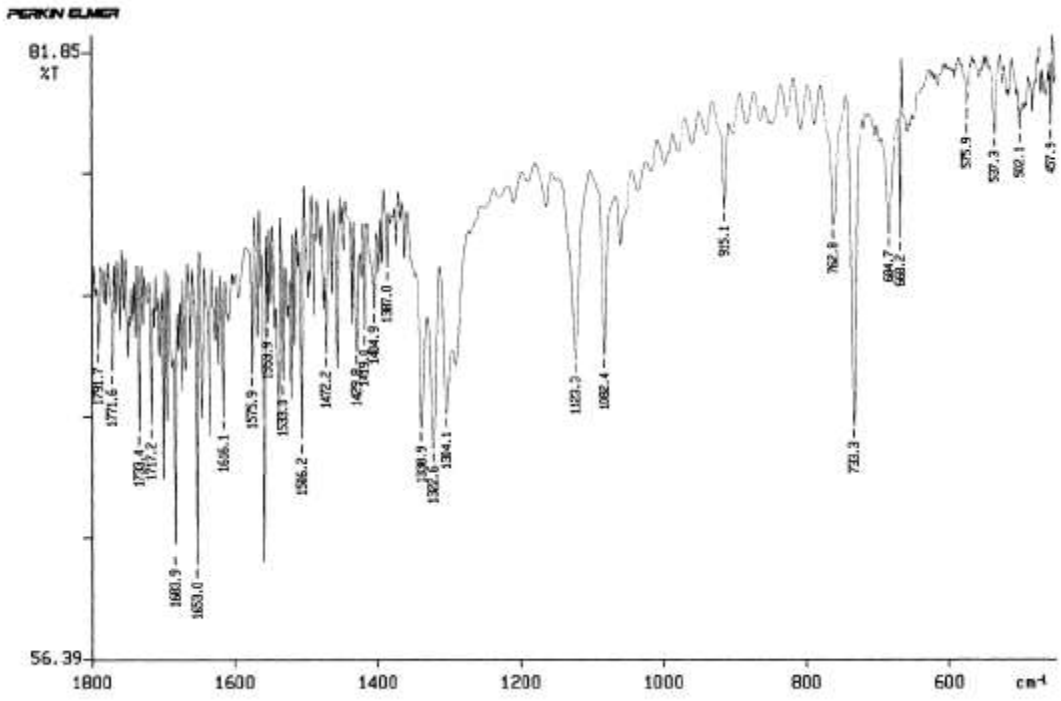

Figure 3.14 IR spectrum of $SiPc[PyCOO]_2$

3.4 Conclusions

The initial aim of the project was to prepare H_2TPP, Fe(III)TPPCl and silicon phthalocyanine *bis* 4-pyridinecarboxylic acid (axially substituted). This part of the experiment was successful.

These compounds were characterised using electronic absorption, IR spectroscopy and mass spectrometry. These confirmed that the $SiPcCl_2$ had been successfully substituted to $SiPc[PyCOO]_2$ and H_2TPP was substituted to Fe(III)TPPCl.

Difficulties were encountered in trying to isolate pure $SiPc[PyCOO]_2$, due to the decomposition of the product on the column, leading to the formation of oligomeric

species and hydroxides with high retention but soluble in solvents in which it is stable.

The NLO properties of the product could not be investigated as accurate measurement of the second harmonic generation and the third harmonic generation requires a higher degree of purity than that achieved in this work.

Recrystallisation of $SiPc[PyCOO]_2$ and Fe(III)TPPCl in chloroform and the attempt to make a larger complex of $[Fe(III)TPP\text{-}OOCPy]_2SiPc$ was unsuccessful. The search for a solvent to provide the most suitable environment for crystallisation of the desired crystal structure was not successful.

The ligand $[4PyCOO]^-$ has a higher affinity towards H^+ than $[Fe(III)TPP]^+$. This is due to steric hindrance and it is also contributed by the solvent chloroform because it is too hygroscopic and therefore any exposure to moisture would have made the crystallisation process impossible.

3.5 References

1. J. E. Falk, *In Comprehensive Biochemist*: *Chemistry and Biochemistry of Porphyrins and Metalloporphyrins,* edited by M. Florkin and E. H. Stotz, Elsevier, New York, **1963**.
2. J. N. Phillips, *In Comprehensive Biochemist*: *Physico-Chemical Properties of Porphyrins*, edited by M. Florkin and E. H. Stotz, Elsevier, New York, **1963**.
3. K. Smith, *In Porphyrins and Metalloporphyrins*: *Spectra of Porphyrins Concerning Isocyclic Ring*, edited by Smith, Elsevier, Amsterdam, **1975**.
4. M. Asanaka, T. Kurimura, H. Toya, J. Ogaki, *J. Anti-HIV activity of photoporphyrin*. **1989**, *Aids 3(6),* 403.

5. E. Ochiai, *Bioinorganic Chemistry*: *Concerning the Metalloenzymes Ascorbate Oxidase.* edited by Allyn and Bacon , Boston, **1977**.
6. http://www.netcomuk.co.uk/~rpeters1/aufe2f.htm
7. A. Bearden, *Bioinorganic Chemistry*, **1975**, 87.
8. B Li, G Gutierrez, L Chen, R Brědy, J. Bernard, G Montague, X Ma, V Bernigaud, B Manil, L Maunoury, B Huber and S Martin, *Journal of Physics: Conference Series*, **2009,** *163*, 12077.
9. http://pubchem.ncbi.nlm.nih.gov/summary/summary.cgi?sid=700018
10. D. M. Collins, R. Countryman and J. L. Hoard, *J. Am. Chem. Soc.*, **1972**, *94(6)*, 2066.
11. I. A. Cohen, C. Jung and T. Governo, *J. Am. Chem. Soc.*, **1972**, *94*, 3003.
12. R.D. Joyner, J. Cekada Jr., R. G. Linck and M. E. Kenney, *J. Inorg. Nucl. Chem.*, **1960**, *15*, 387.
13. R. D. Joyner and M. E. Kenney, *Inorg. Chem.*, **1962**, *1*, 236.
14. P. C. Krueger and M. E. Kenney, *J. Org. Chem.*, **1963**, *28*, 3379.
15. J. N. Esposito, J. E. Lloyd and M. E. Kenney, *Inorg. Chem.*, **1966**, *5*, 1979.
16. M. K. Lowery, A. J. Starshak, S. J. N. Esposito, P. C. Krueger and M. E. Kenney, *Inorg. Chem.*, **1965**, *4*, 128.
17. K. M. Kane, F. R. Lemke and J. L. Peterson, *Inorg. Chem.*, **1997**, *36*, 1354.
18. D. A. Davies, C. Schnick, J. Silver, J. L. Sosa-Sanchez and P. B. Riby, *J. Porphyrins and Phthalocyanines*, **2000**, *4*, 1.
19. S. Pawlenko, *Organosilicon Chemistry*, Walter de Gruyter, Berlin, **1986**, 43.
20. G. Meyer and D. Worhle, *Die. Makrom. Chem.*, **1974**, *175*, 714.
21. A. B. P. Lever, *Adv. Inorg. Radiochem.*, **1965**, *7*, 27.
22. J. N. Esposito, J. E. Lloyd and M. E. Kenney, *Inorg. Chem.*, **1966**, *11*, 1979.

23. A. R. Kane, R. G. Yalman and M. E. Kenney, *Inorg. Chem*., **1968**, *7*, 2588.

24. A. R. Kane, J. F. Sullivan, D. H. Kenny and M. E. Kenney, Inorg. Chem. **1970**, *9*, 1445.

25. T. Koyama, T. Suzuki, K. Hanabusa and H. Shirai, *Inorg. Chem. Acta*., **1994**, *218*, 41.

26. L. E. Sutton and M. E. Kenney, Inorg. Chem., **1967**, *6*, 1869.

27. C. W. Dirk, T. Inabe, K. F. Schoch Jr. and T. J. Marks, *J. Am. Chem. Soc*., **1983**, *105*, 1539.

28. W. Caseri, T. Sauer and G. Wegner, *Makromol. Chem. Rapid Commun*., **1988**, *9*, 651.

29. L. Oddos-Marcel, F. Madeore, A. Block, D. Neher, A. Ferenz, H. Rengel, G. Wagner, C. Kryschi and H. P. Trommsdorff, *J. Phys. Chem*., **1996**, *100*, 11850.

30. D. A. Davies, *PhD Thesis*, Essex University, **1998**.

31. K. Kasuga and Tsuitsui, *Coord. Chem. Rev*., **1980**, *32*, 67.

32. R. L. M. Allen, *Colour Chemistry*, Tomas Nelson and Sons Ltd., London, **1971**, 231.

33. E. Benhur, M. M Zuk, Sc Chin, D. Banerjee, M. E. Kenney and B. Horrowitz, *Photochem. and Photobiol*., **1995**, *62*, 572.

34. A. Segalla, C. Milanesi, G. Jori and K. Schieweck, *Br. J. Cancer*, **1994**, *69*, 817.

35. H. Chen, M. Wang and S. Yang, *J. Polymer Sci. A.*, **1997**, *35*, 959.

36. N. J. Long, *Angew. Chem. Int. Ed. Eng*., **1995**, *34*, 21.

37. G. Dela Torre, T. Torres and F. Agulla-Lopes, *Adv. Mat.*, **1997**, *9*,265.

38. M. Tian, T. Wada, H. Kimura-Suda and H. Sasabe, *J. Mat. Chem.*, **1997**, *7*, 861.

39. J. L.Sosa-Sanchez, *PhD Thesis*, Essex University, **1997**.

40. G. F. Reynolds, *Physics and Chem. Of the Organic Solid State*, edited by. D. Fox, M. M. Labes and A. Weissberger, Wiley InterScience, New York, **1963**, 223.

41. C. Bridle and T. R. Lower, *Acta Cryst.*, **1965**, *19*, 483.

42. L. M. Harwood and C. J. Moody, *Experiments of Organic Chemistry: Principles and Practice*, Blackwell Scientific, Oxford, **1987**.

43. P. J. Jones, *Crystal Growing*, *Chem. In Britain*, **1981**, *17*, 222.

44. T. Kottke and D. Stalke, *Journal of Applied Cryst.*, **1963**,

45. H. E. Buckley, *Crystal Growth*, Wiley, London, **1951**.

46. *Advanced Crystal Growth*, edited by. P.M. Dryburgh, B. Cockayne and K. G. Barraclough, Prentice Hall International (UK) Ltd., **1987**.

47. J Peterson, L. K. Steinrauf and L. H. Jensen, *Acta Cryst.*, **1960**, *13*, 104.

48. J. W. Jeffery and K. M. Rose, *Acta Cryst.*, **1964**, *17*, 343.

49. Raymond Chang, *Physical Chem with Application to Biological Systems*, 2nd edition, MacMillan Publishing Co. Inc., New York, **1981**.

50. R. Rafaeloff, F. J. Kohl, P. C. Krueger and M. E. Kenney, *J. Inorg Nucl. Chem.*, **1966**, *28*, 899.

51. P. J. Marsh, PhD Thesis, Essex University, **1996**.

52. A. Adler, F. R. Longo, J. D. Finarelli, J. Goodmacher, J. Assour and L. Karsakoff, *J. Org. Chem.*, **1967**, *32*, 476.

53. P. Rothemund and R. Menotti, *J. Am. Chem. Soc.*, **1941**, *63*, 267.

54. Professor C. Frampton, Roche Discovery Welwyn, Broadwater Road, Welwyn City Garden, Hertfordshire AL7 3AY.

55. D. D. Perrin and W. L. F. Armarego, *Purification of Laboratory Chemicals*, 3rd Edition, Pergamon Press, Oxford, New York, Beijing, Frankfurt, Sao Paulo, Sydney, Tokyo & Toronto, **1988**.

56. *CRC Handbook of Phys. & Chem*., CRC Press, Boca Raton, 77th edition, **1996**.

57. J. E. Falk, *Porhyrins and Metalloporphyrins* Elsevier Publishing Co., Amsterdam, London, New York, B. B. A. Library, **1964**.

58. E. Ciliberto, K. A. Doris, W. J. Pietro, G. M. Reisner, D. E. Ellis, I. Fragala, F. H. Herbstein, M. A. Ratner and T. J. Marks, *J. Am. Chem. Soc.,* **1984**, *106,* 7748.

59. E. B. Fleischer, J. M. Palmer, T. S. Srivatsa and A. Chatterjee, *J. Am. Chem. Soc.*, **1971**, *93:13,* 3162.

Chapter 4: A High Pressure Mössbauer Spectroscopy Study of 2,3,7,8,12,13,17,18 - Octaethylporphyrin ^{57}iron(III) chloride [^{57}Fe(III)OEPCl]

4.1 Introduction

Porphyrins are ubiquitous class of naturally occurring compounds with many important biological representatives including haems, chlorophylls, haemoglobin, myoglobin and a wide range of cytochromes[1].

There are additionally a multitude of synthetic porphyrinoid molecules that have been prepared from basic research, to functional applications in society[2]. All of these molecules share a common porphyrin macrocycle substructure. The basic structure of the porphyrin macrocycle consists of four pyrollic subunits linked by four methine bridges (Figure 4.1) and the complete system itself is described in detail in Chapter One of this thesis.

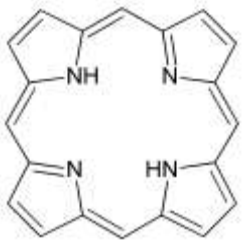

Figure 4.1 Structure of porphyrin macrocycle[3].

Protoporphyrin IX iron(II/III) [PPIXFe(II/III)] (haem) is the most common porphyrin. As a result of the importance of iron porphyrins in biochemistry, the literatures on porphyrins and metalloporphyrins are extensive; reviews regularly appear and an extensive series of books have been written on this subject. Distorted porphyrin macrocycle was recently studied to understand the stabilisation of iron oxidation state by Patra *et al*[4] .

Many synthetic porphyrins have been studied to model the structure and the reactions of haemproteins[5]. One of the reasons for this is that PPIXFe(II/III) is difficult to crystallise but at the same time Fe(III)TTP[6-10], as illustrated in Chapter 3, or Fe(OEP)[11, 12] compounds can readily crystallise.

In this chapter, Mössbauer spectroscopy was used to study the spin state and its changes in [^{57}Fe(III)OEPCl] under high-pressure conditions. This area of study is an extension of previous work on [^{57}Fe(III)PPIXCl] using the same technique[13]. Evidence was found for a change in the spin state from high to its spin admixed $S = \pm 3/2, \pm 5/2$ state.

Fe(III)(OEP) compounds are by reason of their symmetry, high solubility and stability amongst the most important and widely used models for the study of porphyrin chemistry.

4.1.1 The Fe(III)(OEP) and Fe(III)(PPIX) Systems

The structure of the porphyrin core (Figure 4.2) and the numbering of positions that can be substituted are shown in Figure 4.3.

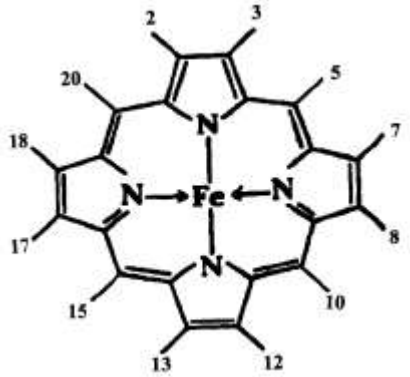

Figure 4.2 Porphyrin core showing substituent numbering system

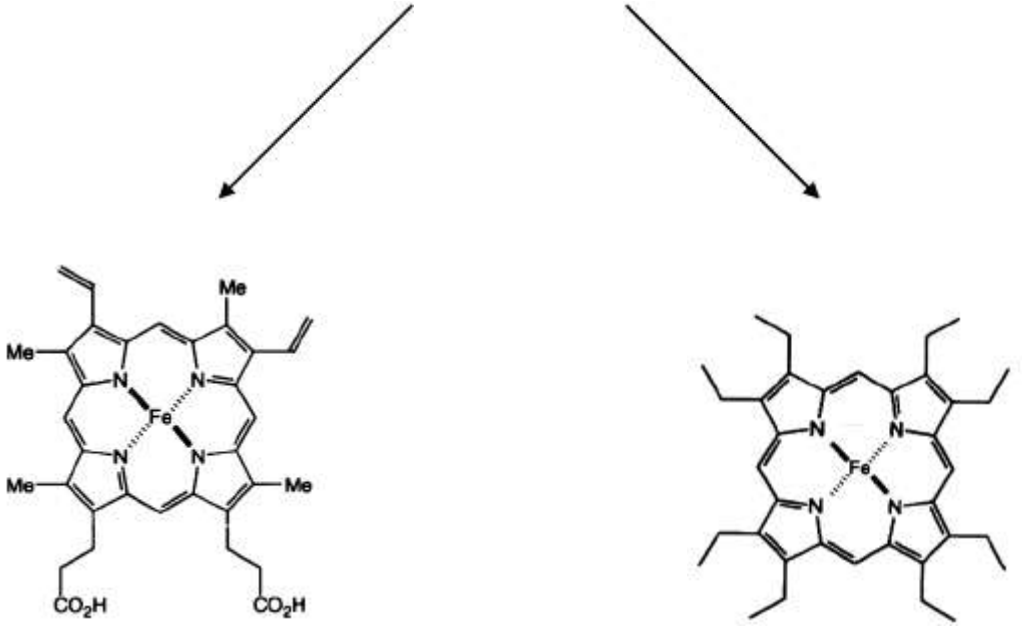

Iron protoporphyrin IX (FePPIX) Iron octaethylporphyrin (FeOEP)

For PPIX: 2, 7, 13, 17 = Me 3, 9 = $CHCH_2$ 12, 18 = CH_2CH_2COOH

For OEP: 2, 3, 7, 8, 12, 13, 17, 18 = CH_2CH_3

Figure 4.3 Porphyrin substitution and compounds[14] studied in this work.

Table 4.1 illustrates the substitution patterns and abbreviations of some porphyrins discussed in this thesis.

Table 4.1 Porphyrin substituents and names.

Porphyrin	2	3	5	7	8	10	12	13	15	17	18	20
TPP			Ph			Ph			Ph			Ph
OEP	E	E		E	E		E	E		E	E	
PPIX	M	V		M	V		M	Pr		Pr	M	
OETPP	E	E	Ph	E	E	Ph	E	E	Ph	E	E	Ph
OMTPP	M	M	Ph	M	M	Ph	M	M	Ph	M	M	Ph
OMTBP	-B-			-B-			-B-			-B-		
TpivPP			N			N			N			N

TPP = tetraphenylporphyrin, OEP = octaethylporphyrin, PPIX = protoporphyrin IX, OETPP = octaethyltetraphenylporphyrin, OMTPP = octamethyltetraphenylporphyrin, OMTBP = octamethylbenzoprophytin and TpivPP = tetra(o-pivalamidephenyl)porphyrin.

Blank space = H, M = CH_3, V = CH_2CH, E = CH_3CH_2, Pr = CH_2CH_2COOH, Ph = C_6H_5,

B = fused dimethyl benzene across bond between two positions and N = o-$NHCOC(CH_3)_3C_6H_4$

The chemistry of Fe(PP)IX and its derivatives has been extensively studied using Mössbauer spectroscopy of solids and frozen solutions[4, 5, 15-18]. This technique gives direct information on both the valence state of the iron and the spin state. The Mössbauer parameters can be compared to the synthetic iron porphyrins with known structures.

The Mössbauer spectra of iron porphyrins and the factors affecting the parameters have been well documented in the literature[4].

Iron(III) porphyrins can be split into three different categories, depending on the spin state, these are: - low spin, $S = {}^{1}/_{2}$, high spin, $S = {}^{5}/_{2}$ and admixed spin, $S = {}^{5}/_{2}$, ${}^{3}/_{2}$. Theoretically it is also possible to have an intermediate spin state, $S = {}^{3}/_{2}$. The spin state[7] depends on the electronic distribution in the *d* orbitals (Figure 4.4).

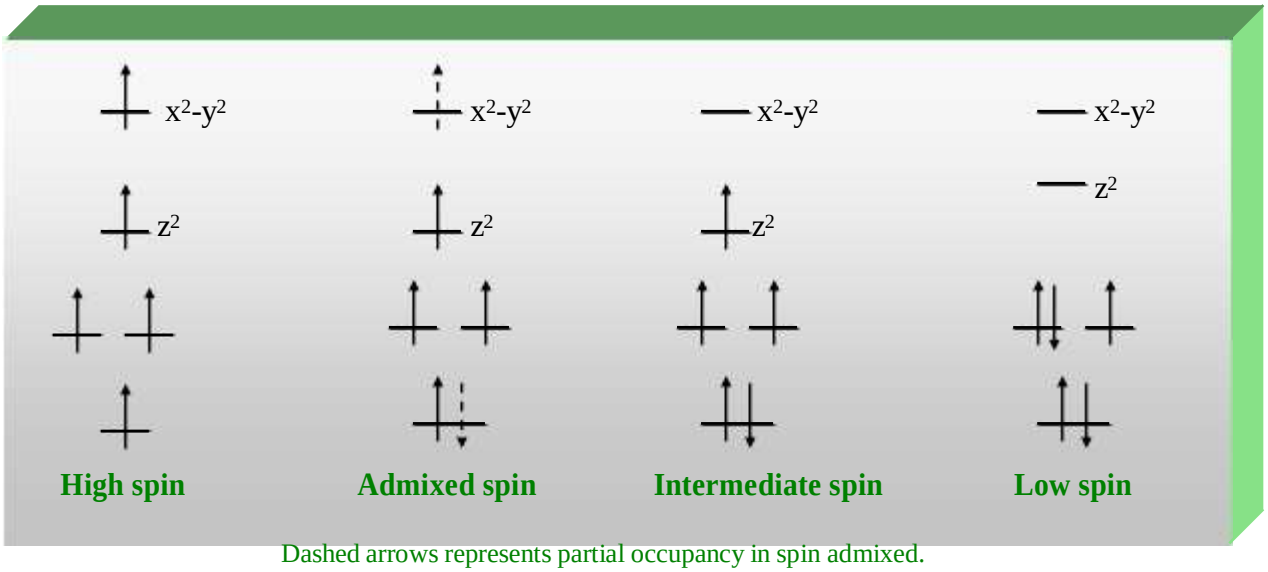

Figure 4.4 Spin states of porphyrins[4].

High spin iron(III) porphyrins are normally five coordinate with the iron resting above the plane of the porphyrin, as shown in Figure 4.5, however some six coordinate high spin iron(III) porphyrins are known where two different ligands coordinate to the axial positions[4]. Examples of five coordination are Fe(III)TPP(Cl) and Fe(III)TPP(NO_3).

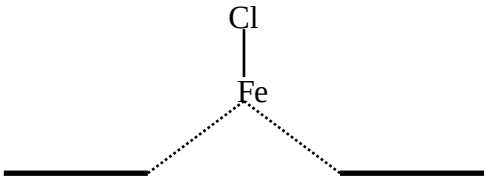

Figure 4.5 Plane of porphyrin on side view. Porphyrin = Fe(III)TPPCl.

The intermediate and admixed spin states of iron(III) porphyrin complexes have been a major interest in research[4-12, 15-25]. It is important to understand their properties in the biologically important haem containing proteins. Complexes of these types are common and found to be more accurately described as quantum mechanical $S = {}^{5}/_{2}, {}^{3}/_{2}$ spin state admixtures at room temperatures rather than truly $S = {}^{3}/_{2}$ intermediate spin[25]. The production of an iron porphyrin system with a pure $S = {}^{3}/_{2}$ spin state has been described; a species that displays a purely $S = {}^{3}/_{2}$ spin state would be a bare iron(III) porphyrin complex, its formulation would be $[Fe(Por)]^{+}$ (Por = porphyrin).

The resulting tetragonal ligand field would cause one *d* orbital (the d_{x2-y2}, the orbital directly facing the porphyrinato nitrogen atoms) to be raised in energy above the other four. This orbital would then be empty in a d^5 state and a pure $S = {}^{3}/_{2}$ state would then exist[26] (see Figure 4.4). However, the synthesis of a pure cationic porphyrin complex of the same type $[Fe(Por)]^{+}$ is not facile. It has been shown that a truly non coordinating ligand does not exist, even in the case of the complex $[Fe(TPP)(SbF_6)]$ the SbF_6 is bonded through a Fe-F bond of 2.105(3)Å. The iron is only a small distance out of the mean porphyrin plane and a nearly pure $S = {}^{3}/_{2}$ spin state occurs. The crystal structure of $FeTPP(ClO_4)$ contains the shortest M-O bond observed for a perchlorate complex.

Other admixed spin iron(III) complexes have been shown to exist as dimers in the solid state, with inner porphyrin plane distances of circa 3.8 Å[9]. It is also interesting to note that the Fe-Cl bond lengths in the spin admixed Fe(OMTPP)Cl [2.24(3) Å] and Fe(OETPP)Cl [2.418(23) Å] compounds appear comparable to that in FeTPPCl

[2.211(1) Å] and that the latter is a high spin complex whereas the two former complexes show spin admixed characteristics[27].

Two perchlorate derivates of 2,4,6-trimethoxyphenylporphyrinato iron(III) have been claimed to be true intermediate spin complexes at room temperature[28]. Complexes such as haemin and haematin have been discussed by others and have been shown to have properties [magnetic moments in the solid state] that are consistent with some admixed $S = 5/2, 3/2$ character, at least in the solid state[29]

These complexes and most of the others with well-characterised $S = 5/2, 3/2,$ spin admixed species are non-naturally occurring methine substituted porphyrins. The only pyrrole ring substituted iron(III) porphyrins showing such an admixed spin state is Fe(III)OEP. The side group (methyl) on the pyrrole ring is electron donating. The total number of substituents on the pyrrole ring of PPIX is eight. These are made up of four methyl groups (electron donating), two vinyl groups (electron withdrawing) and two propionic acid chains (electron withdrawing when protonated) one per pyrrole ring (Figure 4.3). Therefore PPIX is much less electron rich than OEP.

Low spin iron(III) porphyrins result from the coordination of ligands producing a strong field across the axial positions of a distorted octahedral with the equatorial positions coordinating to the porphyrin N atoms[6].

4.2 Experimental

All chemicals were used as purchased [Aldrich] except for isopropanol (IPA), which was dried according to the method to Perrin[30]. Iron-57 was purchased from AMT Chemicals Co. Ltd. Electronic absorption spectra were recorded on a Perkin Elmer λ3 spectrometer. Ambient and high-pressure Mössbauer spectra at room temperature

were recorded using the previously reported apparatus. The spectra and instrument used to measure and record for this experiment was described in detail in Chapter Two. For high pressure Mössbauer the experiment was conducted in Bayerisches Geoinstitut, Universitat Bayreuth, Germany. The spectra were recorded using a modified Merill-Basett diamond anvil cell (DAC) under hydrostatic pressure using the previously reported system[31]. Methanol:ethanol = 4:1 (v/v) was used as the hydrostatic fluid. The pressure in the cell was recorded using the ruby fluorescence method[32].

4.2.1 Methods

4.2.1.1 Synthesis of H_2OEP

The synthesis is multi step and very difficult. After several attempts, H_2OEP was produced from scratch. As illustrated in Figure 4.6, there are several steps involved in obtaining H_2OEP.

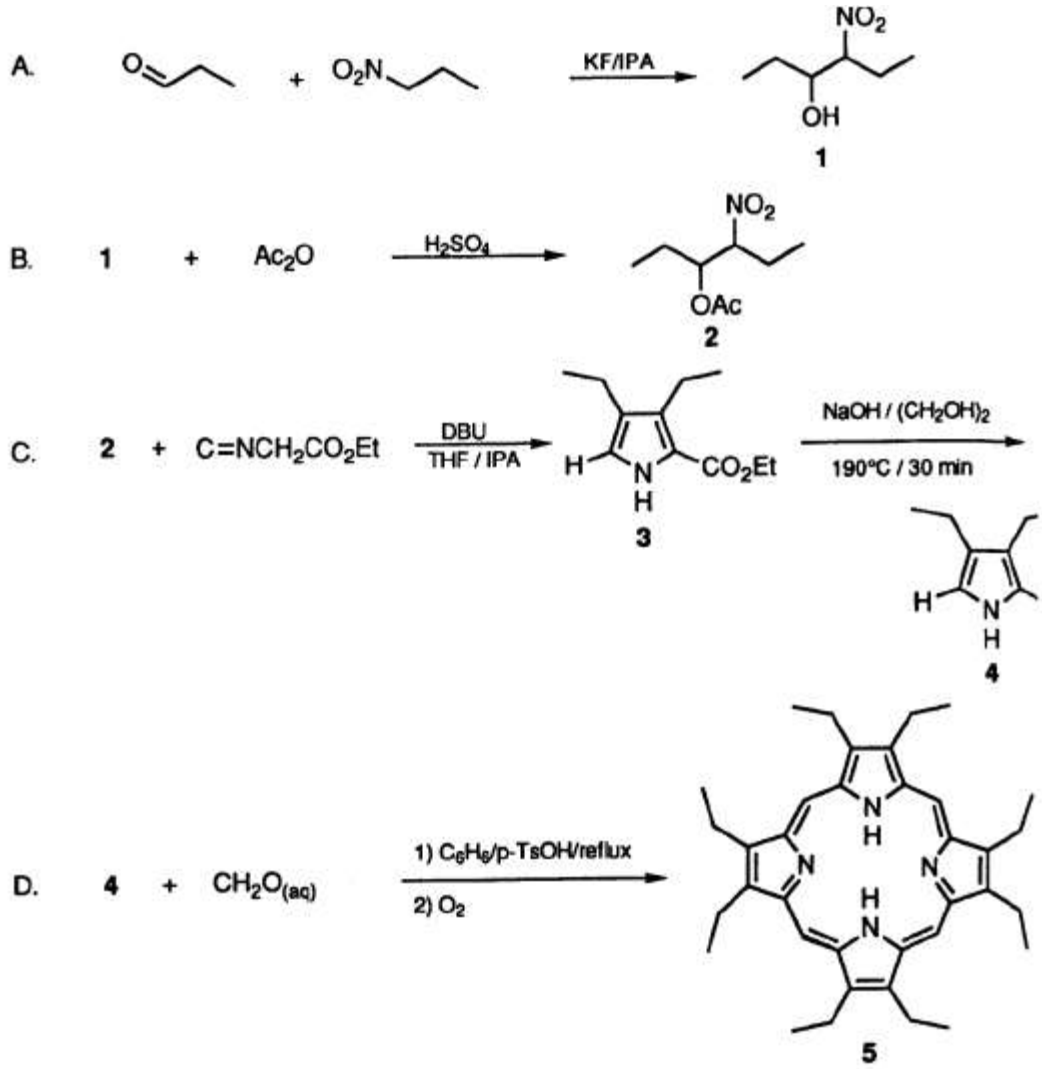

Figure 4.6 Synthesis of H_2OEP[34].

A. Synthesis of 4-Nitro 3-hexanol

Propionaldehyde (174 g, 3 mol) and propan-2-ol (450 mL) were added to a 2 L three necked, round bottomed flask equipped with a mechanical stirrer, thermometer, dropping funnel, and drying tube. To this solution potassium fluoride (KF) (25 g, 0.15 mol) was very carefully added. 1-nitropropane (267.3 g, 3mol) was then added drop wise with continuous stirring and the temperature was maintained below 40ºC with the aid of an ice bath. This flask was then stirred for an additional 24 hours.

The catalyst (KF) was then removed and the filtrate was concentrated under reduced pressure, the ice-bath had been removed at this stage. The residue was then poured

into water (500 mL) and the oil was then extracted with ether (3 x 300 mL). The ethereal layer was dried over anhydrous sodium sulfate (Na_2SO_4) and the solvent was removed under reduced pressure. The remaining liquid was distilled and the fraction boiling at 88-90ºC was collected, yielding 3-nitro-4 hexanol [yielding 285 g, 56%]. The flask containing the product was used directly for the next step.

^{1}H NMR ($CDCl_3$): δ 0.99 (s, 6H CH_3), 1.03 and 1.05 (2s, 2H $O_2NCHCH_2CH_3$), 4.38 (s, 1H $CHNO_2$), 9.78 (s, 1H OH)

B. Synthesis of 4-Acetoxy- 3-nitrohexanol

To a round bottom flask containing 3-nitro-4 hexanol (285 g, 1.93 mol) and 1 mL of concentrated sulphuric acid was added and the reaction was stirred. The reaction mixture was then stirred in an ice bath and acetic anhydride (240 g, 2.35 mol) was added in aliquots, keeping the temperature below 60ºC throughout the addition. After the addition of acetic anhydride was complete, the contents of the flask were stirred for one hour.

The lower boiling components (Ac_2O and AcOH) were removed by evaporation under a pressure of 25 mm Hg by gently heating the stirred contents and keeping the temperature below 100ºC throughout. Upon removal of these components the fraction boiling at 105-107ºC/10 mm was collected and verified using CHN analysis and NMR 1H spectroscopy to be 4-acetoxy 3-nitrohexanol. Yield was 80%

^{1}H NMR ($CDCl_3$): δ 0.98 (s, 6H CH_3), 1.58 (2s, 2H $O_2NCHCH_2CH_3$), 1.99 (s, 2H CH3CO2CHCH$_2$CH$_3$), 4.47 (s, 1H $CHNO_2$) 5.20 (d, 1H CH_3CO_2CH).

[*Anal.* Calc. For $C_8H_{15}NO_4$: C, 50.78; H, 7.99; N, 7.40 %; Found C, 50.12; H, 8.21; N, 7.02 %].

C. Ethyl 3, 4-diethylpyrrole- 2-carboxylate

A 1 L, three necked, round bottomed flask was equipped with a magnetic stirrer bar, a dropping funnel, thermometer and drying tube and was charged with a 4-acetoxy 3-nitrohexane (103 g, 0.54 mol), ethyl isocyanate (50.7 g, 0.45 mol), anhydrous tetrahydofuran (THF) (320 mL) and anhydrous IPA (130 mL).

1, 8-diazabicyclo[5.4.0]undec-7-ene (DBU) (152 g, 1 mol) was added, maintaining the temperature between 20-30ºC at all times with the aid of an ice bath. When the addition of DBU was complete, the orange solution was stirred for 4 hours at room temperature. The solvent was completely removed under reduced pressure (50ºC bath temperature, 20-30 mm Hg) and the residue was poured into a 1L beaker and diluted with warm water (300 mL). To this mixture diethyl ether (300 mL) was then added. The contents of the beaker were poured into a separating funnel. The aqueous layer was drawn off and extracted with an additional two portions of ether (300 mL). The ether layers were combined and washed with aqueous 10% hydrochloric acid (2 x 300 mL) and dried over magnesium sulfate ($MgSO_4$). The ether was removed under reduced pressure, leaving approximately 80g of crude ethyl 3,4-diethylpyrrole 2-carboxylate. This crude product was then isolated as follows:

To the crude product sodium hydroxide (30 g, 0.75 mol) was added, followed by ethylene glycol (300 mL). The contents were held at reflux under nitrogen for 1 hour, cooled, transferred to a 2 L separating funnel and diluted with water (500 mL) and hexane (3 x 300 mL). The hexane layers were combined, dried over $MgSO_4$, and concentrated under reduced pressure. The residue was distilled under reduced pressure, and the fraction boiling at 100ºC was collected, yielding 36% of 3,4-diethylpyrrole (20.25g). ^1H NMR ($CDCl_3$): δ 1.62 (t, 6H CH_2CH_3), 2.47 (q, 4H CH_2CH_3), 6.28 (d, 2H pyrrole H), 7.41 (s, 1H pyrrole 1H).

D. Synthesis of 2,3,7,8,12,13,17,18-Octaethylporphyrin (OEP)

A 500 mL round bottomed flask was wrapped with foil and equipped with a reflux condenser with a Dean-Stark trap, mechanical stirrer and nitrogen inlet. The flask was charged with 3,4-diethylpyrrole (1 g, 8.1 mmol) and *p*-toluenesulfonic acid (0.03 g, 1.7 mmol), 37% solution of aqueous formaldehyde (0.73 mL, 8.9 mmol) and toluene (300 mL).The mixture was stirred and refluxed under a nitrogen atmosphere for approximately an hour using an oil bath and the water was removed by means of a Dean-Stark trap and condenser, this was then replaced with a fritted glass bubbler. Oxygen was bubbled through the brown mixture and the reaction was stirred for 24 hours. Toluene was removed from the flask by distillation under reduced pressure and the residue was dissolved in chloroform (20 mL). The solution was washed with 1N sodium hydroxide (40 mL) and water (2 x 20 mL). The chloroform solution was concentrated to 5 mL in a 100 mL, round bottomed flask, carefully layered over with methanol (approximately 70 mL) and allowed to stand for 24 hours.

The resulting solid was collected by filtration and dried under reduced pressure. The crude material was recrystallised twice from chloroform : hexane (1:1). The final precipitate was collected by filtration and dried under reduced pressure to yield pure 2,3,7,8,12,13,17,18 –OEP(H_2) as a purple solid. The yield was 30% (325mg)

^{1}H NMR ($CDCl_3$): δ -3.70 (s, 2H NH), 1.92 (t, 24H CH_2CH_3), 4.08 (q, 16H CH_2CH_3), 10.14 (s, 4H meso CH).

[*Anal.* Calc. For $C_{36}H_{46}N_4$: C, 80.84; H, 8.68; N, 10.48 %; Found C, 80.45; H, 8.59; N, 10.25 %].

[UV- vis (chloroform) λ : 399, 500, 530, 565 & 620 nm].

4.2.1.2 Synthesis of Fe(III)OEPCl

Fe(III)OEPCl was prepared following the method reported in the literature[35]. Iron(II) chloride was prepared by adding hydrochloric acid to iron wire until there was no further reaction. Excess hydrochloric acid and water were removed at low atmospheric pressure in a Shlenck tube.

H_2OEP (0.1g, 1.65×10^{-4} mol) was dissolved in DMF (50 mL). Anhydrous iron(II) chloride (0.35 g, 3.85×10^{-3} mol), which was prepared earlier was added. The reaction mixture was heated under refluxing conditions. During the reaction a purple precipitate formed.

After 30 minutes, the reaction mixture was allowed to cool to room temperature. Then it was filtered, washed thoroughly with water and dried.

The precipitate was dissolved in dichloromethane and layered onto the top of a neutral activated aluminium oxide column. Dichloromethane was used as the mobile phase. There was a separation into two bands: one remained at the top of the column; the other passed through the column and was collected.

The dichloromethane was removed by rotary evaporation. The purple solid was collected and verified using Mössbauer and electronic spectra to be Fe(III)OEPCl (the experimental spectroscopic data were in excellent agreement with the known values of Fe(III)OEPCl).

4.2.2 Preparation of enriched ^{57}Fe OEP chloride - [^{57}Fe(III)OEPCl]

The preparation of [^{57}FeOEPCl] was according to Borovkov method[36]. Only anhydrous and purified solvents were used for the synthesis. ^{57}Fe foil (0.01 g, 0.18 mmol) was dissolved in deoxygenated concentrated HCl (2ml) under nitrogen. Two drops of 2, 6-lutidine were added to a solution of H_2OEP[31] (5 mg, 0.09 mmol) in chloroform (3 mL) and anhydrous $^{57}FeCl_2$ (was prepared under sealed condition using Shlenck tube for the iron(II) chloride to remain anhydrous) in chloroform. The reaction mixture was stirred at room temperature for 5 hours. Identification of the product - [^{57}FeOEPCl] was achieved by a comparison of the electronic absorption spectrum of a purchased reference sample.

High-pressure Mössbauer spectra were recorded using a Merrill Basset diamond anvil cell (DAC) under hydrostatic pressure[37] (see Chapter Two; *section two*)

4.2.3 Sample Measurements

In this work on ^{57}Fe[OEP]Cl, the material used was from the same sample preparation and was used for the two spectroscopic runs that was carried out (DAC 1 and DAC 2). Both DACs (diamond anvil cell) were working fine. First of all, the DAC was cleaned to remove any traces of debris from both sides of the diamond surfaces. Silver iodide (AgI) powder was used to set the parallel faces of diamond and to obtain the correct alignment (Figure 4.7).

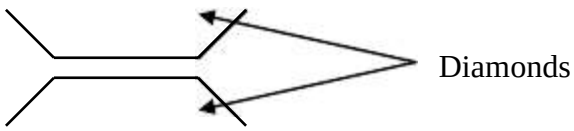

Figure 4.7 Diamond face sitting parallel to each other inside the DAC.

The gasket (tantalum tungsten alloy) then was indented to a thickness of 150 µm and a hole of *circa* 50 µm was drilled. The hydrostatic fluid (4:1 ratio of methanol: ethanol (v/v)) which was used, was prepared prior to use. Then the sample was loaded into the hole in the gasket to obtain all of the measurements (see Figure 4.8). Results from both runs were combined to form a set of results with a trend. It should be noted that repeating a DAC experiment exactly is quite difficult as the application of pressure to the DAC is dependent on the cell, gasket and sample.

Figure 4.8 Picture of a similar DAC and gasket used in the experiment.

In this experiment a Merrill Bassett DAC was used, similar to that shown in Figure 4.8 and where three Allen cap screws required for rotation to achieve a particular pressure. The pressure medium is sealed together with the sample in the gasket hole under microscope. A micrometer is used to measure the thickness for the cell. This makes the actual application of pressure to the sample quite difficult with different

sample loads and required precision work. For the enriched sample, the high pressure Mössbauer spectroscopic measurements each took between 3 to 8 hours to complete.

4.3 Results

The spectra recorded for the variable pressure Mössbauer spectroscopic studies of ^{57}Fe[OEP]Cl are shown in Figures 4.9 and 4.10 The results obtained are presented in Table 4.2. Figures 4.11 and 4.12 show a comparison of the Mössbauer spectra of the ^{57}Fe[PPIX]Cl[13, 38]. The data are presented in Table 4.3.

The results from variable pressure spectra were fitted using software NORMOS 90[39]. In this work ^{57}Fe[OEP]Cl, material from the same sample preparation was used for all spectroscopic work.

The DAC experiment requires several careful operations as it difficult to do. The application of pressure to the DAC is dependent on the cell, gasket and sample. In order to maintain alignment and the parallelism of the anvils it is important to maintain the gasket hole and sample by monitoring the thickness of the sample. The rotation of the Allen cap screws required a fine adjustment to achieve a particular pressure. The data collected during the course of this research are also presented graphically in Figures 4.14, 4.15 and 4.16. Figure 4.13 showed spectra of Fe(PPIX)Cl before and after the application of pressure.

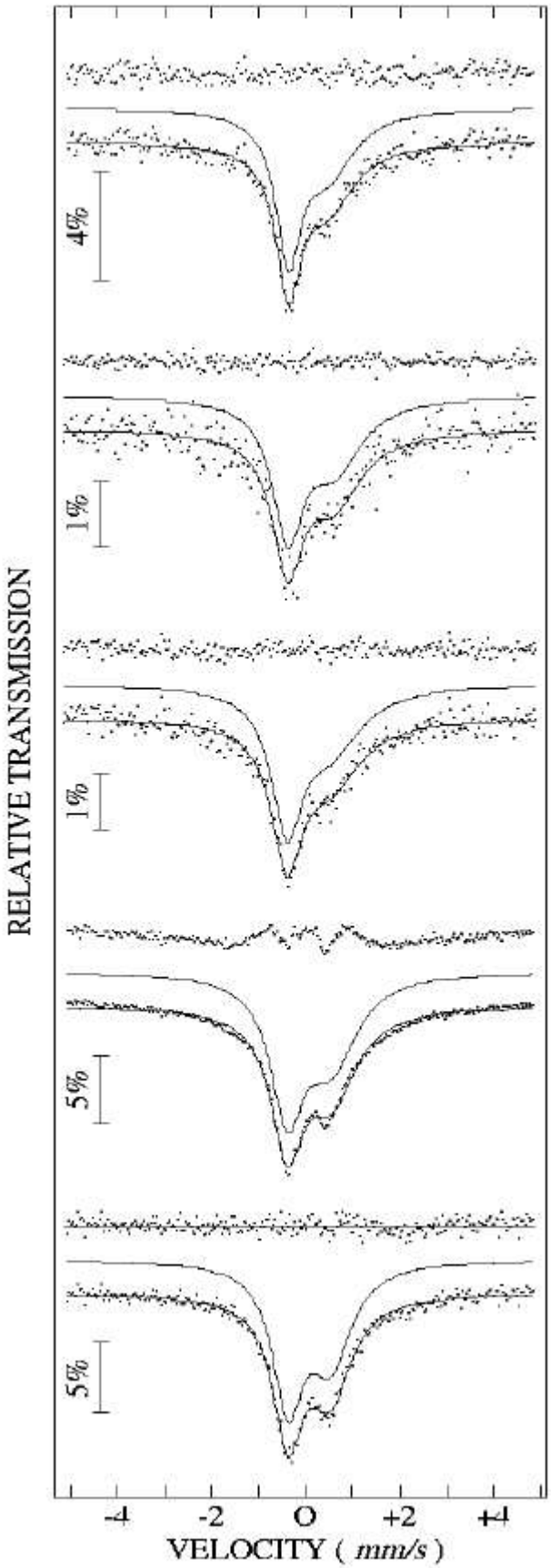

1.38(5) GPa

1.88(5) GPa

2.05(21) GPa

2.57(31) GPa

2.75(20) GPa

Figure 4.9 Mössbauer spectra of varying pressure for ^{57}Fe[OEP]Cl.

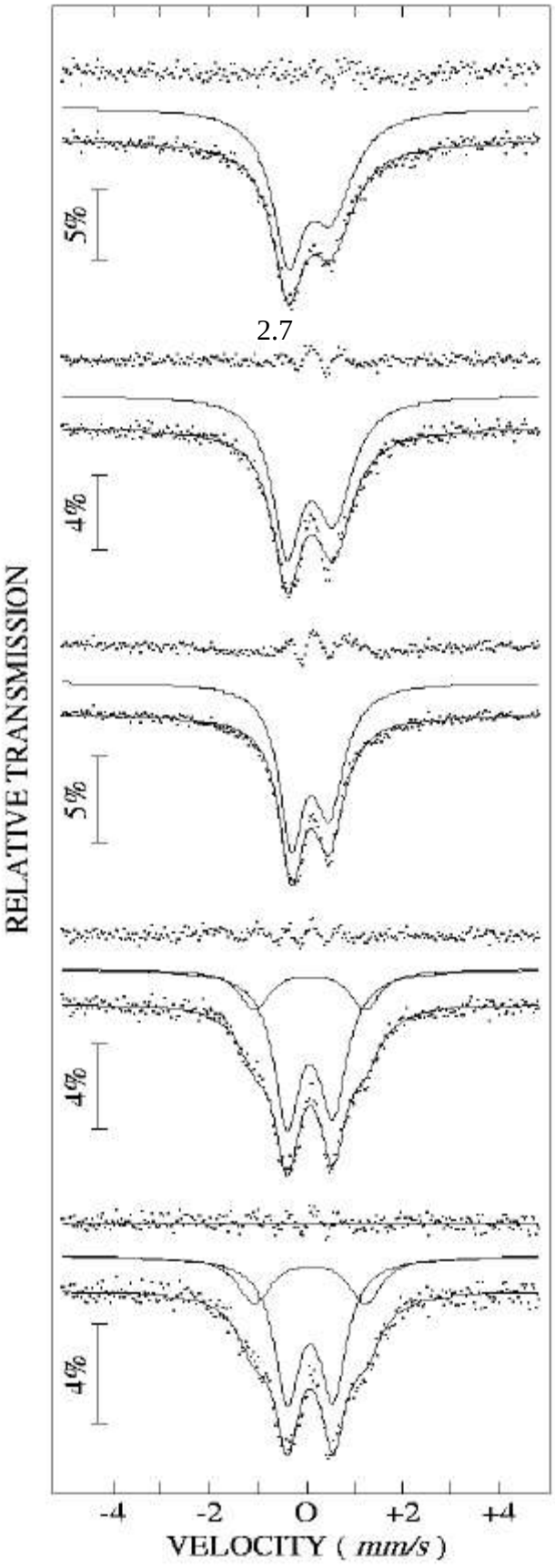

Figure 4.10 Continuing Mössbauer spectra at varying pressure for ^{57}Fe[OEP]Cl.

Table 4.2 Mössbauer spectroscopic parameters for [^{57}FeOEPCl].

Pressure GPa	δ **mms^{-1}**	ΔE_Q **mms^{-1}**	Γ **mms^{-1}**	**% Area**
1.38(5)	0.28(1)	0.82(2)	0.64(2)	100(2)
1.88(5)	0.34(3)	0.98(4)	0.77(5)	100(4)
2.05(21)	0.30(2)	0.91(4)	0.78(3)	100(3)
2.57(31)	0.314(3)	0.937(4)	0.85(1)	100(1)
2.75(20)	0.304(5)	0.898(9)	0.78(1)	100(1)
3.50(23)	0.318(4)	0.968(7)	0.73(1)	100(1)
4.37(24)	0.327(2)	0.783(4)	0.61(1)	100(1)
5.40(33)	0.310(4), 0.31(1)	0.95(1), 2.30(4)	0.65(2), 0.76(6)	76(2), 24(2)
6.30(41)	0.315(1), 0.31*	0.95(1), 2.29*	0.65(2), 0.81(6)	70(2), 30(1)

*Values held in fitting routine.

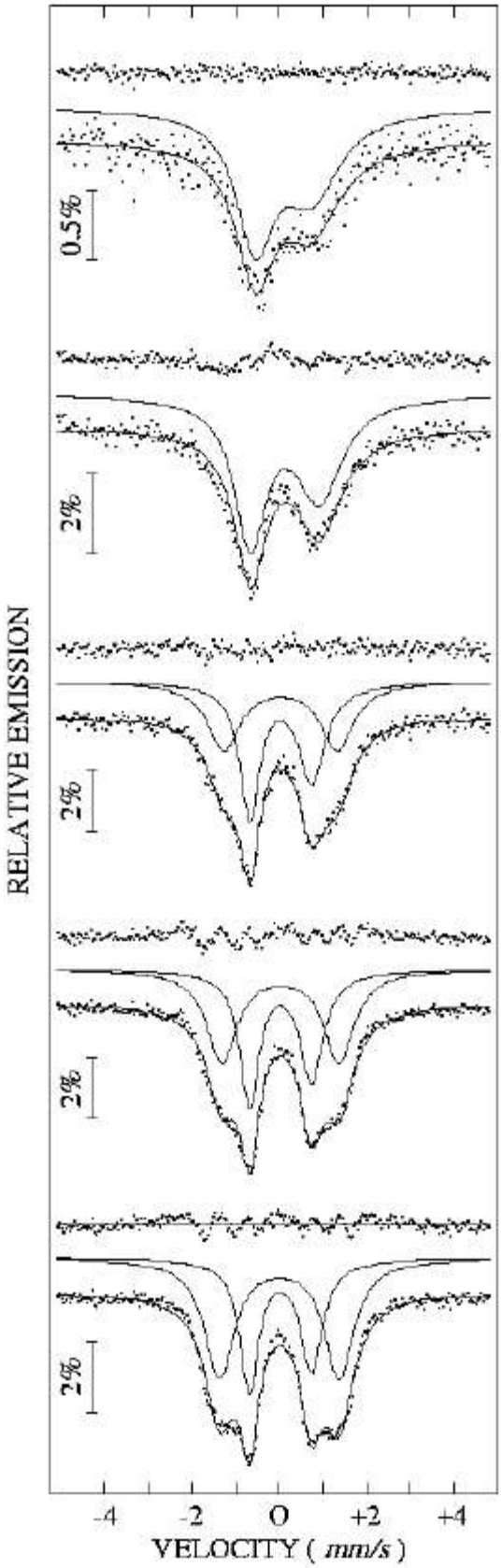

Figure 4.11 Mössbauer spectra of varying pressure for ^{57}Fe[PPIX]Cl.

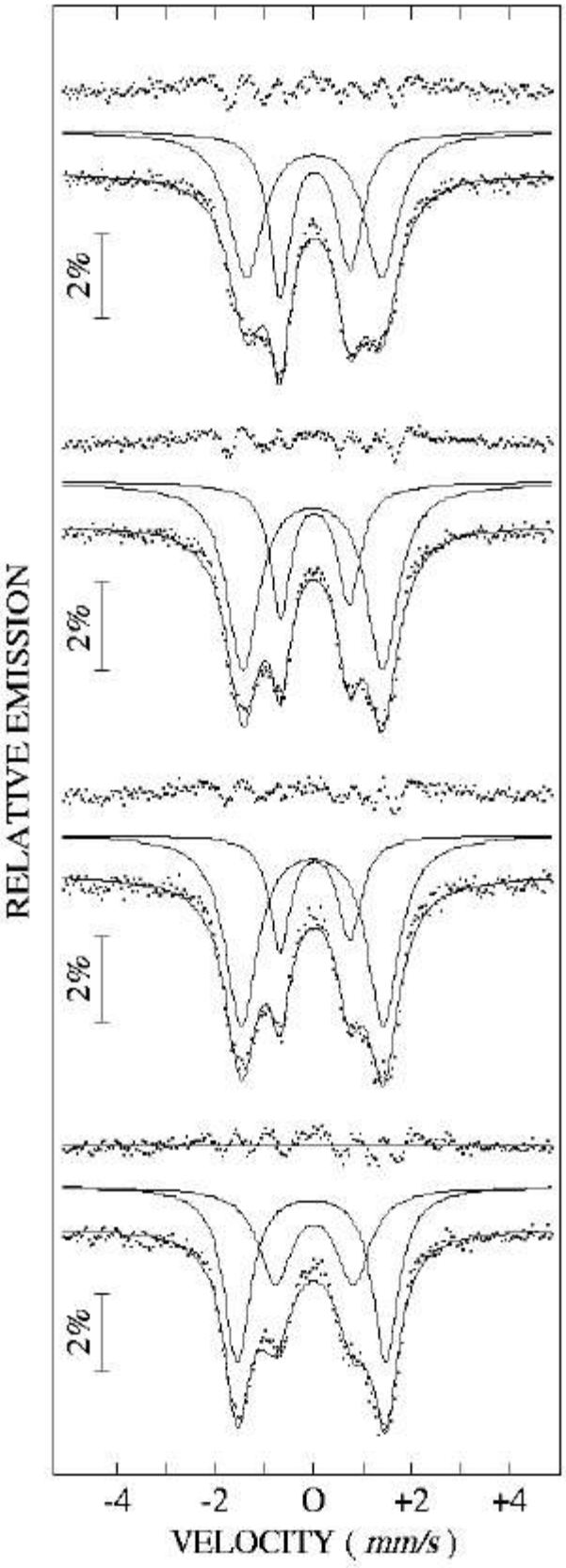

Figure 4.12 Continuing Mössbauer spectra of varying pressure for ^{57}Fe[PPIX]Cl.

Table 4.3 Mössbauer spectroscopic parameters for [^{57}FePPIXCl].

Pressure GPa	δ **mms^{-1}**	ΔE_Q **mms^{-1}**	Γ **mms^{-1}**	**% Area**
0.41(9)	0.361(22)	1.290(37)	1.055	100(3)
1.36(10)	0.312(14) 0.332(25)	1.337(51) 2.369(14)	0.624 1.033	61(9) 39(10)
2.60(24)	0.311(5) 0.302(3)	1.439(15) 2.628(36)	0.565 0.865	55(2) 45(2)
3.14(25)	0.306(1) 0.303(3)	1.405(7) 2.642(14)	0.514 0.865	45(1) 55(2)
3.75(25)	0.295(1) 0.274(8)	1.421(8) 2.754(9)	0.517 0.846	40(1) 60(1)
3.28(25)	0.305(3) 0.251(6)	1.399(3) 2.851(11)	0.459 0.797	30(5) 70(1)
4.51(10)	0.295(3) 0.275(3)	1.422(7) 2.754(11)	0.521 0.793	41(1) 59(1)
4.85(23)	0.290(9) 0.243(3)	1.397(8) 2.876(7)	0.496 0.814	27(7) 73(1)
6.03(56)	0.290(5) 0.225(3)	1.411(11) 2.939(9)	0.554 0.716	27(1) 73(1)

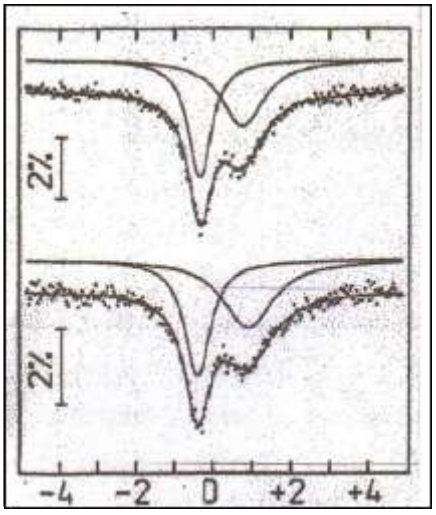

Fig 4.13 Comparison of the Mössbauer spectra of FePPIXCl before and after the application of pressure at room pressure [1 x 10^{-4}] GPa.

4.3 Discussion

The Mössbauer spectroscopic data for 57Fe(III)OEPCl are presented in Table 4.2 and Figures 4.9 and 4.10. The atmospheric pressure Mössbauer data are in agreement with literature values[40] and indicate that the compound contains high spin iron(III). The first effect of applying pressure is to decrease the broadness of the background and as the pressure increases this process steadily continued. These spectra have been fitted as doublets with a height variation allowing for asymmetry and for the ratio of the widths of the two lines to vary. The given linewidth is for the low velocity line.

At 3.50(23) GPa, the quadrupole splitting (ΔEQ) is 0.968(7) mm/s, the highest compared to the rest of the values.

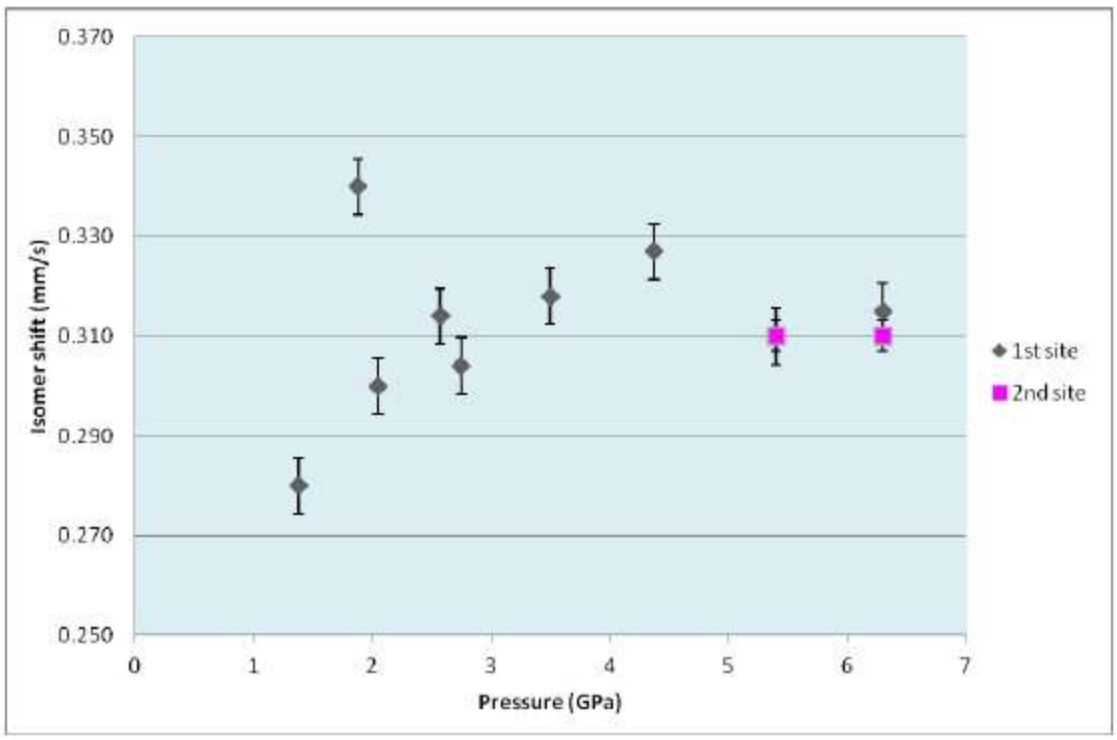

Figure 4.14 Graph of isomer shift (i.s) against pressure (GPa) for ^{57}Fe(III)OEPCl.

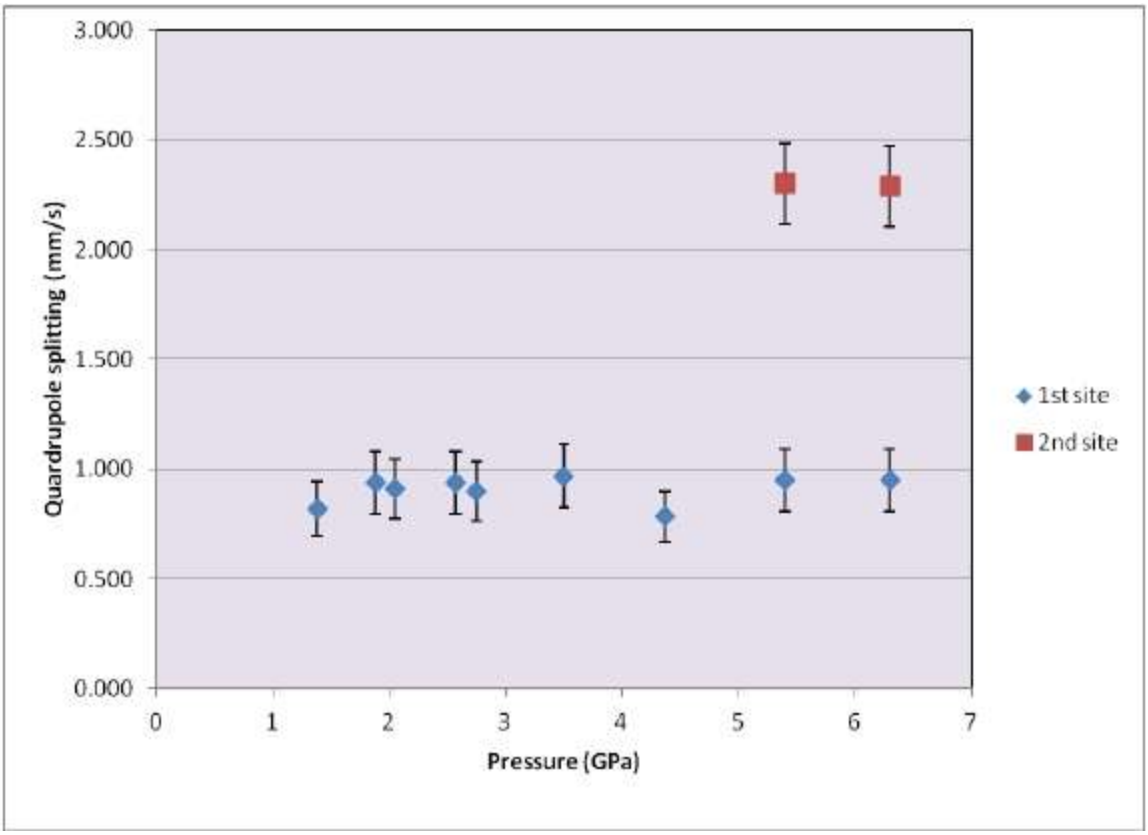

Figure 4.15 Graph of quadrupole splitting (q.s) against pressure (GPa) for ^{57}Fe(III)OEPCl.

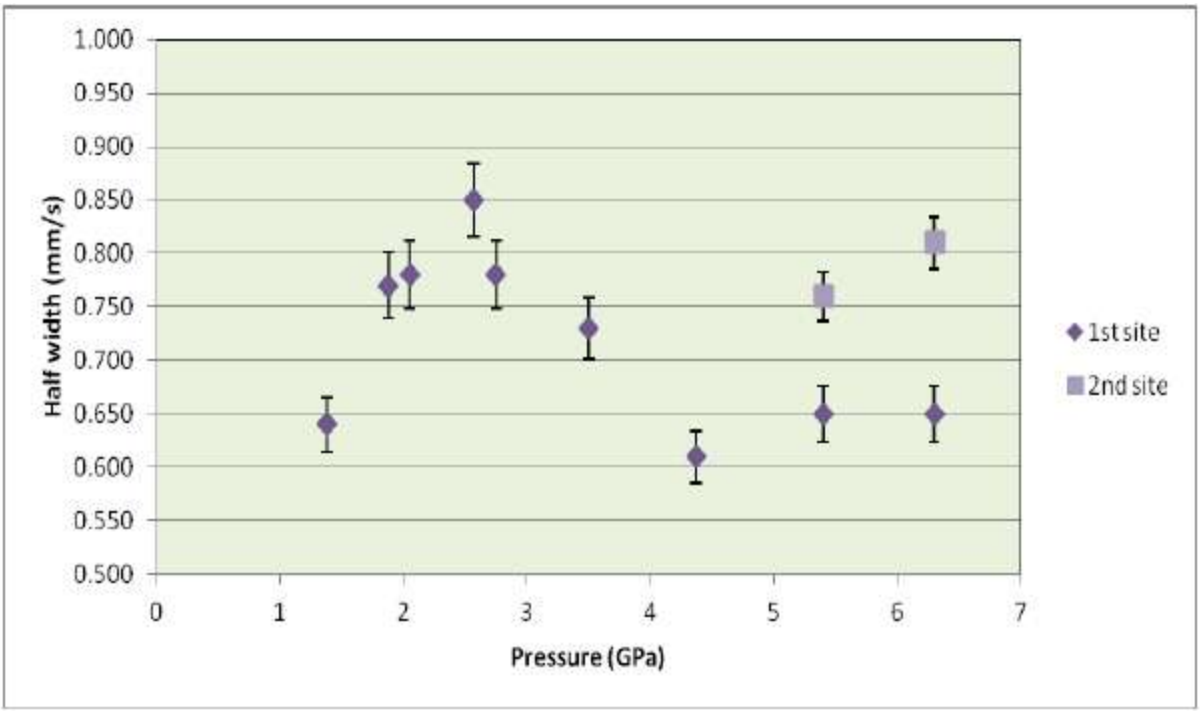

Figure 4.16 Graph of half width (mm/s) against pressure (GPa) for ^{57}Fe(III)OEPCl.

The ΔE_Q for the high spin iron(III) site becomes more clearly resolved as the pressure increases up to 4.37(24) GPa. It then increases at higher pressures. The dominant effect in the ΔE_Q of iron(III) high spin porphyrins is q_{latt}.The reason for the increase can be atttributed to a change in the lattice, which allows a move toward planarity when it happens[40]. This differs for the ΔE_Q of the high spin iron(III) in ^{57}Fe(III)PPIXCl (Figures 4.11 and 4.12), which initially increases with increasing pressure and then levels off. This is in keeping with the experimental findings for 57Fe(III)PPIXCl[38].

At 5.40(33) GPa there is evidence for the development of a second site in the 57Fe(III)OEPCl spectrum which, persists at 6.30(41) GPa. The parameters for this site are compatible with those of an $S = \pm 3/2, \pm 5/2$ spin admixed site. Table 4.4 presents some typical values for spin admixed iron porphyrins. Again, this is in agreement with our findings for 57Fe(III)PPIXCl as in Figures 4.11 and 4.12. However for 57Fe(III)OEPCl, the spin admixed site only occur at higher pressures and the proportion of this site is much less than in 57Fe(III)PPIXCl.

Table 4.4 Mössbauer data for admixed spin iron porphyrins at 298 K.

	δ	ΔEQ	Fe^X	Ref.
$FeOEP(BF_4)$	0.29	3.17	III	4
$FeOEP(ClO_4)$	0.29	3.17	III	4
$FeOEP(EtOH)_2(ClO_4)$	0.28	2.97	III	4
$[FeOEP(3,5\text{-}Cl_2py)_2](ClO_4)$	0.30	3.12	III	11
$FeTPP(C{=}C(p\text{-}ClC_6H_4)_2)$	0.23	2.87	III	15
$FeTPP(C[CN_3])$	0.30	3.18	III	15

[FeTPP(2,3,6-OCH_3)ClO_4].$CHCl_3$	0.41	3.55	III	17
[FeTPP(2,3,6-OCH_3)ClO_4].2THF.$CHCl_3$	0.39	3.28	III	17
FePPIX(CF_3COO)	0.39	3.15	III	17
FePPIX(ClO_4)	0.37	3.32	III	17
FeTPivPP$(THF)_2O_2$	0.29	2.14	II	4
FeTPP	0.39	2.62	II	4
FeOEP	0.54	1.49	II	4
FeOMTBP	0.67	0.56	II	4

It should be noticed that in Figures 4.9, 4.10, 4.11 and 4.12 the asymmetry of the high spin iron(III) site decreases dramatically as the pressure increases. The room pressure asymmetry is due to the presence of Kramer's doublets. This suggests that at higher pressures as the lattice is compressed, the higher energy Kramer's doublet becomes less populated due to pressure increasing the energy differences between these energy levels.

At low temperature (4.2K) and normal pressure, symmetrical Mössbauer spectra are observed, as only the $S_Z = \pm ½$ states are populated and as Blume [41] has explained; the spin-spin relaxation is fast. As the temperature increases, the upper states populate ($\pm 3/2$, $\pm 5/2$) with longer relaxation times, leading to asymmetric Mössbauer spectra - like those at higher pressures in Figures 4.10 and 4.12. This means that the application of pressure has a similar effect on the Mössbauer spectra, to that of lowering temperature, as was reported previously[42, 43].

It is now worth considering what happened to the high spin iron(III) site as the pressure was increased. The ΔE_Q increases on average with pressure, the isomer shift (δ) first increase then decreases at higher pressure.

The change in the ΔE_Q would be in keeping with an increased q_{latt} term arising from a movement of the Fe-Cl bond towards the porphyrin plane and the porphyrin is being pushed towards the iron shortening the Fe-N bonds. The increase in the δ, with increasing pressure is due to the less electron density at the iron nucleus and this would be due to greater shielding effect by the nucleus for *p* and *d* electron orbitals being pushed towards the iron.

The spin admixed site is also caused by squeezing of the iron atom towards the porphyrin plane but would be in keeping with a longer Fe-Cl bond. Lengthening of the Fe-Cl bond of other compounds[44] are presented in Table 4.5. Fe(III)TPPCl, Fe(III)OMTPPCl and Fe(III)OETPPCl showed lengthening of the Fe-Cl bond. The two peripherally substituted TPP complexes are admixed spin compounds and Fe(III)TPPCl has a high spin state. These bond lengths suggest that as the iron atom moved towards the porphyrin plane a number of effects may occur, such as changes in the Fe-Cl bond length and changes in the solid state packing.

Table 4.5 Selected average bond lengths in iron porphyrin chlorides[44].

	Fe(III)(OETPP)Cl	Fe(III)(OMTPP)Cl	Fe(III)(TPP)Cl
Fe-Cl	2.2418(23)Å	2.24(3) Å	2.211(1) Å
Fe-N	2.031(5) Å	2.034(6) Å	2.079(9) Å
N-C	1.386(7) Å	1.387(9) Å	1.383(6) Å
C-C (pyrrole bridge)	1.405(8) Å	1.399(11) Å	1.394(5) Å
Fe-nitrogen plane	0.47 Å	0.46 Å	0.49 Å
Fe-mean porphyrin plane	0.43 Å	0.51 Å	0.57 Å

The data in Table 4.5 suggests that the axial bond lengths around iron have shortened. The admixed spin state the Fe-N bonds have shortened to a greater extent than the Fe-Cl bond (which is unlikely to have shortened in a change to admixed spin and is unlikely to have lengthened under applied pressure). The differences in the two sites are probably controlled by the deformation/puckering of the porphyrin plane, which is effected by solid state packing and intramolecular interactions.

It is apparent that the ethyl groups on the [^{57}FeOEPCl] must first be squeezed towards the planar before the molecules can get closer together. This may be why the compound only shares the admixed spin state at very high pressure. In contrast [^{57}FePPIXCl] only has four of its substituents that can be non planar.

4.5 Conclusions

[^{57}FeOEPCl] under very high pressure shows the presence of two iron(III) sites; one is high spin (S = $^{5}/_{2}$) and the other is spin admixed (S = $^{3}/_{2}$, $^{5}/_{2}$). The pressure at which this occurs is higher than that found for [^{57}FePPIXCl] and this is most probably due to the different substitution on OEP.

From known structural data, the change in spin state must be accompanied by a change in bond lengths. These bond length changes would be expected from a decrease in volume under pressure. The corelation of the electronic properties with geometry provides a further understanding[45] of the S = $^{3}/_{2}$ state of iron porphyrins.

4.6 References

1. *Coordination compounds of Porphyrins and Phthalocyanines* B.P Berezin, John Wiley & Sons Ltd., **1981**.
2. *Porphyrins and Metalloporphyrins* edited by K. M. Smith, Elsevier, Amsterdam, **1975**.
3. *The Porphyrins Vol. 4* J. R. Sams and T. B. Tsin, edited by D. Dolphin, Academic Press, New York, **1979.**
4. R. Patra, S. Bhowmik, S.K. Ghosh and S. P. Rath, *Dalton Trans*., **2010**, *39*, 5795.
5. C. A. Reed, T. Mashiko, S. P. Bentley, M. E. Kastner, W. R. Scheidt and K. Spartalian, *J. Am. Chem. Soc*., **1979**, *101*, 2948.
6. B. E. Serr, C. E. Headford, O. P. Anderson, C. M. Elliot, K. Spartalian, V. E. Fainzilbirg, W. E. Hatfield, B. R. Rohrs, S. E. Eaton and G. R. Eaton, *Inorg. Chem.*, **1992**, *31*, 5450.

7. P. Bartner, D. L. Boxler, R. Brambilla, A. K. Mallams, J. B. Morton, P. Reichert, F. D. Sancillo, H. Surprenant and G. Tomalesky, *J. Am. Chem. Soc*., **1978**, *100*, 666.
8. G. P. Gupta, G. Lang, Y. J. Lee, W. R. Scheidt, K. Shelly and C. A. Reed, *Inorg. Chem.*, **1987**, *26*, 3022.
9. B. E. Serr, C. E. Headford, O. P. Anderson, C. M. Elliot, C. K. Schauer, K. Akabori, K. Spartalian, W. E. Hatfield and B. R. Rhors, *Inorg. Chem.*, **1990**, *29*, 2663.
10. W. R. Scheidt, S. R. Osvath, Y. J. Lee, C. A. Reed, B. Shaevits and G. P. Gupta, *Inorg. Chem.*, **1989**, *28*, 1591.
11. M. Mylrajan, L. A. Anderson, J. Sun, T. M. Moehr, C. S. Thomas, E. P. Sullivan, M. A. Thompson, K. M. Long, O. P. Anderson and S. H. Strauss, *Inorg. Chem.*, **1995**, *34*, 3593.
12. D. A. Davies, *PhD Thesis*, University of Essex, **1998**.
13. *The Colours of Life. An introduction to the Chemistry of Porphyrins and Related Compounds*. Lionel R. Milgrom, Oxford University Press, Oxford, New York, Tokyo, **1997**.
14. D. Mansuy, I. Morgenstern Bandarau, M. Lamge and P. Gans, *Inorg. Chem.*, **1982**, *21*, 1427.
15. O. K. Medhi and J. Silver, *J. Chem. Soc., Dalton Trans*., **1990**, 555.
16. H. Abu-Soud and J. Silver, *Inorg. Chim. Acta*, **1988**, *153*, 139.
17. O. K. Medhi and J. Silver, *J. Chem. Soc., Dalton Trans*., **1990**, 263.
18. A. D. Boersma and H. M. Goff, *Inorg. Chem.*, **1984**, *23*, 1671.
19. H. Goff and E. Shimomura, *J. Am. Chem. Soc*., **1980**, *102*, 31.
20. A. D. Boersma and H. M. Goff, *Inorg. Chem.*, **1982**, *21*, 581.

21. W. E. Hatfield, C. M. Elliot, J. Ensling and K. Akabori, *Inorg. Chem.*, **1987**, *26*, 1930.

22. E. T. Kinter and J. H. Dawson, *Inorg. Chem.*, **1991**, *30*, 4892.

23. H. Abu-Soud and J. Silver, *Inorg. Chim. Acta*, **1988**, *52*, 61.

24. R. G. Little, K. R. Dymok and J. I. Ibers, *J. Am. Chem. Soc*., **1975**, *97*, 4532.

25. K. Shelly, T. Bartczak, W. Scheidt and C. A. Reed, *Inorg. Chem.*, **1985**, *24*, 4325.

26. R. Cheng, P. Chen, P. Gau, C. Chen and S. Peng, *J. Am. Chem. Soc*., **1997**, *119*, 2563.

27. G. E. Toney, L. W. terHaar, J. E. Savrin, A. Gold, W. E. Hatfield and R. Sangaiah, *Inorg. Chem.*, **1984**, *23*, 2561.

28. D. C. Grenoble, C. W. Frank, C. B. Bargeron and H. G. Drickamer, *J. Chem. Phy*., **1971**, *55*, 1633.

29. *Purification of Laboratory Chemicals*, D. D. Perrin and W. L. F. Armarego, 3rd Edition, Pergamon Press, Oxford, New York, Beijing, Frankfurt, Sao Paulo, Sydney, Tokyo & Toronto, **1988**.

30. *Recent Trends in High Pressure Research*, C. A. McCammon, edited by A. K. Singh, Oxford and IBH, New Delhi, **1982**, 824.

31. J. D. Barnett, S. Block and G. J. Piermarinni, *Rev. Sc. Instrum*, **1973**, *44*, 1.

32. J. B. Paine III, W. B. Kirsher, D. W. Moskowitz and D. Dolphin, *J. Org. Chem.*, **1976**, *24*, 3857.

33. J. L. Sessler, A. Mozaffari, M. R. Johnson, *Org. Syn.*, **1991**, *70*, 68.

34. P. J. Marsh, *PhD Thesis*, University of Essex, **1996**.

35. V. V. Borovkov, J. M. Lintuluoto and Y. Inuone, *Synlett.*, **1999**, *1*, 61.

36. A. Jayaraman, *Rev. Mod. Phys.*, **1983**, *55*, 1.

37. W.B. Hopfazel, *High Temperatures-High Pressures*, **1970**, *2*, 241.

38. P. J. Titler, D. A. Davies, J. Silver and C. A. McCammon - presented as a poster at ICAME **1999**, Germany.

39. R. A. Brand, Laboratorium für Angewandte Physik, Universwität Duiburg, D-4708, Germany and U Klein, Wissenschaftliche Elektronik GmbH, Würmstr. 8, D-82319 Stranberg, Germany, **1999**.

40. B. W. Fitzsimmons, J. R. Sams and T. B. Tsin, Chem. Phys. Lett., **1976**, *38(3)*, 588.

41. M. Blume, *Phys. Rev. Lett*., **1967**, *18*, 305.

42. J. Silver, R. M. G. Roberts, D. A. Davies and C. A. McCammon, *Chem. Comm.*, **1996**, *1*, 11.

43. J. Silver, J. R. Miller, D. A. Davies and C. McCammon, *Inorg. Chem*., **1997**, *36*, 4017.

44. *The Porphyrin Handbook, Inorganic, Organometallic & Coordination Chemistry* edited K. M. Kadish, K. M. Smith, R. Guiland, Academic Press, **2000**, Vol. 9, San Diego.

45. Yan Ling and Yong Zhang, *J. Am. Chem. Soc*., **2009**, *131(18)*, 6386.

Chapter 5: Comparative High Pressure Mössbauer Spectroscopic Studies on Low Spin Iron Porphyrins of 2,3,7,8,12,13,17,18-octaethylporphyrin iron(III) di, 4-aminopyridine chloride, [Fe(III)(OEP)(4-$NH_2Py)_2$]Cl and Protoporphyrin IX iron(III) di-imidazole chloride, [Fe(III)(PPIX)$(HIm)_2$]Cl

5.1 Introduction

This chapter deals with comparative studies of two low spin iron porphyrins which model the axial ligands of the haem groups, of cytochrome b proteins and haem compounds. Many studies of bis-ligated porphyrinato iron(III) complexes, $[Fe(III)Por(L)_2]^+$, where the axial ligands L are aliphatic amines[1,2], histidines[3], imidazoles or substituted imidazoles[4-22] have been undertaken to model the active centre of cytochromes b. These model compounds have proved extremely useful as aids to the understanding of the bonding of the haems in such proteins. Conclusions can be drawn that the axial ligand orientation may be an extremely important means of fine- tuning reduction potentials to specific values in particular cytochromes[10]. In this chapter, high pressure Mössbauer spectroscopic investigations were carried out on [Fe(OEP)(4-$NH_2Py)_2$]Cl and the results were compared to those reported for [Fe(III)(PPIX)$(HIm)_2$]Cl as a function of pressure[23,54].

5.1.1 Cytochrome b

Nature's elaboration of the fundamental iron porphyrin structure has resulted in a multiplicity of functions for the haemoproteins. Numerous studies on cytochromes b from various mitochondrial and chloroplast sources showed that haem (iron protoporphyrin IX) is co-ordinated to two-histidine residues[24-31] (Figure 5.1). Cytochrome b_5 from yeast flavocytochrome b_2[24], mitochondrial $b_{562}(b_k)$ and $b_{566}(b_T)$[25],

cytochrome a of cytochrome oxidase[26], chloroplast[27,28], liver[29] and erythrocytes of animals[30] have been identified as having these axial ligands. The principal mechanisms of fine control of haem iron reactivity in haemoproteins arise from the electronic and steric influences of these ubiquitous ligands[31]. Thus oxygen transport in cytochromes c, and oxygen redox chemistry in the cytochromes P_{450} and peroxides are all achieved at an iron-active site by tuning the parameters, which control the haemoprotein structure.

Many physical properties[32-35] found in the cytochromes proteins, have been linked with differences in the orientation of the two imidazole planes of the histidine ligands, steric[26, 35-38] strain of *bis* histidine ligation or hydrogen bonding of axial histidines. Perturbation of the porphyrin ring by various π donor-acceptor interactions between the haem and an aromatic residue such as histidine, phenylaniline or tyrosine has also been proposed as a secondary but no less powerful control mechanism[39].

Protein control of the axial ligation modes of the haem group will reveal much of how it works. The overall objective of this research is to apply the synthetic analogue approach to resolve the structural questions of the haemoproteins. The definitive characterisation of protein-free haem complexes, which are frequently amenable to more detailed scrutiny than the haemoproteins themselves, provides a structural framework for understanding the changes of spin state and oxidation state in the haemoproteins.

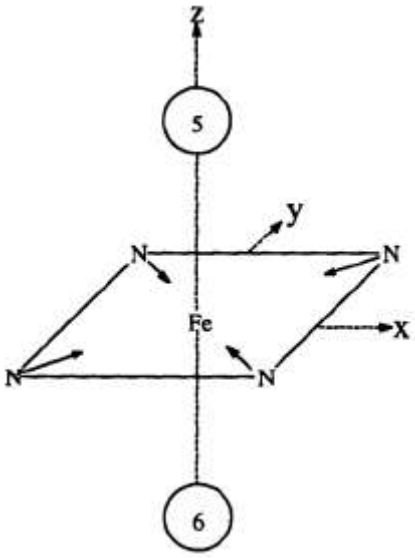

Figure 5.1 Octahedral geometry of [Fe(II)Por(L)$_2$]. The numbers 5 and 6 denote the axial ligand positions.

5.1.2 Models for Cytochrome b

Medhi and Silver have described models for cytochromes b proteins based on complexes of iron(III) protoporphyrin (IX), [Fe(III)PPIX]$^+$ (Figure 5.2), with imidazoles[4], substituted imidazoles and histidine[5] and its substituted derivatives.

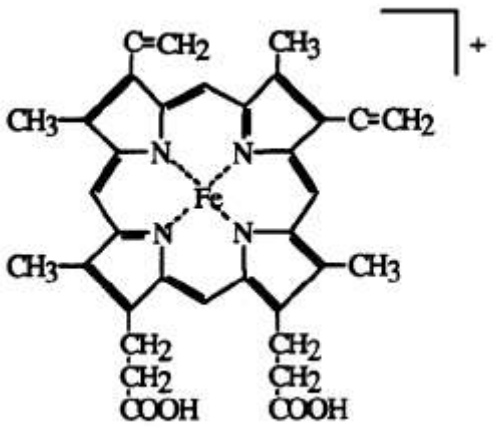

Figure 5.2 [Fe(III)PPIX]$^+$ [4].

In Mössbauer spectroscopic studies of $[Fe(III)PPIX(L)_2]^+$ (L=imidazole or substituted imidazole) complexes in various solvents, Medhi and Silver found a relationship exists between the axial imidazole plane orientation and the observed quadrupole splitting (ΔE_Q) and line shapes[4].

Large ΔE_Q values of around 2.34 - 2.43 mms^{-1} were assigned to structures where the two imidazoles are orientated more or less parallel in alignment; in contrast, values around 1.8 mms^{-1} were assigned to a perpendicular orientation of the imidazole planes (Figure 5.3). In a similar study on *bis* histidine and related complexes they demonstrated that the iron binds the histidine ligands as sterically hindered imidazoles and that the iron imidazole bonds are weak[5]. The magnitude of the ΔE_Q values of 2.14 mms^{-1} and large line widths suggested that there is a large angle between the two imidazole planes[5]. Similar conclusions in regard to the assignment of the Mössbauer parameters and EPR parameters have since been reported by others[10, 40].

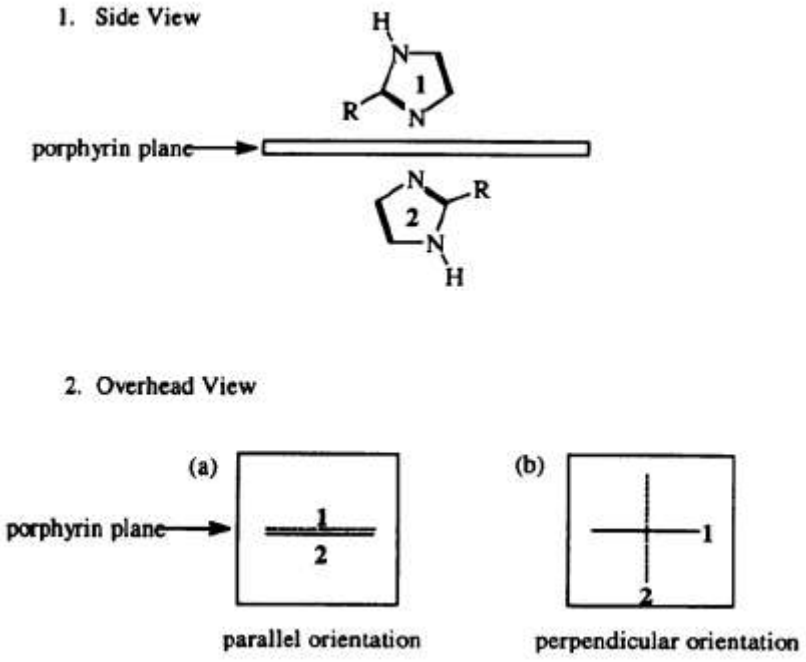

Figure 5.3 Orientation of axial ligands.

The observation, by Medhi and Silver[5] of asymmetric quadrupole doublets together with broad lines is characteristic of slow spin-lattice relaxation of iron, similar to that seen for cyctochrome c[41] and small peptides prepared from cyctochrome c[42-44]. In such cases T1 ≤ 10^{-8} s at 77K were observed. The resulting Mössbauer spectroscopic data for the *bis* histidine complexes were similar to those reported for low spin iron(III) cyctochromes[41, 45] and cyctochrome b_{546}.

Furthermore these studies demonstrated that steric strain arising from the histidine side chains and electrostatic interactions between the charged groups and the porphyrin propionate carboxylates influenced the iron electronic structures and the imidazole plane orientations[5].

In this work, $[Fe(III)OEP(NH_2Py)_2]^+$ was chosen for study because of its position at the boundary between the ^2B and ^2E states[22,54]. ^2B (orbital doublet) or $(d_{xy})^2(d_{xz})^2(d_{xy})^1$ ground state happens when the ligands are parallel to each other. ^2E states (orbital doublet) or $(d_{xy})^2\ (d_{xz},\ d_{xz})^1$ ground state happens when the ligands are perpendicular to each other (Figure 5.3) and in contrast $[Fe(III)PPIX(HIm)_2]^+$ was chosen as it was a good model for natural haemoproteins, as it contains the natural occurring iron porphyrin and a histidine type residue ligand.

5.2 Experimental

5.2.1 Materials

Octaethylporphyrin (OEP), ^{57}Fe and 4-aminopyridine (4-NH_2Py) were purchased from Aldrich (Acros Organics). Chemicals were used as purchased except for $[PPIX]H_2$ (produced in the laboratory) which was purified according to the literature method[47]. Electronic absorption spectra were recorded on a Perkin Elmer λ3 spectrometer. The results showed OEP and 4-amino pyridine present in the solution of

chloroform. High-pressure Mössbauer spectra were recorded using the previously reported apparatus[48]. The spectra and instrument used to measure and record for this experiment was described in detail in Chapter 2. For high pressure Mössbauer the experiment was conducted in Bayerisches Geoinstitut, Universitat Bayreuth, Germany. The spectra were recorded using a modified Merill-Basett diamond anvil cell (DAC) under hydrostatic pressure using the previously reported system[31]. Methanol:ethanol = 4:1 (v/v) was used as the hydrostatic fluid. The pressure in the cell was recorded using the ruby fluorescence method[32].

5.2.2 Preparation of [^{57}Fe(III)OEP(4-NH_2Py)$_2$]Cl

Firstly, [^{57}Fe(III)OEPCl] $^{57}FeCl_2$ was prepared using enriched iron-57 [97%] according to Borovkov's method[49]. Only anhydrous and purified solvents were used for the synthesis. ^{57}Fe foil (0.01 g, 0.18 mmol) was dissolved in deoxygenated concentrated HCl (2 mL) under nitrogen atmosphere. Two drops of 2, 6-lutidine was added to a solution of OEP (5 mg, 0.09 mmol) in $CHCl_3$ (3 mL) and anhydrous $^{57}FeCl_2$ in CH_3Cl. The reaction mixture was stirred at room temperature for 1 hour. Identification of the product - [^{57}Fe(III)OEPCl] was achieved by a comparison of the electronic absorption spectrum with a purchased reference sample.

^{57}Fe(III)OEP(4-NH_2Py)$_2$ was prepared by a slight modification of the method of Hill *et al*[50]. ^{57}Fe(III)OEP(4-NH_2Py)$_2$ was obtained from a hot solution of [57Fe(III)OEPCl] in a mixture of excess 4-aminopyridine (4-H_2NPy), dichloromethane and methanol at a ratio of (1:10:8, v/v/v) in a Schlenk tube. The mixture was reduced under pressure until crystallisation started. The collected sample was pinkish red in colour. High-pressure Mössbauer spectra were recorded using a Merrill Basset diamond anvil cell (DAC) under hydrostatic pressure[51].

5.2.3 Preparation of ^{57}FePPIXCl

^{57}FePPIXCl was prepared by dissolving iron(II) chloride in degassed concentrated HCl (1 mL) under a nitrogen atmosphere, to which (20 mL) of degassed glacial acetic acid was added. The solution of (PPIX)H_2 (0.2 g, 0.38 mmol) previously dissolved in glacial acetic acid (200 mL) was then heated to reflux under a nitrogen atmosphere in a round bottomed flask with a water condenser. Once reflux had been reached, the solution of iron(II) chloride in acetic acid was cannulated into the reaction mixture. The subsequent reaction was followed by electronic absorption spectroscopy carried out hourly and heating was stopped when no further change in the spectra occurred. The reaction mixture was then opened to the air, and a saturated NaCl solution (60 mL) and then water (40 mL) were added to the reactants. Overnight, precipitates formed which were filtered off, redissolved in HPLC grade DMSO and freeze-dried. ^{57}FePPIXCl (0.012 g, 0.02 mL) and imidazole (0.14 g, 1.70 mmol) were dissolved in NaOH solution of pH12; with further addition of diluted HCl (10% concentrated) until a precipitate formed at *circa* pH 7.3. The precipitate was collected by centrifugation and freeze-dried. The sample was black in colour.

[*Anal.* Calc. For $FeC_{46}H_{58}N_8Cl$: C, 67.75; H, 7.17; N, 13.74 %; Found C, 65.75; H, 6.39; N, 13.81 %].

5.2.4 Mössbauer Measurements

Mössbauer spectra were recorded using solid material at 77 K. The ambient pressure spectrum was measured using standard Mössbauer sample holder [Delrin disk] of a 12.7mm and 1mm depth. Sample was loaded into the hole using a small amount of acetone. The sample was mixed with calcium carbonate to fill the hole. A piece of Kapton tape was used to keep the sample from spilling out. The set up

(instrumentation) was described in Chapter 2, *section one*. High pressure measurements were recorded using a Merrill Basset type diamond anvil cell (DAC) on the previously reported high-pressure experimental setup[51] in Chapter Two, *section two.* Some broadening of line-widths due to internal recoil was observed, caused by the use of a high activity point source. 1:1 (Pentane: isopentane (v/v)) was used as the hydrostatic media for both $^{57}FePPIX(HIm)_2Cl$ and for $^{57}FeOEP(4\text{-}NH_2Py)_2Cl$. Accurate recording of pressure within the cell utilised the ruby fluorescence method[52].

5.3 Results

The complexes have been characterised by UV/vis, CHN analysis and Mössbauer spectroscopy.

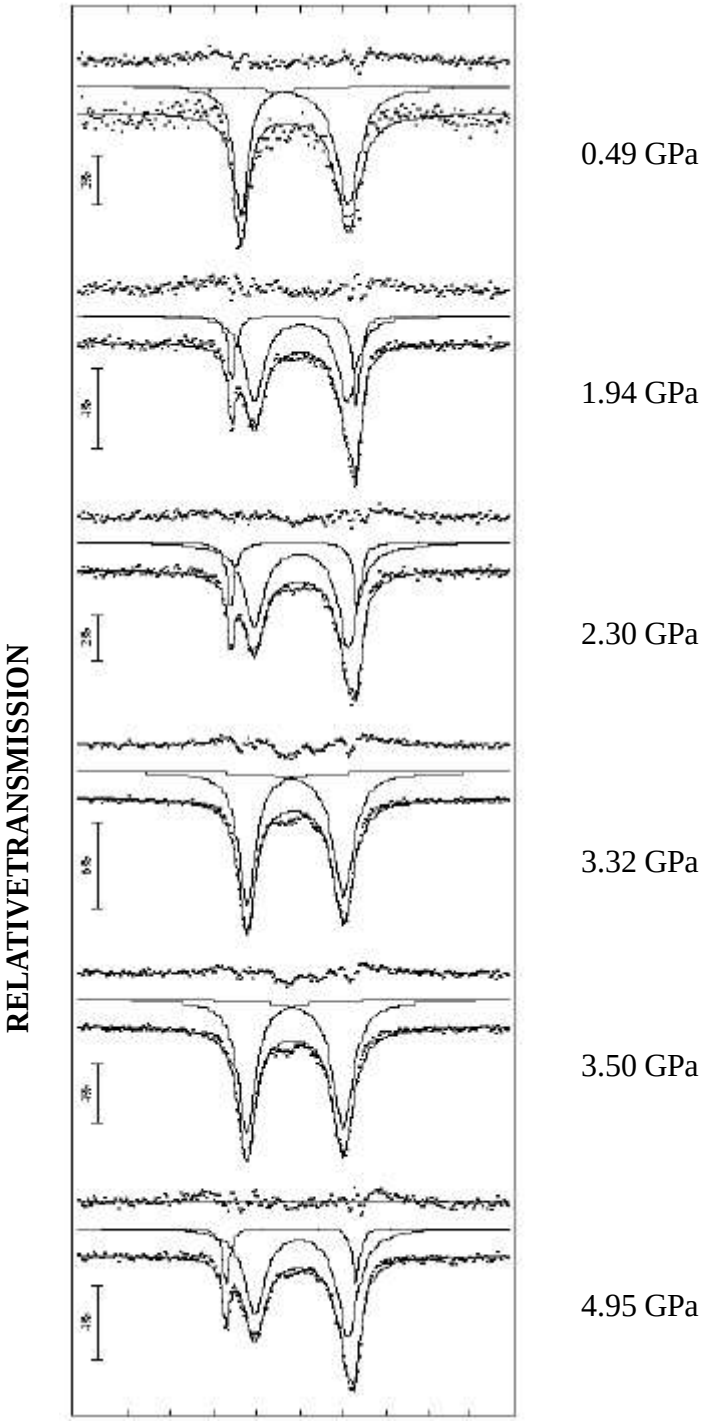

Figure 5.4 Mössbauer spectra at varying pressure for $^{57}Fe(III)OEP(4\text{-}NH_2Py)_2Cl$.

Figure 5.4 clearly indicates the affect of an increase in pressure for the compound of $^{57}Fe(III)OEP(4\text{-}NH_2Py)_2Cl$. At pressures of 0.49, 3.32 and 3.50 GPa only evidence of one electronic site is visible. In this case, (type 1) they are similar to the ambient pressure spectrum at room temperature. This is illustrated in Figure 5.5 (see below). The ΔE_Q values for the type 1 site show little variation with pressure for the ambient pressure, 1.94, 2.30 and 4.95 GPa whereas the 0.49, 3.32 and 3.50 GPa spectra for this site shows evidence of a decrease in the ΔE_Q values with increasing pressure. This possibly indicates some orientation of the angle of the ligand planes.

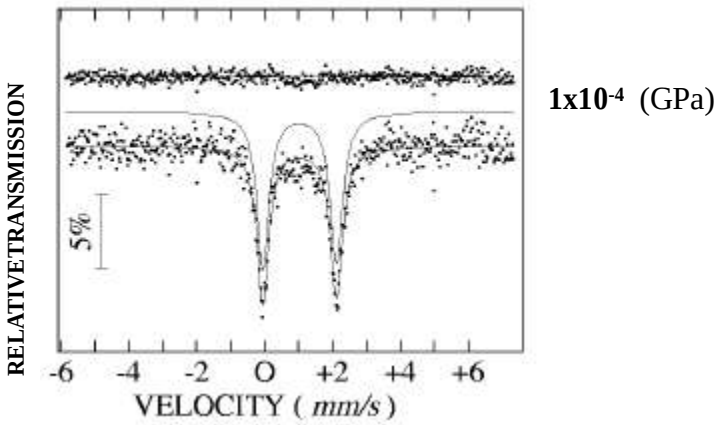

Figure 5.5 Before application of pressure for $^{57}Fe(III)OEP(4\text{-}NH_2Py)_2Cl$.

At pressures of 1.94, 2.30 and 4.95 GPa, two new sites (type 2) of the electronic environment are observed (Figure 5.4).

One of these (type 2) is typical of a low spin Fe(II) site but the ΔE_Q values are lower than those for the original site at all pressures in Table 5.1. The second site shows a much wider ΔE_Q value suggesting that of an intermediate spin or 'spin admixed site'. The isomer shifts for this site are not consistent with such a site as they are low; as yet no explanation of this has been found.

Table 5.1 Mössbauer parameters for [Fe(III)OEP(4-$NH_2Py)_2$]Cl at varying pressure.

Pressure(GPa)	i.s	ΔE_Q in mms^{-1}	% area	Γ* in mms^{-1}	i.s	ΔE_Q in mms^{-1}	% Area	Γ* in mms^{-1}
$1x10^{-4}$ (77K)	0.29(1)	2.42(1)	80(2)	0.42(2)	0.44(2)	0.70(2)	20(2)	0.23(2)
$1x10^{-4}$(298K)	0.21(1)	2.16(1)	100(2)	0.21(1)				
0.49(5)†	0.12(1)	2.49(2)	100(1)	0.39(2) 0.64(3)				
1.94(21)	0.27(1)	2.16(1)	73(2)	0.25(1)	0.15(1)	2.90(2)	27(1)	0.11(1)
2.30(32)	0.28(1)	2.18(1)	71(1)	0.29(1)	0.11(1)	2.91(2)	29(1)	0.13(1)
3.32(15)†	0.16(1)	2.24(1)	100(1)	0.24(1) 0.27(1)				
3.50(26)†	0.13(1)	2.24(1)	100(1)	0.24(1) 0.28(1)				
4.95(28)	0.28(1)	2.17(1)	84(1)	0.29(1)	0.10(1)	3.01(1)	16(0.5)	0.09(1)

† Fitted as two singlets.

* Half width at half height

5.4 Discussion

[Fe(III)OEP($NH_2Py)_2$]Cl has a large ΔE_Q at 77K which is typical of a conformation where the angle between the pyridine rings ($\Delta\phi$) is zero (that is the rings are parallel to each other). The change in the ΔE_Q value between 77 K and room temperature is large and in itself may be expected to represent an angle change. However, this is unlikely as at 0.50 GPa, ΔE_Q returns to 2.49(2) GPa (Figure 5.6) and it have been previously shown that the effect of increasing pressure affects Mössbauer spectroscopic parameters in a similar way to decreasing temperature [53].

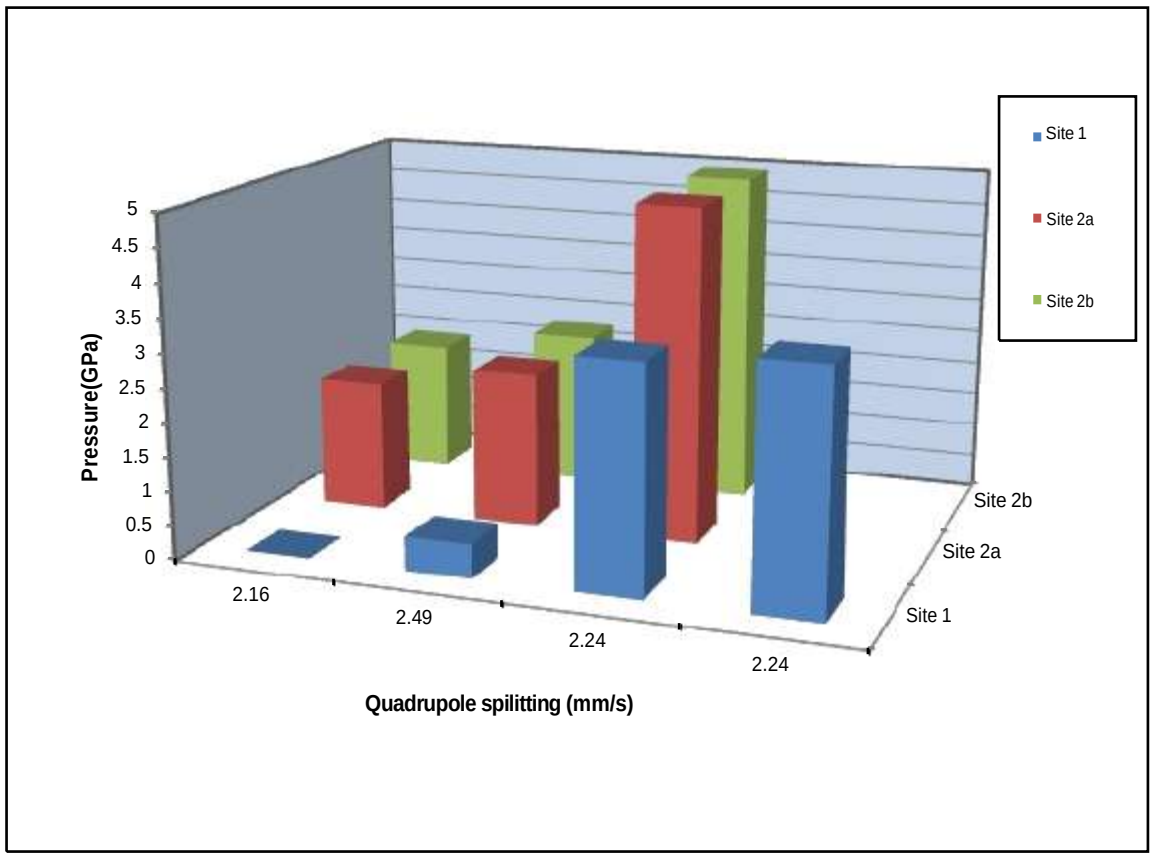

Fig 5.6 Plot of pressure (GPa) against ΔE_Q (mm/s) for ^{57}Fe(III)OEP(4-$NH_2Py)_2$Cl.

The pressure dependence of the ΔE_Q values for [Fe(III)OEP(NH_2Py)$_2$]Cl can be seen in Table 5.1 and Fig. 5.3. Two distinctly different effects are observed.

1. At pressures of 0.49, 3.32 and 3.50 GPa, only evidence of one electronic site is found; the ΔE_Q values decrease after an initial increase, but the basic shape of the spectra are similar. In all three cases, they are like the room temperature spectrum in appearance and low spin iron(III) persists.

2. At pressures of 1.94, 2.30 and 4.95GPa, two new electronic environments (sites) are seen. One is a typical of a low spin site but the ΔE_Q values are lower than those for the original site at all pressures. The second site shows a much wider ΔE_Q value that is suggestive of an intermediate spin or 'spin admixed' site.

The first discussion is: **why do the two kinds of behaviour take place**? The obvious answer is that at each change of pressure a volume change takes place, which involves a shrinking of the available sample space. This causes the [^{57}Fe(III)OEP($4NH_2Py$)$_2$]$^+$ complexes to be pressed closer together. At each pressure change (in the range studied) it appears that there are two possible configurations. In one, only the original site persists (type 1) as the complexes squeezed. In the other (type 2), the molecules are squeezed at the alternative arrangement.

In this case, (a) some can remain in a low spin iron(III) configuration whilst others (b) take on an 'intermediate/spin admixed' conformation.

These (a) and (b) forms must be related as they occur at three pressures, though the amount of spin form increases with increasing pressure. This must be because of the intermediate/spin admixed form requires more space, and is therefore less favourable as the pressure increases. It is known (Table 5.3) that the intermediate/spin admixed forms of [Fe(III)Por(L)$_2$]$^+$ species have parallel L ligand planes ($\Delta\phi = 0$) and also ϕ angles of zero, hence we can assume such a conformation takes place in the type 2b

site. ϕ is the angle between the two ligands (above and below) that bonded to the iron metal.

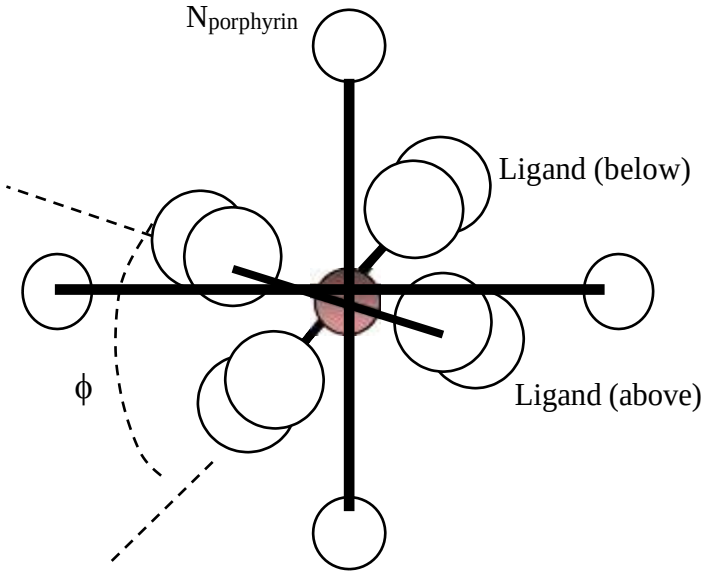

Figure 5.10 Orientation of axial ligands relative to $N_{(por)}$-Fe-$N_{(por)}$ vector. Arial view along $N_{(axial)}$-Fe showing the plane of ligand for the angle ϕ.

Hence, the type 2a low-spin site must be related to this. Therefore, as the pressure increased, the ϕ angle became smaller approaching a value of zero, but concomitant with this, the ligand is forced towards the Fe-N_{por} vector. Thus the compound is predominantly still low spin (type 2a) though a proportion goes into the 'intermediate/spin admixed' site (type 2b). This latter proportion is smaller as the pressure increases and as it necessitates a longer Fe-N_{axial} ligand band. However, the fact is that the ϕ angle has changed with applied pressure due to the packing of the complexes that allows a change in the spin state to occur. Hence, a change in spin state from low spin to intermediate/admixed spin can indeed be pressure induced, and be readily explained.

The variation in isomer shift in $[^{57}Fe(III)OEP(4\text{-}NH_2Py)_2]^+$ is dependent on the electronic environment type. In type 1, the isomer shift decreases from the ambient pressure values but then slightly increases as the pressure increases. This is nearly the same behaviour as found for $[FePPIX(HIm)_2]^+$, and is expected. However, the isomer shift values for type 2a are higher than room pressure and are constant as a function of pressure. These isomer shift values are typical of low spin $[Fe(III)Por(L)_2]^+$ complexes at 77 K[52].

5.4.1 Effects of Pressure on the Line Width of $^{57}Fe(III)OEP(4\text{-}NH_2Py)_2Cl$

As shown, in Table 5.1 for the type 1 site, the line widths of the low spin iron(III) are the same at 77 K and 298 K, but are slightly narrower in the latter case. At 0.49 GPa the high velocity line is much wider and its area is much greater. At 3.32 GPa, the lines width change with higher velocity, becoming less wide, and its area also closer to the low velocity line. The behaviour of the lines at 3.50 GPa is similar to that at 3.32 GPa.

5.4.2 Studies on $[Fe(III)PPIX(HIm)_2]^+$

The room temperature variable pressure Mössbauer data for $[Fe(III)PPIX(HIm)_2]Cl$ are presented in Figure 5.7 and Table 5.2. These spectra were recorded by D. Davies in 1997. This work is summarised here in order to compare it to the results for $[^{57}Fe(III)OEP(4\text{-}NH_2Py)_2]Cl$. After the high-pressure run the sample was allowed to return to ambient pressure and was shown to give the same results, within experimental error, as the starting material[54].

Table 5.2 Mössbauer spectroscopic data for [^{57}FePPIX(HIm)$_2$]Cl[57].

Pressure GPa	**i.s. mms^{-1}**	**ΔE_Q mms^{-1}**	**Γ* mms^{-1}**
1 x 10^{-4}	0.176(10)	1.962(20)	0.319(15)
0.15(5)	0.185(40)	1.974(8)	0.305(6)
1.12(5)	0.173(2)	2.013(4)	0.281(4)
2.52(5)	0.158(2)	2.032(4)	0.263(6)
3.54(12)	0.140(2)	2.033(4)	0.275(3)
3.90(7)	0.137(2)	2.037(3)	0.265(4)
4.70(12)	0.135(2)	2.043(4)	0.272(3)
5.91(45)	0.128(2)	2.042(4)	0.279(2)
1 x 10^{-4}♠	0.185(10)	1.987(18)	0.278(14)

* Half width at half height.

♠ *second run after the sample (DAC) relax into room pressure*

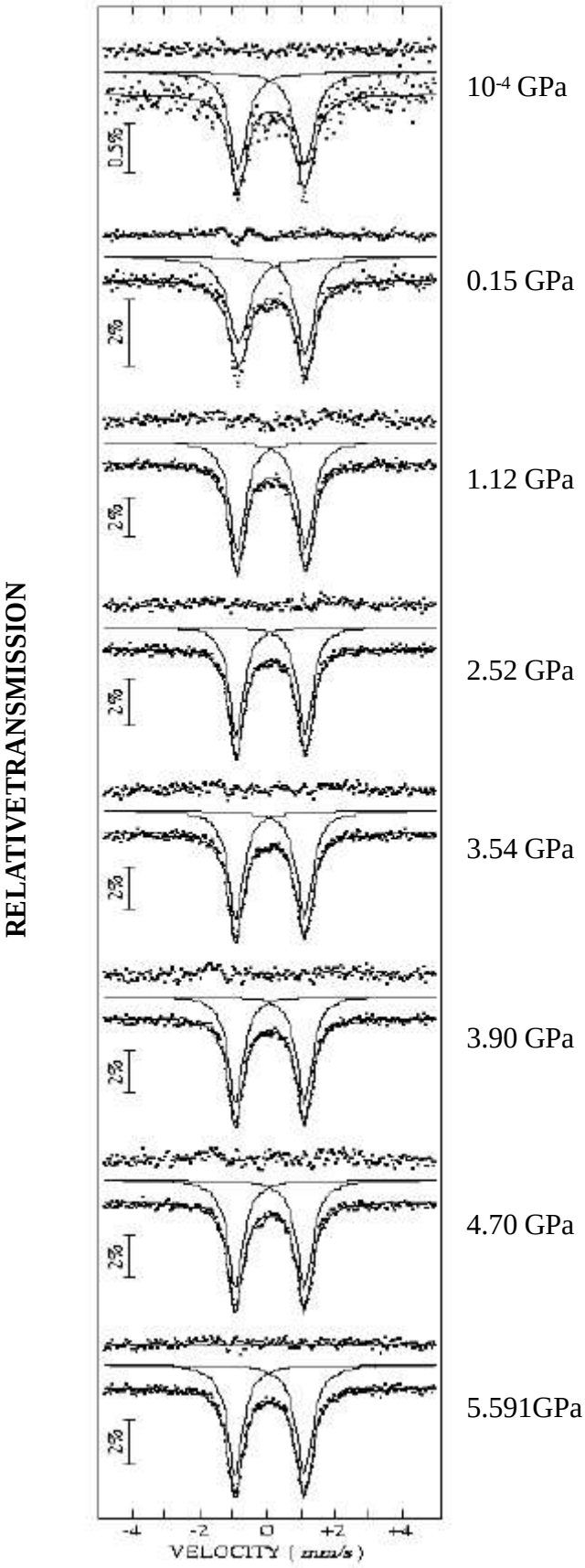

Figure 5.7 Mössbauer spectra at varying pressure for [^{57}Fe(III)PPIX(HIm)$_2$]Cl.

In this work, it was observed that there is no sign of the spectra broadening with increasing pressure, unlike in [^{57}Fe(III)OEP(4-NH_2Py)$_2$]Cl.

There was no evidence of a second site, even one which has a line shape overlapping the line shape of the first site, nor is there any evidence for a second site discrete from the initial site developing. Thus, there is no evidence for a second site developing with pressure. However that was reported in the previous study on [Fe(III)PPIX(HIm)$_2$]Cl[23]. The isomer shift of the ambient temperature and pressure spectra (0.176(10) mms^{-1})[55] was consistent with the Mössbauer parameters reported for similar compounds (≈ 0.15 mms^{-1}) [25, 63]. The isomer shift was found to decrease with the pressure increases as shown in Table 5.1.

In Figure 5.8, the observation of the isomer shifts value is clearly illustrated. The decrease in isomer shift is almost linear to inversely proportional to increase in pressure for [Fe(III)PPIX(HIm)$_2$]Cl[23]. No such effect was observed for either site in [^{57}Fe(III)OEP(4-NH_2Py)$_2$]Cl.

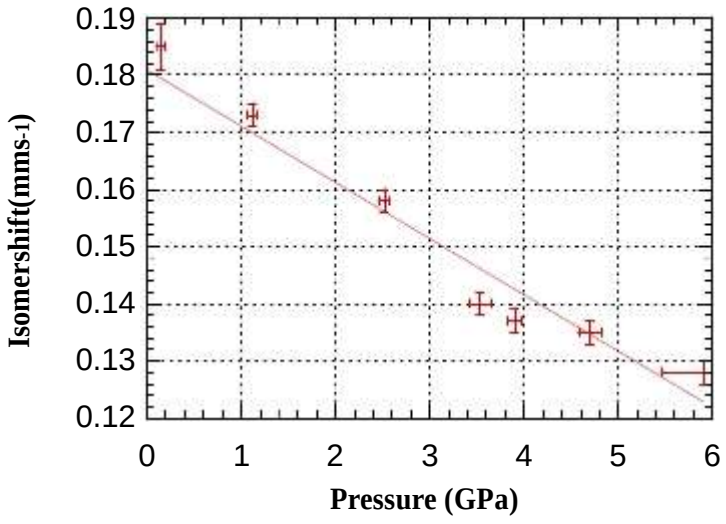

Figure 5.8 Plot of isomer shift against pressure for [^{57}Fe(III)PPIX(HIm)$_2$]Cl.

Drickamer *et al*[23] also observed a decrease in the isomer shift with pressure for [Fe(III)PPIX(HIm)$_2$]Cl before the development of their 'second site', though it decreased at a slower rate than observed by Davies[54].

A decreasing isomer shift is consistent with the decrease in the shielding of the *p* and *d* electron density with increasing pressure. The variation of the Mössbauer line half width at half height against pressure is plotted in Figure 5.9.

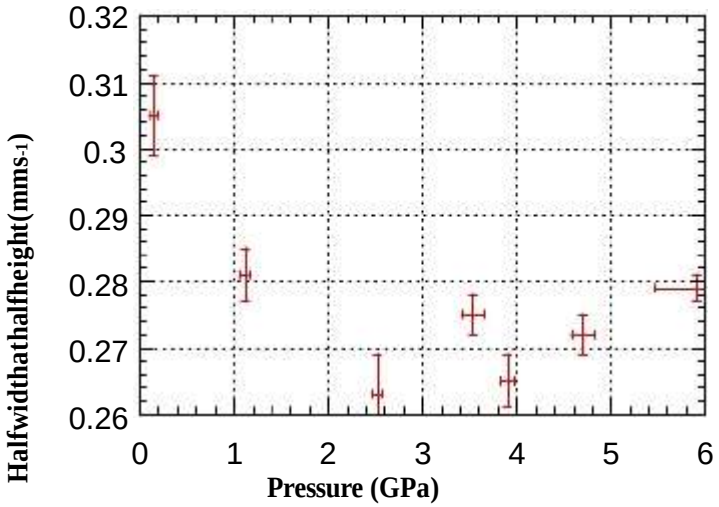

Figure 5.9 Plot of half width at half height against pressure for [^{57}Fe(III)PPIX(HIm)$_2$]Cl.

For the [Fe(III)PPIX(HIm)$_2$]Cl spectra, the variation was small at high pressure and there was no sign of asymmetry at low pressures. The initial narrowing of the line with the application of pressure is probably insignificant and caused by an improvement in the percentage transmittance statistics arising from an increase in f where (f = the fraction of recoil-free events) at higher pressure.

A plot of the ΔE_Q values for [^{57}Fe(III)PPIX(HIm)$_2$]Cl against the applied pressure is presented in Figure 5.10. An initial increase of ΔE_Q values with increasing pressure and then a levelling off was observed.

It has been shown that the alignment of the imidazole ligands can vary in both solution and the solid state[1,4], however the previous solution studies of [Fe(III)PPIX(HIm)$_2$]Cl have produced ΔE_Q values of 2.32 mms^{-1} or greater[4]. A difference in the orientation of the imidazole planes will affect the ΔE_Q of the Mössbauer spectra of the compound[1, 4].

It was shown that the electronic absorption spectra in the solution of the [Fe(III)PPIX(HIm)$_2$]Cl was in good agreement with the literature[54, 56]. Thus it seems that the low ΔE_Q values may be consistent with the solid sample having imidazole planes somewhere between perpendicular and parallel.

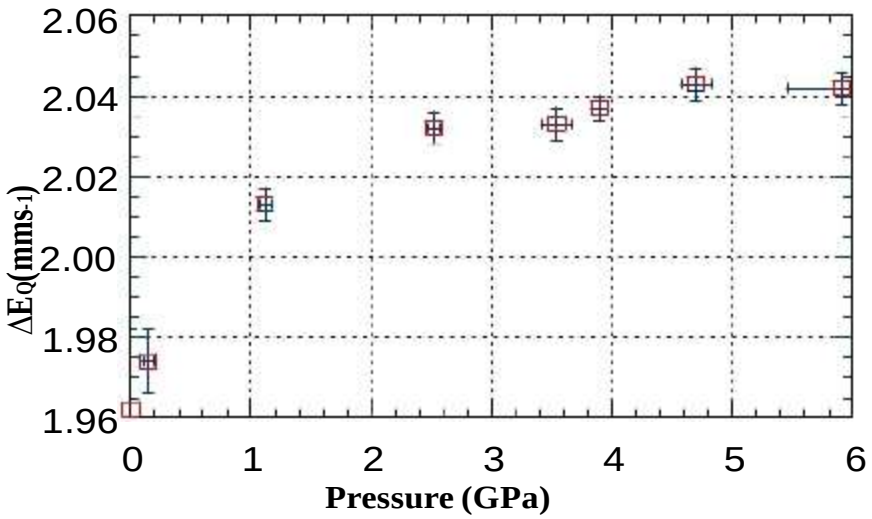

Figure 5.10 Plot of ΔE_Q against pressure for [^{57}Fe(III)PPIX(HIm)$_2$]Cl.

An increase in ΔE_Q values with the increase of applied pressure could be caused by a shortening of the N of the imidazole to iron bond, this would bring about a change in

the axial tetragonal distortion of the compound. This will increase the overlap of σ bonding orbitals, increasing the population of the d_{z2} orbital. Parallel with this will be an increase in the delocalisation of the electron density in the π back bonding orbitals which will reduce the population of the iron orbitals involved in the back bonding. The orientation of the two imidazole ligands will determine which orbitals are affected by this increased delocalisation. It was believed that the orientation was closer to parallel[54]. The delocalisation mainly happens in either the d_{yz} or d_{xz} orbitals. It can be seen, from equation 5.1[55], that:

$$V_{zz} = k\,[n_{x2-y2} - n_{z2} + n_{xy} - {}^{1}/_{2}\,(n_{xz} + n_{yz})] \quad \textit{Equation (5.1)}$$

Both increased in the d_{z2} population and a decrease in the d_{yz} or d_{xz} population will decrease the observed ΔE_Q[55].

The results for [^{57}Fe(III)PPIX(HIm)$_2$]Cl were therefore interpreted to mean that initialising the application of pressure caused the reorientation of the imidazole until about 2.5 GPa at which point the rate of change of the ΔE_Q with pressure increases markedly.

Thus in [^{57}Fe(III)PPIX(HIm)$_2$]Cl the pressure range was studied, no change in spin state was observed, only just a change in axial ligand orientation. In contrast for [^{57}Fe(III)OEP(4-NH$_2$Py)$_2$]Cl there is a change to an intermediate or "spin admixed site" and little evidence for ligand orientation change.

A single high pressure spectrum of enriched FeTPP(HIm)$_2$Cl (ΔE_Q = 2.11(1) mms^{-1} at 298 K) showed a slight decrease in ΔE_Q to 2.05 mms^{-1} at around 4.50 GPa in previous work[56]. In this complex it is believed that the ligands are non parallel and the decrease in ΔE_Q values was caused by an increase in the electric field gradient (EFG) due to change in magnitude of the axial tetragonal distortion. This probably arises from a

slight change in ϕ and Δϕ angles with pressure. The ϕ angles will be expected to decrease more towards a parallel arrangement of the axial ligand.

5.3.3 Previous work

Previous work by Quinn *et al*[14] showed that if the Fe-N bond lengths (porphyrin bonds is plotted against the average of the two Fe-N axial bonds) are considered, the ^2B and ^2E types of low-spin iron(III) porphyrins are distinctly different crystallographically[22] (see Table 5.2). A third group of compounds[10, 40, 52] with the same general formula have a $(d_{xz},d_{yz})^4,(d_{xy})^1$ ground state in these ligands are sterically hindered from the iron, and are more weakly bonded than the porphyrin nitrogen ligands.[22] It has been shown that if the axial ligands are chosen to have a range of basicities, it is possible to progressively shift the ground state from mainly $(d_{xy})^2(d_{xz,}d_{yz})^3$ to predominantly $(d_{xz},d_{yz})^4(d_{xy})^1$ showing that a combination of electronic and conformational factors can dictate the iron ground state[53].

It was shown that the bis-ligated iron(III) octaethylporphyrin complexes $[FeOEP(L)_2]^+$ [43,50] lay in the region near the boundary between the ^2B and ^2E states as mentioned earlier. The compound, $Fe(III)OEP(3\text{-}ClPy)_2ClO_4$ (3-ClPy = 3-chloropyridine) was close to the boundary and is known to exist in three different forms. One is a high spin – low spin equilibrium[54], one has a quantum admixed ($S = {}^3/_2, {}^5/_2$) spin state[55] and the third is said to be in an admixed $S = {}^3/_2$ state.[56]

Another compound $Fe(III)OEP(NMe_2Py)_2ClO_4$[10] (NMe$_2$Py = N-dimethylpyridine) also lies close to the boundary. This compound, along with other $[Fe(III)OEP(L)_2]^+$ compounds has been shown to have a complex spin state behaviour[50, 58].

The fact that some haem compounds can exist in different spin states has also been related to differences in the orientation of the axial ligands[15, 50-52]. For pyridine

ligands, an orientation in which the ligand plane projections on to the porphinato core make small angles with an iron porphyrin nitrogen vector gives an admixed intermediate spin state. If the ligand planes are rotated by ~40° then a low spin state is achieved[15].

5.5 Further Discussion

The question is what is its likely ϕ angle? From Table 5.3, compounds 1 to 12, ϕ can take values from 0° to 41°. To minimise the Fe-N_{axial} distances, it might be expected that the ϕ angle is close to 41°.

Table 5.3 Comparison of major bond lengths and angles around the $[FePor(L)]^{+}$. complexes.

Complex	Fe-N_{por}(Å)	Fe-N_{ax}(Å)	ϕ	Δϕ(°)	Ref.
[Fe(III)OEP(4-$NMe_2Py)_2$]ClO_4	1.987(2)	1.995(2)	41	0	17
[Fe(III)OEP(3-ClPy)$_2$]ClO_4	1.995(2)	2.031(2)	41	0	50
[Fe(III)OEP(2-MeIm)$_2$]ClO_4	2.04(1)	2.275(1)		22	53
[FeOEP(3-ClPy)$_2$]ClO_4	2.006(8)	2.304(7)	6.1	3.8	52
[FeOEP(2-MeIm)$_2$]ClO_4	2.0481)	2.249(1)	32	0	56
[FeOEP(3-CNPy)$_2$]ClO_4	2.012(2)	2.269(6)	4.0	0	54
[FeOEP(3,5-Cl_2Py_2]ClO_4	1.994(10)	2.347(4)	0	0	-
[FeOEP(1-MeIm)$_2$] [Ag(1-MeIm)$_2$]PF_6	2.004(2)	1.975(2)	20	0	45
[Fe(III)OEP{(C_5H_5)(C_4NH_4)Fe}$_2$]O_3 SCF_3	2.014(4)	2.057(5)	23	0	43
[K(K222)][Fe^{III}TPP(4-MeIm)$_2$]	2.003(12) 1.994(12)	1.958(12) 1.928(12)	1 17	18	22
[Fe(III)TPP(4-MeIm)$_2$]Cl	2.001(12)	1.975(2)	3.1(1)	0	29
[Fe(III)TPP(1-MeIm)$_2$]ClO_4	1.979(3) 1.985(3)	1.970(3) 1.978(3)	22 32	10	19
[Fe(III)T2,6-Cl_2PP(1-VinIm)$_2$]ClO_4	1.980(4) 1.977(4)	1.976(4) 1.968(4)	14 20	6	15
[Fe(III)TPP(HIm)$_2$]Cl	1.993(3) 1.993(4)	1.977(3) 1.964(3)	5 41	0 0	13,27
[Fe(III)TPP(*t*-MU)$_2$]SbF_6	1.992(4)	1.983(4)	22	0	21
[Fe(III)TPP(*c*-MU)$_2$]SbF_6	1.995(7) 1.997(7)	1.979(7) 1.967(7)	15 29	0	21
[Fe(III)TPP(HIm)$_2$] [$CuC_4N_2S_2$)$_2$]$_4C_4H_8O$	1.999(3)	1.981(3)	31	0	44
[Fe(III) PPIX(1-MeIm)$_2$]ClO_4	1.993(6) 1.989(5)	1.988(5) 1.966(5)	3 16	13	24
[Fe(III)TMP(1-MeIm)$_2$]ClO_4	1.991(3) 2.002(3)	1.975(3) 1.965(3)	23 36	0	17
[Fe(III)TPP($Py)_2$]ClO_4	1.987(5) 1.977(4)	2.005(5) 2.001(5)	34 38	86	36
[Fe(III)TPP(2-MeIm)$_2$]ClO_4	1.970(4) 1.971(4)	2.015(4) 2.010(4)	32	89	28
[Fe(III)TMP(3-ClPy)$_2$]ClO_4	1.969(7) 1.968(7)	2.018(7) 2.006(7)	29 48	77	47
[Fe(III)TMP(4-CNPy)$_2$]ClO_4	1.956(6) 1.966(6)	2.021(6) 2.001(5)	43 44	90	47
[Fe(III)TMP(3-EtPy)$_2$]ClO_4	1.962(4) 1.965(4)	2.002(4) 1.989(4)	44 44	90	47
[Fe(III)TMP(4-Me2NPy)$_2$]ClO_4	1.960(4) 1.970(4)	1.989(4) 1.978(4)	37 42	79	17
[Fe(III)TPP(4-CNPy)$_2$]ClO_4	1.947(4) 1.958(4)	2.008(4) 1.997(4)	36 35	89	45

There have been relatively few studies on 'intermediate' spin $[Fe(III)Por(L)_2]^+$ species (where L is an aromatic N-heterocyclic ligand). These include both spin admixed systems and systems where the spin state is very close to $S = 3/2$. There has also been much discussion on what really is an intermediate $S = 3/2$ spin state in six co-ordinate iron porphyrin systems.[51-56, 59-64] . Indeed, on first impression, one would not expect a change from low spin to another spin state with the application of pressure.

5.5.1 Drickamer's Results

The interpretation in the earlier study was based on findings in other systems that "most iron(III) compounds studied to date show a pressure induced reduction to iron(II)". Because of this idea the authors thought it was reasonable to fit changes in the spectra to iron(II) spin states and assigned the presence of low spin iron(II) and intermediate state iron(II)[23] .

However, in 1971, there had been no systematic studies on intermediate spin iron(III)porphyrin complexes so the type of Mössbauer parameters to be expected was not known. In their paper, Grenoble *et al*[23] show five of the high pressure spectra obtained for $[FePPIX(HIm)_2]^+$ as well as explaining the way they fitted the spectra based on their assumptions that iron(II)sites are present.

However, inspection of the spectrum at 1.2 GPa and 296 K indicates that the site is clearly a simple iron(III) low spin site, $\Delta E_Q = 2.07$ mms^{-1} and $\delta = 0.16$ mms^{-1}. For the 10.3 GPa spectrum at 296 K, two sites can be fitted: one with a $\Delta E_Q \sim 2.10$ mms^{-1} and $\delta = 0.08$ mms^{-1} and another with a $\Delta E_Q \sim 2.8$ mms^{-1} and $\delta \sim 0.13$ mms^{-1}. At 383 K and 10.3 GPa a similar fit is possible, also at this temperature and 4.6 GPa two sites may be fitted: $\Delta E_Q \sim 2.07$ mms^{-1} and $\delta \sim 0.15$ mms^{-1} (low spin), and the other $\Delta E_Q \sim$

2.6 mms^{-1} and $\delta \sim 0.14$ mms^{-1} (admixed spin $S = {}^{3}/_{2},{}^{5}/_{2}$). However, at 2.4 GPa the spectrum does not easily fit to two such sites although the major part of the spectrum fits a low spin iron(III) site $\Delta E_Q \sim 2.06$ mms^{-1} and $\delta \sim 0.2$ mms^{-1}, and the minor part of the spectrum has a narrow $\Delta E_Q \sim 1.4$ mms^{-1} and $\delta \sim 0.2$ mms^{-1}, which is clearly not intermediate spin iron(III). However this site would be compatible with a $(d_{xz},d_{yz})^4(d_{xy})^1$ ground state that is usually found for axial ligands that are sterically hindered from the iron, and are more weakly bonded than the porphyrin nitrogen ligands. Although there is little evidence for a similar site in the 4.6 GPa spectrum, there is none in the 10.3 GPa spectrum.

So, how can the spectrum be explained? At room pressure the single site has a ΔE_Q slightly higher than the present work but much lower than the $[FePPIX(HIm)_2]^+$ type spectra. This suggests that this site reflects a perpendicular arrangement for the axial ligand planes as the pressure increases the first effect is that the second site ($\Delta E_Q \sim 1.4$ mms^{-1}) appears. The simplest explanation is that some of the axial ligands become sterically hindered though the ligands do not change their orientation. The only way this would occur would be if hydrogen bonding from the imidazole ligands to the chloride ions was strong enough to pull the ligands away from the iron atoms. This explanation would be in keeping with only a small proportion of the molecules being affected and the structure distorting under pressure. At higher pressures this site disappears and only the original site and the intermediate spin iron(III) are present.

As discussed for $[FeOEP(4\text{-}NH_2Py)_2]^+$, the intermediate spin iron(III) complex requires the ligand planes to be parallel and orientated over the Fe-N_{por} vectors. Hence, here in the $[FePPIX(HIm)_2]^+$ complex for the "intermediate" spin iron(III) state the ligands must have re-orientated under the applied pressure. In our sample,

$[FePPIX(HIm)_2]^+Cl$ discussed above, we noted that re-orientation of the ligand planes were taking place with pressure. At the high pressures used by Grenoble *et al*[23] the intermediate spin iron(II) site is accessible in $FePPIX(HIm)_2Cl$. Hence, it is apparent that the application of high pressure can give access to a range of iron(III) environments in a naturally occurring iron porphyrin.

5.6 Conclusions

The formation of a new low spin $Fe(III)OEP(NH_2Py)_2Cl$ compound has been confirmed by the high pressure Mössbauer spectroscopy and the comparative data of $Fe(III)PPIX(HIm)_2Cl$ and previous work presented in this chapter.

The Mössbauer data for these compounds when compared with a whole range of $[Fe(III)Por(L)_2]^+$ complexes provided a better understanding into the nature of all these compounds. A study using computation and interpretation of Mössbauer parameters gives a complete understanding of the work achieved here [60]. The dynamics of iron porphyrin compounds can be further studied using aggregates of iron porphyrin to accelerate the spin-spin relaxation[61].

5.7 References

1. P. J. Marsh, J .Silver, M. C. R. Symons, F. A. Taiwo, *J. Chem Soc., Dalton Trans.* **1996**, 2361.
2. H. M. Marques, O. Q. Munro, M. L. Crawcour, *Inorg. Chim. Acta*. **1992**, *96*, 221.
3. R. Keller, O. Groudinsky, K. Wuthrich, *Biochim. Biophys. Acta*, **1973**, *328*, 233.
4. O. K. Medhi, J. Silver, *J. Chem. Soc., Dalton Trans.* **1990**, 263.

5. O. K. Medhi, J. Silver, *J. Chem. Soc., Dalton Trans.* **1990**, 555.

6. W. R. Scheidt, S. R. Osvath, Y. J. Lee, *J. Am. Chem. Soc.* **1987**, *109*, 1958.

7. D. M. Collins, R. Countryman, J. L. Hoard, *J. Am. Chem. Soc.* **1972**, *94*, 2066.

8. K. Hatano, M. K. Safo, F. A. Walker, W R. Scheidt, *Inorg. Chem.* **1991**, *30*, 1643.

9. F. A. Walker, B. H. Huynh, W. R. Scheidt, S. R. Osvath, *J. Am. Chem. Soc.* **1986**, *108*, 5288.

10. M. K. Safo, G. P. Gupta, F. A. Walker, W. R. Scheidt, *J. Am. Chem. Soc.* **1991**, *113*, 5497.

11. T. Yoshimura, T. Ozaki, *Arch. Biochem. Biophys.*, **1984**, *230*, 466.

12. T. B. Higgins, M. K. Safo, W. R. Scheidt, *Inorg. Chim. Acta*, **1990**, *178*, 261.

13. M. Nakamura, K.Tajima, K.Tada, K. Ishizu, N. Nakamura, *Inorg. Chim. Acta*, **1994**, *224*, 113.

14. R Quinn, J. S. Valentine, M. P. Byrn, C. E. Strouse, *J. Am. Chem. Soc.* **1987**, *109*, 3301.

15. R. Quinn, C. E. Strouse, J. S. Valentine, *Inorg. Chem.*, **1983**, *22*, 3934.

16. F. A. Walker, D. Reis, V. L. Balke, *J. Am. Chem. Soc.*, **1984**, *106*, 6888.

17. R. G. Little, K. R. Dymock, J. A. Ibers, *J. Am. Chem. Soc*., **1975**, *97*, 4532.

18. L. M. Epstein, D. K. Straub, C. Marricondi, *Inorg. Chem.*, **1967**, *6*, 1720.

19. W. R. Scheidt, D. M. Chipman, *J. Am. Chem. Soc.*, **1986**, *108*, 1163.

20. S. M Soltis, C. E. Strouse, *J. Am. Chem. Soc.*, **1988**, *110*, 2824.

21. W. R. Scheidt, J. L. Kirner, J. L. Hoard, C. A. Reed, *J. Am. Chem. Soc.* **1987**, *109*, 1963.

22. J. Silver, P. J. Marsh, M. C. R. Symons, D. A. Svistunenko, C. S. Frampton, G. R. Fern, *Inorg. Chem*., **2000,** *39*, 2874.

23. D. C. Grenoble, C. W. Frank, C. B. Bangeron, H. G. Drickamer, *J. Chem. Phys.*, **1971**, *55*, 1633.

24. G. T. Babcock, P. M. Callahan, M. R. Ondrias, I. Salmeen, *Biochemistry*, **1981**, *20*, 959.

25. *Cytochrome Oxidase*, W. E Blumberg, J. Peisach, edited by T. E. King, Y. Orii, B. Chance, K. Okuniki, Elsevier, Amsterdam, **1979**.

26. G. T. Babcock, W. R. Widger, W. A. Cramer, W. A. Oertlings, J. Mertz, *Biochemistry*, **1985**, *24*, 3638.

27. W. R. Widger, W. A. Cramer, R. G. Herrman, A. Trebst, *Proc. Natl. Acad. Sci. USA*, 1984, *81*, 674-678.

28. F. S. Matthews, E. W. Czerwinski, P. Argos, In: *The Porphyrins*: Dolphin, D., Ed. Academic Press: New York, **1979**, *Vol. 7*, 108.

29. T. Iyanagi, *Biochemistry*, **1977**, *16*, 2725.

30. G. R. Moore, R. J. P. Williams, *FEBS Lett*. **1977**, *79*, 229.

31. M. F. Perutz, L F. Ten Eyck, *Cold Spring Harbor Symp. Quant. Biol.* **1971**, *36*, 295.

32. J. R. Salerno, *J. Biol. Chem.*, **1984**, *259*, 2331.

33. A. Tsai and G. Palmer, *Biochim. Biophys. Acta*, **1983**, *722*, 349.

34. D. L Brautigan, B. A. Feinberg, B. M. Hoffman, E. Margoliash, J. Peisach and W. E. Blumberg, *J. Biol. Chem.*, **1977**, *252*, 574.

35. K. R. Carter, A. Tsai and G. Palmer., *FEBS Lett.*, **1981**, *132*, 243

36. F. A. Walker, B. H. Hunyh, W. R. Scheidt and S. R. Osvath, *J. Am Chem. Soc*., **1986**, *108*, 5288.

37. F. A. Walker, D. Reiss and V. L. Balke, *J. Am. Chem. Soc*., **1984**, *106*, 6888.

38. W. R. Scheidt and D. M. Chipman, *J. Am. Chem. Soc*., **1986**, *108*, 1163.

39. *Charge Transfer Interaction of Biomolecules*, M. F. Slifkin, Acad. Press, London, **1971**.

40. M. K. Safo, G. P. Gupta, C. T. Watson, U. Simonis, F. A. Walker, W. R. Scheidt, *J. Am. Chem. Soc.* **1992**, *114*, 7066.

41. T. A. Kent, E. Münck, W. R. Dunham, W. F. Filter, K. L. Finding, T. Yoshida and J. A. Fee, *J. Biol. Chem*., **1982,** *275*, 1248.

42. J. Peterson, J. Silver, M. T. Wilson, and I. E. G. Morrison, *J. Inorg. Biochem*., **1980,** *13*, 75.

43. J. Peterson, M. M. Saleem, J. Silver, M. T. Wilson, and I. E. G. Morrison, *Inorg. Biochem*., **1983,** *19*, 165.

44. P. Adams, R. C. de L. Milton, J. Silver, *Biometals*, **1994**, *7*, 217.

45. E. Münck, *Methods. Enzymol*., **1978**, *54*, 1434.

46. O. K. Mehdi, J. Silver., *Inorg. Chim Acta*., **1989**, *164*, 231.

47. Y. Hamed, R. C. Hider and J. Silver, *Inorg. Chem. Acta.*, **1982**, *66*, 13.

48. C. A. McCammon in "*Recent Trends in High pressure Research*", edited by A. K. Singh, Oxford and IBH, New Delhi, **1982**, 824.

49. V. V. Borovkov, J. M. Lintuluoto and Y. Inuone, *Synlett.*, **1999**, *1*, 61.

50. H. A. O. Hill, P. D. Skyte, J. W. Buchler, H. Lueken, M. Tonn, A. K. Gregson, G. J. Pellizer, *J. Chem. Soc. Chem. Comm*., **1979**, 151.

51. A. Jayaraman, Rev. Mod. Physics, **1983**, *55*, 1.

52. M. K. Safo, F. A. Walker, A. M. Raitsimring, W. P. Walters, D. P. Dolata, P. G. Debrunner, W. R. Scheidt, *J. Am. Chem. Soc.* **1994**, *116*, 7760.

53. B. R. Serr, C E L Headford, C. M. Elliot, C. P. Anderson, *Acta Cryst*., **1990**, C46, 500.

54. M. Cesario, C. Gianotti, J. Guilhem, J. Silver, J. Zakrzewski, *J. Chem. Soc., Dalton trans.,* **1997**, 47.

55. W. R Scheidt, D. K. Geiger, K.J. Haller, *J. Am. Chem. Soc*. **1982**, *104*, 495.

56. W. R Scheidt, D. K. Geiger, R. G. Hayes, G. Lang, *J. Am. Chem. Soc*. **1983**, *105*, 2625.

57. D. A. Davies, *PhD Thesis*, University of Essex, **1998**.

58. W. R Scheidt, D. K. Geiger, Y. J. Lee, C. A. Reed, G. Lang, *Inorg. Chem*., **1987**, *26*, 1039.

59. A. K. Gregson, *Inorg. Chem*., **1981**, *20*, 81.

60. http:/extra.springer.com/2011/Grodzicki_computation.pdf.

61. K. Dziedzic-Kocurek, J. Stanek and K Burda, *Hyperfine Interactions*, **2008**, *87*, 185.

Chapter 6

6.1 Summary and General Conclusions

It is evident from the work presented in this thesis that the chemistry of porphyrin and the related phthalocyanine compounds are interesting, important and varied.

In nature, haemoproteins are integral components in a number of diverse biochemical pathways including electron transport (cyctochromes and the related chlorophylls), oxygen transport (haemoglobin), oxygen storage (myoglobin), hydroxylation reactions (cyctochrome P450) and molecular rearrangement (cobalamin enzymes).

In Chapter 3, H_2TPP, Fe(III)TPPCl and SiPc[PyCOO]$_2$ were successfully synthesised. Phthalocyanines are not found in nature, though they are stable molecules. Phthalocyanines are used widely in dye industry. SiPc[PyCOO]$_2$ was very difficult to isolate due to its nature : high retention for water and formation of oligomeric species and hydroxides in solvents in which it is very stable. The attempt to form a large complex structure between Fe(III)TPPCl and SiPc[PyCOO]$_2$ was not successful. However, detailed studies of some physical and chemical aspects of these compounds were achieved. There was less success when a series of substituted imidazoles were used to form a new type of complex with Fe(III)TPPCl.

High-pressure Mössbauer spectroscopy was used (Chapter 4), in studies of ^{57}FeOEPCl and ^{57}FePPIXCl.These compounds were prepared using enriched iron-57, as very small quantities of sample were required (<1 mg).

These studies highlighted some of the theory behind the spin state of the compound when pressure was applied.

In Chapter 5, [^{57}Fe(III)OEP(4-NH_2Py)$_2$]Cl and [^{57}FePPIX(HIm)$_2$]Cl were the focus. Again, high-pressure Mössbauer spectroscopic technique was applied to gain

understanding of the spin states that occur in these compounds when pressure was applied. The formation of new low spin [Fe(III)OEP($NH_2Py)_2$]Cl compounds have been confirmed and the comparative data of [Fe(III)PPIX($HIm)_2$]Cl and previous work presented in this chapter. The Mössbauer data for these compounds when compared with a whole range of $[Fe(III)Por(L)_2]^+$ complexes provided a better understanding into the nature of all these compounds.

6.2 Future work

There is still a need to study many more low spin iron(III) porphyrins under high pressures by Mössbauer spectroscopy. This is more to learn about the factors that affect the spin state.

In addition it would be useful to make parallel high pressure studies on the structural changes that occured using Raman spectroscopy. The porphyrin derivatives that been synthesised here and have very important biological applications. Ideally Synchrotron radiation spectroscopy will improve the speed of data collections and solving structures that will leads to obtain structural information (i.e bond lengths and angles) on a timescale allows a promising study. This results/study could be correlated with Mössbauer spectroscopic parameters.

Appendix

Conference Poster Presentations/Publications

1. Poster presentation:
   "A High Pressure Mössbauer Spectroscopic Study of
   [^{57}Fe(III)OEPCl]

   S. Anandan *et al*., ICAME Conference, Oxford University, **2000**

2. Publication:
   High Pressure Mössbauer Spectroscopic Studies of Molecular Solids. The Importance of 'Free' Space in Molecular Lattices.

   J. Silver, **S. Ananadan**, D. A. Davies, G. R. Fern, P. J. Marsh, J. R. Miller, P. J. Titler and C. A. McCammon, *Hyperfine Interactions*, **2002** *142/142*, 109-117.

A High Pressure Mössbauer Spectroscopy Study of [^{57}FeOEPCl]

S. Anandan[1], J. Silver[1], G. R. Fern[1], P. J. Titler[1], C. A. McCammon[2].

[1]School of Chemical and Life Sciences, University of Greenwich, Wellington Street, Woolwich, London, SE18 6PF. E-mail s.anandan@gre.ac.uk.

[2]Bayerishes Geoinstitut, Universität Bayreuth, D-95440, Bayreuth, Germany.

Introduction

Iron porphyrins are widespread in nature, being found as the active sites in hemoglobin, myoglobin and a wide range of cytochromes[1]. The most common porphyrin is Protoporphyrin IXiron(II)/(III) [PPIXFe(II)/(III)] (haem), however this complex is difficult to crystallise and its chemistry is often modelled using man made porphyrins. We have previously studied [Fe^{III}PPIXCl][2] by high pressure Mössbauer spectroscopy and found evidence of a change of spin from high spin state to a spin admixed state S = +/- $^3/_2$, +/- $^5/_2$.

To extend our work in this area we present here the results of a high pressure Mössbauer spectroscopic study produced 2,3,7,8,12,13,17,18-octaethylporphyrin ^{57}iron(III) chloride [$^{57}Fe^{III}$OEPCl]. The reason for choosing this porphyrin is that it has ethyl side groups substituted in the same positions on the macrocycle ring as the side groups in PPIX and thus a better model for the latter than tetraphenylporphyrins.

Experimental

The preparation of [^{57}FeOEPCl] was prepared according to a literature method[3]. Only anhydrous and purified solvents were used for the synthesis. ^{57}Fe foil (0.01g, 0.18 mmol) was dissolved in deoxygenated conc. HCl (2ml) under nitrogen. Two drops of 2, 6-lutidine were added to a solution of H_2OEP[4] (5mg, 0.09 mmol) in $CHCl_3$ (3ml) and anhydrous $^{57}FeCl_2$ in CH_3Cl. The reaction mixture was stirred at room temperature for 5 hours. Identification of the product - [^{57}FeOEPCl] was achieved by a comparison of the electronic absorption spectrum of a purchased reference sample.

High pressure Mössbauer spectra were recorded using a Merill Basset diamond anvil cell (DAC) under hydrostatic pressure. 4:1 Methanol:Ethanol was used as the hydrostatic pressure fluid[5]. The ruby fluorescence method was used to measure the pressure in the DAC[6].

Results

Table 1 Mössbauer Spectroscopic Parameters for [^{57}FeOEPCl]

Pressure GPa	δ mms^{-1}.	ΔE_Q mms^{-1}	Γ mms^{-1}	% Area	δ mms^{-1}.	ΔE_Q mms^{-1}	Γ mms^{-1}	% Area
1.38(5)	0.28(1)	0.82(2)	0.64(2)	100(2)				
1.88(5)	0.34(3)	0.98(4)	0.77(5)	100(4)				
2.05(21)	0.30(2)	0.91(4)	0.78(3)	100(3)				
2.57(31)	0.314(3)	0.937(4)	0.85(1)	100(1)				
2.75(20)	0.304(5)	0.898(9)	0.78(1)	100(1)				
3.50(23)	0.318(4)	0.968(7)	0.73(1)	100(1)				
4.37(24)	0.327(2)	0.783(4)	0.61(1)	100(1)				
5.40(33)	0.310(4)	0.95(1)	0.65(2)	76(2)	0.31(1)	2.30(4)	0.76(6)	24(2)
6.30(41)	0.315(1)	0.95(1)	0.65(2)	70(2)	0.31*	2.29*	0.81(6)	30(1)

* values held in fitting routine.

Figure 1

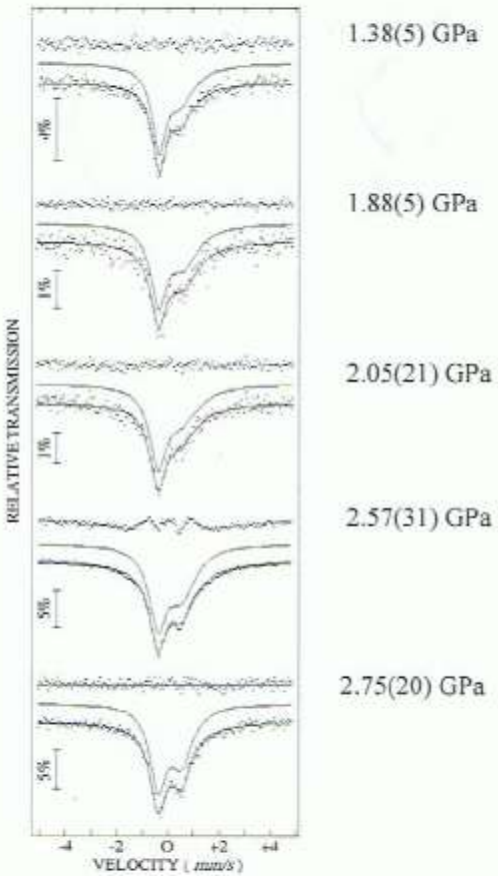

Figure 2

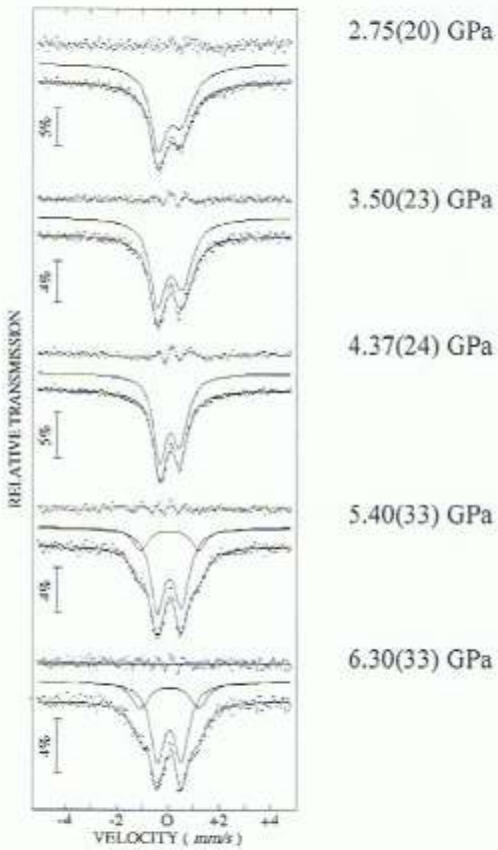

Figure 1 and 2 of ^{57}Fe Mössbauer spectra under high pressure of [^{57}FeOEPCl], with increasing pressure from 1.38(5) GPa to 6.30(41) GPa.

Figure 3

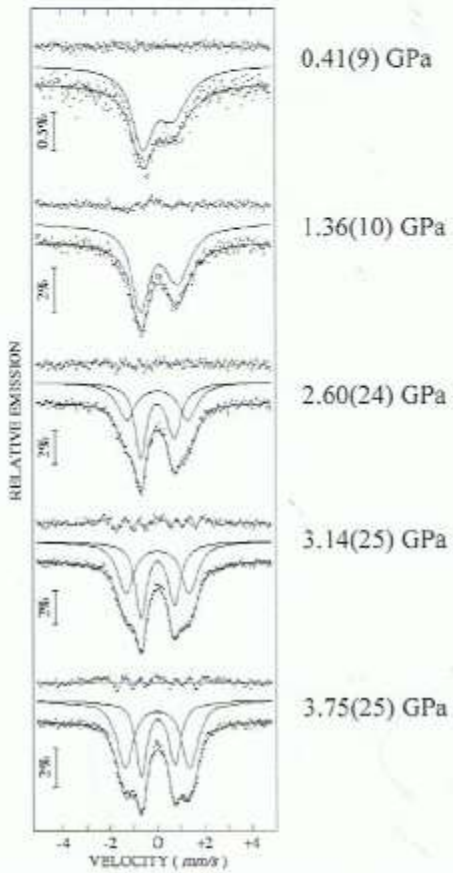

Figure 4

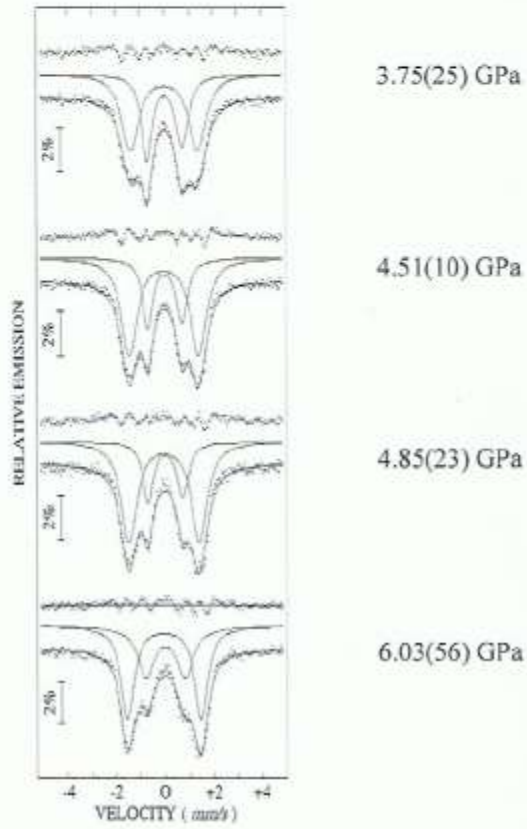

Figure 3 and 4 of ^{57}Fe Mössbauer spectra under high pressure of [^{57}FePPIXCl], with increasing pressure from 0.41(9) GPa to 6.03(56) GPa.

Discussion

The Mössbauer spectroscopic data for [^{57}FeOEPCl] are presented in Table 1 and in figs. 1 and 2. The room temperature Mössbauer spectroscopic data are in agreement with literature values[7] and indicate that the compound contains high spin Fe^{III}. The first effect of applying pressure was to decrease the broadness of the background and as the pressure increased this process steadily continued. These spectra were fitted as doublets with a height variation allowing for asymmetry and for the ratio of the widths of the two lines to vary. The given linewidth is for the low velocity line. The quadrupole splitting (ΔE_Q) for the high spin Fe^{III} site becomes more obviously resolved as the pressure increased to 4.37(24) GPa. It then increased at higher pressures. This differed for the ΔE_Q of the high spin Fe^{III} in [^{57}FePPIXCl](fig. 3 and 4) which initially increased with increasing pressure and then levelled off. This was in keeping with our findings for [^{57}FePPIXCl] (figs. 3 and 4).

At 5.40(33) GPa there is evidence for the development of a second site in the spectrum, which persists at 6.30(41) GPa. The parameters for this site are compatible with those of an S = +/- $^3/_2$, +/- $^5/_2$ spin admixed state. Again this is in agreement with our findings for [^{57}FePPIXCl] (figs. 3 and 4). However for the [^{57}FeOEPCl] the spin admixed site only occurs at higher pressures and the proportion of this site is much less than in [^{57}FePPIXCl].

It should be noticed that in both figs. 1 and 2 and figs. 3 and 4 the asymmetry of the high spin Fe^{III} site decreased dramatically as the pressure increased. The room pressure asymmetry is due to the presence of Kramer's doublets. This suggests that at higher pressures as the lattice is compressed, the higher energy Kramer's doublet becomes less populated due to pressure increasing the energy differences between these energy levels.

At low temperature (4.2K) and normal pressure, symmetrical Mössbauer spectra are observed, as only the S_z = +/- ½ states are populated and - as Blume[8] has explained, the spin-spin relaxation is fast. As the temperature increases, the upper states populate (+/- $^3/_2$ +/- $^5/_2$) with longer relaxation times, leading to asymmetric Mössbauer spectra - like those at higher pressures in figs. 2 and 4. This means that the application of pressure has a similar effect on the Mössbauer spectra, to that of lowering temperature, as we have reported previously[9-10].

Acknowledgements

High-pressure experiments were performed at the Bayerisches Geoinstitut under the E. C. 'Human Capital and Mobility' - Access to large scale facilities programme. (Contract No. ERBCHGET940053 to D. C. RUBIE).

References

[1] B.P Berezin, "Coordination compounds of Porphyrins and Phthalocyanines", John Wiley & Sons Ltd., (1981).
[2] P.J. Titler, D.A. Davies, J. Silver and C.A. McCammon - unpublished results, presented as a poster at ICAME 1999.
[3] V.V. Borovkov, J. M. Lintuluoto andY. Inuone, Synlett., 1(1999) 61.
[4] J. Sessler, A. Mozaffari, M. Johnson, Org. Synth., 70(1991) 68.
[5] A. Jayaraman, Rev. Mod. Phys., 55(1983) 1.
[6] J. D. Barnett, S. Block and G. J. Piermarinni, Rev. Sc. Instrum, 44(1973) .
[7] B. W. Fitzsimmons, J. R. Sams and T. B. Tsin, Chem. Phys. Lett., 119(1997) 2563.
[8] M. Blume, Phys. Rev. Lett., 18(1967) 305.
[9] J. Silver, R. M. G. R. Roberts, D. A. Davies and C. A. McCammon, Chem. Commun., (1996) 11.
[10] J. Silver, J.R. Miller, D.A. Davies, and C.A. McCammon, Inorg. Chem., 36(1997) 4017.

A High Pressure Mössbauer Spectroscopy Study of [^{57}FeOEPCl]

S. Anandan[1], J. Silver[1], G. R. Fern[1], P. J. Titler[1], C. A. McCammon[2].

[1]School of Chemical and Life Sciences, University of Greenwich, Wellington Street, Woolwich, London, SE18 6PF. E-mail s.anandan@gre.ac.uk.

[2]Bayerishes Geoinstitut, Universität Bayreuth, D-95440, Bayreuth, Germany.

Introduction

Iron porphyrins are widespread in nature, being found as the active sites in hemoglobin, myoglobin and a wide range of cytochromes[1]. The most common porphyrin is Protoporphyrin IXiron(II)/(III) [PPIXFe(II)/(III)] (haem), however this complex is difficult to crystallise and its chemistry is often modelled using man made porphyrins. We have previously studied [Fe^{III}PPIXCl][2] by high pressure Mössbauer spectroscopy and found evidence of a change of spin from high spin state to a spin admixed state S = +/- $^3/_2$, +/- $^5/_2$.

To extend our work in this area we present here the results of a high pressure Mössbauer spectroscopic study produced 2,3,7,8,12,13,17,18-octaethylporphyrin ^{57}iron(III) chloride [$^{57}Fe^{III}$OEPCl]. The reason for choosing this porphyrin is that it has ethyl side groups substituted in the same positions on the macrocycle ring as the side groups in PPIX and thus a better model for the latter than tetraphenylporphyrins.

Experimental

The preparation of [^{57}FeOEPCl] was prepared according to a literature method[3]. Only anhydrous and purified solvents were used for the synthesis. ^{57}Fe foil (0.01g, 0.18 mmol) was dissolved in deoxygenated conc. HCl (2ml) under nitrogen. Two drops of 2, 6-lutidine were added to a solution of H_2OEP[4] (5mg, 0.09 mmol) in $CHCl_3$ (3ml) and anhydrous $^{57}FeCl_2$ in CH_3Cl. The reaction mixture was stirred at room temperature for 5 hours. Identification of the product - [^{57}FeOEPCl] was achieved by a comparison of the electronic absorption spectrum of a purchased reference sample.

High pressure Mössbauer spectra were recorded using a Merill Basset diamond anvil cell (DAC) under hydrostatic pressure. 4:1 Methanol:Ethanol was used as the hydrostatic pressure fluid[5]. The ruby fluorescence method was used to measure the pressure in the DAC[6].

Results

Table 1 Mössbauer Spectroscopic Parameters for [^{57}FeOEPCl]

Pressure GPa	δ mms^{-1}.	ΔE_Q mms^{-1}	Γ mms^{-1}	% Area	δ mms^{-1}.	ΔE_Q mms^{-1}	Γ mms^{-1}	% Area
1.38(5)	0.28(1)	0.82(2)	0.64(2)	100(2)				
1.88(5)	0.34(3)	0.98(4)	0.77(5)	100(4)				
2.05(21)	0.30(2)	0.91(4)	0.78(3)	100(3)				
2.57(31)	0.314(3)	0.937(4)	0.85(1)	100(1)				
2.75(20)	0.304(5)	0.898(9)	0.78(1)	100(1)				
3.50(23)	0.318(4)	0.968(7)	0.73(1)	100(1)				
4.37(24)	0.327(2)	0.783(4)	0.61(1)	100(1)				
5.40(33)	0.310(4)	0.95(1)	0.65(2)	76(2)	0.31(1)	2.30(4)	0.76(6)	24(2)
6.30(41)	0.315(1)	0.95(1)	0.65(2)	70(2)	0.31*	2.29*	0.81(6)	30(1)

* values held in fitting routine.

Figure 1

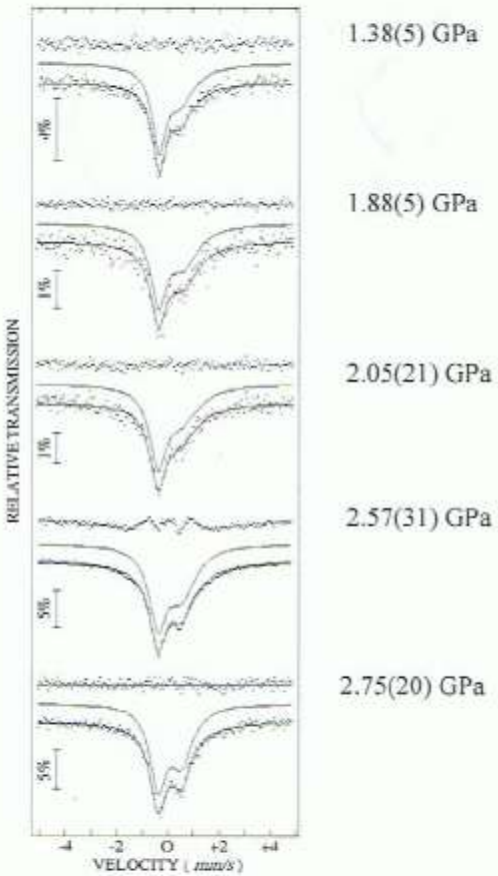

Figure 2

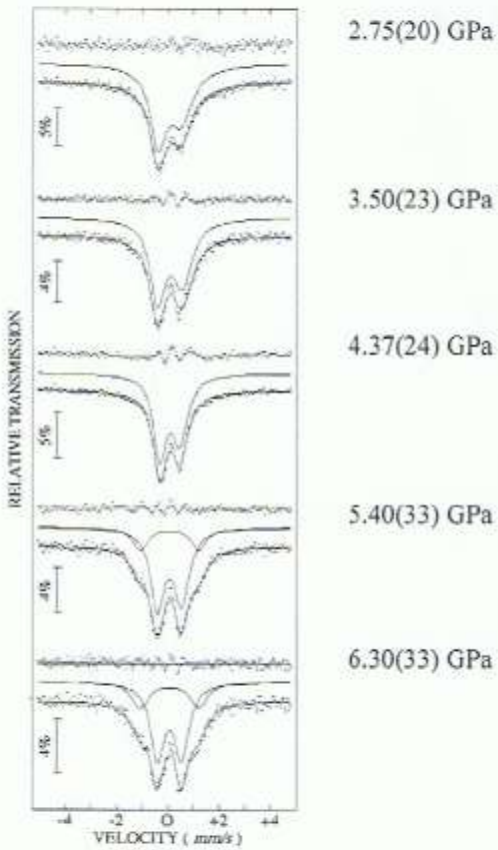

Figure 1 and 2 of ^{57}Fe Mössbauer spectra under high pressure of [^{57}FeOEPCl], with increasing pressure from 1.38(5) GPa to 6.30(41) GPa.

Figure 3

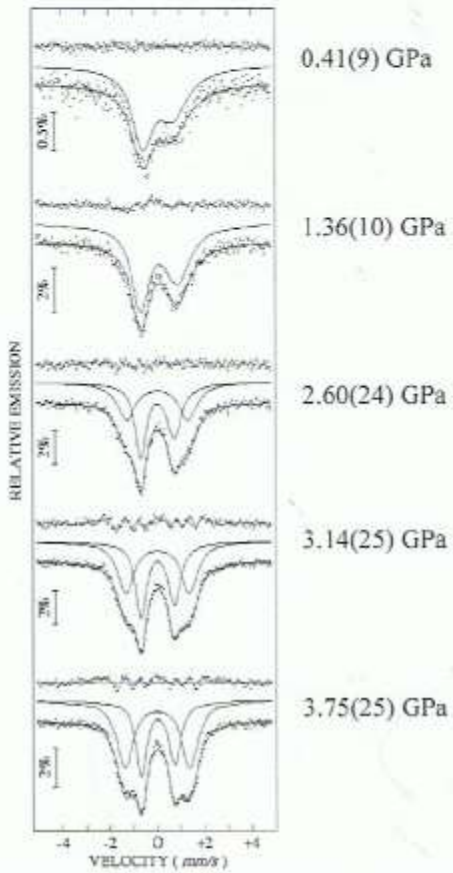

Figure 4

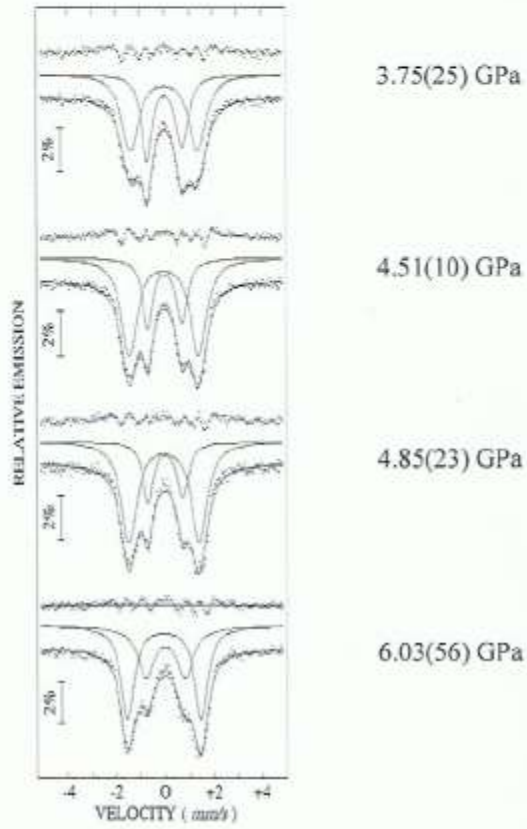

Figure 3 and 4 of ^{57}Fe Mössbauer spectra under high pressure of [^{57}FePPIXCl], with increasing pressure from 0.41(9) GPa to 6.03(56) GPa.

Discussion

The Mössbauer spectroscopic data for [^{57}FeOEPCl] are presented in Table 1 and in figs. 1 and 2. The room temperature Mössbauer spectroscopic data are in agreement with literature values[7] and indicate that the compound contains high spin Fe^{III}. The first effect of applying pressure was to decrease the broadness of the background and as the pressure increased this process steadily continued. These spectra were fitted as doublets with a height variation allowing for asymmetry and for the ratio of the widths of the two lines to vary. The given linewidth is for the low velocity line. The quadrupole splitting (ΔE_Q) for the high spin Fe^{III} site becomes more obviously resolved as the pressure increased to 4.37(24) GPa. It then increased at higher pressures. This differed for the ΔE_Q of the high spin Fe^{III} in [^{57}FePPIXCl](fig. 3 and 4) which initially increased with increasing pressure and then levelled off. This was in keeping with our findings for [^{57}FePPIXCl] (figs. 3 and 4).

At 5.40(33) GPa there is evidence for the development of a second site in the spectrum, which persists at 6.30(41) GPa. The parameters for this site are compatible with those of an S = +/- $^3/_2$, +/- $^5/_2$ spin admixed state. Again this is in agreement with our findings for [^{57}FePPIXCl] (figs. 3 and 4). However for the [^{57}FeOEPCl] the spin admixed site only occurs at higher pressures and the proportion of this site is much less than in [^{57}FePPIXCl].

It should be noticed that in both figs. 1 and 2 and figs. 3 and 4 the asymmetry of the high spin Fe^{III} site decreased dramatically as the pressure increased. The room pressure asymmetry is due to the presence of Kramer's doublets. This suggests that at higher pressures as the lattice is compressed, the higher energy Kramer's doublet becomes less populated due to pressure increasing the energy differences between these energy levels.

At low temperature (4.2K) and normal pressure, symmetrical Mössbauer spectra are observed, as only the S_z = +/- ½ states are populated and - as Blume[8] has explained, the spin-spin relaxation is fast. As the temperature increases, the upper states populate (+/- $^3/_2$ +/- $^5/_2$) with longer relaxation times, leading to asymmetric Mössbauer spectra - like those at higher pressures in figs. 2 and 4. This means that the application of pressure has a similar effect on the Mössbauer spectra, to that of lowering temperature, as we have reported previously[9-10].

Acknowledgements

High-pressure experiments were performed at the Bayerisches Geoinstitut under the E. C. 'Human Capital and Mobility' - Access to large scale facilities programme. (Contract No. ERBCHGET940053 to D. C. RUBIE).

References

[1] B.P Berezin, "Coordination compounds of Porphyrins and Phthalocyanines", John Wiley & Sons Ltd., (1981).
[2] P.J. Titler, D.A. Davies, J. Silver and C.A. McCammon - unpublished results, presented as a poster at ICAME 1999.
[3] V.V. Borovkov, J. M. Lintuluoto andY. Inuone, Synlett., 1(1999) 61.
[4] J. Sessler, A. Mozaffari, M. Johnson, Org. Synth., 70(1991) 68.
[5] A. Jayaraman, Rev. Mod. Phys., 55(1983) 1.
[6] J. D. Barnett, S. Block and G. J. Piermarinni, Rev. Sc. Instrum, 44(1973) .
[7] B. W. Fitzsimmons, J. R. Sams and T. B. Tsin, Chem. Phys. Lett., 119(1997) 2563.
[8] M. Blume, Phys. Rev. Lett., 18(1967) 305.
[9] J. Silver, R. M. G. R. Roberts, D. A. Davies and C. A. McCammon, Chem. Commun., (1996) 11.
[10] J. Silver, J.R. Miller, D.A. Davies, and C.A. McCammon, Inorg. Chem., 36(1997) 4017.

A High Pressure Mössbauer Spectroscopy Study of [$^{57}Fe^{III}$OEPCl]

S. Anandan[1], J. Silver[1], G. R. Fern[1], P. J. Titler[1], C. A. McCammon[2]

[1]School of Chemical and Life Sciences, University of Greenwich, Wellington Street, Woolwich, London SE18 6PF.

[2]Bayerisches Geoinstitut, Universität Bayreuth, D-95440 Bayreuth, Germany.

the UNIVERSITY of GREENWICH

Introduction

Iron porphyrins are widespread in nature, being found as the active sites in hemoglobin, myoglobin and a wide range of cytochromes[1]. The most common porphyrin is Protoporphyrin IX iron(II)/(III) [PPIXFe(II)/(III)] (haem), however this complex is difficult to crystallise and its chemistry is often modelled using man made porphyrins. We have previously studied [Fe^{III}PPIXCl][2] by high pressure Mössbauer spectroscopy and found evidence of a change of spin from high spin to its spin admixed S = +/- $^1/_2$, +/- $^5/_2$.

To extend our work in this area we present here the results of a high pressure Mössbauer spectroscopic study of 2,3,7,8,12,13,17,18-octaethylporphyrin ^{57}iron(III) chloride [$^{57}Fe^{III}$OEPCl]. The reason for choosing this porphyrin is that it is substituted in the same positions as PPIX and thus a better model for the latter than tetraphenylporphyrins.

Experimental

The preparation of [^{57}FeOEPCl] was prepared according to a literature method[3]. Only anhydrous and purified solvents were used for the synthesis. ^{57}Fe foil (0.01g, 0.18 mmol) was dissolved in deoxygenated conc. HCl (2ml) under nitrogen. Two drops of 2, 6-lutidine were added to a solution of OEP[4] (5mg, 0.09 mmol) in $CHCl_3$ (3ml) and anhydrous $^{57}FeCl_2$ in CH_3Cl. The reaction mixture was stirred at room temperature for 5 hours. Identification of the product - [^{57}FeOEPCl] was achieved by a comparison of the electronic absorption spectrum of a purchased reference sample.

High pressure Mössbauer spectra were recorded using a Merill Basset diamond anvil cell (DAC) under hydrostatic pressure. 4:1 Methanol:Ethanol was used as the hydrostatic pressure fluid[5]. The ruby fluorescence method was used to measure the pressure in the DAC[6].

Results

Table Mössbauer Data for [^{57}FeOEPCl]

Pressure (GPa)	δ (mms^{-1})	ΔE_Q mms^{-1}	Γ (mms^{-1})	% Area	δ (mms^{-1})	ΔE_Q (mms^{-1})	Γ (mms^{-1})	% Area
1.38(5)	0.28(1)	0.62(2)	0.64(2)	100(2)				
1.88(5)	0.34(3)	0.66(4)	0.77(5)	100(4)				
2.05(21)	0.30(2)	0.81(4)	0.75(3)	100(3)				
2.57(31)	0.31(2)	0.93(4)	0.85(1)	100(1)				
2.75(20)	0.30(4)	0.98(6)	0.78(1)	100(1)				
3.50(23)	0.31(4)	0.98(7)	0.75(1)	100(1)				
4.37(24)	0.32(2)	0.78(4)	0.81(1)	100(1)				
5.40(33)	0.31(4)	0.95(1)	0.46(2)	76(2)	0.37(1)	2.30(4)	0.78(6)	24(2)
6.30(41)	0.31(2)	0.95(1)	0.65(2)	70(2)	0.91*	2.29*	0.81(6)	30(1)

*values held in fitting routine

Figure 1

^{57}Fe Mössbauer spectra under high pressure of ^{57}FeOEPCl with increase in pressure from 1.38(5) GPa to 2.75(20) GPa

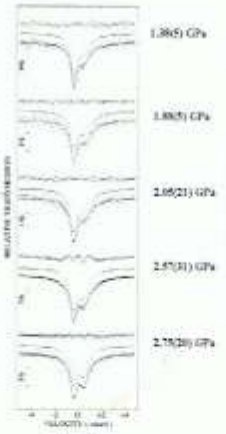

Figure 2

^{57}Fe Mössbauer spectra under high pressure of ^{57}FeOEPCl with increase in pressure from 2.75(20) GPa to 6.30(41) GPa

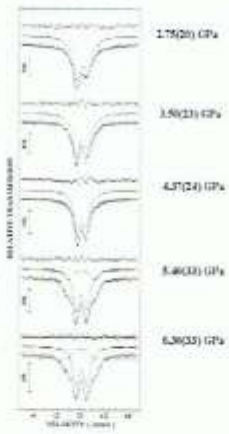

Figure 3

^{57}Fe Mössbauer spectra under high pressure of ^{57}FePPIXCl with increase in pressure from 0.41(9) GPa to 3.75(25) GPa

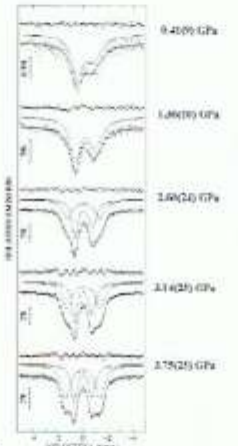

Figure 4

^{57}Fe Mössbauer spectra under high pressure of ^{57}FePPIXCl, increase in pressure from 3.75(25) GPa to 6.05(56) GPa

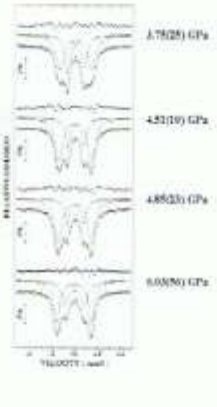

Discussion

The Mössbauer spectroscopic data for [^{57}FeOEPCl] are presented in the Table and in figs. 1 and 2. The room temperature Mössbauer data are in agreement with literature values[7] and indicate that the compound contains high spin Fe(III).

The first effect of applying pressure is to decrease the broadness of the background and as the pressure increases this process steadily continues. These spectra have been fitted as doublets with a height variation allowing for asymmetry and for the ratio of the widths of the two lines to vary. The given linewidth in the Table is for the low velocity line. The quadrupole splitting (ΔE_Q) for the high spin Fe^{III} site becomes more obviously resolved as the pressure increases up to 4.37(24) GPa. It then increases at higher pressures. This differs for the ΔE_Q of the high spin Fe^{III} in [^{57}FePPIXCl](fig. 3 and 4) which initially increases with increasing pressure and then levels off. This is in keeping with our findings for [^{57}FePPIXCl] (figs. 3 and 4).

At 5.40(33) GPa there is evidence for the development of a second site in the spectrum which persists at 6.30(41) GPa. The parameters for this site are compatible with those of an S = +/- $^1/_2$, +/- $^5/_2$ spin admixed site. Again this is in agreement with our findings for [^{57}FePPIXCl] (figs. 3 and 4). However for the [^{57}FeOEPCl] the spin admixed site only occur at higher pressures and the proportion of this site is much less than in [^{57}FePPIXCl].

It should be noticed that in both figs. 1 and 2 and figs. 3 and 4 the asymmetry of the high spin Fe^{III} site decreases dramatically as the pressure increases. The room pressure asymmetry is due to the presence of Kramer's doublets. This suggests that at higher pressures as the lattice is compressed, the higher energy Kramer's doublet becomes less populated due to pressure increasing the energy differences between these energy levels.

At low temperature (4.2K) and normal pressure, symmetrical Mössbauer spectra are observed, as only the S_z = ± ½ states are populated and - as Blume[8] has explained -the spin-spin relaxation is fast. As the temperature increases, the upper states populate (± $^3/_2$ ± $^5/_2$) with longer relaxation times, leading to asymmetric Mössbauer spectra - like those at higher pressures in figs. 2 and 4. This means that the application of pressure has a similar effect on the Mössbauer spectra to that of lowering temperature, as we have reported previously[9-10].

References

1) "Coordination Compounds of Porphyrins and Phthalocyanines", D.P Bernton, John Wiley & Sons Ltd., 1981.
2) P. J. Titler, D. A. Davies, J. Silver and C. A. McCammon - unpublished results, presented as a poster at ICAME 1999.
3) V. V. Borovkov, J. M. Lintuluoto & Y. Inoone, Synlett., 1, 61-62, 1999.
4) J. Sessler, A. Mozaffari, M. Johnson, Org. Synth., 70, 68, 1991.
5) A. Jayaraman, Rev. Mod. Phys., 55, 1, 1983.
6) J. D. Barnett, S. Block and G. J. Piermarini, Rev. Sc. Instrum., 44, 1973.
7) B. W. Fitzsimmons, J. R. Sams and T. B. Tsin, Chem. Phys. Lett., 38, 588, 1976.
8) M. Blume, Phys. Rev. Lett., 18, 305, 1967.
9) J. Silver, R. M. G. R. Roberts, D. A. Davies and C. A. McCammon, Chem. Commun., 11, 1990.
10) J. Silver, J. R. Miller, D. A. Davies and C. A. McCammon, Inorg. Chem., 36, 4017, 1997.

Hyperfine Interactions **141/142:** 109–117, 2002.

High Pressure Mössbauer Spectroscopic Studies of Molecular Solids. The Importance of 'Free' Space in Molecular Lattices

J. SILVER[1], S. ANANADAN[1], D. A. DAVIES[1], G. R. FERN[1], P. J. MARSH[1], J. R. MILLER[1], P. J. TITLER[1] and C. A. McCAMMON[2]

[1] *School of Chemical and Life Sciences, University of Greenwich, Woolwich Campus, Wellington Street, Woolwich, London, SE18 6PF, UK; e-mail: sj29@gre.ac.uk*
[2] *Bayerisches Geoinstitut, Universität Bayreuth, D-95440 Bayreuth, Germany*

Abstract. The behaviour of a number of different molecular solids (both neutral and charged) to applied pressure is discussed. It is shown that the geometry of the molecules, the presence of and number of charges, and the ability of the molecules to alter their shape are all important in the response of their respective lattices to applied pressure. The presence of 'free' space in the lattices at room pressure is shown to be a major factor that needs to be taken into account in order to understand their behaviour.

Key words: high pressure, porphyrins, molecular lattices, ferrocenes

1. Introduction

Relatively few Mössbauer spectroscopic studies have been carried out at high pressure on neutral or ionic molecular solids. When ionic solids are subjected to pressure, the distances between anions and cations are restricted so that they are forced to move closer together. In such lattices there is no 'free' *space* so all the ions in the lattice immediately feel the full effect of being subjected to pressure, leading either to lattice contraction (decrease in one or more cell parameters) or to a phase change or to both.

Technical advances in the design of the cells have now allowed high pressure Mössbauer spectroscopy to become a widespread solid state probe [1, 2]. Initially, such work was limited to very few groups [3–8]. Recent high pressure Mössbauer spectroscopic studies have been predominantly in the fields of solid state physics and geochemistry [9, 10], although some work has also been carried out on high pressure phase changes in molecular solids [11, 12]. Though, potentially, such studies are of immense interest, much must be known about the structure and Mössbauer spectroscopic parameters of the compound or similar

compounds at normal pressure before the high pressure parameters can be understood.

Molecular solids in which the molecules are either neutral or charged present a very different scenario to simple ionic solids when subjected to pressure. For neutral molecular solids, changes experienced by the molecules when the lattice is under pressure will depend on: (1) the shape of the molecules – which in turn will affect how they pack – which will affect how much 'free' space is present in the lattice, (2) how the molecules vibrate – which will, of course, depend on the lattice energy and be related to temperature, and (3) the interaction between the vibrating molecules and the way they pack.

Under pressure molecular solids in which either the anions or the cations (or both) are molecules will also be affected by ionic repulsion/attraction forces. If the shape of the cations are different to the anions or if they carry more than one charge, this will give rise to further complication. If the molecular ions are not rigid, they may also change their geometry/configuration.

Mössbauer spectroscopy (at room pressure) has now been applied to iron(II)/(III) molecular solids for over forty years and there is a wide understanding of the factors that influence the parameters. Substituent effects on the Mössbauer spectroscopic parameters, of three types of iron sandwich compound, have been explained in terms of bonding models [13–15], and the effects of pressure on the electronic absorption spectra and Mössbauer spectra of ferrocene **(1)** have also been reported previously [16, 17].

Dynamic reorientation of molecular species and plasticity in lattices are of interest in many areas of science [18–23]. Naturally occurring dynamic properties of compounds may be altered by changes in physical conditions, potentially making them useful in the fields of molecular electronics and nanotechnology [22]. Mössbauer spectroscopy has been used to probe dynamic effects [20–25], but until recently [24, 25] such studies involved only changes in temperature [18–23].

Variable temperature Mössbauer spectroscopic studies [19] aided by differential scanning calorimetry (DSC) and X-ray diffraction [19], provide evidence that cyclopentadienyl fluorobenzene iron(II) cation of the salts [(η^6-PhF)(η^5-Cp)Fe][AF_6] where A = P **(2)**, As, Sb, are in a state of rapid isotropic reorientation at room temperature which is halted at lower temperatures. The ^{57}Fe Mössbauer spectra are sharp singlets at room temperature but broaden and separate into quadrupole doublets on cooling. We considered this system as a 'molecular rollerball' [24], and showed it could be halted on the Mössbauer spectroscopic time scale by the application of pressure [24, 25]. Two of the three compounds studied, **(2)** and [(η^6-Ph)(η^5-Cp)Fe][PF_6] **(3)** had previously been shown to contain molecules that manifested dynamic reorientation and, in the third, [(η^6-PhMe)(η^5-Cp)Fe][PF_6] **(4)**, no such movement was present [27]. We demonstrated that:

(1) the dynamic reorientation in compounds **(2)** and **(3)** could be turned off (at least as viewed on the time scale of the Mössbauer event) by the application of pressure,

(2) the extrapolation of experimental quadrupole splitting E_Q data gave stationary E_Q values at 298 K and 10^{-4} GPa which are consistent with the previous low temperature data,

(3) the extrapolated E_Q value for **(3)** is larger than the experimental 'outer' E_Q at ambient temperature showing that the latter site is also dynamic at room temperature and 10^{-4} GPa,

(4) that explanations of the observed decreases in E_Q of the stationary sites with applied pressure are consistent with suggestions that the ring plane to metal distances are reduced by increasing applied pressure.

The temperature dependence of the Mössbauer spectrum of the ferrocene thiourea clathrate initially resembles both **(2)** and **(3)**, but the interpretation of the data differs [23]. The ferrocene molecules are guests within the hexagonal channels of the thiourea lattice [23, 26], and can take up three possible orientations; parallel with the channels (Z), or perpendicular (X and Y) [26]. At ambient temperature the spectrum is a singlet which was interpreted as very rapid reorientation between X and Y with rapid orientation between X or Y and Z [23]. This reorientation was consistent with the X-ray structure as the ring atoms of the ferrocene (but not the iron atom) were unresolved [26]. Below 141 K the spectra has a E_Q of a similar magnitude to that of ferrocene [23].

Here, we report high pressure Mössbauer spectra of ferrocene **(1)** and ferrocene thiourea clathrate **(5)**. The former is a neutral molecule in a molecular lattice, the latter can be considered as a neutral molecule in a hydrogen bonded cage. The results are discussed in relation to our findings for the mono-cations in compounds **(2)–(4)** and will also be compared to the iron sandwich dications in bis(hexamethylbenzene)iron(II) hexafluorophosphate **(6)**.

As examples of more multi-charged molecular species other than **(6)**, we have previously reported the effect of pressure on the Mössbauer spectra of models for the $[4Fe\text{-}4S]^{2+}$ clusters of iron sulfur proteins [27]. These compounds had the general formula $[Cat]_2[Fe_4S_4(S^tBu)_4]$ where $[Cat]^+ = [NMe_4]^+$ **(7)**, $[NEt_4]^+$ **(8)**, $[NPr_4]^+$ **(9)**, $[NPen_4]^+$ **(10)** and $[PPh_4]^+$ **(11)** [27]. Of these, **(7)**, **(8)** and **(10)** had been structurally characterised and **(9)** has been shown to be isomorphous with the first two [27]. The structure and Mössbauer spectroscopic data for $[PPh_4]_2[Fe_4S_4(SCH_2CO_2C_2H_5)_4]$ **(12)** were also reported [27]. Here, the results found for these complexes are discussed and the spectra for $[NEt_4]_2[Fe_4S_4Cl_4]$ **(13)** is easily understood in the light of our previous findings [27].

The effect of applied pressure on iron porphyrin compounds is somewhat more complex than for the other molecular species. As examples of what might be expected, changes observed in bis(imidazole) protoporphyrin(IX) iron(III) chloride **(14)** and in bis(imidazole)octaethylporphyrin(IX) iron(III) chloride **(15)** are also reported herein.

2. Experimental

Compound preparations have been described elsewhere [24, 25, 27–30], as has the high pressure Mössbauer spectroscopy details [27].

3. Results and discussion

3.1. IRON SANDWICH COMPOUNDS

The variation of isomer shift (i.s.) with pressure for compounds **(1)**–**(6)** are shown in Figures 1 and 2 and the Mössbauer spectroscopic data for compounds **(1)**–**(6)** are given in refs. [27] and [30]. Within experimental error the i.s. decreased with increasing pressure, consistent with previous reports [10], and is ascribed mainly to increasing electron density at the iron nucleus. The average rate of change of i.s. with pressure is highest for **(4)** and lowest for **(1)** with the other compounds having similar rates of decrease. If it is assumed that the least change in the Mössbauer parameters with pressure is found where there is most space in the lattice, then in the neutral ferrocene lattice the molecules have much space available to them (this is probably reflected by the fact that all structures of ferrocene to date show evidence of disorder).

Compound **(4)** is expected to have little free lattice space at room temperature as, unlike **(2)** and **(3)**, it does not show dynamic reorientation of the iron sandwich cations [25]. Hence, the application of pressure immediately affects the ions in the lattice and a fairly smooth change in the i.s. is observed [25], providing evidence that there is no pressure induced phase change. Thus the iron atoms experience the ever closer proximity of the anionic charges as well as a gradual change in charge distribution within their own sandwich molecules. In contrast, **(2)** and **(3)**, which

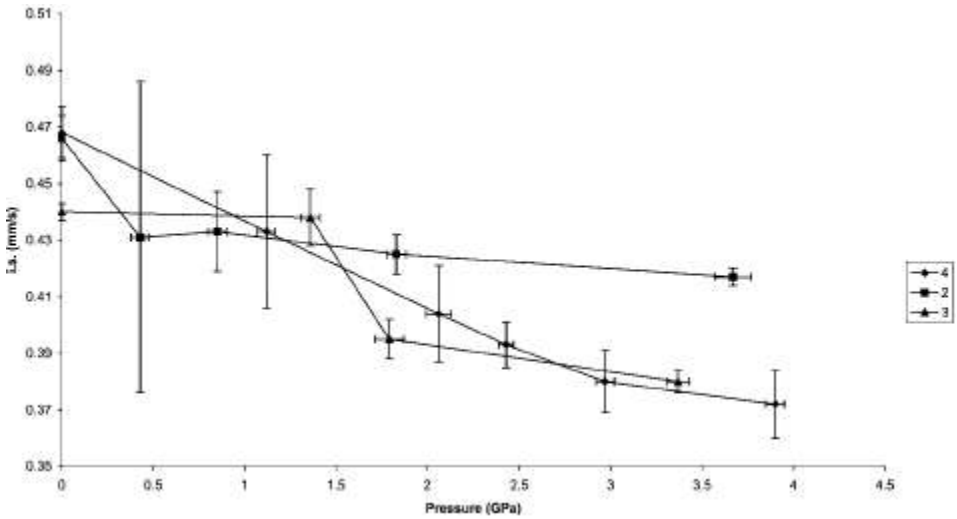

Figure 1. Plot of i.s. against pressure for **(2)**, **(3)**, **(4)**.

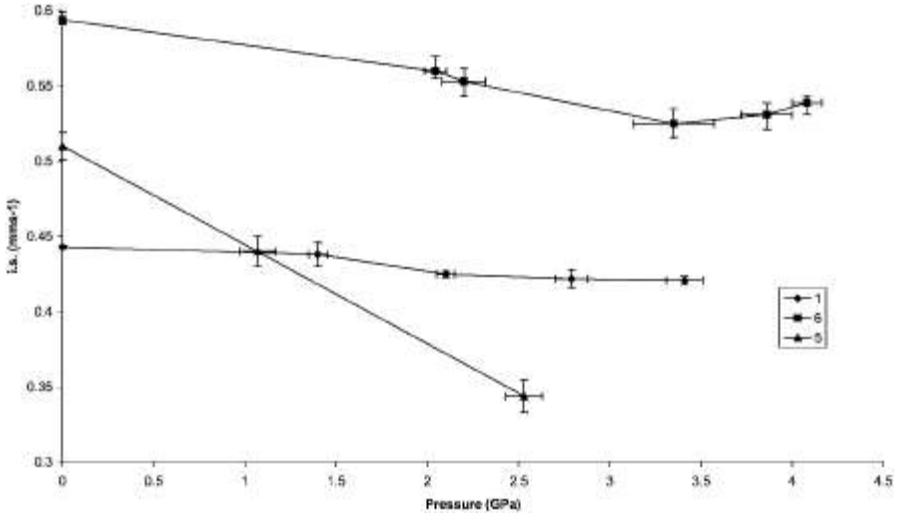

Figure 2. Plot of i.s. against pressure for **(1)**, **(5)**, **(6)**.

manifest dynamic reorientation of the iron sandwich cations must have free space at room pressure (and 298 K). When this space is restricted (when motion ceases on the Mössbauer time scale (~0.85 GPa for **(2)** and below 1.36 GPa for **(3)**), then the i.s. values drop with applied pressure, though that of **(2)** does not drop as much (possibly due to the presence of the F− substituent packing less well, leaving some free space in the lattice).

Compound **(6)** manifests no dynamic process at room pressure (at 298 K) suggesting little free space is present, and so as pressure is applied, the iron atoms immediately experience the effect of the anionic field. However, the dication iron sandwich molecules in **(6)** manifest less change in i.s. with pressure than **(4)**.

The behaviour of the E_Q values of these compounds with pressure is shown in Figures 3 and 4. **(1)** shows the least change, whereas the non-dynamic **(4)** shows a greater rate of change. The final E_Q values of compounds **(4)** and **(6)** are much smaller than the 80 K values [15] (Figure 4) showing the effect of forcing the rings towards the iron atom. **(2)** also manifests a large change with pressure when its motion has ceased on the Mössbauer time scale but **(3)** shows less of a change. This may again be due to the presence of the F− substituent on the iron sandwich cation.

In the ferrocene thiourea clathrate, **(5)**, at room temperature the ferrocene undergoes dynamic reorientation [23]. At high pressure (1.07 GPa) this motion ceases (on the Mössbauer time scale) though the increase in E_Q at 2.53 GPa may indicate that the motion had not fully ceased at 1.07 GPa (see ref. [25] for discussion of slight differences in $[FeCpPhH]^+[PF_6]^-$ E_Q values at room temperature). At 2.1 GPa the ferrocene in the thiourea clathrate manifests an i.s. much smaller than that of ferrocene around this pressure and a E_Q value that is also much smaller. In fact, if the plots of i.s. and E_Q against pressure for ferrocene are extrapolated

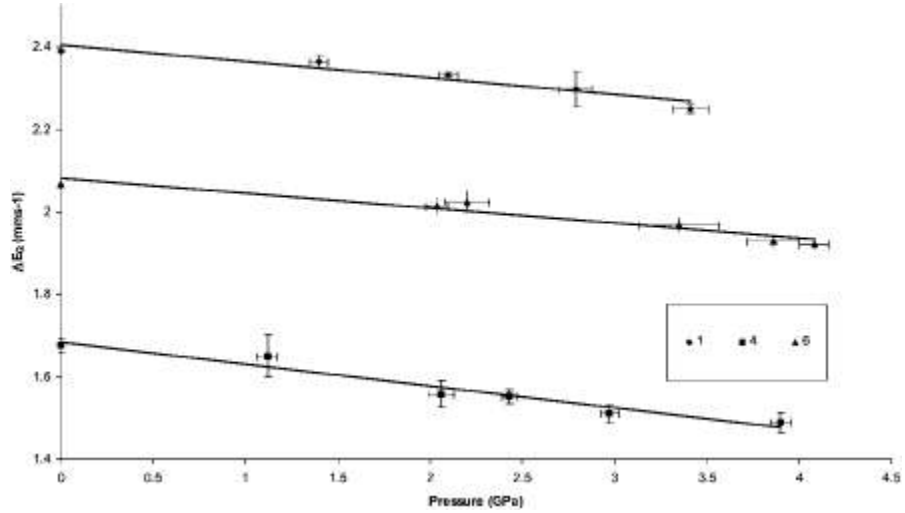

Figure 3. Plot of E_Q against pressure for **(1)**, **(4)** and **(6)**.

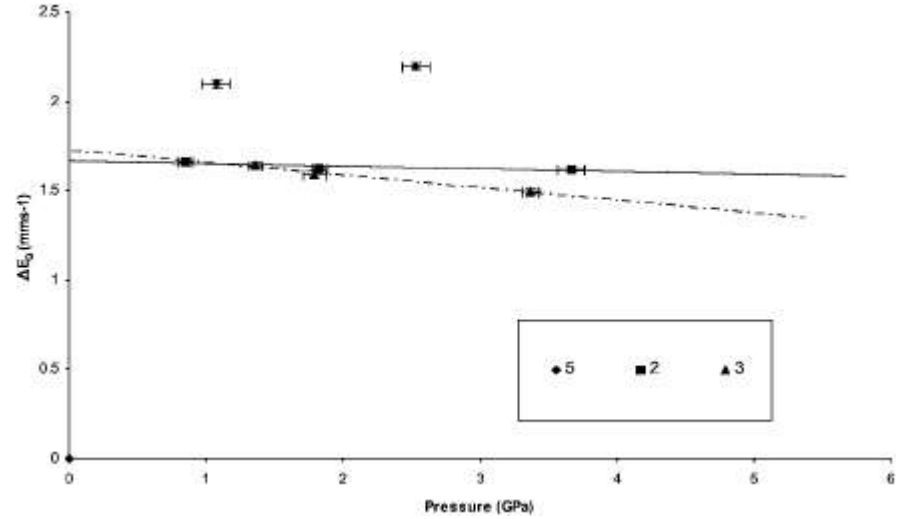

Figure 4. Plot of E_Q against pressure for the stationary sites of **(2)**, **(3)** and **(5)**.

to values of 0.344 mm s^{-1} for the i.s. and 2.197 mm s^{-1} for the E_Q then this corresponds to pressures of around 15 GPa and 5 GPa, respectively. Thus the effects of applying pressure to **(5)** (i.e. on the ferrocene molecules) are magnified by the thiourea cage (once dynamic reorientation has ceased). Moreover the fact that the E_Q and i.s. are not in line with those of pure ferrocene may suggest that the magnification is anisotropic, and the thiourea network is acting as a *molecular vice*.

Thus, where there is least free 'space' between molecules in the lattices of in iron sandwich compounds, the effect of pressure on the iron Mössbauer parameters is the greatest.

3.2. IRON–SULFUR COMPLEXES

The Mössbauer spectroscopic data for **(7)**–**(12)** have been discussed [27]. It was found that for the $[4Fe–4S]^{2+}$ clusters, the iron atoms became less electronically symmetric as temperature is lowered or pressure increased. It was possible to arrange these compounds into three classes depending on their response to the application of pressure. **(7)** had an ordered lattice and it was possible to squeeze the lattice back to its E_Q value at 78 K and, indeed, past that value. In the case of the disordered lattices of compounds **(8)**–**(12)**, it was not possible to do this. **(7)** was assigned to Class A, which is the hard (highly ordered) lattice case [27] in which the cations can be thought of as hard spheres that do not distort with temperature in the range 78–298 K, or with pressure up to at least 5.15(18) GPa. Class B contained compounds **(8)**–**(10)** which had the softer cations that display disorder at 298 K and keep the lattice pinned open when pressure is applied, effectively protecting the cluster cores from the external pressure. Class C was intermediate between the first two and contains cations that are symmetric, less likely to distort than class B, but softer than class A. **(11)** and **(12)** fit into class C, both contain $[PPh_4]^+$ cations. Thus, in compounds **(7)**–**(12)**, free space was again important and it is packing considerations that are most important in the lattice rather than the number of charges on the anions. The crystal structure of **(12)** manifested some disorder in the $SCH_2CO_2C_2H_5$ chains on the $[4Fe–4S]^{2+}$ clusters, which was evidence for free space in the lattice at room temperature. It is likely that this space is initially lost on the application of pressure and any other changes caused by pressure do not cause further loss of freedom to the electronic environment of the iron atoms [27].

Compound **(13)**, like **(7)**–**(12)**, has a cubane core but now the exterior SR^- groups are replaced by Cl^- ions making the overall cluster much smaller. The E_Q value increases from its room pressure/temperature value (0.61(2) mm s^{-1}) to a value of 0.88(2) mm s^{-1} at 3.30(7) GPa. It then decreases to 0.78(2) at 3.53(17) GPa and shows only a little increase (0.82(2) mm s^{-1}) at 4.61(37) GPa. There is no change in the i.s. until 3.30(7) GPa, but above this pressure it drops sharply by 0.06 mm s^{-1}. The behaviour of **(13)** to 3.30(7) GPa shows that it fits to a type A lattice (little free space) [27], then a reversible pressure induced phase change occurs. In these lattices the overall effect of loss of space is to distort softer ions (here cations) most.

3.3. IRON–PORPHYRIN COMPLEXES

The orientation of the axial ligands in compounds of the type $[PorFe(III)L_2]Cl$ (where Por is a porphyrin and L is a imidazole or pyridine type ligand) have been

shown to be important in controlling the ground state and electronic properties of the molecules. It has been shown that the choice of axial ligand has a dominant effect on the resulting ground state of the molecule [28]. The results of applying pressure to **(14)** and **(15)** indicate that the orientation of the axial ligands change to compensate for the lack of space in the lattice [29]. The changes in ligand orientation for **(14)** lead to changes in the ground state of the molecules and also to a spin state change from $S = 1/2$ to $S = 5/2, 3/2$ (admixed spin state) for some of the molecules. For **(15)** there is evidence of two slightly different orientations of the low spin iron ground state and also for a spin admixed spin state. These spin admixed states are not expected as they necessitate an increase in molecular volume. However, this is offset by overall closer molecular packing.

Here the response of a lattice of molecular ions to applied pressure leads to modification of the shape of the ions to accommodate the restrictions imposed by loss of 'free' space.

4. Conclusions

We have shown in this work that the effect of applied pressure on neutral or charged molecules (in molecular lattices) is dependent in the shape of the molecules and the charges present. To accommodate the loss of free space the closer packing of the molecules may necessitate changes in their shape. These changes may affect physical properties such as dynamic reorientation, ground states, or even spin states.

Acknowledgements

High pressure experiments were performed at Bayerisches Geoinstitut under the E.C. 'Human Capital and Mobility – Access to Large Scale Facilities' programme (Contract No. ERBCHGECT940053 to D.C. RUBIE).

References

1. Taylor, R. D. and Pasternak, M. P., *Hyp. Interact.* **53** (1990), 159.
2. Noak, R. and Holzapfel, W. B., In: K. D. Timmerhaus and W. D. Barber (eds), *High Pressure Science and Technology*, Plenum Press, New York, 1979, p. 748.
3. Pound, R. V., Benedek, G. B. and Drever, R., *Phys. Rev. Lett.* **7** (1961), 405.
4. Pipkorn, D. N., Edge, C. K., DeBrunner, P., de Pasquali, G., Drickamer, H. G. and Frauenfelder, H., *Phys. Rev. A* **135** (1964), 1604.
5. DeBrunner, P., Vaughan, R. W., Champion, A. R., Cohen, J., Monzis, J. and Drickamer, H. G., *Rev. Sci. Inst.* **37** (1966), 1310.
6. Fitch, R. A., Slykhouse, T. E. and Drickamer, H. G., *J. Opt. Soc. Amer.* **47** (1957), 1015.
7. Drickamer, H. G. and Frank, C. W., *Electronic Transitions and High Pressure Chemistry*, Chapman Hall, London, 1973.
8. Holzapfel, W. B., *High Temperatures – High Pressures* **19** (1970), 241.
9. Pasternak, M. and Taylor, R. D., *Hyp. Interact.* **47** (1989), 415.

10. Armthauer, G., *High Pressure Research in Geosciences*, Schweizbart'sche, Verlagsbuchhandlung, Stuttgart, 1982, p. 269.
11. Konig, E., Ritter, G. and Waigel, J., *J. Chem. Phys.* **83** (1985), 3055.
12. Koppen, H., Meissner, E., Wiehl, L., Spiering, H. and Gutlich, P., *Hyp. Interact.* **52** (1989), 29.
13. Houlton, A., Miller, J. R., Roberts, R. M. G. and Silver, J., *J. Chem. Soc., Dalton Trans.* (1990), 2181; *ibid* (1991), 467.
14. Brown, R. A., Houlton, A., Roberts, R. M. G., Silver, J. and Slade, E., *J. Chem. Soc., Dalton Trans.* (1994), 1519.
15. Brown, R. A., Houlton, A., Howe, S. D., Roberts, R. M. G. and Silver, J., *J. Chem. Soc., Dalton Trans.* (1993), 3329.
16. Vaughan, R. W. and Drickamer, H. G., *J. Chem. Phys.* **47** (1967), 468.
17. Zahner, J. C. and Drickamer, H. G., *J. Chem. Phys.* **35** (1961), 375.
18. Sherwood, J., *The Plastically Crystalline Solid*, Wiley, Chichester, 1979, p. 1.
19. Fitzsimmons, B. W. and Sayer, I., *J. Chem. Soc., Dalton Trans.* (1991), 2907.
20. Fitzsimmons, B. W. and Hume, A. R., *J. Chem. Soc., Dalton Trans.* (1980), 180.
21. Fitzsimmons, B. W. and Marshall, W. G., *J. Chem. Soc., Dalton Trans.* (1992), 73.
22. Fitzsimmons, B. W., *J. Phys. C* **41** (1980), 33.
23. Gibb, T. C., *J. Phys. C* **9** (1979), 2627.
24. Silver, J., Roberts, R. M. G., Davies, D. A. and McCammon, C. A., *J. Chem. Soc. Chem. Commun.* (1996), 11.
25. Silver, J., Miller, J. R., Davies, D. A. and McCammon, C. A., *Inorg. Chem.* **36** (1997), 4017.
26. Hough, E. and Nicholson, D. G., *J. Chem. Soc., Dalton Trans.* (1978), 15.
27. Silver, J., Fern, G. R., Miller, J. R., McCammon, C. A., Evans, D. J. and Leigh, G. J., *Inorg. Chem.* **38** (1999), 4256 and references therein.
28. Silver, J., Marsh, P. J., Symons, M. C. R., Svistunenko, D. A., Frampton, C. S. and Fern, G. R., *Inorg. Chem.* **39** (2000), 2874.
29. Silver, J., Davies, D. A., Anandan, S., Titler, P. J., Fern, G. R., Marsh, P. J. and McCammon, C. A., *J. Am. Chem. Soc.* (2001), submitted.
30. Davies, D. A., Ph.D. Thesis, University of Essex, 1998.